The Effects of Clinically Relevant Concentrations of Metal Ions after Hip Replacement on Bone Cell Physiology

Karan Mehul Shah

Thesis submitted in accordance with the requirements of The University of Sheffield for the degree of Doctor of Philosophy.

Department of Human Metabolism
Faculty of Medicine, Dentistry & Health

February 2014

Acknowledgements

Statement of Attribution

I would like to acknowledge the following people for their contribution to the data in the project:

Dr Rebecca Andrews for her data on the effects of individual metal ions on developing osteoclasts (2 experimental repeats for Co^{2+}) and mature osteoclasts (1 experimental repeat for Co^{2+} and Cr^{6+} each) (Chapter 4).

Mr Peter Orton for quantification of one case-control pair of osteoclast cultures assessing the effects of circulating metal ions on osteoclast survival and function (Chapter 4).

Mr Nick Mani for his optimisation of *in vitro* MLO-Y4 culture (Chapter 5).

Dr Paul Quinn for the analyses of µXRF and µXANES data for intracellular distribution and speciation of metal ions in bone cells.

List of awards, publications and presentations

Awards:

Orthopaedic Research Society - William H. Harris Award for the paper '*Understanding the Tissue Effects of Tribo-corrosion: Uptake, Distribution, and Speciation of Metal in Human Bone Cells*' to be awarded at the Orthopaedic Research Society Annual Meeting, New Orleans, USA (2014).

Bone Research Society - Best Basic Science Poster awarded for '*MicroXRF and XANES Study to Investigate the Speciation and Distribution of Metal Ions in Osteoblasts*' at the Osteoporosis and Bone Conference held jointly by National Osteoporosis Society and Bone Research Society (2012).

Publications:

Shah KM, Quinn PD, Wilkinson JM, Gartland A. (2014). Understanding the Tissue Effects of Tribo-corrosion: Uptake, Distribution, and Speciation of Metal in Human Bone Cells *(manuscript prepared to be submitted to Journal of Orthopaedic Research).*

Andrews RE, **Shah KM**, Wilkinson JM, Gartland A. (2011) Effects of cobalt and chromium ions at clinically equivalent concentrations after metal-on-metal hip replacement on human osteoblasts and osteoclasts: implications for skeletal health. *Bone. 49(4):717-23*

List of presentations:

2014   **Oral Presentation** at the Annual Orthopaedic Research Society, New Orleans, USA.
Understanding the Tissue Effects of Tribo-corrosion: Uptake, Distribution, and Speciation of Metal in Human Bone Cells
Shah KM, *Quinn PD, Gartland A, Wilkinson JM*

2013   **Oral Presentation** at British Orthopaedic Research Society and Bone Research Society Joint Meeting, Oxford, UK
Effect of Metal Ions and Particles on Osteoblast Mineralisation on Grit-Blasted, Titanium-Coated and Hydroxyapatite-Coated Prosthesis Surfaces.
Shah KM, *Draper ER, Gartland A, Wilkinson JM*

2013   **Oral Presentation** at British Orthopaedic Research Society and British Hip Society joint meeting, Bristol, UK
Effect of clinically relevant metal ion combinations on osteoblast and osteocyte survival and function in vitro.
Shah KM, *Gartland A, Wilkinson JM*

2013	**Oral Presentation** at the Annual Orthopaedic Research Society, San Antonio, USA. *Effect of clinically relevant metal ion combinations on osteoblast survival and function in vitro* **Shah KM**, *Gartland A, Wilkinson JM*
2012	Poster Presentation at the Osteoporosis and Bone conference jointly held by National Osteoporosis Society and Bone Research Society, Manchester, UK. *MicroXRF and XANES Study to Investigate the Speciation and Distribution of Metal Ions in Osteoblasts.* **Shah KM**, *Quinn PD, Wilkinson JM, Gartland A*
2012	**Oral Presentation** at UK Purine Meeting, Norwich, UK *Cellular Uptake of Metal Ions by Osteoblasts – a possible role for P2X7 receptors?* **Shah KM**, *Wilkinson JM, Gartland A*
2011	**Oral Presentation** at the 11th International Symposium on Metal ions in Biology and Medicine. *Effect of Metal Ion Combinations on Osteoblasts in vitro.* **Shah KM**, *Wilkinson JM, Gartland A*
2011	Poster presentation at the 3rd joint meeting of the BRS and BORS, Cambridge, UK *Effect of Metal Ion Combinations on Osteoblasts in vitro.* **Shah KM**, *Wilkinson JM, A Gartland*

Summary

In the last decade, metal-on-metal (MOM) hip replacements have been a popular alternative to conventional total hip arthroplasty (THA) in younger more active patients requiring hip replacement surgery, due to their improved wear and lubrication characteristics. However, these prostheses have a relatively poor clinical outcome compared to THA. The most frequent reasons for failure include osteolysis, aseptic loosening, femoral neck fracture and periprosthetic inflammatory masses attributed to the adverse local tissue reactions to metal ions and particles released from the prosthesis. More recently, similar adverse events have been associated with modular conventional hip implants due to corrosion and wear at metal junctions.

Most implants rely on good periprosthetic bone health for fixation and survival. This warrants the understanding of the effects of prostheses related metal ions and particles on bone cell survival and function. This project investigates the effects of clinically relevant concentrations and combinations of metal ions (Co^{2+}, Cr^{3+} and Cr^{6+}) on survival and function of osteoblasts, osteoclasts and osteocytes. Furthermore, it describes the intracellular distribution and speciation of metal ions in bone cells and investigates the possible mechanisms of their cellular entry.

The results from this group of studies suggest that in the local periprosthetic environment, there is inhibition of bone cell activity with implications for primary fixation of the implant and its survivorship. Over a narrow systemic concentration range, the metal ions increased osteoblast differentiation and mineralisation, consistent with a small increase in bone mineral density observed clinically. The results of sub-cellular distribution suggest different mechanisms of cellular entry for metal ions based on the cell type and stage of differentiation, whilst the speciation data confirms the intracellular reduction of Cr^{6+}, with no change in oxidation stage observed for Co^{2+} and Cr^{3+}. Furthermore, the cellular entry of Co^{2+} was reduced with P2X7R antagonist in osteoblasts but not osteoclasts, offering a cell specific therapeutic target to alter bone remodelling in the periprosthetic environment. The main limitation of the study was the use immortalised cell-lines which, whilst being convenient and useful tool, may not accurately represent the clinical setting.

Contents

List of Figures

List of tables

List of Abbreviations

˚C	Degree Celsius
µg	Microgram
µM	Micromolar
µm	Micrometer
µ-XANES	Micro X-ray absorption near edge structure
µ-XRF	Micro X-ray fluoroscence
ALP	Alkaline phosphatase
AP-1	Activator protein-1
Asp	Aspartame
ATP	Adenosine triphosphate
AUC	Area under curve
BMP	Bone morphogenetic protein
BMU	Bone multicellular unit
Ca	Calcium
CATK	Cathepsin K
Cd	Cadmiuim
CI	Confidence interval
Co	Cobalt
COC	Ceramic-on-ceramic
Cr	Chromium
Cu	Copper
Cx43	Connexin 43
Da	Dalton
Dmp-1	Dentin matrix protein 1
DMSO	Dimethyl sulfoxide
DMT-1	Divalent metal transporter-1
DNA	Deoxyribonucelic acid
dsDNA	Double stranded DNA
ECM	Extracellular matrix
EDXA	Energy dispersive X-ray analysis
FCS	Foetal calf serum
Fe	Iron
F-Oc	Forming oscteoclast
FSD	Functional secretory domain
GB	Grit blasted
GJ	Gap junction
Gly	Glycine
GPa =	Giga Pascals
GSH	Glutathione
H	Histidine
HA	Hydroxyapatite
HIF1α	Hypoxia inducible factor-1α
hr	Hour
IARC	International Agency for Research on Cancer
IC_{50}	Inhibitory concentration (50%)
IL	Interleukin
IU	International units

L	Litre
M	Molar
MCP-1	Monocyte chemotactic protein -1
M-CSF	Macrophage-colony stimulating factor
Mg	Magnesium
min	Minute
Mn	Manganese
Mo	Molybdenum
M-Oc	Mature osteoclast
MOMHR	Metal-on-metal hip resurfacing
MOMTHR	Metal-on-metal total hip replacement
MOP	Metal-on-polyethylene
MSC	Mesenchymal stem cell
MT1-MMP	Membrane type-1 metalloproteinase
MV	Matrix vesicle
NFAT	Nuclear factor of activated T-cells
Ni	Nickel
nM	Nanomolar
NO	Nitric oxide
NP	Nanoparticle
NRAMP2	Natural resistance-associated macrophage protein 2
OA	Osteoarthritis
Ob	Osteoblast
Oc	Osteoclast
OPG	Osteoprotegrin
OSHA	Occupational Safety and Health Administration
P2X7R	P2X7 receptor
PBMC	Peripheral blood mononuclear cell
PBS	Phosphate buffer saline
PGE-2	Prostaglandin E2
Pi	Inorganic phosphate
PMMA	Polymethylmethacrylate
pNPP	paraNitrophenyl phosphate
PPi	Inorganic pyrophosphate
PTH	Parathyroid hormone
RANKL	Receptor activator of nuclear factor kappa-B ligand
RGD	Arg-Gly-Asp
ROS	Reactive oxygen species
SD	Standard Deviation
THA	Total hip arthroplasty
Ti	Titanium coated
TNAP	Tissue non-specific alkaline phosphatase
TNF-alpha	Tumor necrosis factor-alpha
TRAcP	Tartrate resistant acid phosphatase
XAS	X-ray absorption spectroscopy
Zn	Zinc

Chapter 1 - Introduction

Musculoskeletal related disorders, after mental and behavioural disorders, are the second largest contributors to disability worldwide, estimated to affect 22.7% of the global population (Vos*, et al* 2012). Of all musculoskeletal disorders, osteoarthritis (OA) has had the greatest increase in incidence between 1990 and 2010, with incidence of hip OA increasing by 60% (Vos*, et al* 2012), probably due to the increase in life-span and improved diagnosis. The term hip replacement describes an orthopaedic surgical procedure in which a diseased native hip joint is replaced with artificial implants, with the aim of restoring activity and alleviating pain and disability. Hip OA is the main indication for replacement surgery with 91% of all hip procedures in 2012 having OA as its primary cause (NJR 2013). This has led to a worldwide increase in hip replacement surgeries, with number of procedures in England and Wales up by 35% over the last seven years (NJR 2013).

The majority of hip replacement surgeries are done in patients over 60 years of age. Nevertheless, the increase in number of total procedures has led to a larger number of younger more active patients (<60 years) having hip replacements. This change in population demographics made the use of hips with metal-on-metal (MOM) articulations more popular over the last decade, due to better wear and lubrication characteristics that permitted higher activity levels (Chan*, et al* 1999, Clarke*, et al* 2000). These included metal-on-metal hip resurfacings (MOMHR) that preserve the patient femoral bone, and metal-on-metal total hip replacement (MOMTHR) which is similar to conventional stemmed metal-on-polyethylene THA, but with metal-on-metal articulation. However, both MOMHR and MOMTHR have a poor clinical outcome with higher mid-term failure rates compared to cemented and uncemented THA that do not use a MOM bearing (Smith*, et al* 2012a, Smith*, et al* 2012b). This poor performance is attributed to the adverse reactions to metal ions released into the periprosthetic environment due to wear and corrosion at the MOM articulating surfaces (Langton*, et al* 2010).

The main objective of this project is to characterise the effects of prosthesis-derived metal ions on bone cells at systemic and local concentrations to obtain a greater insight into mechanisms for implant failure, as bone-related complications are the main reason for prosthesis failure. The introduction to this thesis will

provide a brief overview regarding the development of MOM hip replacements and the problems associated with it. It will describe the basic concepts of bone biology and review the known effects of metal ions on bone cells, before stating the hypothesis and the aim of this project.

1.1 History of Hip Arthroplasty

Treatment for OA of the hip gradually developed from rudimentary surgery such as amputation of the limb in the late 1700's, the first excision arthroplasty by Anthony White in 1821; to the first interpositional arthroplasty by Vitezlav Chlumsky in 1880's, who experimented with various materials, from metals like zinc to tissues such as muscle (Gomez and Morcuende 2005).

The first use of prosthesis is credited to Pierre Delbet who used rubber for the femoral part of the joint in 1919 (Gomez and Morcuende 2005). Smith-Peterson, in 1923, used a glass hemi-arthroplasty which had limited success due to the brittle nature of the material (Smith-Petersen 2006). Gradually, the prosthesis evolved into a metal implant first used by Wiles in 1938, and by Austin Moore in 1940 (Moore and Bohlman 2006). A fenestrated stem that depended upon osseointegration for fixation by bone ingrowth was described for the first time by Moore in 1952 (Gomez and Morcuende 2005). Later, Kenneth McKee and Edward Haboush, developed a prosthesis which used dental acrylic cement for fixation (Gomez and Morcuende 2005). Metal-on-metal articulation in a cementless implant was developed by Peter Ring in 1964 (Gomez and Morcuende 2005), but all these prostheses gave way to John Charnley's model which made used of a metal-on-polyethylene bearing for low friction and it remains the template of modern THA (Amstutz and Grigoris 1996).

1.2 Total Hip Arthroplasty

Conventional THA involves the removal of the femoral head and proximal femoral neck along with the cartilaginous tissue and subchondral bone from the acetabulum (Siopack and Jergesen 1995). A metal stem with a spherical metal head is implanted in the proximal femoral medullary canal, and a polyethylene component is inserted into the pelvic acetabulum, forming a metal-on-polethylene (MOP) articulation (Siopack and Jergesen 1995).

The implants may be cemented to the bone using polymethylmethacrylate (PMMA) cement or uncemented in which the implant surface has a porous coating or is roughened, and relies on bone ingrowth or ongrowth for implant fixation (Siopack and Jergesen 1995). The development of the cementless prostheses was prompted by the high failure rates of first generation cemented THAs (Yamada, *et al* 2009), sometimes as high as 34% for Charnley-Muller prosthesis after 7 years (Olsson, *et al* 1981). The poor outcomes were attributed to aseptic loosening of the prostheses due to the presence of PMMA cement debris (Harris, *et al* 1976, Learmonth, *et al* 2007), and thus the aim of developing uncemented implants was to remove this material from THA. This view was evidenced by the observation that PMMA particles induced an inflammatory response via the release of pro-inflammatory cytokines and chemokines (Glant, *et al* 1993, Nakashima, *et al* 1999). This inflammatory response has been associated with an increase in bone resorption which eventually plays a role in the loosening of the implant (Glant, *et al* 1993, Quinn, *et al* 1992).

The 7-year cumulative hazard for revision for uncemented hip replacements was observed to be higher at 5.59% compared to cemented prostheses at 2.09% (Makela, *et al* 2014, NJR 2013). This improved survivorship of cemented implants has been a result of better cementing techniques with lavaging of the endosteal surface (Breusch, *et al* 2000) and application of pressure for better fixation (Askew, *et al* 1984). The persistence of osteolysis and prosthetic loosening in absence of cement suggested the involvement of other factors, and a study by Schmalzried et al.(1992) showed an association between lytic bone loss and polyethylene debris from joint wear, identified by its birefringence under polarized light (Schmalzried, *et al* 1992). Higher levels of activity, typical of younger patients, also influence wear rates and increases their chances of periprosthetic loosening and implant failure (Jasty, *et al* 1997). These observations established wear and the generation of particulate debris from the bearing surface, and not from fixation using PMMA cement, as the major factor causing osteolysis and loosening in conventional THA.

Modern THA is considered to be one of the most successful surgical interventions with an implant survival after 10 years being 90% as shown by many (Callaghan,

et al 2000, Eskelinen*, et al* 2006, Ulrich*, et al* 2008). However, 10-year implant survival drops to about 80% for patients under the age of fifty and at longer follow-ups of twenty-five years the survivorship drops down to about 70% (Berry*, et al* 2002, Malchau*, et al* 2002). To overcome the problem of osteolysis, implant loosening and joint instability, alternative bearing surfaces such as metal-on-highly crosslinked polyethylene (MOHXLPE), ceramic-on-ceramic (COC), and metal-on metal (MOM) were developed with the aim of reducing the volumetric wear at the articular bearing. Metal-on-metal bearings show less wear compared to implants using conventional polyethylene (Scholes*, et al* 2001); however, there are concerns regarding metal ion release which will be discussed in detail later (section 1.5) (Manley and Sutton 2008).

1.3 Metal-on-Metal Hip Implants

A MOM articulation was first used by Phillip Wiles in 1938, and was made from stainless steel to reconstruct a complete hip joint (Amstutz and Grigoris 1996). Later, vitallium (an alloy of cobalt, chromium and molybdenum) based MOM implants developed by McKee-Farrar become popular and were widely used during the 1950's and 1960's (Long 2005). However, increasing rates of early component loosening along with the promising clinical results for Charnley's metal-on-polyethylene prostheses caused MOM articulations to fall out of favour (Amstutz and Grigoris 1996, Long 2005).

The initial failure of these implants was attributed to the limitations of manufacturing processes which resulted in an equatorial contact between the femoral and the acetabular components (Figure 1.1). This resulted in an increase in frictional torque and inefficient lubrication between the articular surfaces which increased the risk of failure and implant seizing (Kim*, et al* 2008, Walker and Gold 1971). Technical advances now allow a polar bearing contact pattern (Figure 1.1) which permits fluid ingress that subsequently forms a fluid film between the bearing surfaces. This provides better lubrication resulting in lower wear and hence lower osteolysis, with better load bearing characteristics. Metal-on-metal hip resurfacing (MOMHR) and metal-on-metal total hip replacement (MOMTHR) are the two most commonly used hip prostheses with MOM articulations.
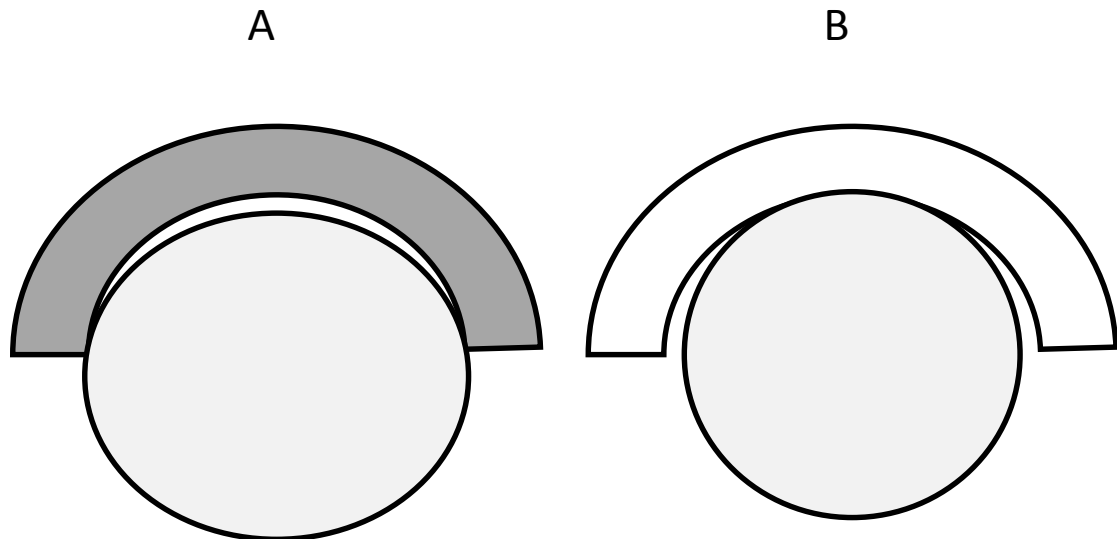
Figure 1.1 Bearing contact patterns.

A) Equatorial contact results in inefficient lubrication and increased frictional torque which increases the risk of failure. B) A polar contact now possible in new generation MOM articulation permits fluid ingress allowing better lubrication with lower wear and thus better load bearing characteristics.

1.3.1 Metal-on-metal hip resurfacing and metal-on-metal total hip replacements

Hip resurfacing is a procedure of joint reconstruction which removes less bone at the proximal femur, provides superior stress transfer characteristics and permits the use of large femoral heads that improve stability, reducing the rate of hip dislocation (Amstutz, *et al* 1998) (Figure 1.2).

The first total hip resurfacing prosthesis is credited to John Charnley who used a Teflon-on-Teflon implant, which although had excellent friction-related attributes experienced poor survivorship (Howie, *et al* 1993). In the 1970's, several attempts at resurfacing primarily having a metal femoral component and a polymer acetabular component failed to improve the survivorship and were abandoned. The causes for failure were presumed to be the osteonecrosis of femoral head or the increased frictional torque due to large-diameter femoral heads. In fact, the decreased survivorship of these early resurfacings is now attributed to polyethylene wear mediated osteolysis, as verified by retrieval studies (Howie, *et al* 1993).
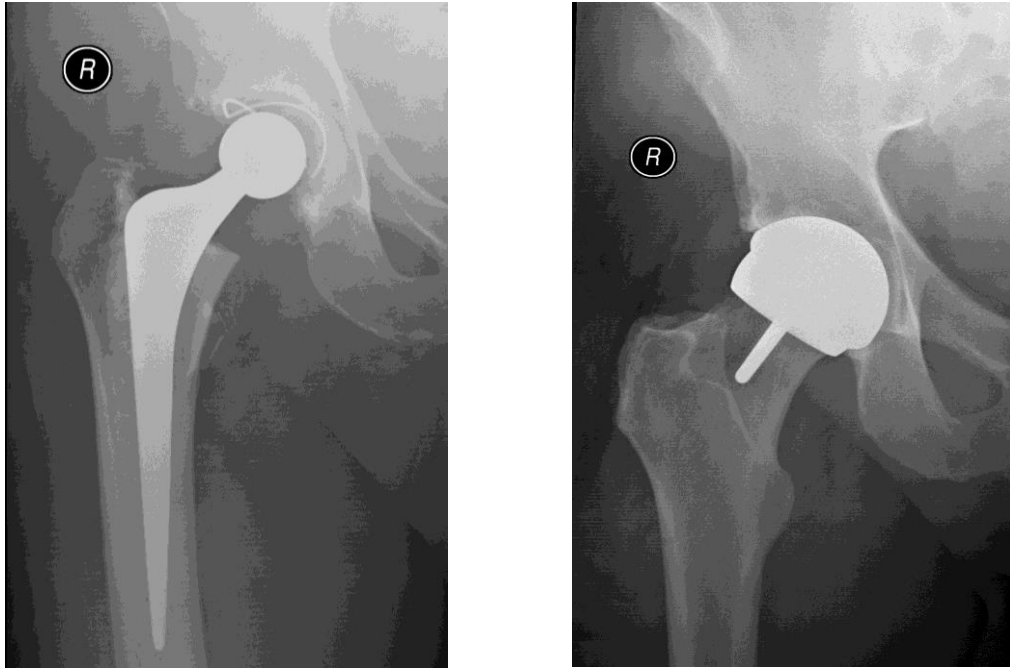
Figure 1.2 THA and MOMHR X-ray radiographs

Left – A conventional THA with complete excision of the femoral head. Right – A MOMHR with the femoral head conserved that aids in revision to THA.

Interest in metal-on-metal bearing surfaces was renewed when studies evaluating the long-term outcome of the first metal-on-metal prostheses showed promising results (Andrew*, et al* 1985, August*, et al* 1986). High failure rates of conventional THA in younger active patients due to increased wear related osteolysis (Dorr*, et al* 1994, Kilgus*, et al* 1991) further prompted a revival in low wear MOMHR. MOMTHR, a stemmed alternative to MOMHR also became popular in light of reports suggesting association of femoral neck fractures, osteonecrosis and low survival of femoral components with MOMHR (Amstutz*, et al* 2004, Garbuz*, et al* 2010, Ullmark*, et al* 2009, Zustin*, et al* 2010).

1.3.2 MOM hip replacements versus THA

In addition favourable tribological characteristics described previously, MOM hip replacements showed several advantages over THA.

Lower wear: Hip simulator studies have suggested approximately 70 fold decrease in volumetric wear after 10 years for MOM bearings compared to conventional bearings (Clarke*, et al* 2000, Scholes*, et al* 2001). With wear-related osteolysis being the primary reason for failure of conventional THA, MOM hips were perceived to be a promising alternative. The lower wear for this articulation is attributed to the use of larger femoral heads that reduces contact pressure and increases the contact area (Liu*, et al* 2005). Additionally, the formation of a mixed or fluid film lubrication between the hard-on-hard articulating surfaces reduces friction and wear compared to MOP bearings that largely functions in boundary lubrication regimes (Jin*, et al* 1997) (Figure 1.3).
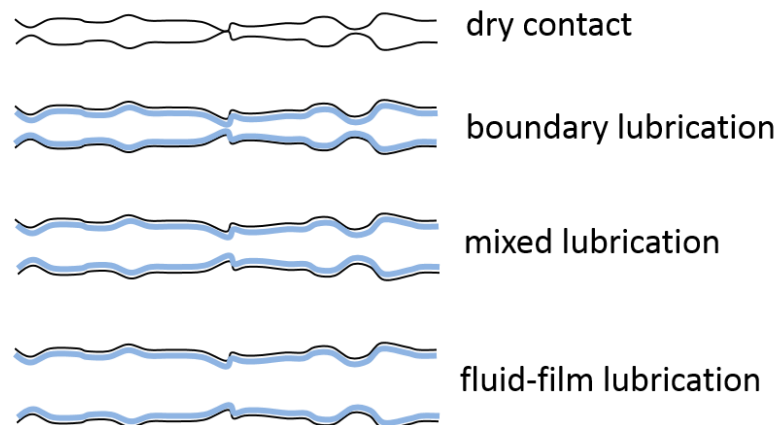
Figure 1.3 Lubrication regimes operating between articulating surfaces

The black line represents the surface of the material and the blue represents adsorbed molecules on the surfaces. Dry contact lubrication has the greatest coefficient of friction followed by boundary lubrication (associated with MOP bearing). Fluid-film lubrication prevents contact between the two surfaces and has coefficient of friction two orders of magnitude lower than boundary conditions. Coefficient of friction for mixed lubrication varies between boundary and fluid-film regimes. MOM articulation have a mixed or fluid-film lubrication and thus function with lower friction and subsequent wear.

Rates of dislocation: Several studies have reported a lower rate of early dislocation in MOM prostheses compared to conventional THA (Peters*, et al* 2007, Plate*, et al* 2012, Stroh*, et al* 2013). The dislocation rates with THA range from 2% to 5% whereas hips with MOM bearings offer a much lower dislocation rate of 0.2% to 0.4% (Lieske*, et al* 2008, Peters*, et al* 2007). The reduced rates of dislocation for MOM hip articulation have been attributed to better interfacial forces during lubrication as a result of smaller separation between the surfaces (Clarke*, et al* 2003b), and a better head:neck ratio, especially for MOMTHR, that prevents impingement (Singh*, et al* 2013).

Increased levels of activity: MOMHR permits higher activity levels and reduced pain in a study comparing 57 MOMHR to 93 THA with minimum follow-up of 2 years (Mont*, et al* 2008, Reito*, et al* 2013, Vail*, et al* 2006). A recent study reported MOMHR to be an attractive option for patients under the age of 30 due to improved functional outcomes as measured by Harris hip scores and UCLA activity scores after a 50 month follow-up (Krantz*, et al* 2012).

The perceived advantages led to a rapid increase in the use of MOM hip implants over the last decade peaking with 16% (11,290) of all hip procedures in England and Wales in 2008 (NJR 2013) (Figure 1.3). It is currently estimated that approximately 80000 patients in the UK have an indwelling MOM prosthesis (NJR 2013).
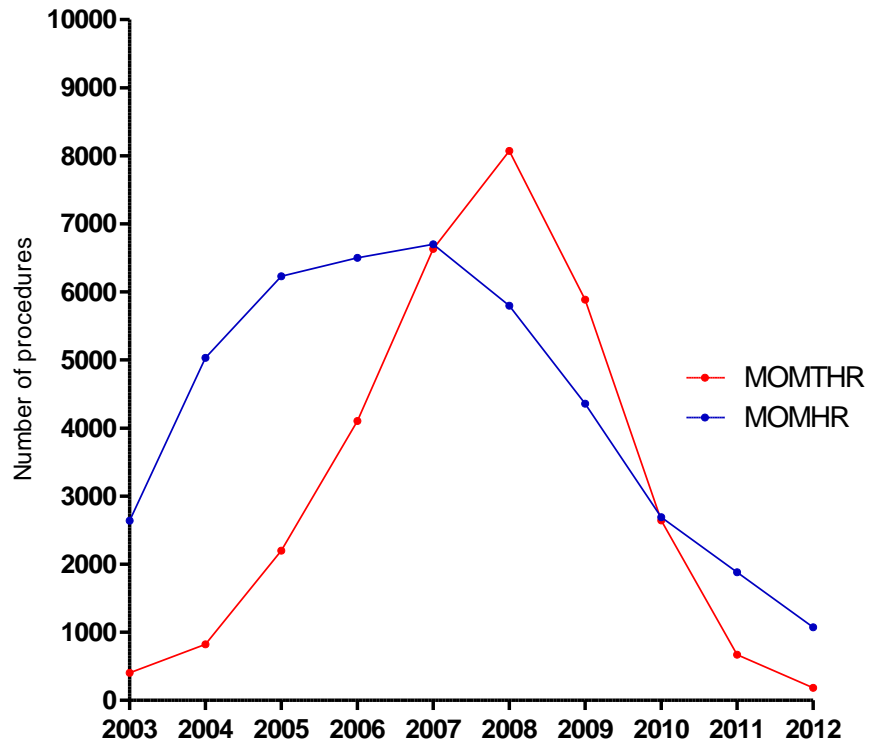
Figure 1.4 Number of prosthesis with MOM articulation between 2003 and 2012.

The graphs illustrate the rapid increase and decrease in popularity over the last decade of metal-on-metal hip resurfacing (MOMHR) and metal-on-metal total hip replacement (MOMTHR) in England and Wales. Data from the National Joint Registry 10th Annual report.

1.3.3 Survivorship of MOM hip replacements

Despite the reported advantages of lower wear (Scholes*, et al* 2001) and dislocations (Smith*, et al* 2005), the survivorship of MOM hip implants is much lower compared to conventional total hip arthroplasty with 5-year revision rates of 5.8% (5.5-6.1) for MOMHR, and 6.3% (95%CI, 4.9-8.0) for cemented and 7.6% (7.3-8.0) for uncemented MOMTHR compared to 1.5% (1.4-1.6) for cemented and 2.5% (2.3-2.6) uncemented conventional total hip arthroplasty (NJR 2013) (Figure 1.4). The reduced survivorship of these implants is attributed to adverse reactions in the surrounding tissue to metal ions and particles released from the prostheses, as evidenced by a positive correlation between implant failure and metal ion concentrations in patient blood (Langton*, et al* 2013).

1.4 Adverse events following metal-on-metal hip replacements

1.4.1 Pseudotumors

A study examining the periprosthetic tissue following metal-on-metal hip replacement observed perivascular infiltration of lymphocytes which was more severe in cases of aseptic loosening than in samples received during autopsy (Davies*, et al* 2005). This reaction, now termed as a 'pseudotumor' as it manifests as a periprosthetic inflammatory mass (Pandit*, et al* 2008), and is believed to be due to a delayed hypersensitivity response to implant-related metal debris and correlates with increased wear (Grammatopoulos*, et al* 2013, Willert*, et al* 2005). Initially thought to affect 1% of all MOMHR patients (Pandit*, et al* 2008), recent studies report up to 28% prevalence in MOMHR patients with failure rates of 5.6% over 5-years (Bisschop*, et al* 2013). Additionally, the incidence of pseudotumours in patients with MOMTHR was recently observed to be as high as 39% with 12% undergoing revision surgeries at a mean follow-up of 3.6 years (Bosker*, et al* 2012).

1.4.2 Bone related adverse events

According to the Canadian Arthroplasty Society, bone related adverse events make up 71% of all early failures (mean follow-up 3.4 years) following MOMHR (Canadian Arthroplasty Society2013) (Figure 1.5). The predominant causes for failures include femoral neck fracture and loosening of implant components. *Femoral Neck Fracture:*

Studies and data has shown that femoral neck fracture is one of the most common reasons for failure of hip resurfacing with the risk ranging from 0.7% to about 2.5% (Canadian Arthroplasty Society2013, Amstutz, *et al* 2004). The etiology of femoral neck fracture following MOMHR is unclear but possible causes include stress shielding, avascular necrosis of the femur head, misalignment of the femoral component and femoral neck notching (Nabavi, *et al* 2009, Richards, *et al* 2008, Steffen, *et al* 2005). Recent reports suggest that femoral neck narrowing is an early event that occurs within the first 3 months of the surgery (Wang, *et al* 2013). Although the causes for the narrowing of the femoral neck are unclear, increased bone resorption as a result of stress shielding, or osteonecrosis following restriction of blood supply are believed to play a role (Brennan, *et al* 2013, Spencer, *et al* 2008).

Osteolysis and aseptic loosening:

Osteolysis and aseptic loosening are the causes of nearly 32% of all MOMHR revision surgeries (Canadian Arthroplasty Society2013). The overall incidence of aseptic loosening in MOMHR has been reported to be about 1% after 3 year (Carrothers, *et al* 2010). MOMTHR is reported to have a much higher failure rate of 4% at 6 years compared to 3% at 10 years for conventional THA (Herberts and Malchau 2000, Korovessis, *et al* 2006). The main cause for early osteolysis is thought to the hypersensitivity reaction of the surrounding tissue to the metal ions and particles released from the implant (Park, *et al* 2005a). In addition to the immune response, metal ions have direct detrimental effects on bone cells which are responsible for osseointegration of the prosthesis (section 1.10-1.13) (Purdue, *et al* 2006).
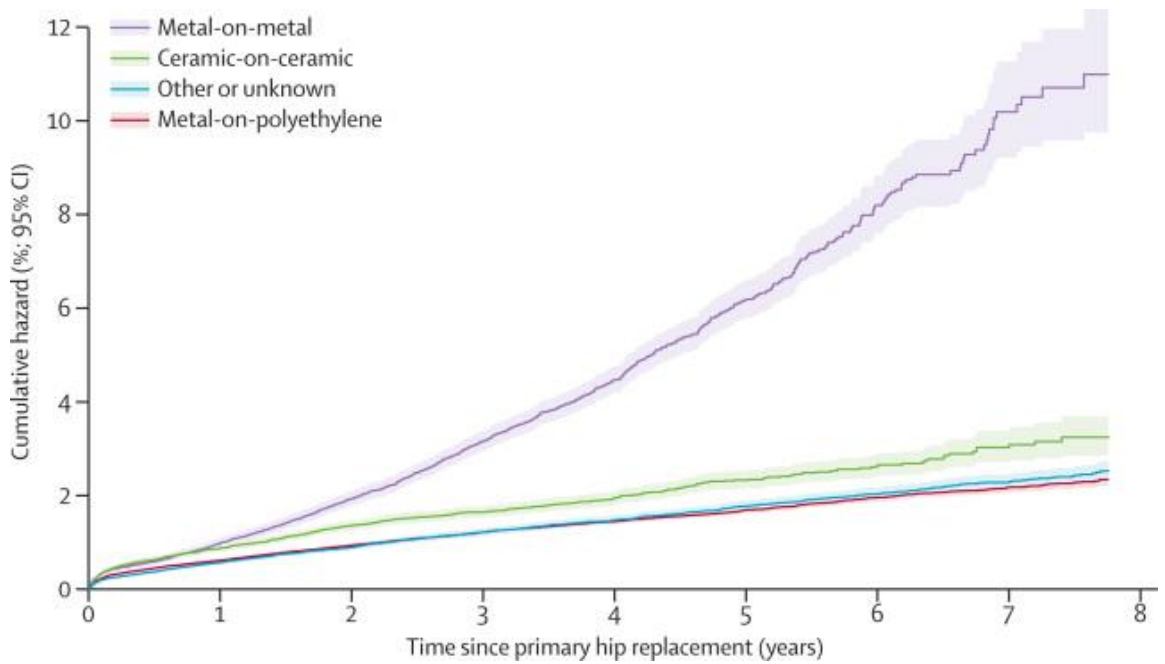
Figure 1.5 Risk of revision by articulating surfaces.

Revision rates for prostheses with metal-on-metal bearing surfaces are higher over 8 years after primary surgery compared other bearing surfaces. *Reprinted from 'The Lancet', (379):9822, Smith, AJ et al. Failure rates of stemmed metal-on-metal hip replacements: analysis of data from National Joint Registry of England and Wales, 1119-204., 2012, with permission from Elsevier.*
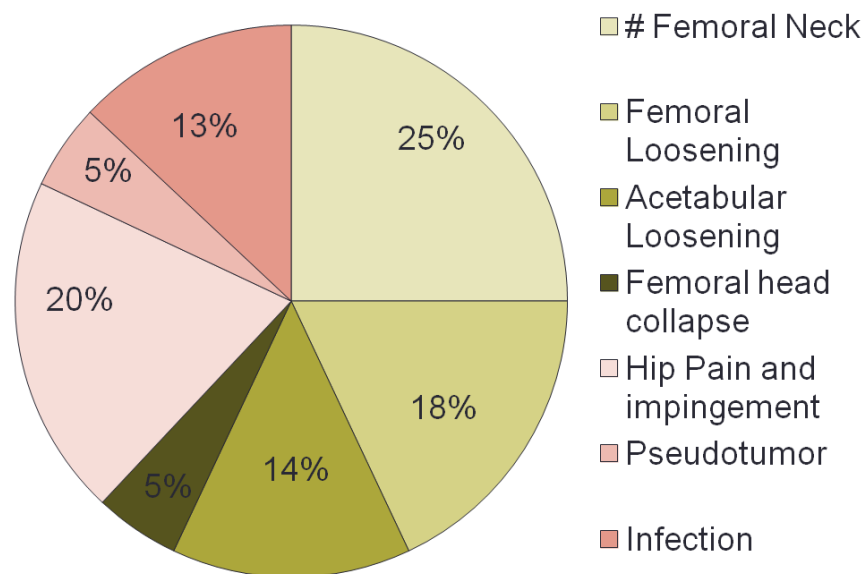
Figure 1.6 Reasons for early failure of MOMHR

Bone related adverse events (green shades) are the cause of 71% of all MOMHR failures. Data with a mean follow-up of 3.4 years for 2773 MOMHR with 101 failures (Canadian Arthroplasty Society2013).

1.5 Release of metal ions from hip implants

Cobalt-chromium-molybednum (Co-Cr-Mo) alloy (ASTM F75) is the one of the most common material to be used in orthopaedic applications and extensively used for metal-on-metal hip replacements. Co-Cr based alloys are biocompatible and highly resistant to corrosion due to passivation via an oxide layer in physiological conditions (Nasab and Hassan 2010). They have superior resistance to fatigue and wear, and elastic modulus (220-230GPa) an order of magnitude higher than cortical bone (20-30GPa) (Nasab and Hassan 2010). The higher elastic modulus results in reduced transfer of load, with possible loss of periprosthetic bone due to stress shielding (Navarro, *et al* 2008).

Several studies have described an increase in the systemic concentrations of metal ions compared to normal physiological range of <0.5µg/L (Savarino, *et al* 2008), following metal-on-metal hip replacements, which peak during the first year after surgery but remain persistently elevated to at least 10 years after surgery (summarised in Table 1.1). Median concentrations of 27.9µg/L (range: 1.6-271) for Co and 1.8µg/L (range: 0.45-143) for Cr have been reported systemically at 2-year follow-up (Langton, *et al* 2009, Williams, *et al* 2011). Median concentrations in the periprosthetic environment, as measured in the synovial fluid from patients with failed MOMHR were reported to be 797µg/L (range: 7-17764) for Co and 1388µg/L (range: 20-136115) for Cr (Davda, *et al* 2011). The actual metal load in the synovial fluid is significantly higher as evidenced by Davda et al. who reported levels of 1496µg/L (range: 11-24262) for Co and 5072µg/L (range: 13-185731) for Cr following acid digestion that liberated the metal from its molecular bonds (Table 1.1).

The release of metal ions from the prosthesis can occur via electrochemical corrosion, physical wear or a combination of the two – termed tribocorrosion (Figure 1.6). The electrochemical corrosion involves the loss of electrons from the metals, a phenomenon which depends on the equilibrium potentials of the metal. Metal alloys have a negative potential which means they oxidise spontaneously. This leads to a formation of a passive oxide layer on the surface of the metal that forms a kinetic barrier to further corrosion. During articulation,

the integrity of the passive layer might get compromised, revealing fresh metal surface that can undergo electrochemical corrosion (Figure 1.6), until a passivation layer reforms (Liao*, et al* 2013).

Study	Follow-up (months)	Sample	[Co]µg/L	[Cr]µg/L
(Heisel, et al 2008)	12	Serum	0.4-15	0.5-20
(Clarke, et al 2003a)	16	Serum	0.8-8.5	1.5-8.6
(Langton, et al 2009)	24	Whole blood	0.4-271	1.5-70
(Witzleb, et al 2006)	24	Serum	4.3	5.1
(Beaule, et al 2011)	24	Serum	0.8-13	0.9-6.7
(Williams, et al 2011)	24	Serum	0.4-196	0.5-143
(Moroni, et al 2008)	58	Serum	0.3-5.6	0.5-11
(Langton, et al 2010)	63	Whole blood	0.6-147	2.4-40
(Holland, et al 2012)	115	Whole blood	0.5-20	0.4-15
(Savarino, et al 2008)	121	Serum	0.3-1.6	0.3-2.2
(Davda, et al 2011)	36	Synovial fluid	7-17764	20-136115
(Kwon, et al 2011)	61	Synovial fluid	206-1802	221-1322
(Davda, et al 2011)	36	Synovial fluid (Acid digested)	11-24262	13-185731

Table 1.1 Concentration of Co and Cr following MOMHR

The table lists the reported systemic and local concentration ranges of elemental Co and Cr following metal-on-metal hip replacement at various follow-up times up to 10 years.

Tribocorrosion is believed to be a dominant mechanism for release of metal ions from the articulating surfaces (Catelas and Wimmer 2011, Mathew, *et al* 2012), with evidence for pitting (Hallam, *et al* 2004) and galvanic corrosion (Koerten, *et al* 2001) also observed in retrieved implants. The *in vivo* corrosion of wear particles has the potential to further add to the concentrations of metal ions in the periprosthetic environment (Shahgaldi, *et al* 1995).

Additionally, the release of metal ions is not only limited to implants with MOM bearings. Recently, adverse reactions to metal debris similar to that observed following MOM hip replacement, including pseudotumors, have been witnessed in patients with modular MOP, ceramic-on-polyethylene (COP) or ceramic-on-ceramic (COC) hip prosthesis (Cook, *et al* 2013, Cooper, *et al* 2012, Kurtz, *et al* 2013). Wear-accelerated corrosion and fretting at the head-neck taper has been identified as a primary source for the release of metal ions (Cooper, *et al* 2012, Kurtz, *et al* 2013). In fact, the lower survivorship of MOMTHR described previously (section 1.3.3), may be due to the increased release of metal debris from the head-neck taper compared to non-modular MOMHR (Matthies, *et al* 2013, Nassif, *et al* 2014).

While a sharp decrease in the use of MOM hip articulations has been observed worldwide, the use of hip prostheses with modular junctions is indispensable. In the last year, approximately 74,000 modular implants have used in patients in UK, with 545,000 modular prostheses been implanted over the last decade (NJR 2013). This presents a very urgent clinical need to understand the effects of metal ions and particles in the survivorship of the implant.
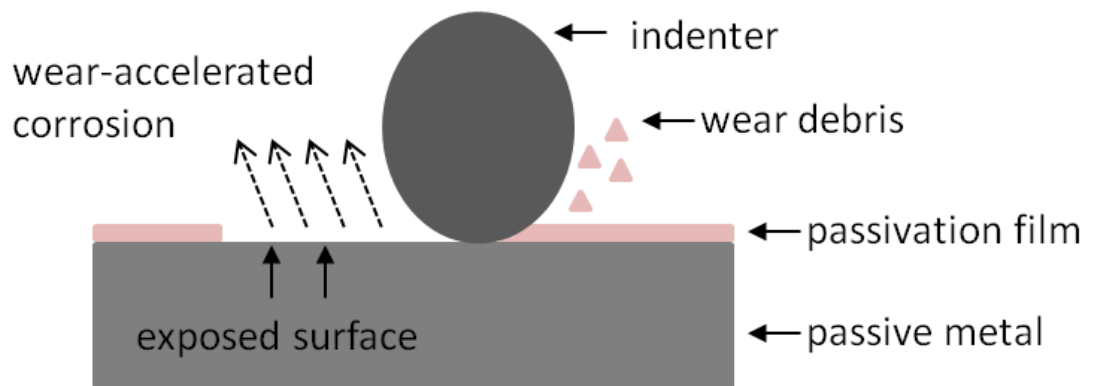
Figure 1.7 Tribocorrosion – a simultaneous combination of wear and corrosion.

Wear of the passive oxide layer (pink) at the articulating surfaces, represented here by the indenter and passive metal exposes a fresh metal surface. Electrochemical corrosion occurs at the exposed surface till it repassifies. This phenomena is also referred to as wear-accelerated corrosion

1.6 Cobalt

1.6.1 Chemistry

Cobalt (Co) is a transitional element with an atomic number of 27 and molecular mass of 58.93. While Co does occur in the oxidation state of +3, it is most stable in the state of +2, especially in an aqueous environment. Studies have shown that Co from Co-Cr alloy hip prostheses is present in the surrounding environment in the +2 oxidation state (Goode, *et al* 2012, Hart, *et al* 2010b).

1.6.2 Physiological role

Cobalt is an essential trace element and is a constituent of vitamin B_{12} or cobalamin, the only required form of cobalt in the body, which is vital for fat and protein metabolism (Cartwright 1955). Intracellularly, vitamin B_{12} is converted to adenosylcobalamin and methylcobalamin, its two active cofactors (Coelho, *et al* 2008). Adenosylcobalamin is a coenzyme for mitochondrial methylmalonyl-coenzyme-A mutase, responsible for fatty acid and amino acid catabolism, whereas methylcobalamin is a coenzyme for methionine synthase that is essential for one-carbon metabolism which in turn regulates important intracellular processes such as methylation, DNA synthesis and neurotransmitter metabolism (Coelho, *et al* 2008, Moretti, *et al* 2004, Weissbach and Dickerman 1965).

According to the Committee on the Medical Aspects of Food Policy report of 1991, the recommended daily amount for cobalamin was set to 1.5µg/day for adults and 2µg/day during lactation. The physiological concentration of Co in whole blood of healthy individuals is 0.5µg/L. Prolonged deficiency is initially characterised by symptoms such as fatigue, weakness, pallor and sore tongue (Seetharam and Alpers 1982). Perinicious anaemia caused by mal-absorption of cobalamin is one of the severe effects of the deficiency (Frost and Goldwein 1958). Long term deficiency is also linked with impairment of the normal myelination and demyelination of neurons causing a neuropathy that leads to paresthesia in feet and fingers (Dror and Allen 2008, Seetharam and Alpers 1982, von Schenck, *et al* 1997).

1.6.3 Transport and excretion

The mean absorption fraction of ingested inorganic cobalt varies from 0.03 to 0.4, whereas organic cobalt shows a mean absorption fraction of 0.57 (Harp and Scoular 1952, Leggett 2008). Cobalt is similar to iron in its chemistry and it shares similar mechanisms for absorption in the small intestine and transport via blood which can occur via albumin, transferrins or ferritins and are thought to enter cells via specific transporter proteins (Leggett 2008, Mabilleau, *et al* 2008). Upon oral administration, unabsorbed cobalt is primarily excreted via faeces, whist the rest is excreted via urine. Nearly half the ingest Co is cleared from the body within the first 6-12h (Paustenbach, *et al* 2013).

1.6.4 Toxicity

Occupational Safety and Health Administration (OSHA) has set the permissible exposure limit for cobalt metal, dust, and fume as $0.1mg/m^3$ of air as an 8 hour time weighted-average concentration. Inhalation of cobalt is associated with various respiratory disorders such as occupational asthma, diagnosed in diamond polishers, and hypersensitivity pneumonitis with possible evolution to pulmonary fibrosis in hard metal (tungsten carbide) industry workers (Krakowiak, *et al* 2005, Nemery, *et al* 2001). Hard metal industry workers also often present with a 'cobalt-lung' which is characterised by presence of multinucleated giant cells in the bronchoalveolar lavage, diagnosed as giant cell interstitial pneumonitis (Nemery, *et al* 2001, Sundaram, *et al* 2001).

The ingestion of high levels of cobalt has been associated with cardiomyopathy as observed in beer drinkers of United States and Canada where cobalt salts were used as foam stabilizers in the 1960s (Morin and Daniel 1967). Excessive erythrocytosis has also been associated with increased serum cobalt levels (>16.9nmol/L) and a study with chickens suggested association of excess cobalt to right ventricular hypertrophy and ascites (Diaz, *et al* 1994, Jefferson, *et al* 2002).

Cobalt exposure has been linked to impairment of base and nucleotide excision repair of the DNA which may result in mutations associated with cancer (Hartwig and Schwerdtle 2002). Cobalt ions and particles are known to induce oxidative

stress by free radical generation which may cause a cellular redox imbalance associated with oncogenicity (Valko, *et al* 2006). Cobalt exposure in rats via subcutaneous injections has been associated with sarcomas and inhalation of 1-3mg/m^3 significantly increased the incidence of bronchoalveolar neoplasm (De Boeck, *et al* 2003). An increased lung cancer risk has also been observed in humans with occupational exposure to cobalt compounds (De Boeck, *et al* 2003).

1.7 Chromium

1.7.1 Chemistry

Chromium is also a transitional metal with an atomic number 24 and molecular mass of 52.01. It can occur in valence states from -2 to +6 but only the ground state 0, +2, +3 and +6 are common in nature with +3 state the most stable (Mertz 1969).

1.7.2 Physiological Role

The trivalent state of chromium (Cr^{3+}) is the biologically active form and is widely distributed in our daily food supply (Moukarzel 2009). Chromium is known to play a role in lipid and glucose metabolism by potentiating the activity of insulin (Moukarzel 2009). Some studies show a beneficial effect with elevated intakes of chromium in type 2 diabetes patients (Albarracin, *et al* 2008, Anderson, *et al* 1997). The physiological concentrations of Cr in healthy people ranges from 0.1-0.5µg/L (Savarino, *et al* 2008)

The adequate intake amount for chromium was set in the range of 50-200µg/day which was seldom met (Preuss and Anderson 1998), but was later revised to 30 µg/day which would be available in a self-selected diet (Vincent 2010). Hence, chromium deficiency is seldom seen and is most common in patients on total parenteral nutrition (Vincent 2010). The symptoms observed in these patients include peripheral neuropathy, hyperglycaemia, weight loss and glucose intolerance which were managed by addition of chromium in their diet (Moukarzel 2009, Vincent 2010).

1.7.3. Transport and Excretion

On absorption, chromium binds to siderophillin, also known as transferrin, which is an iron binding protein (Mertz 1969). In case of excess chromium, binding occurs to other proteins in the plasma once the binding sites for transferrin are saturated (Mertz 1969). The chromium uptake into the tissue is dependent on its chemical state, with some states being excreted fairly quickly compared to others (Mertz 1969).

1.7.4 Chromium Toxicity

Trivalent chromium, when ingested, is not considered toxic due to its low absorption and is an essential micronutrient. However, concerns regarding Cr^{3+} have arisen due to some *in vitro* studies suggesting DNA damage in human lymphocytes exposed to Cr^{3+} (Blasiak and Kowalik 2000, Speetjens*, et al* 1999), but no such evidence has been seen clinically (Moukarzel 2009). Although, there have been some cases of renal failure and impaired liver function with ingestion of extremely elevated levels over prolonged periods (Moukarzel 2009).

Chromium (VI), not naturally present in food, is known to be much more toxic both with acute and chronic exposure and its compounds are regulated by the Dangerous Substances Directive (67/548/EEC) (Unceta*, et al* 2010). It is also recognised to be a class-1 human carcinogen by the International Agency for Research on Cancer (IARC) (Unceta*, et al* 2010). Contact dermatitis, as a result of an allergy to chromium (VI) was identified in cement workers exposed to 4-25ppm of chromium, with levels of 20ppm or more causing skin ulcers (Shelnutt*, et al* 2007).

Other occupations that possess risk to chromium exposure include pigment manufacturing, welding, chrome-plating and leather tanning (Gatto*, et al* 2010, Rastogi*, et al* 2008). Inhalation of hexavalent chromium has been associated with increased risk of respiratory disease, fibrosis and lung cancer (Beveridge*, et al* 2010, Halasova*, et al* 2009, Langard and Norseth 1975, Nickens*, et al* 2010). The permissible levels of chromium (VI) in air were set to $52\mu g/m^3$ by OSHA in 1971, but in view of the following findings, it was reduced to $5\mu g/m^3$ (Nickens*, et al* 2010).

Ingestion of chromium (VI) is known to be hazardous with a study rat intestinal cells showing reduced intestinal functional efficacy (Upreti, *et al* 2005). An association between increased cancer mortality and ingestion of chromium (VI) has been suggested in a Chinese population (Beaumont, *et al* 2008), however no study has yet confirmed the carcinogenicity of ingested chromium (VI). The carcinogenicity of chromium (VI) is suggested to be via the formation of reduced species of chromium (V), chromium (IV) and chromium (III) which are known to mediate DNA damage and inhibit DNA replication (Nickens, *et al* 2010, O'Brien, *et al* 2001). The reduction of chromium (VI) also produces reactive oxygen species (ROS) and free radicals which are known to damage DNA, RNA proteins and lipids (Donkena, *et al* 2010, Klaunig and Kamendulis 2004, Nickens, *et al* 2010).

1.8 Bone

Bone is a dynamic connective tissue that is integral to the skeletal system, and consists of an organic matrix of type-1 collagen, within which inorganic hydroxyapatite $[Ca_5(PO_4)_3OH]$ is deposited to give structural integrity (Marks and Odgren 2002). The tissue provides mechanical support to the body, permits locomotion, acts as metabolic store for mineral salts and provides protection to vital organs such as brain and heart (Stevens and Lowe 1997). Bone tissue consists of three main cell types – the osteoblasts, the osteoclasts and the osteocytes. The survival and function of these cells are tightly coupled to regulate bone homeostasis via remodelling. Understanding of the normal cellular physiology of these cells is essential to understand the effect metal ions may have on them and effectively target interventions.

1.8.1 Osteoblasts

Osteoblasts are mononuclear cells with a mesenchymal origin that form bone by producing an extracellular collagenous matrix which subsequently gets mineralized by hydroxyapatite deposition (Jensen*, et al* 2010, Marks and Odgren 2002). The commitment of these mesenchymal stem cells to one of the many possible lineages such as, adipocytic, chondrocytic or osteoblastic, is governed by expression of specific transcriptional regulators, with *Runx2* being essential for osteoblastogenesis (Jensen*, et al* 2010). This is evidenced by studies which report complete lack of osteoblast maturation and ossification in *Runx2* deficient mice (Komori*, et al* 1997). The *Runx2* expression is in turn governed by TGF-β/SMAD signalling via the bone morphogenetic proteins (BMPs), all of which are members of the TGF-β family (Canalis 2009).

A second major pathway for osteoblast formation is the canonical Wnt/β-catenin signalling pathway (Rodda and McMahon 2006). The activation of Wnt leads to cytoplasmic accumulation of β-catenin that translocates to the nucleus, interacts with transcription factor TCF/LEF (T-cell factor/lymphoid enhancer factor) and regulates the expression of genes responsible for osteoblast proliferation (Lin and Hankenson 2011). Several studies have described crosstalk between these two pathways including combined regulation of several target genes (Hussein*, et al* 2003, Zhang*, et al* 2013)

Mature osteoblasts express high levels of alkaline phosphatase (ALP) on their cell surface which serves as a marker for their state of differentiation and is important for hydrolysing inorganic pyrophosphate (PPi), an inhibitor of matrix mineralisation (Addison*, et al* 2007). Mature osteoblasts can further differentiate into either bone lining cells or get embedded in the matrix to form osteocytes.

1.8.2 Osteocytes

Osteocytes are the most abundant cell type in bone, and belong to the mesenchymal lineage. During the process of bone formation, some osteoblasts get embedded in the mineralising osteoid matrix, differentiating into cells with dendritic processes - typical of osteocytes. These cells are known to express key osteocytic genes such as connexin 43, osteocalcin and beta actin (Mason*, et al* 1996). These actin-rich dendritic processes extend through canaliculi of mineralised matrix, connecting the cell to other osteocytes and cells on the bone surface.

Osteocytes are known to regulate bone remodelling by orchestrating the activities of both osteoblasts and osteoclasts. Fatigue induced microcracks in bone due to physiological wear causes osteocyte apoptosis that initiates bone resorption at the site of damage, leading to the process of remodelling (Verborgt*, et al* 2000). The molecular mechanisms responsible for the osteoclastogenic response are unclear, but studies have shown that media from apoptotic osteocytes contain increased amounts of RANKL that can promote osteoclast differentiation (Al-Dujaili*, et al* 2011). In addition, it has been suggested that osteocyte apoptotic bodies induce TNF-alpha production in osteoclast precursors, which acts in a paracrine manner promoting osteoclastogenesis independent of RANKL (Kogianni*, et al* 2008). In contrast, osteoblasts are negatively regulated by osteocytes which constitutively secrete sclerostin that antagonises the Wnt/β-catenin signalling integral to osteoblast differentiation (Li*, et al* 2005b, Poole*, et al* 2005).

Additionally, osteocytes mediate the process of adaptive remodelling of bone in response to loading and mechanical strain. The complex dendritic network performs the mechanosensing function by interacting with pericellular canalicular

walls via tethering filaments (You, *et al* 2004). These filaments sense the drag forces of canalicular fluid flow, a consequence of external loading, and cause cytoskeleton rearrangements and subsequent downstream signalling (Han, *et al* 2004, Wang, *et al* 2007). Mechanically loaded osteocytes positively regulate osteoblasts, favouring an osteogenic response by decreasing sclerostin production (Robling, *et al* 2008) and releasing prostaglandin E2 (PGE2) (Ajubi, *et al* 1999, Forwood 1996, Hartke and Lundy 2001). Mechanical loading is also associated with reduced osteoclast activity (Hillam and Skerry 1995), which is mediated at least in part via release of nitric oxide (NO) (Tan, *et al* 2007) that is anti-apoptotic to osteocytes (Tan, *et al* 2008).

1.8.3 Osteoclasts

Osteoclasts are multinucleated cells formed by fusion of progenitor cells of monocyte/macrophage lineage of hematopoietic origins and are responsible for resorbing bone (Marks and Odgren 2002). The differentiation of hematopoietic precursors into fully mature osteoclasts is mediated by two factors – the TNF family cytokine RANKL and macrophage-colony stimulating factor (M-CSF) produced both by marrow cells and osteoblasts (Boyle, *et al* 2003). These factors drive osteoclast formation and differentiation by activating transcription factors such as nuclear factor κB (NF- κB), activator protein-1 (AP-1) and nuclear factor of activated T-cells cytoplasmic 1 (NFATc1). Studies in mice, which functionally lack either of the two factors, show a dense bone phenotype known as osteopetrosis, reiterating the importance of these factors in osteoclast formation and activity (Kong, *et al* 1999, Yoshida, *et al* 1990). These cytokines are also known to induce the expression of tartrate resistant acid phosphatase (TRAcP) and cathepsin K (CATK) genes which are characteristic of mature osteoclasts and are vital for resorbing bone (Boyle, *et al* 2003).

During resorption mature osteoclasts get polarised and anchor to the bone via integrin $\alpha_v\beta_3$, forming a sealed zone beneath the cell. H+-ATPase pumps located at the ruffled cell membrane of the sealed zone and in vacuoles acidifies the sealed zone to causing degradation of the enclosed matrix (Blair, *et al* 1989). The acidification dissolves the mineral while the secretion of lytic enzymes such as pro-CATK and matrix metalloproteinases (MMPs) results in the formation of a

resorption pit (Boyle, *et al* 2003). Following bone resorption, the degraded matrix components are endocytosed by the osteoclasts and transferred through the cell before being excreted by the functional secretory domain (FSD) present on the basolateral membrane (Nesbitt and Horton 1997). Osteoclastic bone resorption is regulated by various factors including hormones such as parathyroid hormone (PTH) and oestrogen; cytokines such as TNF-α and IL-1β as well as 1, 25 (OH)$_2$ vitamin D$_3$ (Li, *et al* 2000). Most of these factors act by affecting the levels of RANKL or osteoprotegrin (OPG), a decoy ligand for RANK secreted by osteoblasts (Li, *et al* 2000).

1.9 Bone modelling and remodelling

As mentioned previously, bone is a dynamic tissue and exists in a constant state of modelling and remodelling. Modelling is responsible for the normal growth of the bone and its adaptive response to mechanical loads. The osteoblast and osteoclast activity during modelling may be different anatomical sites, free of coupling. Moreover, modelling becomes less common with age, with conditions like hypoparathyroidism (Ubara, *et al* 2003) and renal osteodystrophy (Ubara, *et al* 2005) causing it to increase.

In contrast, remodelling is the process by which damaged bone is replaced by new bone to maintain strength and mineral homeostasis. This process is thought to occur in a temporary compartment of bone described as the bone multicellular unit (BMU) involving tight coupling of the osteoblast and osteoclast activity (Raggatt and Partridge 2010). The process of remodelling has been categorised into 5 distinct stages – activation, resorption, reversal, formation and termination (Figure 1.7).

The activation stage involves the detection of a signal indicating initiation of bone remodelling (Raggatt and Partridge 2010). This signal can be in the form of systemic factors such as oestrogen or PTH, or a local factor such as mechanical strain causing osteocyte cell death (Aguirre, *et al* 2006, Crockett, *et al* 2011). The resorption stage is characterised by the recruitment of osteoclasts precursors to the BMU by osteoblasts. In addition to secreting monocyte chemo-attractant

protein (MCP-1) (Li*, et al* 2007), osteoblasts also modulate the expression of pro osteoclastogenic proteins such as M-CSF and RANKL which causes formation of mature osteoclasts that resorb bone as described previously (Ma*, et al* 2001).

Once bone resorption has occurred, the reversal stage sets in, during which reversal cells, suspected to be from the osteoblast lineage, remove the remnants of collagen and prepare the surface for bone formation (Raggatt and Partridge 2010). The osteoblasts are then recruited to the site by coupling signals which can be mediated via cell contact (EphB4/ephrin-B2 signalling) or by soluble factors (such as sphingosine-1 phosphate) to lay a new extracellular matrix and mineralise it in the formation stage (Pederson*, et al* 2008, Raggatt and Partridge 2010, Zhao*, et al* 2006). Once the resorbed bone is replaced, termination signals, suspected to be the loss of sclerostin expression by osteocytes, results in apoptosis of mature osteoblasts, or their differentiation to bone lining cells or osteocytes if embedded in the matrix, returning the bone to its resting state (Raggatt and Partridge 2010).

Osseointegration is similar to a bone healing response and involves a bone remodelling process that results in the formation of new bone at the implant interface ensuring fixation (Mavrogenis*, et al* 2009). Any imbalances in the dynamics of bone cells surrounding the implant may result in the failure of osseointegration. Thus, it is vital to investigate the effect of prosthesis-derived metal ions on the surrounding bone to understand the mechanisms for implant failure.
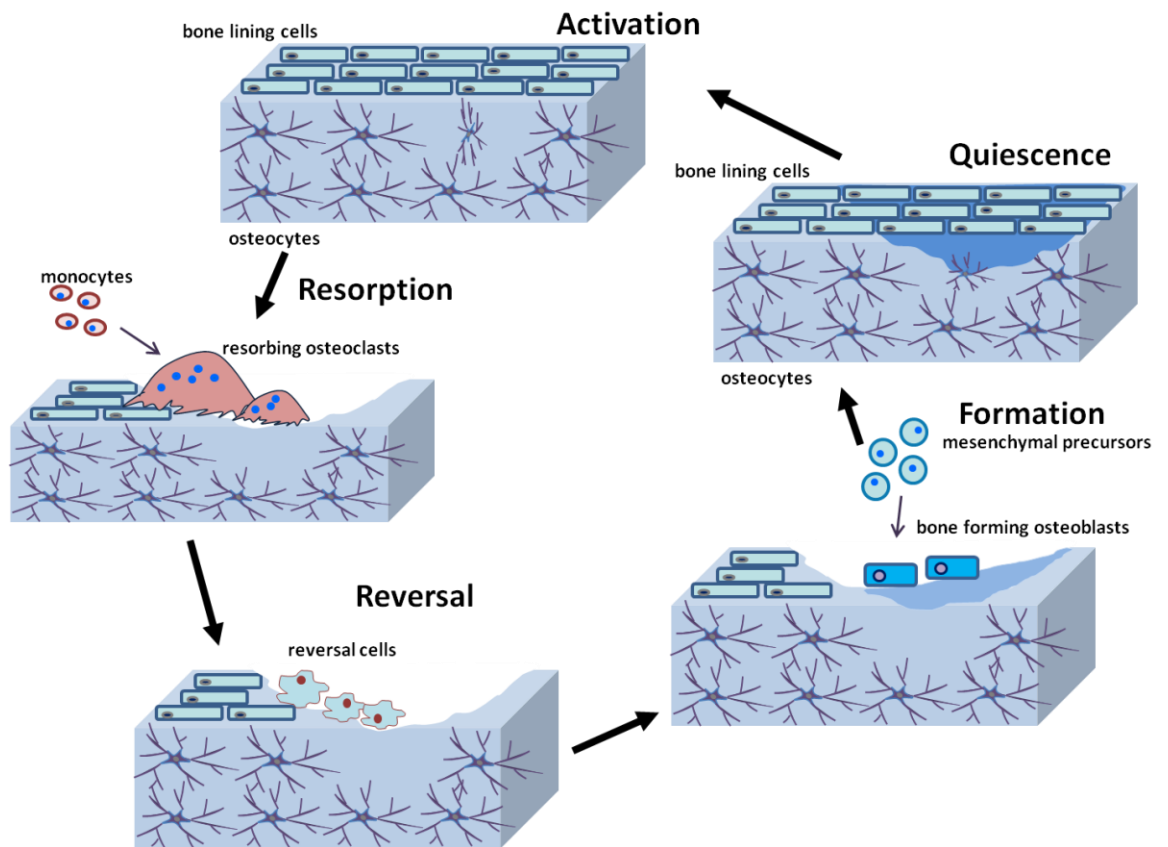
Figure 1.8 Bone remodelling cycle

Bone remodelling cycle is **activated** by a stimulus such as apoptosis of osteocyte here. Following activation, monocytes are recruited which differentiate into osteoclasts that **resorb** bone. Subsequently, osteoclasts undergo apoptosis and **reversal** cells remove remnants of the resorption phase preparing the surface for formation. Osteoblast progenitors are recruited to the site for **formation** of new bone following which the bone returns to a state of **quiescence**.

1.10 Effect of cobalt and chromium on osteoblasts

Osteoblast survival and function in the periprosthetic environment is vital for the osseointegration hip prostheses. Several studies including ours have investigated osteoblast viability and osteogenic potential in presence of particulate and ionic metal exposure. Allen et al., (1997) reported no change in osteoblast viability with Cr and CoCr particles, whilst Co proved cytotoxic at concentrations of 0.1mg/mL. A dose dependent decrease in ALP activity and osteocalcin secretion was observed with all particles (Allen, *et al* 1997). A similar study by Lohmann et al. (2000) reported the phagocytosis of polyethylene, titanium alloy and CoCr alloy wear particles by osteoblast-like cells, with a chemical composition specific response to different of particles. Treatment with CoCr particles increased osteoblast viability but decreased its osteogenic potential as evaluated by measuring ALP activity (Lohmann, *et al* 2000). A more recent study described an increase in the secretion of inflammatory cytokines such as IL-6 and TNF-alpha following CoCr exposure which may have implications for the regulation of bone remodelling (Dalal, *et al* 2012).

Fleury et al. (2006) described a dose dependent decrease in cellular viability for osteoblast like cells in the presence Co^{2+} and Cr^{3+}, with Co^{2+} being more cytotoxic. They reported an increase in markers for oxidative stress suggesting the oxidative stress as the potential mechanism for toxicity (Fleury, *et al* 2006). A study with primary murine calvarial osteoblasts suggested induction of dormancy with exposure to Co^{2+} and Cr^{3+} accompanied with reduction in ALP activity and increased apoptosis (Dai, *et al* 2011). More recently, a study by us described a dose dependent decrease in osteoblast survival and osteogenic ability as measured by ALP activation and mineralisation ability with exposure to clinically relevant concentrations of Co^{2+}, Cr^{3+} and Cr^{6+} (Andrews, *et al* 2011). Similar to the effects of particulate metal exposure, metal ions have also been shown to induce the expression of proinflammatory cytokines and chemokines (Hallab, *et al* 2002, Queally, *et al* 2009) and alter the ratio of OPG/RANKL in the periprosthetic environment (Zijlstra, *et al* 2012).

1.11 Effect of cobalt and chromium on osteocytes

Although osteocytes are the most abundant cells in the bone, the effects of prosthesis related metal ions and particles are unclear. Only two studies till date describe the effects of CoCr alloy particles on murine MLO-Y4 osteocyte cells. Kanaji et al.,(2009) describe an increase in gene expression of pro-inflammatory cytokine, TNFα, in response to CoCr particles. The study also described an increase in osteocyte apoptosis as measured by caspase 3, 7 activity (Kanaji*, et al* 2009). In a subsequent study, the group describe the activation of calcineurin/NFAT as the upstream regulator for the increase in expression of TNFα observed previously (Orhue*, et al* 2011). The vital role of osteocyte in orchestration of bone remodelling warrants further investigations into their responses to metal ions and particles for better understanding of periprosthetic and systemic bone health following MOM hip replacement.

1.12 Effect of cobalt and chromium on osteoclasts

Particulate and ionic debris from prostheses has been implicated in mediating periprosthetic osteolysis via osteoclastic resorption. A few studies have described the differentiation of monocyte/macrophage cells exposed to Co-Cr particulate debris into mature resorbing osteoclasts in co-culture experiments with osteoblast-like cells (Pandey*, et al* 1996, Sabokbar*, et al* 1998). Studies have shown that prosthetic wearing produces particles that induce macrophages to release inflammatory cytokines such as TNF-α, IL-1β and IL-6 which are implicated to be resorptive factors (Haynes*, et al* 1993, Masui*, et al* 2005). Another study described increased cytotoxicity and hence reduced osteoclastogenesis from CD14+ monocytes in presence of increasing exposure to CoCr microparticles (Neale*, et al* 2000).

A study on rat bone marrow derived osteoclast precursors cells demonstrated a delayed toxicity with Co^{2+} with concentrations up to 10µg/mL. The study indicated that metal ions at sub lethal, physiologically relevant concentrations suppress bone resorption by inhibiting osteoclast activity (Nichols and Puleo 1997). Rousselle et al, demonstrated that acute exposure of cobalt and chromium ions (24h) at concentrations of 10µg/mL respectively, do not induce apoptosis in

mature rabbit osteoclasts but resulted in smaller cell size and decreased resorption (Rousselle, *et al* 2002). A more recent study described an increase in osteoclast differentiation and resorptive function for cells cultured on calcium phosphate substrate with up to 10μM Co^{2+} incorporated or adsorbed on its surface, or present in the free ionic form in the media (Patntirapong, *et al* 2009).

1.13 Hypothesis and aims of the project

As a result of concerns raised by the Medicine and Healthcare Regulatory Agency recently, the use of MoM prostheses has declined sharply to <3% in 2012, compared to 16% in 2008 (NJR 2013). Nevertheless, it is estimated that around 80,000 patients in the UK currently have an indwelling MoM prosthesis. Moreover, although the understanding of metal ion mediated detrimental effects on bone cells was prompted by lower survivorship of MOM hip replacements, the worldwide use of modular prostheses still makes this clinically relevant.

The association of metal ion release from MOM bearings with local bone-related adverse events suggests that prosthesis-derived metal ions, may have implications for bone health. This project is based on the hypothesis that metal ions released from hip prostheses are detrimental to survival and function of bone cells in the local and systemic environment; and that these effects are mediated following their cellular entry through mechanisms dependant on the metal species.

To test these hypotheses, the specific aims of the project are:

1) *To determine the effect of metal ions on bone cells.* This will be achieved by measuring the survival and functional responses of osteoblast-like SaOS-2 cells, primary human osteoclasts and murine osteocyte cell lines (MLO-A5 and MLO-Y4) to clinically relevant concentrations and combinations of Co^{2+}, Cr^{3+} and Cr^{6+}. Furthermore, to mimic the effect on osseointegration, the osteogenic response of SaOS-2 cells will be assessed on implant surfaces in the presence of metal ions and particles.

2) *To investigate the intracellular distribution and speciation of metal ions in bone cells.* This study will help characterise the different mechanisms of cellular uptake of metal ions and their intracellular reactions. The study will be conducted in osteoblasts and osteoclasts using X-ray absorption spectroscopy using synchrotron-based high intensity X-rays.

3) *To investigate the role of implicated transport systems in cellular uptake of metal ions in bone cells.* To achieve this, fluorescence-based real-time monitoring of Co^{2+} uptake in the presence of specific transporter antagonists will be conducted in osteoblasts and osteoclasts.

Completion of these aims will provide a better understanding cellar dynamics of bone cells in response to metal ions in the periprosthetic and systemic environment post hip replacement. It will also shed light onto the mechanisms of their cellular entry and intracellular interactions that might be exploited to improve the survivorship of hip implants.

Chapter 2 - Materials and Methods

2.1 Metal ion preparation

Cobalt (II) hexahydrate ($CoCl_2.6H_2O$) and chromium (III) chloride hexahydrate ($CrCl_3.6H_2O$) (Fluka, Gillingham, UK) served as salts for Co^{2+} and Cr^{3+} respectively. Hexavalent chromium was purchased as chromium (VI) oxide (CrO_3) from BDH Laboratory Supplies (Poole, UK). The salts were dissolved in double distilled water (ddH_2O) to a concentration of 10^7µg/L (~0.2M), sterile filtered, aliquoted and stored at -20°C.

Prior to cell culture treatment, all stock solutions were diluted to 100X of the final working concentrations in sterile distilled water. These were further diluted 1:100 in appropriate feeding media, both for individual and combination treatments, to reach the final working concentrations. Control treatment contained equivalent volume of sterile distilled water to maintain conditions.

The correlation between metal ion solutions and its actual concentrations was confirmed after 3 days by Ms Rebecca Andrews previously, during her BMedSci, using flame-atomic absorption spectroscopy. Measurements for Co^{2+}, Cr^{3+} and Cr^{6+} showed close agreement with the predicted concentrations (linear regression, r^2 = 1.00, 0.85 and 0.98 for Co^{2+}, Cr^{3+} and Cr^{6+} respectively) (Andrews, *et al* 2011). The precipitation of Cr^{3+} at concentrations of 26000µg/L (~500µM) and above caused a deviation from predicted concentrations and a lower r^2 value.

2.2 Osteoblast culture

2.2.1 Materials

Dulbecco's Modified Eagle Medium (DMEM© GLUTAMAX™) containing sodium pyruvate and 4.5 g/L glucose, foetal calf serum (FCS), dimethyl sulfoxide (DMSO) penicillin (10000 units/mL) and streptomycin (10000µg/mL), 0.25% Trypsin-EDTA 4Na and phosphate buffer saline (PBS) (pH-7.4, Ca^{2+} and Mg^{2+} free) were purchased from Gibco (Paisley, UK). Trypan-blue dye (T8154) was obtained from Sigma (Poole, UK). T75 flasks were from Nunclon (Roskilde, Denmark); 96 multiwell plates were bought from Costar® (Corning, New York, USA).

2.2.2 Maintenance of osteoblast-like SaOS-2 cells

SaOS-2 is a human osteosarcoma cell-line isolated from an 11 year old Caucasian female, and with confirmed osteoblastic properties of alkaline phosphatase activity, mineralisation and expression of genes such as *Runx2* and osteocalcin (Czekanska*, et al* 2013, Rodan*, et al* 1987). SaOS-2 cells were maintained at 37°C in a humidified atmosphere of 95% air and 5% CO_2 with DMEM© GlutaMAX™ containing 100U/mL penicillin, 100µg/mL streptomycin and 10% FCS (referred to as complete DMEM). The cells were passaged every 2-3 days when 80% confluent, for a maximum of 30 passages to avoid phenotypic instability associated with long-term cultures (Hausser and Brenner 2005). Frozen stocks of SaOS-2 cells were maintained in FCS supplemented with 10% DMSO in liquid nitrogen.

2.3 Cellular activity assay

Cellular activity was measured using CellTiter 96® AQueous Non-Radioactive Cell Proliferation Assay according to the manufacturer's instructions (Promega, Southampton, UK). The assay involves the reduction of a tetrazolium compound [3-(4, 5-dimethylthiazol-2-yl)-5-(3-carboxymethoxyphenyl)-2-(4-sulfophenyl)-2H-tetrazolium, inner salt (MTS), as a consequence of dehydrogenase enzymes in metabolically active cells. The reaction occurs in presence of an intermediate electron acceptor phenazine methyl sulphate (PMS), and forms a soluble purple product known as formazan (Figure 2.1) with absorbance maxima at 490nm (Berridge*, et al* 2005, Cory*, et al* 1991).
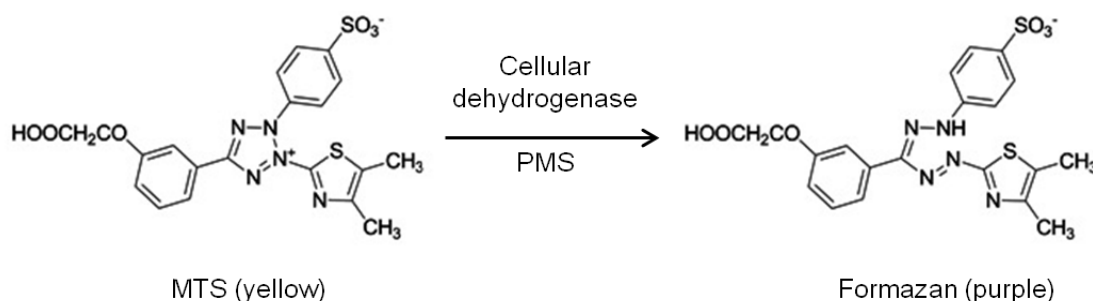
Figure 2.1 Principle for cellular activity assay using MTS.

In presence of cellular dehydrogenases, MTS (yellow) is converted to soluble formazan (purple) product. Cellular activity is proportional to the formation of formazan measured absorbance at 490nm.

SaOS-2 cells were seeded in a 96-well plate at a density of 5×10^3 cells per well in 0.2mL complete medium and left to adhere for the first 24 hours (Appendix-1). The media was then replaced to DMEM© GlutaMAX™ containing 100U/mL penicillin, 100µg/mL streptomycin and 0.5% FCS (referred to hereon as vehicle) ± metal ion treatments till day 3 or 7 at 37˚C in a humidified atmosphere of 95% air and 5% CO_2. The vehicle and metal ion treatments were replenished at day 4 for the 7 day cultures.

At each assay time point a previously prepared 1mL aliquot of MTS and PMS mixture in the ratio of 20:1 was diluted in 9mL of phenol-free DMEM (Gibco® Invitrogen, Paisley, UK) to obtain the working concentration. Subsequently, the growth media was removed from the wells and cells were washed with phenol-free DMEM. The MTS+PMS mixture at its working concentration was added to each well (0.1mL) and the plates incubated for 2 hours at 37˚C in a humidified atmosphere of 95% air and 5% CO_2. The absorbance at 490nm was measured using SpectraMax M5^e (Molecular Devices, Sunnyvale, USA) and cellular activity was expressed as a percentage response relative to vehicle.

2.4 Alkaline Phosphatase Activity

Alkaline phosphatase (ALP) is a metalloenzyme with Zn^{2+} and Mg^{2+} centres which catalyses the hydrolysis of phosphomonoester bonds (Kozlenkov, *et al* 2002). Tissue non-specific ALP (TNAP) isoenzyme is expressed in osteoblasts, and is predominantly present on the cell surface where it attaches via a glycosylphosphatidylinositol anchor (Harrison, *et al* 1995). TNAP is known to hydrolyse pyrophosphate (PPi), a known inhibitor of matrix mineralisation, and thereby providing inorganic phosphate (Pi) for the formation of hydroxyapatite (Hessle, *et al* 2002). The role of ALP in osteoblast differentiation and mineralisation is well established with genetic mutations in the TNAP gene known to cause hypophosphatasia, a disease characterised by low bone mineral density (Weiss, *et al* 1988).

ALP activity was measured for cell lysates by hydrolysing para-nitrophenyl phosphate (pNPP, Sigma-Aldrich, Dorset, UK) (Figure 2.2), and normalising to DNA content measured by Quant-iT™ PicoGreen® dsDNA Assay Kit (Invitrogen, Paisley, UK). PicoGreen® is a proprietary asymmetrical cyanine dye with 1000-fold increase in fluorescence when bound to dsDNA (Singer, *et al* 1997). It has high sensitivity (up to 25pg/mL) and allows quantitation of dsDNA in presence of equimolar concentrations of ssDNA and RNA with minimal interference.
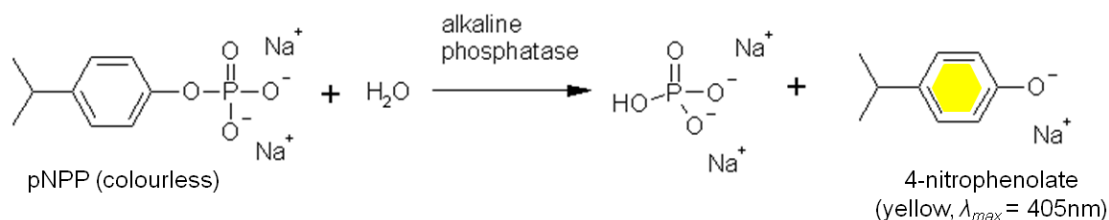
Figure 2.2 Principle of Alkaline Phosphatase activity assay.
ALP catalyses the conversion of para-nitrophenyl phosphate (colourless) to 4-nitrophenolate (yellow). The absorbance is measured as 405nm to assess the formation of the product.

2.4.1 ALP assay

SaOS-2 cells were seeded in a 96-well plate at a density of 5×10^3 cells per well in 0.2mL complete medium and left to adhere for the first 24 hours. The media was then replaced with vehicle ± metal ion treatments till day 3 or 7 at 37°C in a humidified atmosphere of 95% air and 5% CO_2. The vehicle and metal ion treatments were replenished at day 4 for the 7 day cultures. At the assay time points, cells were washed with PBS and frozen with nuclease-free water at -80°C. Cell lysate were obtained by two further freeze-thaw cycles.

The ALP assay solution contained 1mg/mL pNPP substrate, 20mM Tris (pH 8.0-8.3), 1mM $MgCl_2$ and 5μl/mL Quant-iT™ PicoGreen reagent in ddH_2O. The assay solution was brought to 37°C and 150μL was added to each well containing 50μL cell lysate. The absorbance was measured at 405nm over 30 minutes with a 5 minute intervals using SpectraMax M5^e (Molecular Devices, Sunnyvale, USA) maintained at 37°C. Subsequently, fluorescence associated with dsDNA bound PicoGreen® was measured at an excitation and emission wavelength of 485nm and 530nm respectively.

The ALP activity was calculated using the following equation:

$$ALP\ activity\ (\mathrm{U/mL}) = \frac{(A_t - A_0)\ x\ v\ x\ d}{t\ x\ \varepsilon\ x\ l}$$

where,

A_t = absorbance at endpoint 't'

A_0 = absorbance at initial time

V = total volume in the well (150µL assay solution + 50µL sample = 200µL in this experiment)

d = dilution factor of the sample in the total volume (200:50 = 4 for this experiment)

t = time between initial and final reading in minutes (30min)

ε = molar extinction coefficient for pNPP (18.75 mM^{-1} cm^{-1})

l = path length in cm (0.639cm for this experiment)

The dsDNA content for each well was calculated by interpolating the fluorescence readings from a standard curve, also measured in the same ALP substrate buffer. The ALP activity calculated using the equation above was normalised by the dsDNA content of the samples and expressed as percentage response relative to the vehicle.

2.5 Mineralisation Assays

Osteoblasts are bone forming cells that produce an extracellular collagenous matrix that subsequently gets mineralised by hydroxyapatite deposition. Previous studies have demonstrated the ability of osteoblast-like SaOS-2 cells to mineralise extracellular matrix within 7 days when cultured osteogenic media supplemented with ascorbic acid, dexamethasone and a source for inorganic phosphates (Coelho and Fernandes 2000, Jiang, *et al* 2013, McQuillan, *et al* 1995). Ascorbic acid promotes collagen secretion and serves as a cofactor for prolyl hydroxylase which catalyses the hydroxylation of proline residues, integral to the stability of collagen triple helix (Franceschi, *et al* 1994, Murad, *et al* 1981). In addition, ascorbic acid and dexamethasone are known to upregulate osteoblastic genes for ALP and osteocalcin (Franceschi, *et al* 1994, Rickard, *et al* 1994). Inorganic phosphates initiate mineralisation by providing a source of phosphates to osteoblasts for the formation of hydroxyapatite (Bellows, *et al* 1992).

2.5.1 Mineralisation in multiwell plates

Mineralisation by SaOS-2 cells was assessed using Alizarin Red stain, an anthraquinone dye that binds to calcium deposits as confirmed by energy dispersive X-ray spectroscopy (Chang, *et al* 2000). SaOS-2 cells were seeded in 48-well plates at a density of $10x10^3$ cells per well in 0.5mL complete media till they reached confluence (usually day 3). The media was then replaced with vehicle ± metal ion treatments supplemented with 10nM dexamethasone and 50µg/mL L-ascorbic acid (Sigma-Aldrich, Dorset, UK) (referred to as osteogenic media). Vehicle ± metal ion treatments in osteogenic media was replenished every 2-3 days until two days prior to the end of experiment, when 5mM inorganic phosphates (100X solution containing 4 parts of 500mM Na_2HPO_4 and 1 part of 500mM NaH_2PO_4) was added to the osteogenic media to promote mineralisation. On day 7 from the start of treatments, the cells were washed with PBS and fixed overnight in 100% ethanol. To stain for calcium deposits, the wells were washed with PBS and incubated with 40mM Alizarin red stain (pH 4.2; Sigma-Aldrich, Dorset, UK) for 90 min on an orbital shaking platform. The excess stain was washed with 95% ethanol and plates air-dried. The plates were scanned on a flatbed scanner and percentage area of mineralisation per well was quantified using ImageJ (NIH: http://imagej.nih.gov/ij/) (Figure 2.3) and expressed as percentage response to vehicle.

2.5.2 Mineralisation on implant surfaces

Mineralisation by SaOS-2 cells was assessed on grit-blasted (GB), plasma sprayed titanium coated (Ti) and plasma sprayed hydroxyapatite coated (HA) surfaces provided by JRI Orthopaedics Ltd (Sheffield, UK). Xylenol orange, a fluorochrome that incorporates at sites of calcification was used to overcome the opacity of these implant surfaces to transmitted light (Shu, *et al* 2003, Wang, *et al* 2006). Moreover, unlike Alizarin Red S and von Kossa staining, xylenol orange does not bind to HA surfaces, thereby enabling the analysis of cell mediated mineralisation on these surfaces.

Prior to cell seeding, the implant surfaces were washed with PBS and pre-wetted with serum-free DMEM© GLUTAMAX™ for 60 min. SaOS-2 cells were seeded

in 6-well plates containing implant surfaces at a density of 1.5×10^5 cells per well in 3mL complete media till they reached confluence (usually day 3). Subsequently, the cells were treated with osteogenic media containing equivalent combination of Co^{2+} and Cr^{3+} at 1000µg/L, or 1.5×10^7 nanoparticles each of Co and Cr_2O_3 (gift from Dr Ferdinand Lali, Imperial College, London, UK), calculations for which are described below. The treatments were replenished every 2-3 days until 4 days prior to the end of experiment, when 5mM inorganic phosphates and 20µM xylenol orange (Sigma-Aldrich, Dorset, UK) were further supplemented in the osteogenic media. On day 21, the cells were washed with PBS and fixed with 10% buffered formalin for 30min. Subsequently, the surfaces were washed with PBS and imaged with inverted fluorescent widefield microscope (Leica DMI 4000B) using the N3 filter. The images were analysed for percentage mineralisation using ImageJ (NIH: http://imagej.nih.gov/ij/) (Figure 2.4).

Calculation and preparation of nanoparticles treatments

The number of nanoparticles was calculated based on its specific surface area as described below.

- Specific surface area (SSA) for Co particles = $50 m^2/gm$
- The radius of the particles = 40nm
- The surface area for a spherical particle = $4\pi r^2$

$$= 4 \times 3.142 \times 40 nm^2$$

$$= 2.0106 \times 10^{-14} m^2$$

- Thus number of particles per gm $= 50 m^2 / 2.0106 \times 10^{-14} m^2$

$$= 24.868 \times 10^{14}$$

$$= 2.4868 \times 10^{12} \text{ particles/mg}$$

Similarly for Cr_2O_3,

- SSA = $140 m^2/gm$
- Particle radius = 30nm
- Thus number of particles per gm = 1.238×10^{16}

$$= 1.238 \times 10^{13} \text{ particles/mg}$$

1mg of Co and Cr_2O_3 nanoparticles were resuspended in 1mL of 100% ethanol and sonicated For 5 min each to disaggregate the particles. Based on the above counts, the particles were serially diluted in 100% ethanol to obtain 1000x of the working concentrations. The particles were sonicated for 5 min at each dilution to prevent aggregation. The nanoparticle suspension was observed under a microscope to confirm absence of reaggregation. Finally, the particles were diluted 1000 times in osteogenic media to obtain the working concentration. The vehicles media contained equivalent amount of ethanol to keep the conditions consistent.

2.5.3 Calculation for combined interactions of metal ions

The interactions between Co and Cr ions were analysed using the fractional product methods described by Chou and Talalay (Chou 2006). The method follows the equation

$(1 − Fa) × (1 − Fb) = x$,

If $(1 − x)$ = the observed effect then it was said to be additive;

If $(1 – x)$ < the observed effect then it was considered to be antagonistic;

And if $(1 – x)$ > the observed effect, it was considered synergistic.

For example, for an inhibition of 30% for Co^{2+} and 40% for Cr^{6+} treatments, the calculations will be –

$(1-F_{Co2+}) \times (1-F_{Cr6+}) = (1-0.3) \times (1-0.4) = 0.7 \times 0.6 = 0.42$

$(1-0.42)=0.58$

Therefore, if the observed effect of $Co^{2+}:Cr^{6+}$ combination is an inhibition by 58%, then the interactions is said to be additive, while if the inhibition is more than 58% then the interaction was considered synergistic.
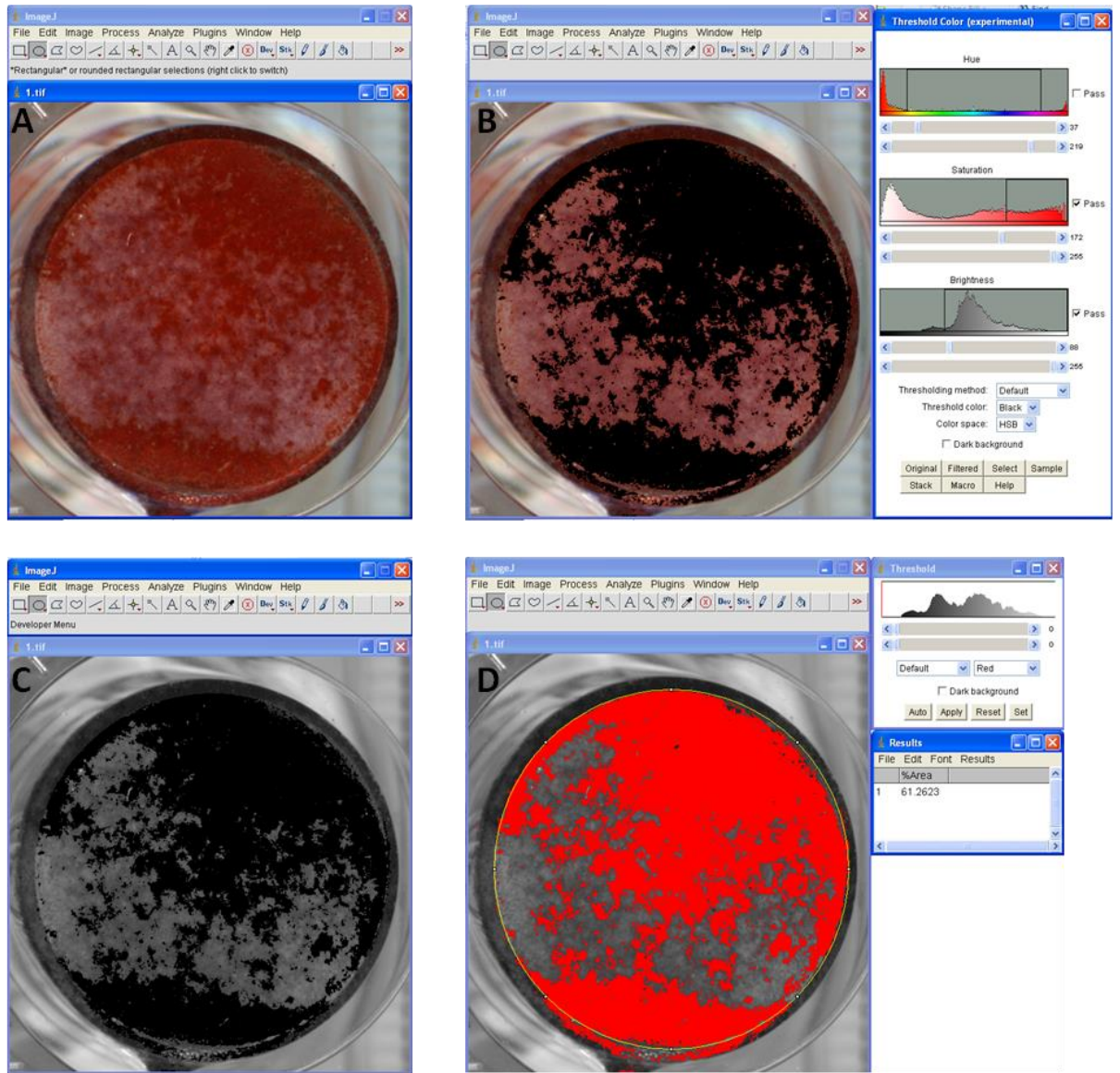
Figure 2.3 Quantification of mineralisation using ImageJ

Representative image of a mineralisation experiment stained with alizarin red (A). The image was colour thresholded (black) to select the deep red stained mineral deposits (B). The thresholding was kept consistent for all wells stained at the same time. Colour thresholded image was converted to a greyscale 8-bit image (C). The greyscale image was thresholded (red) to select the previously colour thresholded black region (D), and the area fraction of mineralisation for the well was measured.
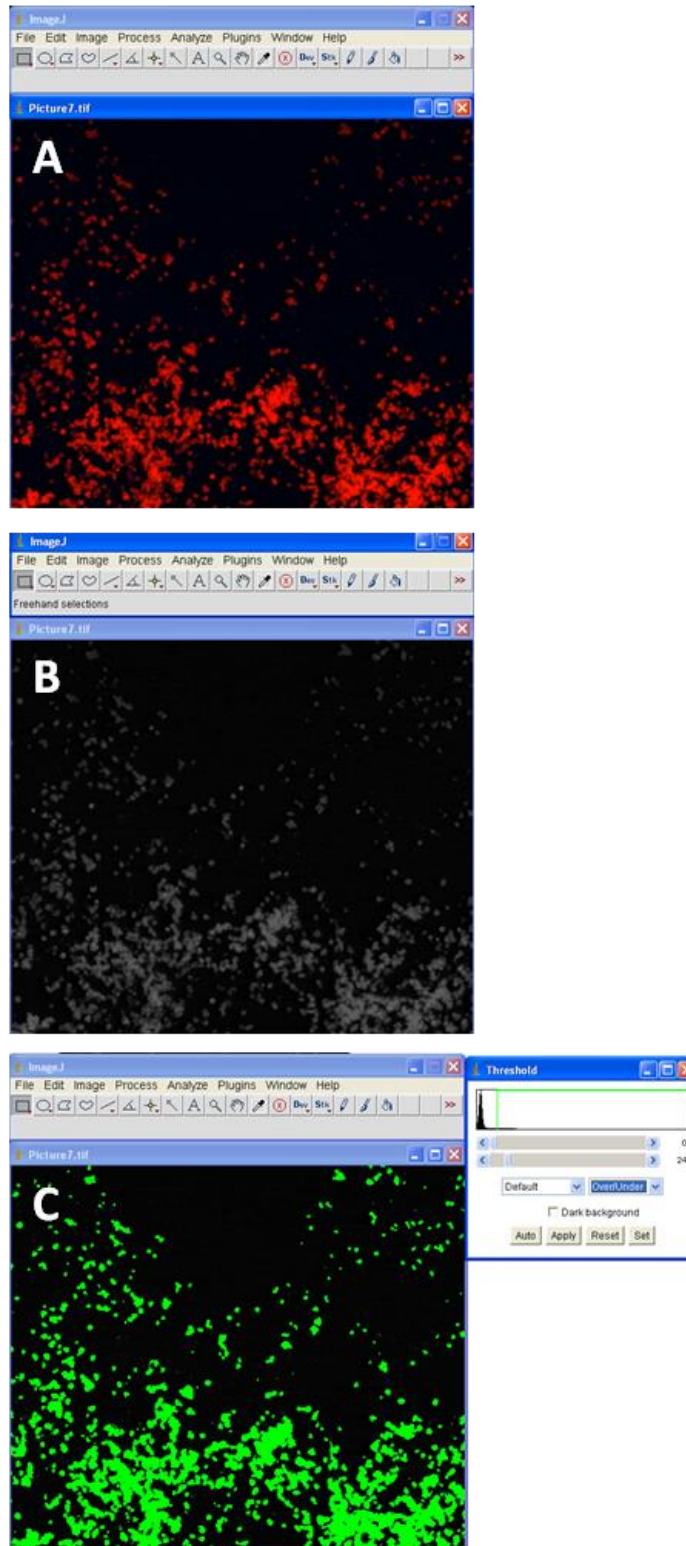
Figure 2.4 Quantification of mineralisation on implant surfaces.

The fluorescent image (A), taken with Leica DMI 4000B using N3 filter, was converted to a gray scale image (B) using ImageJ. This gray scale image was thresholded (C) and percentage area of mineralisation obtained for the field.

2.6 Osteoclast cell culture

2.6.1 Materials

Alpha- Modification of Minimum Essential Medium with GlutaMax™ (α-MEM), Phosphate Buffer Saline (PBS) (pH-7.4 Ca^{2+} and Mg^{2+} free), UltraPure™ 0.5M EDTA (pH 8.0) and Bovine Albumin Fraction V Solution (7.5% BSA) was purchased from Gibco (Paisley, UK). Human recombinant RANKL was obtained from Insight Biotechnology Ltd. (Wembley, UK). Histopaque®-1077 (Sigma-Aldrich, Poole, UK), human recombinant M-CSF (Cambridge, MA, USA) and 96-well culture plates were purchased from Costar® (Corning, New York, USA). CD14 Microbeads and MS columns for magnetic selection of CD14+ monocyte/macrophage population were purchased from Miltenyi Biotec Ltd. (Bisley, UK). Lithium-Heparin and BD SST™ vacutainers (BD Biosciences, Oxford, UK) were used to collected peripheral blood and serum from study volunteers, respectively.

2.6.2 Preparation for culture

Prior to culture, dentine disks were punched using a standard paper-hole punch from elephant ivory wafers; cut using a water-cooled Labcut 1010 low-speed diamond saw (Agar Scientific Ltd., Stansted, UK). The disks were 5mm in diameter and no thicker than 60μm. The dentine disks were sterilised by sonicating twice (10min each) in distilled water and stored in 70% ethanol for minimum of 24 hours. Prior to use in culture, the disks were washed in PBS and then pre-wetted in α-MEM at 37°C for at least an hour. Glass coverslips of 6mm diameter (Richardson's of Leicester, Leicester, UK) were sterilized by dry heating at 175°C for at least 2 hours.

2.6.3 Generation of primary osteoclasts from human peripheral blood

To study the effect of metal ions on osteoclast differentiation and function *in vitro*, peripheral blood (up to 100mL) was collected in lithium-heparin vacutainers from healthy volunteers recruited to SMBRER36 study approved by the University of Sheffield Research Ethics Committee. A separate study investigating the effect of circulating metal ion exposure on osteoclast differentiation and function was performed using peripheral blood from donors with well-functioning metal-on-metal hip replacements (MOMHR) and conventional total hip arthroplasty (THA)

controls matched for age, sex and time-since surgery. The study was approved by South Yorkshire Research Ethics Committee (Reference 09/H1310/62) and informed consent from the volunteers was obtained prior to sample collection.

To generate osteoclasts, the blood was mixed with ice-cold PBS supplemented with 2mM EDTA (Buffer 1) in equal proportion. Peripheral blood mononuclear cell (PBMCs) fraction was separated by density gradient centrifugation using Histopaque®-1077, for 30min at 400g. Subsequently, the PBMC fraction was washed twice with buffer 1 at 300g and 200g, for 10min each. A cell count was performed using a Neubauer chamber with 0.5% acetic acid for lysing red blood cells. Following the count, the cells were washed with buffer 1 by centrifugation at 300g for 10min. The cell pellet was resuspended in buffer 2 (buffer 1 + 0.5% BSA) containing the magnetic microbeads conjugated with anti-human monoclonal CD14 antibody, according to cell number obtained from the cell count (every 10^7 cells were resuspended in 100µL of buffer 2 supplemented with microbeads at 5:1). The cell suspension was incubated for 15min at 4°C to allow antibody binding.

The CD14+ cell fraction (osteoclast precursors) was separated from the unlabelled CD14- cells using a MS-column mounted on an appropriate magnetic separator. The CD14 enrichment process was confirmed using flow cytometry to assess the percentage of CD14+ cells obtained from the total population (courtesy Ankita Agarwal). The separated CD14+ cells were counted and seeded on sterile dentine disks or glass coverslips at a density of 4.5 x 10^3 per well in a 96-well plate. These osteoclast precursor cells were cultured at 37°C and 7% CO_2, in α-MEM supplemented with 10% FCS, 100 IU/mL penicillin, 100µg/mL streptomycin, 25ng/mL M-CSF and 30ng/mL RANKL; hereon referred to as osteoclastogenic media.

2.6.4 Treatments for osteoclast cultures
For investigating the effects of metal ions on osteoclast differentiation and function:
To study the effects of metal ions on development of osteoclasts, the precursor cells were treated with varying concentrations of Co^{2+}, Cr^{3+} and Cr^{6+} (0-

10000µg/L) (see section 2.1) in osteoclastogenic media, 48 hours post seeding (day 2). The media was replaced with fresh treatments made in osteoclastogenic media every 2-3 days till the end of culture at 7 days post onset of resorption (usually day 21). The onset of resorption was established by monitoring the cultures from day 10 by fixing the dentine disks in 10% buffered formalin and staining them for 2min with 1% Toluidine blue prepared in 0.5% sodium tetraborate solution. The excess stain was washed with 70% ethanol and the disks examined for resorption under a microscope.

To assess the effect of metal ions on the function of mature osteoclasts, osteoclast precursors were cultured in normal osteoclastogenic media until the onset of resorption, typically 14 days post seeding. From the onset of resorption, the cells were treated with varying concentrations of Co^{2+}, Cr^{3+} and Cr^{6+} (0-10000µg/L) in osteoclastogenic media for a week, replenished every 2-3 days.

For investigating the effect of circulating metal ions on osteoclast differentiation and function:
The effect of metal ions circulating in patient serum post MOMHR was assessed in mature osteoclasts, following the onset of resorption. The experimental design involved treating osteoclasts from patients with MOMHR and THA with normal cell culture media, autologous donor serum or serum from matched pair (Figure 2.5), plus RANKL and MCSF. For obtaining serum, peripheral blood from the donors was collected in BD SST™ Vacutainers (BD Biosciences, Oxford, UK), incubated for 20min at room temperature and centrifuged at 1100g for 10min. The separated serum was filter sterilised and frozen in aliquots for subsequent use. The cells were treated for 7 days with treatments being replaced every 2-3 days.
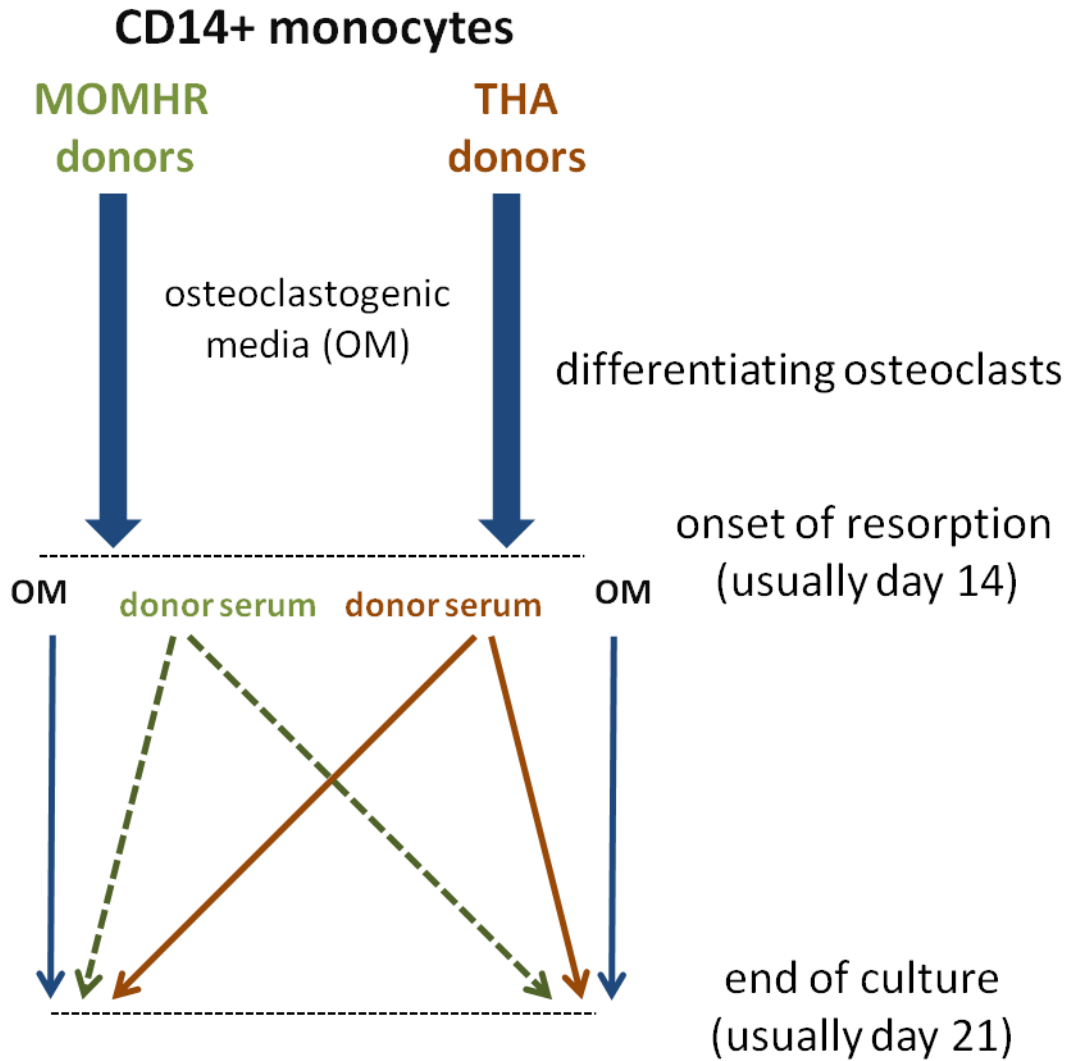
Figure 2.5 Experimental design for investigating the effect of circulating metal ions on osteoclast differentiation and function.

CD14+ monocytes were isolated from donors with MOMHR or THA. The cells were differentiated into mature resorbing osteoclasts in osteoclastogenic media (OM) containing M-CSF and RANKL. From the onset of resorption, the cells were treated for 7 days with OM, autologous serum or serum from the matched pair. The serum treatments were supplemented with RANKL and M-CSF at equivalent concentrations to that of OM.

At the end of all osteoclast cultures, the disks were fixed in 10% formalin, stained for tartrate resistant acid phosphatase and quantified for number of total osteoclasts, number of resorbing osteoclasts and percentage resorption using CellD® Software, Olympus UK.

2.6.5 Tartrate resistant acid phosphatase staining

Tartrate resistant acid phosphatase (TRAcP) is an isoenzyme defined by its ability to resist inhibition by L(+) tartrate and it promotes the hydrolysis of substrates such as phosphoproteins and nucleotides (Hayman, *et al* 2000). It has been identified as a marker enzyme for cytochemical identification of osteoclasts (Baron, *et al* 1986, Cole and Walters 1987) as well as osteoclast function (Minkin 1982).

The protocol used involves the hydrolysation of naphthol AS-BI phosphate by TRAcP, which then couples with pararosaniline, a hexazotized dye, to form a coloured complex that precipitates at the site of activity.

2.6.5.1 Materials

Acetic acid (10001 CU) and Hydrochloric acid (10125 4H) were purchased from VWR (Lutterworth, UK). Naphthol AS-BI phosphate, pararosaniline, sodium acetate trihydrate, sodium nitrite, sodium tartrate dihydrate were all purchased from Sigma (Poole, UK). Dimethylformamide was obtained from Fisher, (Loughborough, UK). DPX mountant was from BDH Laboratory (Poole, UK).

2.6.5.2 Methodology

To TRAcP stain the osteoclast cultures, the fixative were removed from the wells and cells incubated with acetate buffer (0.1M Sodium tartrate in 0.2M sodium acetate, pH 5.2) for 5 minutes at 37°C. The buffer was than discarded and the cells incubated in acetate-tartrate buffer containing 20mg/mL Naphthol AS-BI phosphate/dimethylformamide for 30 minutes at 37°C. Subsequently, the cells were incubated in acetate-tartrate buffer containing hexazotized pararosaniline solution for 15 minutes at 37°C. The wells were then counterstained with Gill's haematoxylin for 30-40 seconds and washed with tap water to remove excess stain. The coverslips were removed from the wells and dried and finally mounted

in DPX. The dentine disks were dried and stored at room temperature for quantification.

2.7 Quantification of osteoclasts on dentine disks

Osteoclasts were identified as TRAcP positive cells with three or more nuclei. Osteoclasts on or in close proximity to resorption pits were classified as resorbing osteoclasts. The cultures were quantified for the parameters of osteoclast number, resorbing osteoclasts and percentage area resorbed. Osteoclast cultures were quantified by point counting or via CellD Imaging Software, Olympus, (Southend-on-Sea, UK).

2.7.1 Point counting

A 10x10 grid with 100 points was superimposed on the field of view and the number of points that overlap with resorption pits was counted to obtain the percentage of area resorbed as described previously (Walsh*, et al* 1991). Osteoclast number and resorbing osteoclasts were counted from the same field in accordance to the definitions above. Eight fields of view were quantified from each dentine disk as per the image below (Figure 2.6).
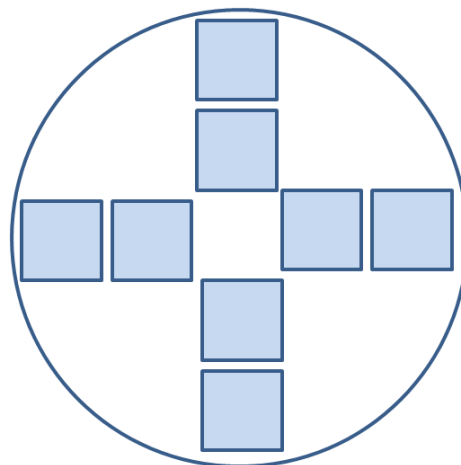
Figure 2.6 Field of view used for point counting osteoclasts.

Each dentine disk was divided into 8 fields which were quantified for osteoclast number, resorbing osteoclasts and percentage resorption.

2.7.2 Quantification using CellD Imaging Software, Olympus

Using the Multiple Image Alignment tool on CellD, 6 separate images on 50X magnification were obtained using Olympus BX51 Microscope and aligned to obtain one complete disk (Figure 2.7A). The osteoclast number, resorbing osteoclasts and percentage of area resorbed were identified manually for the entire disk using the wand tool in the software (Figure 2.7B).

2.8 TRAcP activity

TRAcP activity was assessed as described previously (Koh*, et al* 2006) for both developing and mature osteoclasts (see section 2.6). Briefly, cells were lysed in 50µL lysis buffer (0.2% Triton-X in dH_2O). The lysates was incubated at 37°C for 1h with a substrate buffer (50µL) containing 5.5mM phosphate substrate and 10mM sodium tartrate in 50mM citrate buffer (pH 4.5). Following the incubation, the reaction was stopped by adding 0.1N sodium hydroxide solution (100µL) and absorbance read at 405nm on a SpectraMax M5^e (Molecular Devices, Sunnyvale, USA).

The data was corrected for protein content as measured by bicinchoninic acid (BCA) assay to assess the total TRAcP activity. To measure the effect of metal ions on the TRAcP enzyme functioning, the TRAP activity was normalised to the concentration of TRAcP obtained using human TRAP 5b a sandwich-ELISA (Cusabio, Hubei, China) according to the manufacturer's protocol.

A.

B.
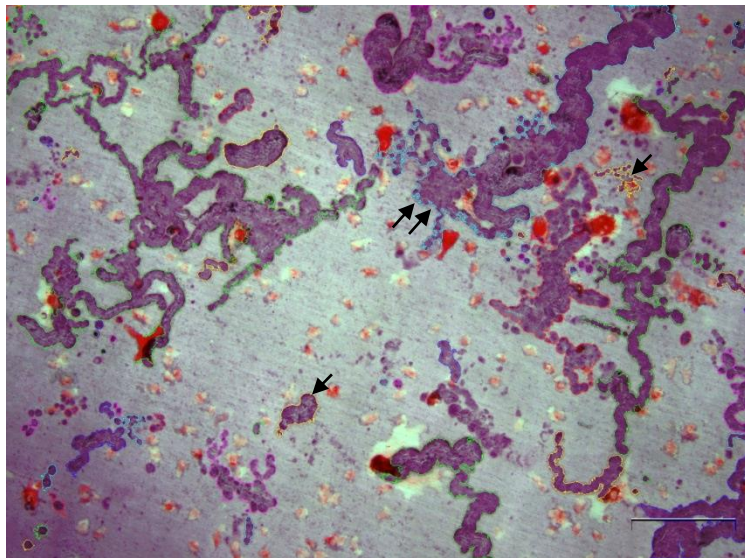
Figure 2.7 Quantification of osteoclasts using CellD.

A) Multiple image alignment of 6 separate images to form a complete dentine disk. B) Representative image outlining resorption pits (marked by arrows) using the wand tool.

2.9 Osteocyte culture

2.9.1 Materials

Alpha- Modification of Minimum Essential Medium with GlutaMax™ (α-MEM), α-MEM with ribonucleosides and deoxyribonucleosides (α-MEM+), foetal calf serum (FCS), dimethyl sulfoxide (DMSO), penicillin (10000 units/mL) and streptomycin (10000μg/mL), 0.25% Trypsin-EDTA 4Na and phosphate buffer saline (PBS) (pH-7.4, Ca^{2+} and Mg^{2+} free) were purchased from Gibco (Paisley, UK). Iron supplemented bovine calf serum (BCS) was purchased from Hyclone and rat-tail type-1 collagen solution was purchased from BD Bisosciences (Oxford, UK). Trypan-blue dye was obtained from Sigma (Poole, UK). T75 flasks were from Nunclon (Roskilde, Denmark); 96 multiwell plates were bought from CoStar® (Corning, New York, USA).

2.9.2 Maintenance of MLO-A5 cells

MLO-A5 cells were previously isolated from long bones of mice expressing T-antigen driven by an osteocalcin promoter and are believed to represent a post osteoblast – pre-osteocyte phenotype capable of mineralisation (Kato, *et al* 2001). MLO-A5 cells were maintained at 37˚C in a humidified atmosphere of 95% air and 5% CO_2 with α-MEM GlutaMAX™ containing 100U/mL penicillin, 100μg/mL streptomycin and 10% FCS (referred to as complete α-MEM). The cells were passaged every 2-3 days when 80% confluent, and frozen stocks maintained in FCS supplemented with 10% DMSO in liquid nitrogen.

2.9.3 Maintenance of MLO-Y4 cells

MLO-Y4 cells were derived from the same transgenic mice as the MLO-A5 cells, but exhibit a more mature osteocyte phenotype with characteristic dendritic morphology complemented with expression of osteocytic genes such as osteocalcin and connexin 43 (Kato, *et al* 1997). The cells were grown in rat-tail type 1 collagen coated T75 flasks (0.15mg/mL in 0.02M acetic acid) and maintained at 37˚C in a humidified atmosphere of 95% air and 5% CO_2, with α-MEM+ containing 100U/mL penicillin, 100μg/mL streptomycin, 2.5% FBS and 2.5% BCS (complete α-MEM+) (Rosser and Bonewald 2012). The cells were passaged every 2-3 days when 60% confluent, and frozen stocks maintained in FCS supplemented with 10% DMSO in liquid nitrogen.

2.10 MLO-A5 mineralisation

Mineralisation by MLO-A5 cells was assessed using Alizarin Red staining, similar to mineralisation by SaOS-2 cells (section 2.5.1). However, the seeding density used for MLO-A5 cells was altered to $2x10^4$ cells in 48-well plate, to achieve confluence at day 3.

2.11 MLO-Y4 survival and dendricity

To assess survival and dendricity, MLO-Y4 cells were cultured overnight in collagen coated (see section 2.8.3) 96-well plates at 2500 cells/well in complete α-MEM+ at 37°C in a humidified atmosphere of 95% air and 5% CO_2. Subsequently, the cells were washed gently with PBS and treated with vehicle (0.5% FCS supplemented α-MEM+) ± metal ion treatments (individual and in combination, see section 2.1). After 24h incubation, the cells were washed with PBS and fixed with 10% buffered formalin (15min) and stained with 0.1% crystal violet stain (10min). The excess stain was washed with dH_2O and the plates left to air-dry overnight.

To quantify MLO-Y4 cell survival, cell numbers were counted from 5 non-overlapping random fields of view per treatment with 4 wells quantified for each treatment. The dendricity was assessed by counting the number of dendrites per cell and the average length of dendrites, for dendrites greater than 5μm in length (Figure 2.8). Quantification was done using CellD imaging software (Olympus, Southend-on-Sea, UK) on 200X magnified images with Leica DMI4000B microscope.
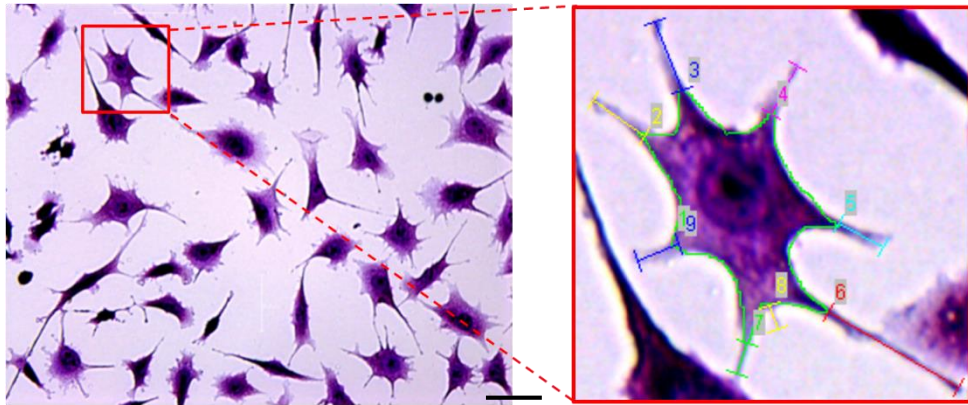
Figure 2.8 Quantification of osteocyte dendricity.

Osteocyte dendricity assessed by counting the number of dendrites per cell and average length of dendrites using CellD. A typical field of view for crystal violet stained osteocytes with dendrite measurements depicted in zoomed image. Scale bar 50µm

2.12. Synchrotron based Microfocus X-ray Spectroscopy

A synchrotron provides high intensity brilliant x-rays suitable for microfocus X-ray spectroscopy permitting elemental analysis of hydrated samples, such as biological specimens, at a submicron scale. It requires minimal sample preparation and causes less radiation artefacts than other microanalytical techniques for chemical characterisation (Adams*, et al* 1998). The working of a synchrotron is described in Figure 2.9.

2.12.1 Microfocus X-ray fluorescence

The I18 microfocus x-ray spectroscopy beamline at the Diamond Light Source synchrotron facility (Harwell Science and Innovations Campus, Didcot, UK) was used for determination of intracellular distribution and speciation of metal ions. For each sample, an initial map of metal distribution was generated using microfocus X-ray fluorescence (µ-XRF), a spectroscopic technique used to observe elemental distribution at a cellular level (Kemner*, et al* 2004, McRae*, et al* 2006, Ortega*, et al* 2009, Yang*, et al* 2005). µ-XRF involves the ejection of electrons from inner orbits of atoms by incident high intensity X-rays (Figure 2.10). The electronic instability of the ionised atom triggers a transition of an electron from an outer to the inner orbital releasing energy in the form of an X-ray photon, a phenomena termed as fluorescence. The energy of this emitted X-ray photon corresponds to the difference in energies between orbitals, and is characteristic for an element, thus identifying the source elemental atom.
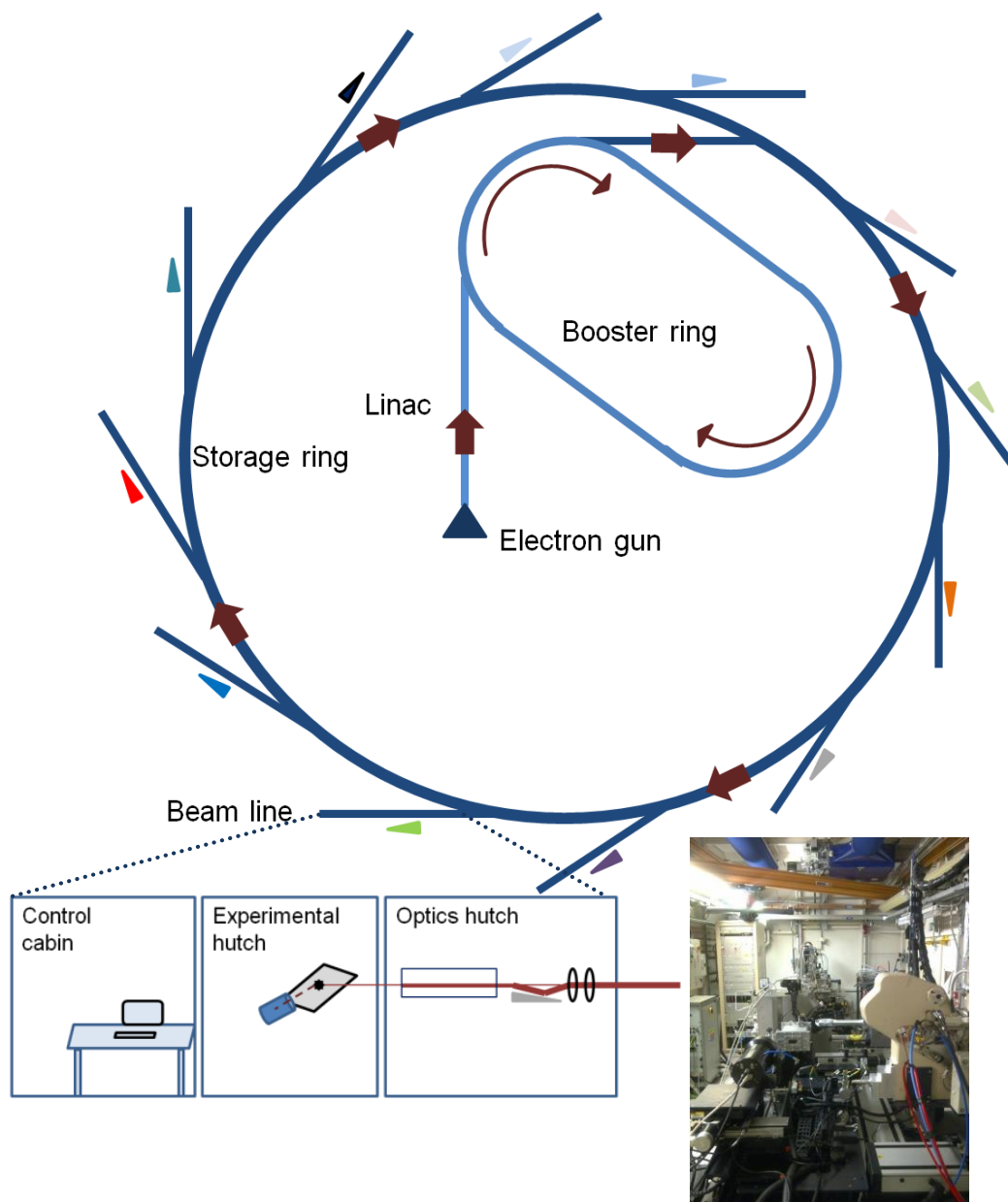
Figure 2.9 Working of a synchrotron

A synchrotron consists of a source of electrons (electron gun) which are linearly accelerated (linac) into a booster ring. In the booster ring, they are further accelerated to near-light speeds before being released into a large storage ring. The bending of electrons around the circular storage ring releases energy in the form of radiation which is used for experimentation in beam-lines. The beamline consists of an optics hutch, where the incoming radiation is filtered and focused on the sample in the experimental hutch (imaged alongside).
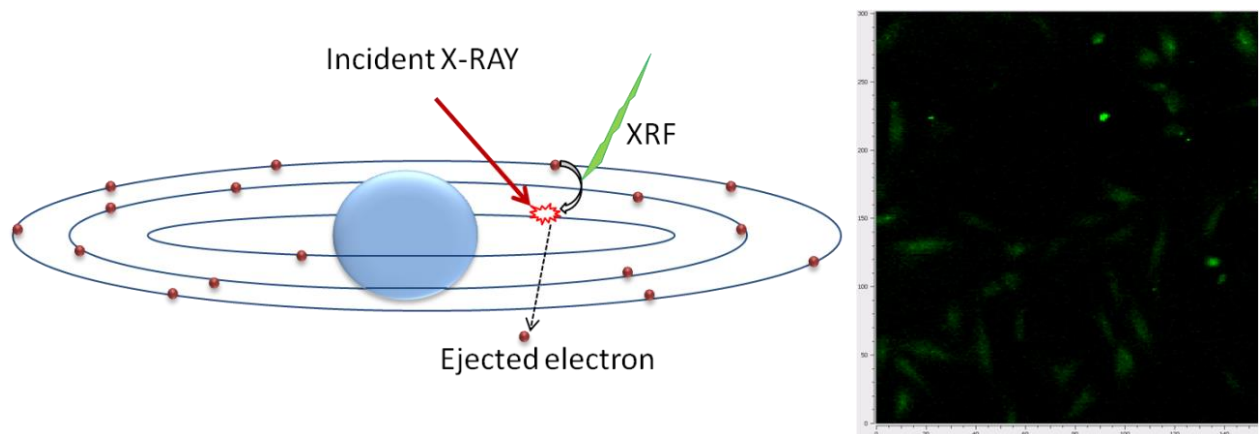
Figure 2.10 Principle for X-ray fluorescence (XRF)

Synchrotron generated high intensity x-rays ionise the sample by ejecting electrons from the inner shell of atoms. An electron from the outer shell loses transits to the inner shell to fill the void by losing energy in the form of fluorescence (XRF).The energy released during this transition is characteristic of an element and is detected for its identification. The XRF map alongside, for Co^{2+} treated osteoblasts shows the presence of intracellular Co (green).

2.12.2 X-ray Absorption Near-Edge Structure

The µ-XRF mapping of elemental metal in cells was followed by generation of X-ray absorption spectra (XAS) to identify the metal speciation. With increasing energies of incident X-rays, atoms absorb the energy monotonically till a characteristic wavelength, where a sharp increase in absorption is observed. This is manifested as an absorption edge on the spectra and it corresponds to the energy which causes the excitation of electrons to high energy states. The spectrum near the absorption edge, ranging from 10eV below the edge to 50eV above it, is termed as the X-ray Absorption Near-Edge Structure (XANES) region (Figure 2.11). In this region of the spectra, the photoelectron has low kinetic energy and experiences multiple scattering by the surrounding atoms (Figure 2.12). These interactions with the surrounding atoms manifest as features in the XANES spectrum, which provide information about the oxidation state, electronic configuration and site symmetry.

2.12.3 Methodology

Preparation of cells

To observe intracellular distribution and speciation of metal ions, human osteosarcoma osteoblast-like cells (SaOS-2) were seeded in complete DMEM at 1.5×10^4 cells per silicon-nitride window (Silson Ltd, Northampton, UK) in a 24 well-plate. After the first 24 hours, the cells were washed with phosphate buffered saline (PBS) and treated with 100µM Co^{2+}, 100µM Cr^{3+} or 5µM Cr^{6+} for 3 days in vehicle media (see section 2.1). At the end of the treatment, cells were fixed in 10% EM-grade formalin (TAAB Laboratories, Aldermaston, UK).

The intracellular state of metal ions was investigated in both developing and mature osteoclasts. Isolated CD14+ monocytes (see section 2.6) were seeded on silicon-nitride windows at a density of 10^4 cells per well in a 48-well plate and treated with 10µM Co^{2+}, 10µM Cr^{3+} or 1µM Cr^{6+} from day 3 till the onset of resorption (checked with a parallel culture on dentine disks). Mature multinuclear resorbing osteoclasts were treated for a week from the onset of resorption (typically on day 14) with 10µM Co^{2+}, 100µM Cr^{3+} or 10µM Cr^{6+} in osteoclastogenic media. The treatments were replenished every 2-3 days and

cells fixed with 10% electron microscopy-grade formalin at the end of the experiment.

µ-XRF mapping of cells

A two-dimensional elemental distribution map was generated for 2 or 3 cells per treatment by raster scanning samples with 4 µm x 2 µm step-size, 1000ms collection per step with an incident X-ray energy of 8.5keV. The XRF maps were analysed using PyMCA 4.4.1 (Solé*, et al* 2007).

µ-XANES spectroscopy

µ-XANES spectra were obtained for metal ion treated samples at sites with high signal within the µ-XRF maps. The X-ray absorption spectra were collected to 200eV beyond the absorption edge and compared to known metal standards of different oxidation states. Data were analysed using Athena (Ravel and Newville 2005) and PySpline (Tenderholt*, et al* 2007) and plotted using GraphPad Prism version 5.04 for Windows (GraphPad Inc, La Jolla, CA, United States).
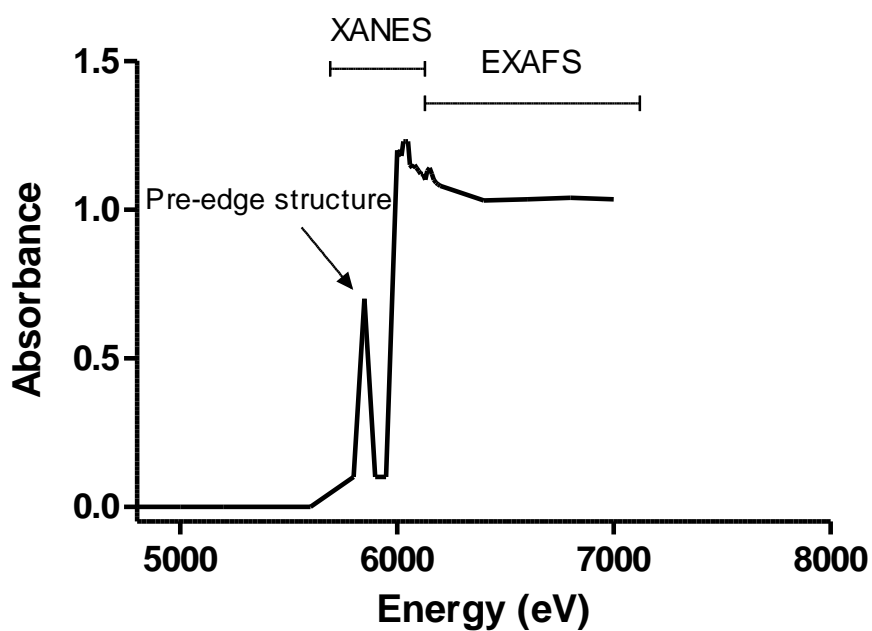
Figure 2.11 X-ray absorption spectra.

The spectrum depicts a sharp increase in absorption corresponding to the excitation of electron to a high energy state. The area near the absorption edge termed as the XANES region and area beyond the edge is termed as EXAFS region.
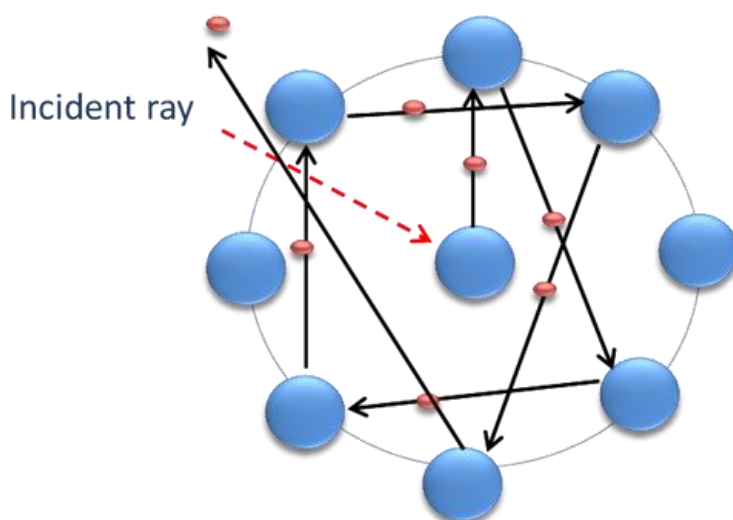
Figure 2.12 Scattering of photoelectron in XANES.

XANES region is dominated by low energy excited electron (red) that undergoes multiple scattering (arrows) amongst surrounding atoms.

2.13 Immuofluorescence for DMT-1 expression

Expression of DMT-1 transporter was assessed in osteoblasts and osteoclasts using a rabbit polyclonal anti-DMT-1 antibody (Abcam, Cambridge, UK). The cells grown on glass coverslips were blocked with 5% normal goat serum (Invitrogen, Paisley, UK) for 60min. Subsequently, they were washed with PBS and stained with the primary antibody for 1hr at a concentration of 0.01mg/mL in 1% normal goat serum. The cells were then washed thrice with PBS andincubated in Alexa-488 conjugated goat anti-rabbit IgG secondary antibody Invitrogen, Paisley, UK) at a concentration of 0.02mg/mL. The cells were counterstained for F-actin (Rhodamine-phalloidin) and nuclei (Hoescht 33342), mounted in ProLong® Gold Antifade reagent (Life technologies, Paisley, UK) and imaged using Leica DMI4000B microscope. Appropriate isotype IgG and 'no primary' controls were used to validate the specificity of the antibodies.

2.14 Cellular uptake of Co^{2+} in SaOS-2 and primary human osteoclasts

The cellular entry of Co^{2+} was assessed by fluorescence quenching of intracellular calcein. Calcein-AM, an uncharged acetoxymethyl ester derivate of calcein readily permeates cell membranes where intracellular non-specific esterases hydrolyse the ester group forming a fluorescing charged molecule that is trapped inside the cells. Calcein possesses diamine tetra-acetic chelating arms, similar to EDTA, which complexes with metal ions (Co^{2+}, Fe^{2+}, Ni^{2+} and Cu^{2+}) and quenches its fluorescence (Breuer, *et al* 1995, Thomas, *et al* 1999). Calcein-AM quenching has been widely used to assess the cytoplasmic entry of divalent metal ions in a variety of cell types (Breuer, *et al* 1995, Forbes and Gros 2003, Picard, *et al* 2000). Calcein-AM only binds to Ca^{2+} at a strong alkaline pH and is unlikely to cause interference at physiologically buffered pH used in the present assay (Lewin, *et al* 1969).

2.14.1 Receptor antagonists

A740003, a specific antagonist for P2X7R, was purchased from Tocris Biosciences (Bristol, UK) and dissolved in DMSO to a stock concentration of 10mM, aliquoted and stored at -80°C. NSC306711, an inhibitor of divalent metal transporter 1 (DMT-1), was procured from the National Cancer Institute,

Developmental Therapeutics Program, Diversity Set, USA. A stock concentration of 7.5mM was made in DMSO, aliquoted and stored at -20˚C.

2.14.2 Preparation of cells

SaOS-2 cells were seeded in a 96-well plate at a density of 5×10^3 cells per well in complete media and left overnight to adhere prior to the assay on the following day. Osteoclasts were generated in 96-well plates from peripheral blood of healthy volunteers as described above. The assay for cellular entry for cobalt was conducted on multinucleated mature osteoclasts, usually at day 14 of the culture.

2.14.3 Fluorometric assay for Co^{2+} uptake

Cells were washed with PBS and incubated with 0.25µM of Calcein-AM (Life Technologies Invitrogen, Paisley, UK) in α-MEM Glutamax™ supplemented with 25mM HEPES and 0.05% bovine serum albumin (Gibco® Invitrogen, Paisley, UK) for 30 minutes at 37˚C. Subsequently the cells were washed with PBS and incubated with phenol-free DMEM (Gibco® Invitrogen, Paisley, UK) ± 40nM A740003 or 50µM NSC306711 for 30 min at 37˚C. The wells were imaged with excitation/emission of 490/515 (L5 filter cube) with the Leica AF6000 time-lapse fluorescent microscope maintained at 37˚C, with 3 minute interval for 60 minutes. Co^{2+}, prepared as 10X stocks (for 5-50000µg/L) in phenol-free DMEM was added to the wells following the first 6 minutes which served as baseline. A 'vehicle' treatment of equivalent volume of phenol-free DMEM without metal ions served as a control. Cellular fluorescence was measured for individual cells using ImageJ (Schneider, *et al* 2012). The average change in cellular fluorescence relative to its own baseline for each concentration was plotted, and the area under curve calculated using GraphPad Prism version 5.04 for Windows (GraphPad Inc, La Jolla, CA, United States) and expressed relative to vehicle with no antagonist.
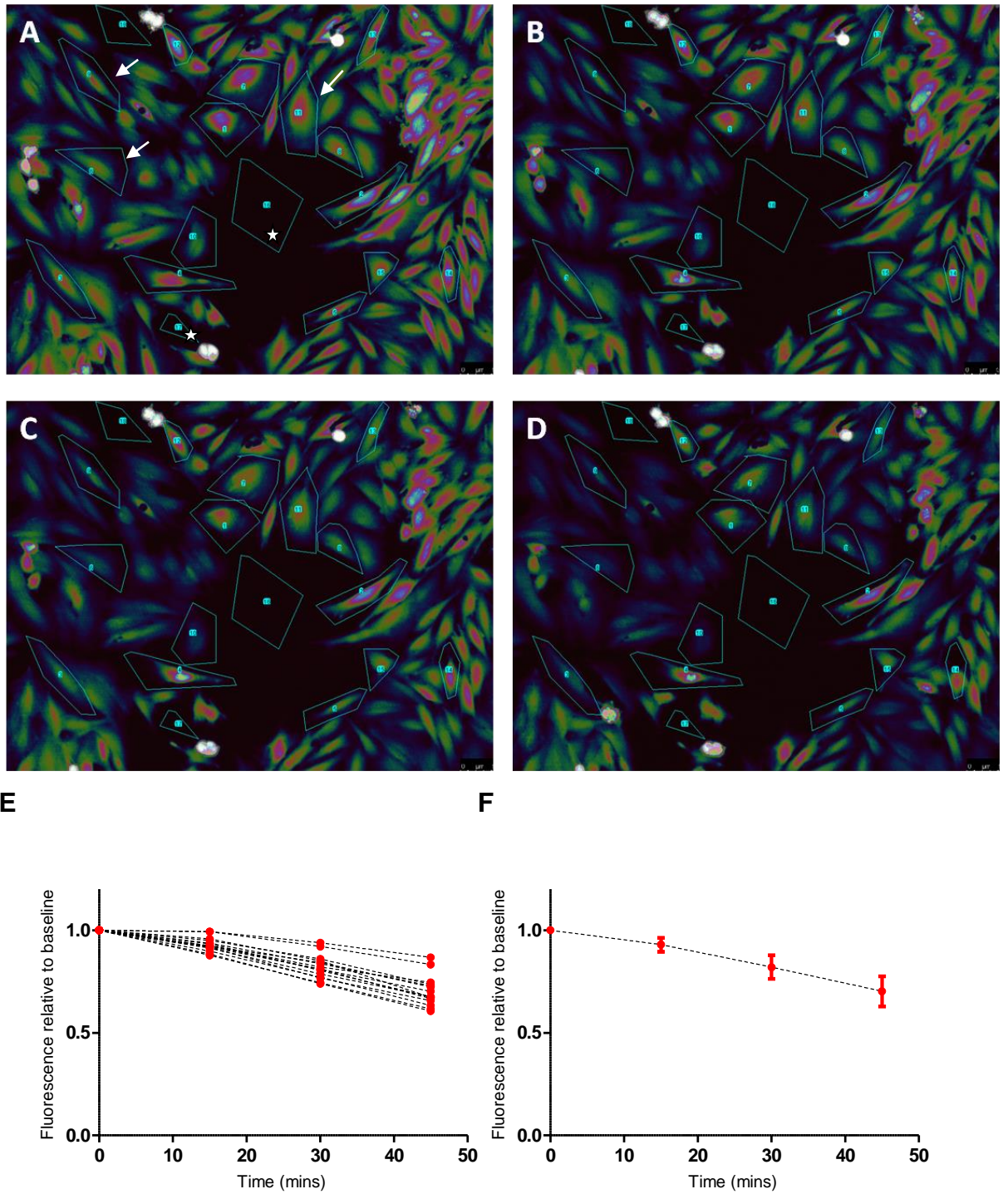
Figure 2.13 Analysis of calcein quenching by Co^{2+}

Time lapse images of calcein-loaded osteoblasts in presence of 5000µg/L Co^{2+} captured at 0, 15, 30 and 45 minutes respectively (A-D). Regions of interests for background (marked by stars in A) and 20 random individual cells (arrows in A) were selected and mean fluorescence measured. The fluorescence quenching in individual cells after subtraction of background is expressed relative to the baseline for that cell (E). The data is then expressed as the average change in fluorescence for all cells for that treatment (F).

2.14 Statistical analysis

All data was analysed using GraphPad Prism version 5.04 for Windows (GraphPad Inc, La Jolla, CA, United States) and illustrated as mean ± 95%CI. Outliers in the data were removed using the Grubb's outlier test (http://graphpad.com/quickcalcs/Grubbs1.cfm) and normality tested using the D'Agostino and Pearson omnibus normality test. Statistical significance was tested using parametric or non-parametric tests as appropriate. For comparing two groups, a student's t-test was used, with Mann-Whitney post-test for non-parametric data. For comparing more than two groups, One- way ANOVA was used with Tukey or Dunnett comparison for parametric data, or Kruskal-Wallis test with Dunn's comparison for non-parametric data. The difference was considered significant for $p < 0.05$.

Chapter 3 - Effect of metal ions on survival and function of osteoblast-like cells

3.1 Introduction

Hip replacements (resurfacing and stemmed types) that use a metal-on-metal bearing usually rely on cementless component osseointegration on the acetabular side, and cementless component osseointegration on the femoral side in the case of stemmed prostheses. Osseointegration of the prosthesis is therefore critical for the long term survival of these implants. Indeed, as per the National Joint Registry of England and Wales (National Joint Registry2013), higher revision rates witnessed with MOMHR are predominantly attributed to aseptic loosening and pain, the patient-time incident rates for which are 2.62 (2.37-2.90 95%CI) and 3.82 (3.52-4.15) per 1000 patient years respectively (National Joint Registry2013). A recent retrospective cohort study reported loosening of the acetabular or femoral component as the cause for 32% of all MOMHR failures (Canadian Arthroplasty Society2013).

Osseointegration is a complex coordinated cellular process, similar to bone healing following fractures, involving an inflammatory response, an osteogenic response followed by a process of remodelling (Mavrogenis, *et al* 2009, Ramazanoglu and Oshida 2011). Osteoblasts play a key role in osseointegration by forming an initial non-collagenous osteoid matrix that leads to the formation of woven bone at the implant interface. This matrix is rich in proteins such as osteopontin and bone sialoprotein that facilitate the recruitment of monocyte precursors and osteoclasts which initiate the process of remodelling (Mavrogenis, *et al* 2009, Reinholt, *et al* 1990). The remodelling of initial matrix results in the formation of new lamellar bone by osteoblasts which ensures implant osseointegration (Mavrogenis, *et al* 2009). This vital role of osteoblasts in implant osseointegration and its subsequent survivorship warrants the investigation of the effects prosthesis-derived metal particles and ions have on osteoblast survival and function.

Previous studies by us and others have demonstrated the detrimental effects of particulate and ionic forms of cobalt and chromium debris on osteoblast survival and function (section 1.10) (Andrews, *et al* 2011, Anissian, *et al* 2002, Dalal, *et al* 2012, Fleury, *et al* 2006, Lochner, *et al* 2011, Zijlstra, *et al* 2012). We observed a

significant dose-dependent reduction in osteoblast-like SaOS-2 cell activity, alkaline phosphatase (ALP) activity and its ability to mineralise, with Cr^{6+} being the most detrimental followed by Co^{2+} and Cr^{3+} having the least negative effect (Andrews, *et al* 2011).

Most studies have investigated the effects of cobalt and chromium ions in isolation. Only recently, Zijlstra et al. (2011) described an increased reduction in cell number with Co^{2+} and Cr^{3+} combined treatment compared to Co^{2+} and Cr^{3+} alone, at 1:2 ratios to reflect clinically observed concentrations following metal-on-metal total hip arthroplasty. Furthermore, the detrimental effects of CoCr alloy particles observed previously (Allen, *et al* 1997, Dalal, *et al* 2012) are likely to be mediated, at least in part, via the simultaneous exposure to cobalt and chromium ions as a result of their intracellular oxidation (Shahgaldi, *et al* 1995) or dissolution in acidic lysosomal vacuoles (Lohmann, *et al* 2000). Whilst studying the effects of individual metal ions helps us discern their contribution to the observed detrimental effects, it does not provide us with an understanding of the overall combined effect they have *in vivo*.

Study of the cellular response to combined cobalt and chromium ions will also highlight any additive or synergistic interactions between ions. It will also give insight into downstream pathways, for example an additive effect would suggest that the treatments act on similar or complementary pathway whilst a finding of synergism would imply independent downstream mechanisms. To analyse whether interactions between cobalt and chromium were additive, synergistic or antagonistic, the fraction product method first described by Chou and Talalay (1984) was used (2.5.3). Interactions are defined as additive when the combined effect is an approximate sum of individual effects of the toxicants and synergistic when they are greater than the sum of individual effects.

This chapter presents the results of osteoblast (SaOS-2) survival and function as evaluated *in vitro* by its cellular activity, ALP activity and its ability to mineralise in presence of combinations of cobalt and chromium at concentrations clinically relevant to MOMHR. A preliminary study conducted by Jennifer Prentice (BMedSci) measuring serum metal ion levels in 25 subjects with asymptomatic

MOMHR suggested a 1:1 correlation between Co:Cr (R^2=0.9635) (Appendix 2). This suggests that the cells are exposed to broadly similar concentrations of cobalt and chromium ions, and is the rationale for the combination treatments in this chapter. However, the study assumes that the 1:1 correlation observed in the serum also reflects the local hip aspirate environment. Only a few studies have measured metal levels at hip aspirates with corelations between Co and Cr ranging from 1:1.7 to 1:7.5 (Davda, *et al* 2011, Kwon, *et al* 2011). The ratios used in this study are therefore a conservative approximation of the physiological setting.

The concentration range for metal ions (0-5000µg/L) used in this study is derived from previously reported patient levels for different physiological compartments (section 1.5). In addition, metal ion concentrations used for experiments with Cr^{6+} were 10-fold lower compared to those used for Cr^{3+} due to its previously established higher toxicity (Andrews, *et al* 2011).

3.2 Results

3.2.1 Effect of Co^{2+} and Cr^{3+} on osteoblast activity

Osteoblast cells (SaOS-2) were treated with a range of clinically relevant concentrations (0, 5, 50, 500 and 5000μg/L) of Co^{2+}, Cr^{3+} or a combination of Co^{2+} and Cr^{3+} ($Co^{2+}:Cr^{3+}$) at equal concentrations for 3 days and 7 days. The effect of metal ions on cell activity was measured by an MTS assay detailed in section 2.3.

After 3 days, a significant reduction in osteoblast activity was only observed at the highest concentration of 5000μg/L for Co^{2+} (mean ± SD; 83.11±16.62), Cr^{3+} (79.83±12.92) and $Co^{2+}:Cr^{3+}$ (76.95±22.76) compared to the untreated control (100±13.47). There was no significant difference between the various treatments for any concentrations (Figure 3.1A). The results corresponding to clinically relevant partitions of metal ion concentrations are illustrated in Figure 3.1B.

In comparison to day 3, SaOS-2 activity at day 7 showed a significant reduction at a lower concentration of 500μg/L with Cr^{3+} (86.25±4.32) and $Co^{2+}:Cr^{3+}$ (89.77±7.12) when compared to an untreated control (100±8.97). A significant reduction in cell activity was also observed for the highest concentration of 5000μg/L with all metal ion treatments (63.43±21.67 Co^{2+}, 72.8±9.55 Cr^{3+} and 47.13±18.53 $Co^{2+}:Cr^{3+}$).

Cell activity with combination treatment of $Co^{2+}:Cr^{3+}$ (47.13±18.53) had an additive effect at 5000μg/L, being significantly lower compared to Co^{2+} (63.43±21.67) and Cr^{3+} (72.8±9.55) individually (Figure 3.2A). The results corresponding to clinically relevant partitions of metal ion concentrations are illustrated in Figure 3.2B.

A.

B.

Figure 3.1 Effect of Co^{2+} and Cr^{3+} on osteoblast activity after 3 days

Following initial 24 hr incubation, SaOS-2 cells were treated with metal ions for 48 hr and their activity measured by MTS assay. The data shown is relative to activity of untreated cells. **A)** Comparison between Co^{2+} (purple), Cr^{3+} (green) and Co^{2+}:Cr^{3+} (red) combined treatments. The control and its SD are depicted by dashed lines. **B)** Effect on osteoblast activity depicted at clinically relevant concentrations corresponding to normal physiology, patient serum and hip aspirate post-MOMHR. All values are mean ± SD of 3 experiments with 4-6 replicates in each (*** $p<0.0001$).

Figure 3.2 Effect of Co^{2+} and Cr^{3+} on osteoblast activity after 7 days

Following initial 24 hr incubation, SaOS-2 cells were treated with metal ions for 6 days and their activity measured by MTS assay. The data shown is relative to activity of untreated cells. **A)** Comparison between Co^{2+} (purple), Cr^{3+} (green) and Co^{2+}:Cr^{3+} (red) combined treatments. The control and its SD are depicted by dashed lines. **B)** Effect on osteoblast activity depicted at clinically relevant concentrations corresponding to normal physiology, patient serum and hip aspirate post-MOMHR. All values are mean ± SD of 3 experiments with 4-6 replicates in each. * indicates significant comparisons between metal concentrations and control, whilst 'a' and 'c' indicate significance between different metal ion treatments (*a $p<0.05$; ** $p<0.01$; ***c $p<0.0001$).

3.2.2 Effect of Co^{2+} and Cr^{6+} on osteoblast activity

The effect of Co^{2+} and Cr^{6+} on SaOS-2 activity was measured by an MTS assay after 3 days and 7 days. The cells were treated with a range of clinically relevant concentrations (0, 0.5, 5, 50 and 500µg/L) of Co^{2+}, Cr^{6+} or a combination of Co^{2+} and Cr^{6+} (Co^{2+}:Cr^{6+}) at equal concentrations. Due to the high toxicity observed with Cr^{6+} in previous studies (Andrews, *et al* 2011), a narrower concentration range was used compared to experiments with Cr^{3+}.

No change in cell activity was observed with Co^{2+} compared to untreated control after 3 days. A significant reduction was observed with Cr^{6+} at 50µg/L (mean ± SD; 86.61±6.32) and 500µg/L (20.01±6.77) when compared to untreated control (100±4.3). Combination treatment with Co^{2+}:Cr^{6+} resulted in a significant reduction in cell activity at 0.5µg/L (88.47±11.0), 50µg/L (87.14±5.3) and 500µg/L (20.25±6.58) compared to the untreated control (Figure 3.3A).

Cell activity with combination treatment of Co^{2+}:Cr^{6+} (88.47±11.0) was significantly lower at 0.5µg/L compared to Co^{2+} (101.6±3.00) and Cr^{6+} (102.8±6.20) and compared to Co^{2+} (93.56±15.03) at 500µg/L, suggesting synergism (Figure 3.3A). The results corresponding to clinically relevant partitions of metal ion concentrations are illustrated in Figure 3.3B. While longer exposure to Co^{2+} had no effect on osteoblast activity at 7 days, Cr^{6+} resulted in a monophasic detrimental response reaching significance at 50µg/L (86.75±7.96) and 500µg/L (14.94±0.60) compared to untreated control (100±3.94). The Co^{2+}:Cr^{6+} treatment seemed to have a small biphasic element to the response, with a significant increase in cell activity at 5µg/L (105.4±7.24) and a decrease at 50µg/L (89.47±8.5) and 500µg/L (15.14±0.53) compared to the untreated control (Figure 3.4A).

Combined Co^{2+}:Cr^{6+} treatment had a stimulatory effect on cell activity with an increase compared to individual Co^{2+} (98.34±5.70) and Cr^{6+} (97.50±4.34) treatments at 5ug/L. A decrease was observed for Cr^{6+} (86.75±7.96) and Co^{2+}:Cr^{6+} (89.47±8.5) compared to Co^{2+} at 50μg/L (97.20±6.37) and 500μg/L (97.88±5.27 versus 14.94±0.60 and 15.14±0.53 for Co^{2+}, Cr^{6+} and Co^{2+}:Cr^{6+} respectively). The results corresponding to clinically relevant compartments of metal ion concentrations are illustrated in Figure 3.4B.

Figure 3.3 Effect of Co²⁺ and Cr⁶⁺ on osteoblast activity after 3 days

Following initial 24 hr incubation, SaOS-2 cells were treated with metal ions for 48 hr and their activity measured by MTS assay. The data shown is relative to activity of untreated cells. **A)** Comparison between Co^{2+} (purple), Cr^{6+} (green) and $Co^{2+}:Cr^{6+}$ (red) combined treatments. The control and its SD are depicted by dashed lines. **B)** Effect on osteoblast activity depicted at clinically relevant concentrations corresponding to normal physiology, patient serum and hip aspirate post-MOMHR. All values are mean ± SD of 3 experiments with 4-6 replicates in each. * indicates significant comparisons between metal concentrations and control, whilst 'c' indicates significance between different metal ion treatments (** $p < 0.01$; ***c $p < 0.0001$).

Figure 3.4 Effect of Co²⁺ and Cr⁶⁺ on osteoblast activity after 7 days

Following initial 24 hr incubation, SaOS-2 cells were treated with metal ions for 6 days and their activity measured by MTS assay. The data is shown relative to activity of untreated cells. **A)** Comparison between Co²⁺ (purple), Cr⁶⁺ (green) and Co²⁺:Cr⁶⁺ (red) combined treatments. The control and its SD are depicted by dashed lines. **B)** Effect on osteoblast activity depicted at clinically relevant concentrations corresponding to normal physiology, patient serum and hip aspirate post-MOMHR. All values are mean ± SD of 3 experiments with 4-6 replicates in each. * indicates significant comparisons between metal concentrations and control, whilst 'a', 'b' and 'c' indicate significance between different metal ion treatments (*a $p<0.05$; **b $p<0.01$; ***c $p<0.0001$).

3.2.3 Effect of Co^{2+} and Cr^{3+} on ALP activity

The effect of Co^{2+} and Cr^{3+} on ALP activity was assessed after 3 days and 7 days by measuring pNPP hydrolysis by the cell lysate. The cells were treated with a range of clinically relevant concentrations (0, 5, 50, 500 and 5000µg/L) of Co^{2+}, Cr^{3+} or a combination of Co^{2+} and Cr^{3+} ($Co^{2+}:Cr^{3+}$) at equivalent concentrations. The ALP activity of the cell lysate was corrected for cell number by normalising the data to the total double-stranded DNA content in the lysate as measured by Quant-iT Picogreen dsDNA Assay (section 2.4.1).

After 3 days, a significant reduction in ALP activity was observed for all concentrations of Co^{2+}, Cr^{3+} and $Co^{2+}:Cr^{3+}$ combination treatment compared to the untreated control (Figure 3.5A). A significantly higher ALP activity was observed for $Co^{2+}:Cr^{3+}$ combination treatment (mean ± SD; 88.61±17.04) compared to Cr^{3+} (75.49±23.61) at 50µg/L. However, at the highest concentration of 5000µg/L corresponding to the patient hip aspirates, ALP activity for $Co^{2+}:Cr^{3+}$ (34.97±10.04) was significantly lower to both Co^{2+} (58.79±17.02) and Cr^{3+} (74.39±17.60), with Co^{2+} being significantly lower to Cr^{3+} (Figure 3.5A).

In contrast to the 3 day results, longer exposure of metal ions significantly reduced ALP activity only at the highest concentration of 5000µg/L Co^{2+} (70.61±16.74) and $Co^{2+}:Cr^{3+}$ (29.83±10.12) compared to untreated control (100±9.18) (Figure 3.6A). Comparisons amongst different treatments at 5000µg/L showed a significantly lower ALP activity with $Co^{2+}:Cr^{3+}$ compared to Co^{2+} and Cr^{3+} (90.61±20.05), with Co^{2+} being significantly lower to Cr^{3+} (Figure 3.6A). The ALP activity after 3 days and 7 days corresponding to clinically relevant partitions of metal ion concentrations are illustrated in Figure 3.5B and Figure 3.6B respectively.
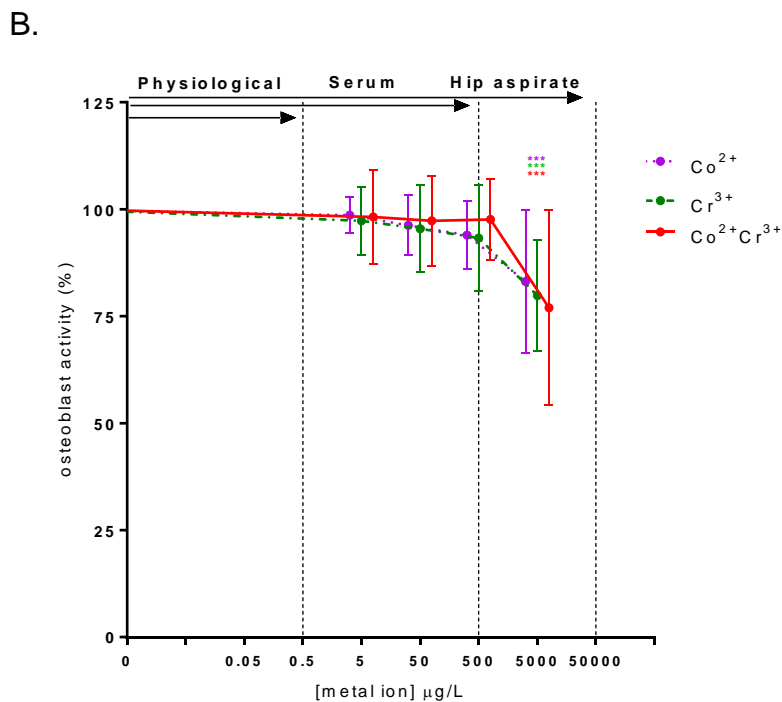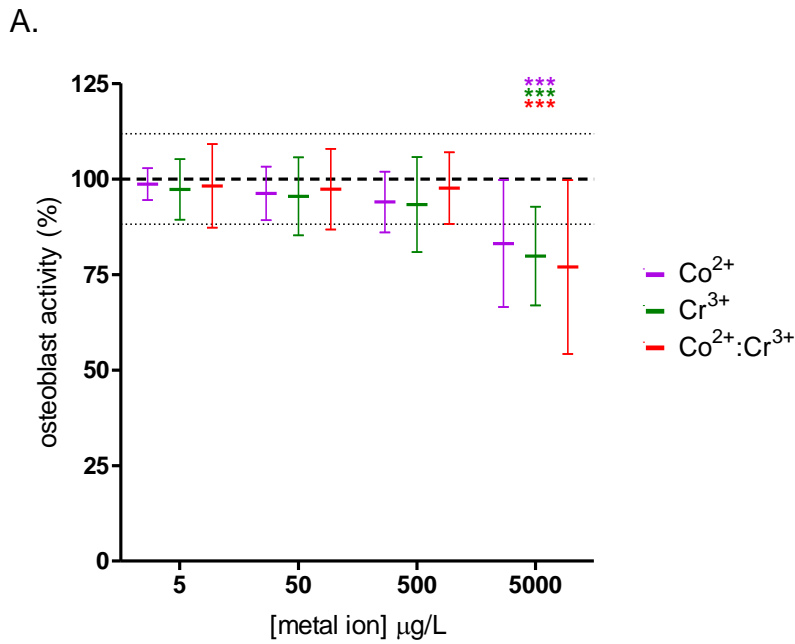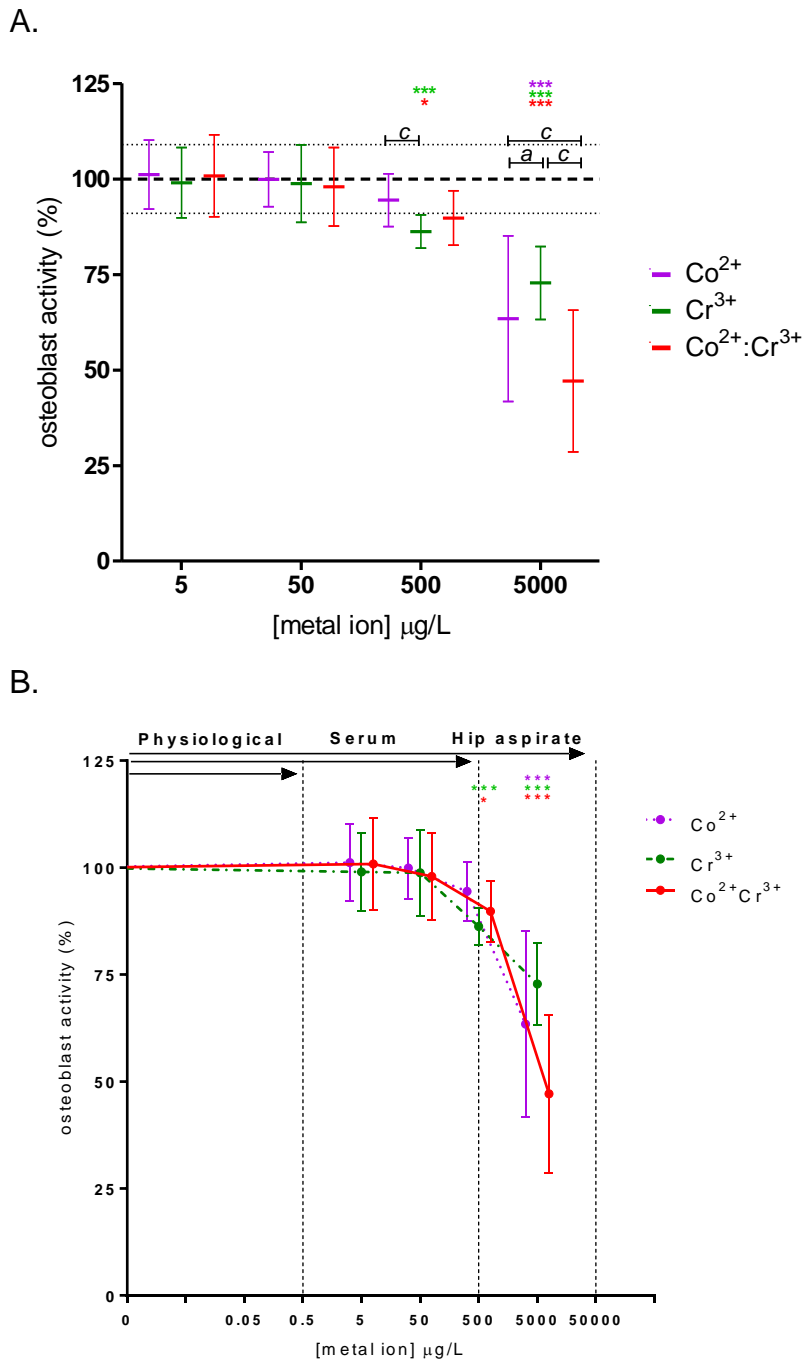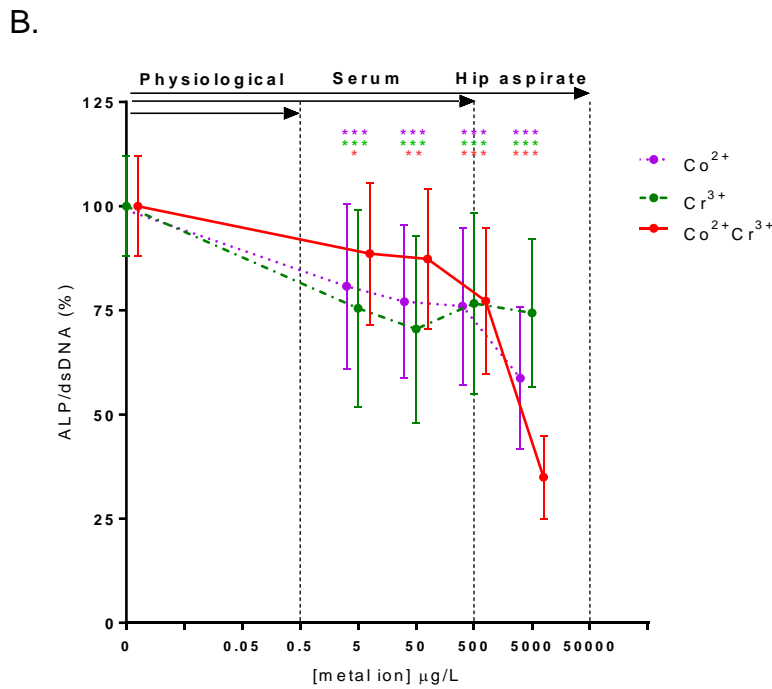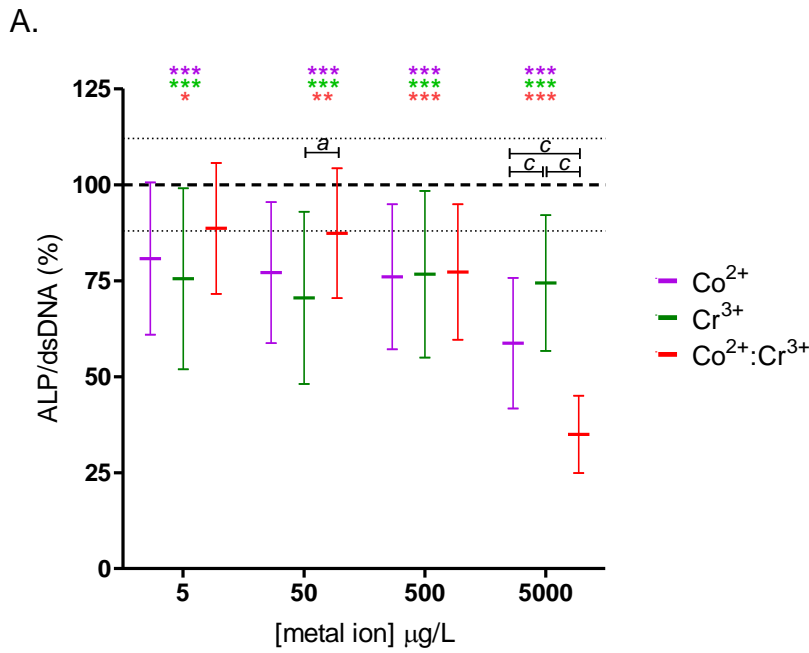
Figure 3.5 Effect of Co²⁺ and Cr³⁺ on osteoblast ALP activity after 3 days

Following initial 24 hr incubation, SaOS-2 cells were treated with metal ions for 48 hr, lysed and ALP activity was measured by pNPP hydrolysis. The data shown is relative to ALP activity of untreated cells. **A)** Comparison between Co^{2+} (purple), Cr^{3+} (green) and Co^{2+}:Cr^{3+} (red) combined treatments. The control and its SD are depicted by dashed lines. **B)** Effect on osteoblast proliferation depicted at clinically relevant concentrations corresponding to normal physiology, patient serum and hip aspirate post-MOMHR. All values are mean ± SD of 4 experiments with 4-6 replicates in each. * indicates significant comparisons between metal concentrations and control, whilst 'a' and 'c' indicate significance between different metal ion treatments (*a $p<0.05$; ** $p<0.01$; ***c $p<0.0001$).

A.

B.

Figure 3.6 Effect of Co^{2+} and Cr^{3+} on osteoblast ALP activity after 7 days

Following initial 24 hr incubation, SaOS-2 cells were treated with metal ions for 6 days, lysed and the ALP activity was measured by pNPP hydrolysis. The data shown is relative to ALP activity of untreated cells. **A)** Comparison between Co^{2+} (purple), Cr^{3+} (green) and Co^{2+}:Cr^{3+} (red) combined treatments. The control and its SD are depicted by dashed lines. **B)** Effect on osteoblast proliferation depicted at clinically relevant concentrations corresponding to normal physiology, patient serum and hip aspirate post-MOMHR. All values are mean ± SD of 3 experiments with 4-6 replicates in each. * indicates significant comparisons between metal concentrations and control, whilst 'c' indicates significance between different metal ion treatments (***c p<0.0001).

3.2.4 Effect of Co^{2+} and Cr^{6+} on ALP activity

The effect of Co^{2+} and Cr^{6+} on ALP activity was assessed at a range of clinically relevant concentrations (0, 0.5, 50, and 500 µg/L) of Co^{2+}, Cr^{6+} or a combination of Co^{2+} and Cr^{6+} ($Co^{2+}:Cr^{6+}$) at equivalent concentrations. The ALP activity of the cell lysate was corrected for cell number by normalising the data to the total double-stranded DNA.

Short-term exposure resulted in a significantly reduced ALP activity for all treatments at 50µg/L and 500µg/L, with Cr^{6+} also resulting in a significant reduction at a lower concentration of 0.5µg/L (mean ± SD; 82.96±19.55) compared to the untreated control (100±14.94), Co^{2+} (95.59±14.23) and $Co^{2+}:Cr^{6+}$ (99.35±13.69) (Figure 3.7A).

The ALP activity after 7 days was significantly elevated for $Co^{2+}:Cr^{6+}$ at 5µg/L (108.2±4.06), whilst a reduction was observed with 50µg/L (91.22±7.14) and 500µg/L (38.25±10.07) compared to the untreated control (100±3.7). ALP activity was also significantly lower for Cr^{6+} treated cells at 500µg/L (52.50±12.15), with Co^{2+} having no effects at any concentration (Figure 3.8A). Comparisons between the different treatments show a significant reduction with $Co^{2+}:Cr^{6+}$ compared to 50µg/L and 500µg/L Co^{2+} (102.70±13.94 and 94.77±8.94 respectively). $Co^{2+}:Cr^{6+}$ was also significantly lower compared to Cr^{6+} at 500µg/L (52.50±12.15). The results corresponding to clinically relevant partitions of metal ion concentrations are illustrated in Figure 3.7B and 4.8B.
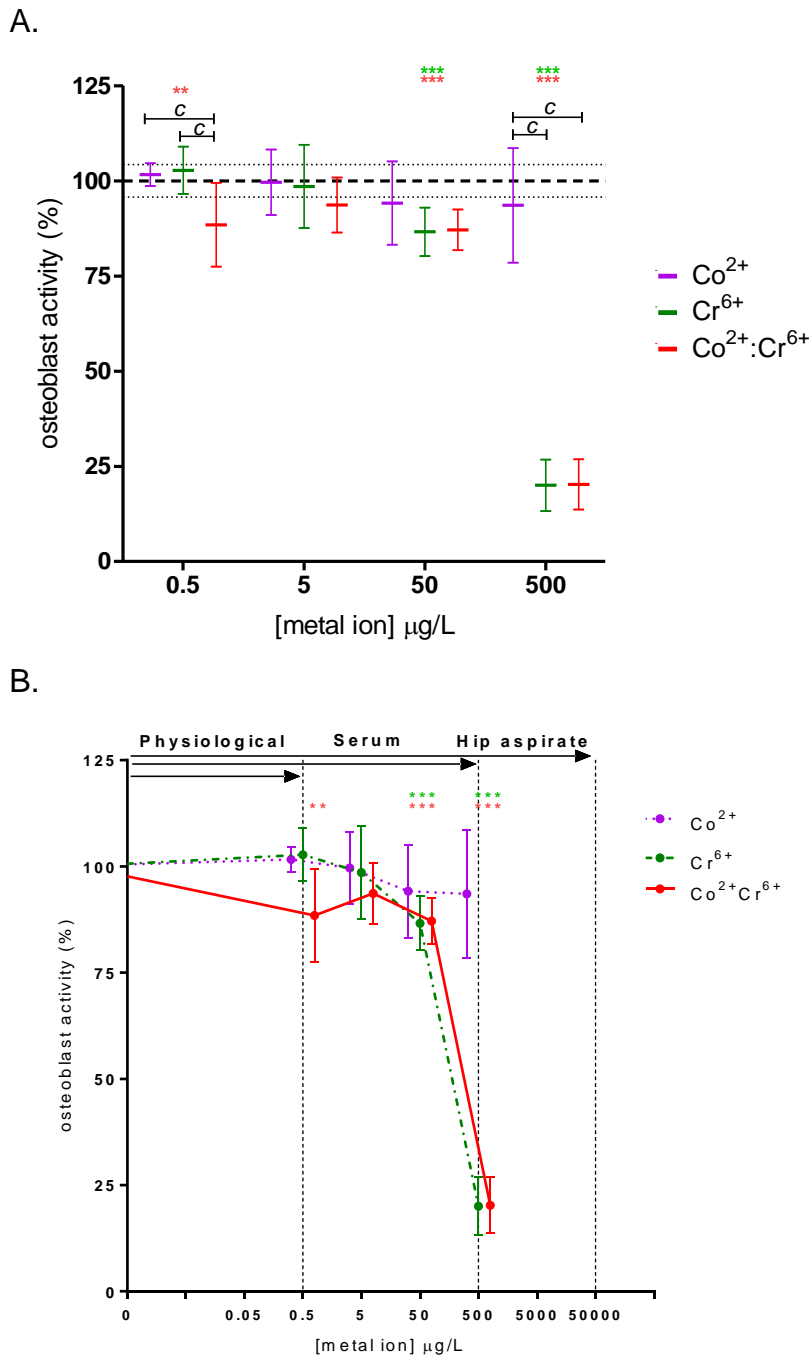
A.

B.
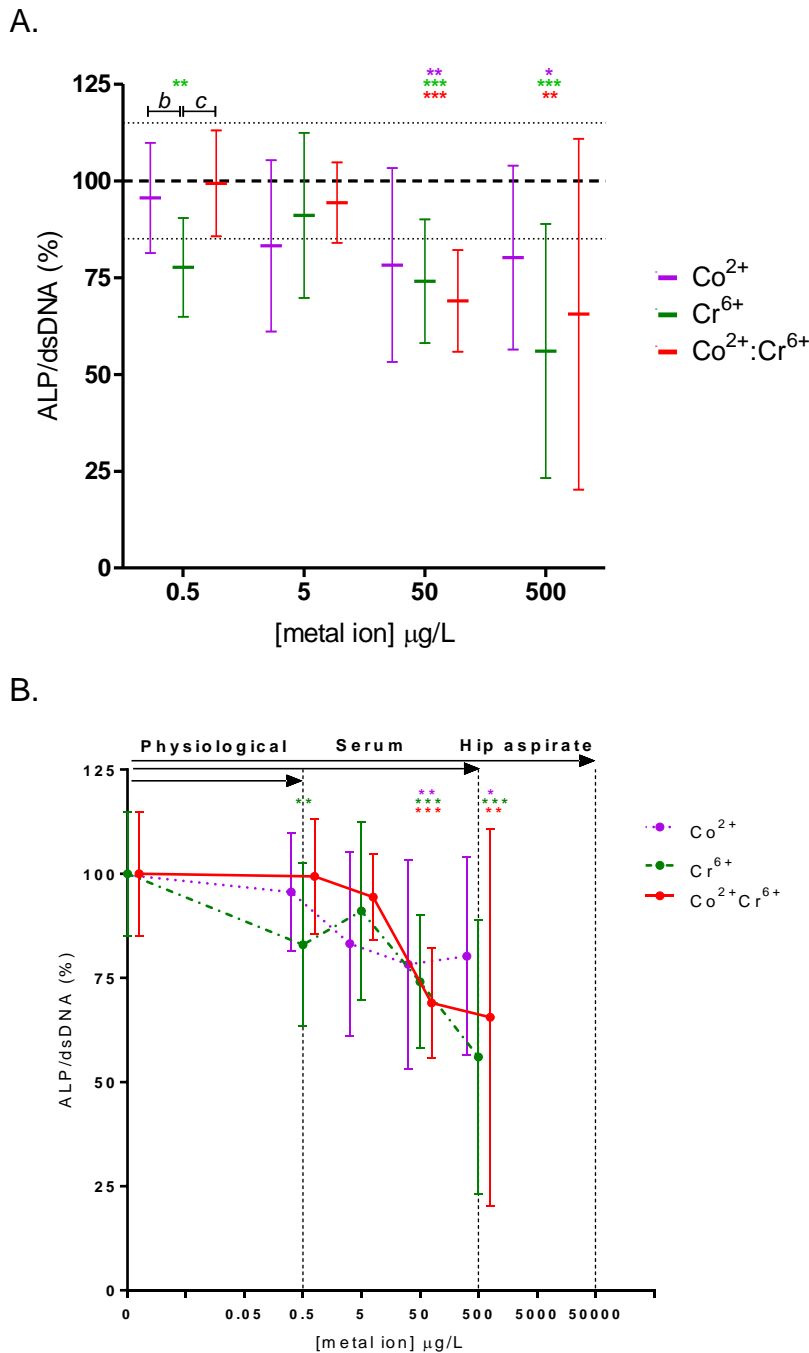
Figure 3.7 Effect of Co²⁺ and Cr⁶⁺ on osteoblast ALP activity after 3 days

Following initial 24 hr incubation, SaOS-2 cells were treated with metal ions for 48 hr, lysed and the ALP activity was measured by pNPP hydrolysis. The data shown is relative to ALP activity of untreated cells. **A)** Comparison between Co²⁺ (purple), Cr⁶⁺ (green) and Co²⁺:Cr⁶⁺ (red) combined treatments. The control and its SD are depicted by dashed lines. **B)** Effect on osteoblast proliferation depicted at clinically relevant concentrations corresponding to normal physiology, patient serum and hip aspirate post-MOMHR. All values are mean ± SD of 4 experiments with 4-6 replicates in each. * indicates significant comparisons between metal concentrations and control, whilst 'b' and 'c' indicate significance between different metal ion treatments (* $p<0.05$; **b $p<0.01$; ***c $p<0.0001$).
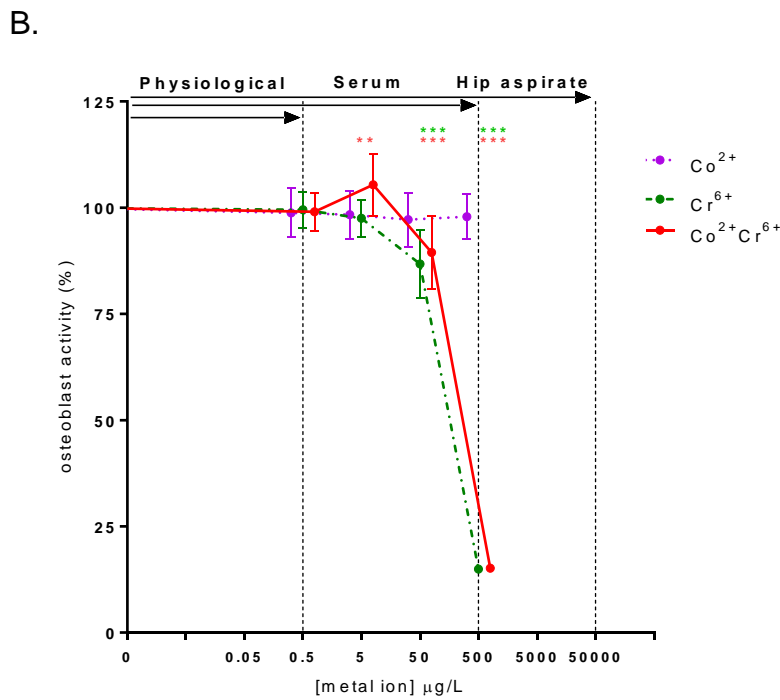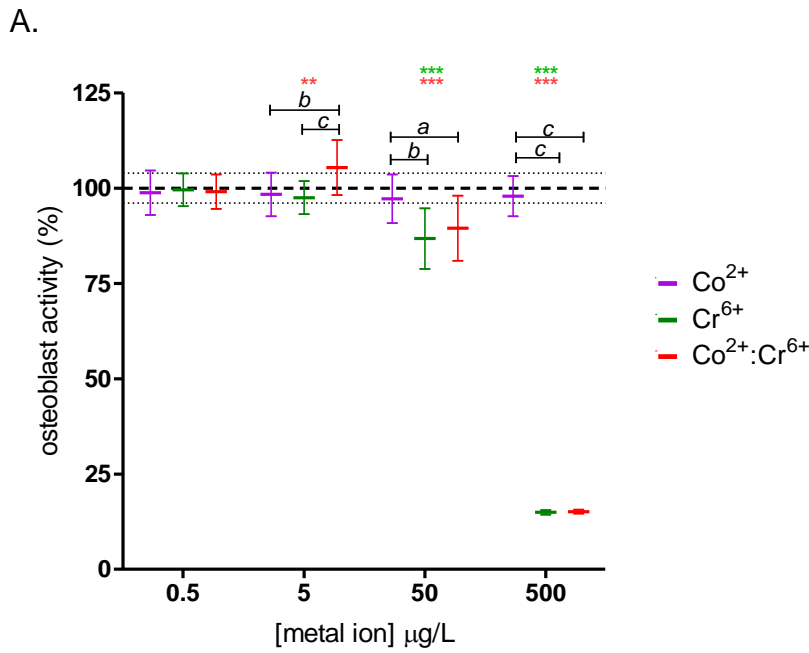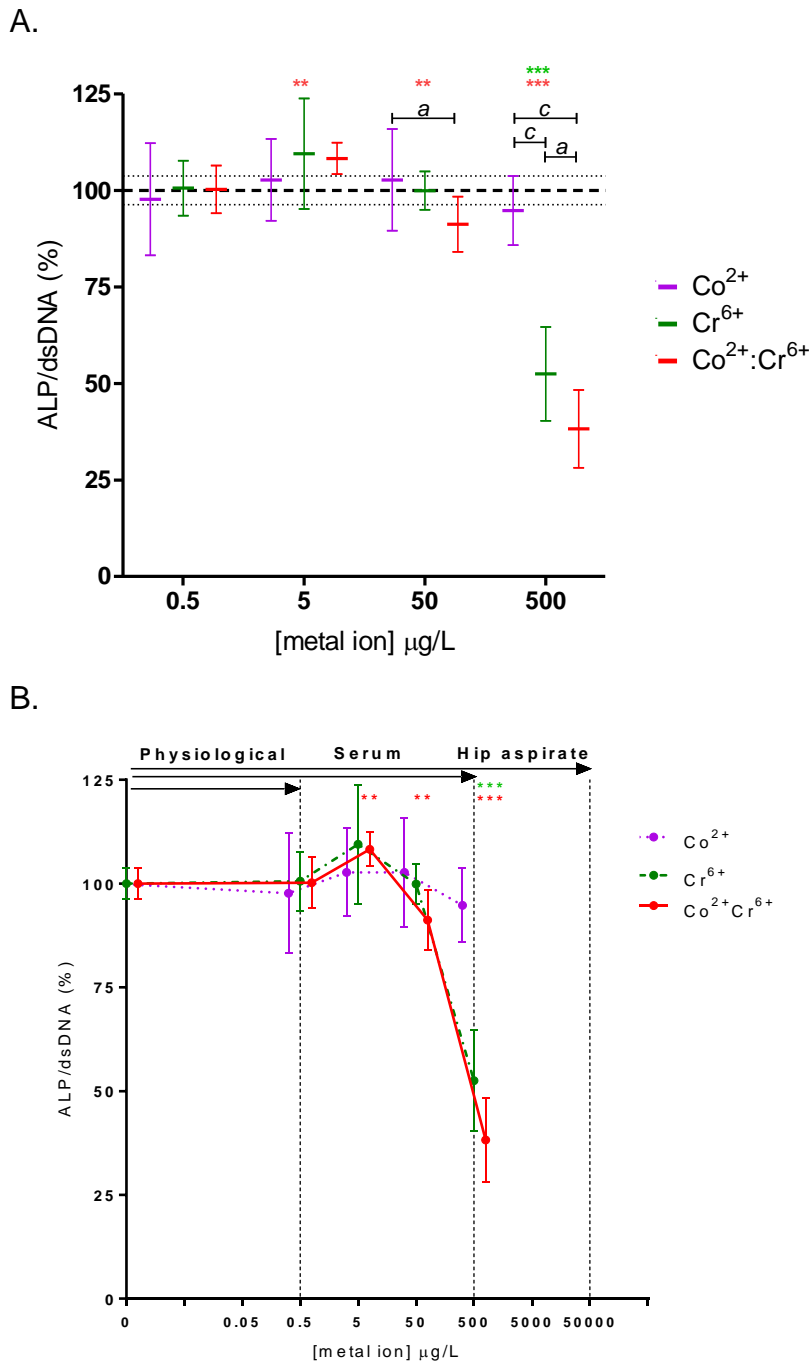
Figure 3.8 Effect of Co²⁺ and Cr⁶⁺ on osteoblast ALP activity after 7 days

Following initial 24 hr incubation, SaOS-2 cells were treated with metal ions for 6 days, lysed and the ALP activity was measured by pNPP hydrolysis. The data shown is relative to ALP activity of untreated cells. **A)** Comparison between Co²⁺ (purple), Cr⁶⁺ (green) and Co²⁺:Cr⁶⁺ (red) combined treatments. The control and its SD are depicted by dashed lines. **B)** Effect on osteoblast proliferation depicted at clinically relevant concentrations corresponding to normal physiology, patient serum and hip aspirate post-MOMHR. All values are mean ± SD of 3 experiments with 4-6 replicates in each. * indicates significant comparisons between metal concentrations and control, whilst 'a' and 'c' indicate significance between different metal ion treatments (*a* $p<0.05$; ** $p<0.01$; ***c* $p<0.0001$).

3.2.5 Effect of Co^{2+} and Cr^{3+} on osteoblast mineralisation

The ability of SaOS-2 cells to mineralise in presence of clinically relevant concentrations and combinations of Co^{2+} and Cr^{3+} was assessed by measuring the area of Alizarin red stained calcium deposits.

A significant decrease in mineralised area was observed for Cr^{3+} treated cells at 500µg/L (57.64±39.89) and 5000µg/L (32.54±34.20), whilst $Co^{2+}:Cr^{3+}$ exposure had a biphasic response with significant increase at 500µg/L (141.10±68.86) and a decrease at 5000µg/L(13.02±14.13) compared to the untreated control (100.00±35.00)(Figure 3.9A). Co^{2+} treatment significantly reduced mineralisation area only at the highest concentration of 5000µg/L (27.21±24.93) corresponding to the hip aspirate. The increase in mineralisation area with 500µg/L of $Co^{2+}:Cr^{3+}$ was also significantly higher compared to similar concentrations of Co^{2+} (76.30±41.87) and Cr^{3+} (57.64±39.89) (Figure 3.9A). The results corresponding to clinically relevant partitions of metal ion concentrations are illustrated in Figure 3.9B.

3.2.6 Effect of Co^{2+} and Cr^{6+} on osteoblast mineralisation

A biphasic response in mineralisation area was observed with Cr^{6+} exposure with 5µg/L resulting in a significant increase (140.4±50.42) and 500µg/L causing a significant decrease (26.36±15.74) compared to the untreated control (100.00±33.82). $Co^{2+}:Cr^{6+}$ treatment significantly decreased mineralisation area at the highest concentration of 500µg/L (33.35±24.76), with Co^{2+} treatment alone having no effect at any concentrations (Figure 3.10A). At 500µg/L Cr^{6+} and $Co^{2+}:Cr^{6+}$ treatments resulted in a significantly lower mineralisation compared to Co^{2+} (91.65± 35.17) (Figure 3.10A). The results corresponding to clinically relevant partitions of metal ion concentrations are illustrated in Figure 3.10B.

A.

B.
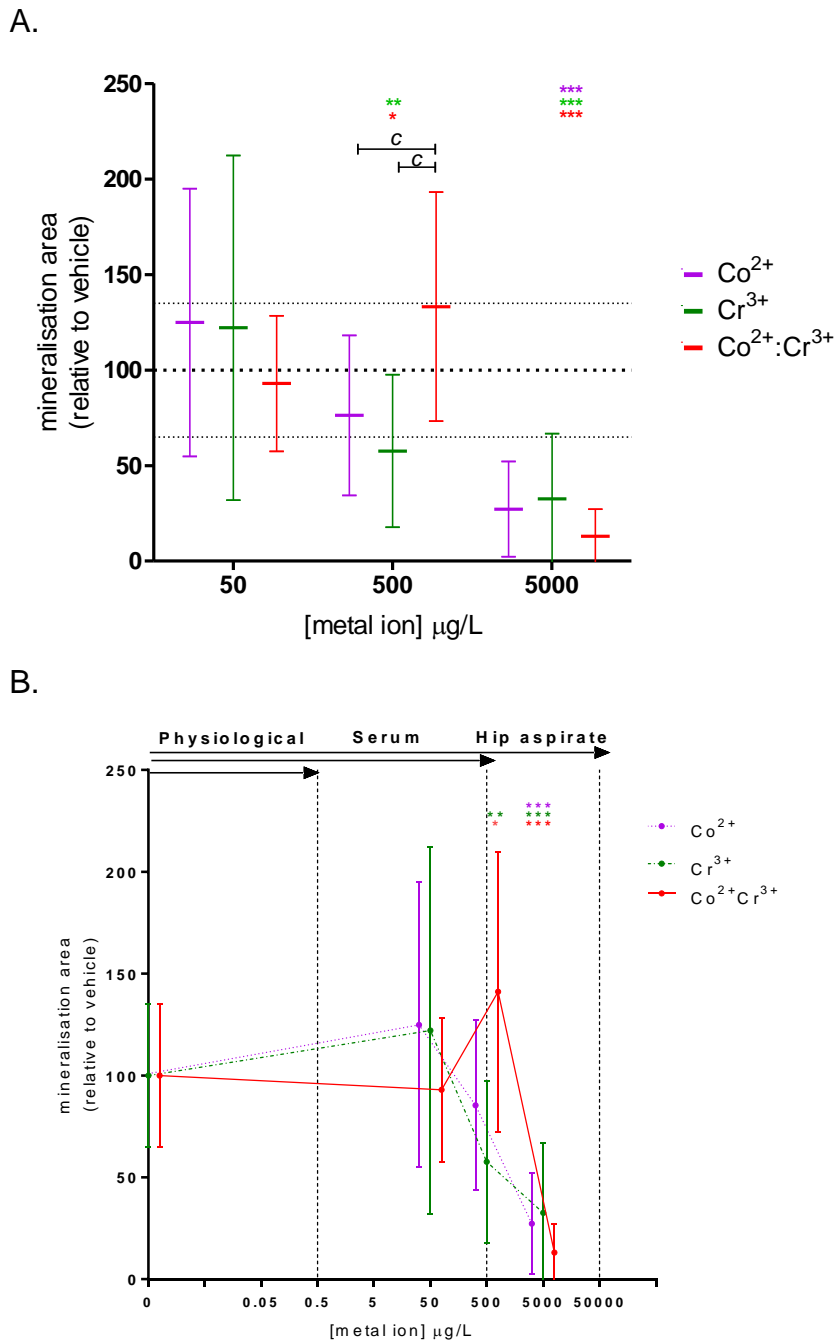
Figure 3.9 Effect of Co^{2+} and Cr^{3+} on osteoblast mineralisation over 7 days

Following confluence, SaOS-2 cells were treated with metal ions for 7 days in osteogenic media and mineralisation assessed by Alizarin Red staining. The data is shown relative to mineralisation area of untreated cells. **A)** Comparison between Co^{2+} (purple), Cr^{3+} (green) and Co^{2+}:Cr^{3+} (red) combined treatments. The control and its SD are depicted by dashed lines. **B)** Effect on mineralisation area depicted at clinically relevant concentrations corresponding to normal physiology, patient serum and hip aspirate post-MOMHR. All values are mean ± SD of 4 experiments with 4-6 replicates in each. * indicates significant comparisons between metal concentrations and control, whilst 'c' indicates significance between different metal ion treatments (*$p < 0.05$; ** $p < 0.01$; ***c $p < 0.0001$).
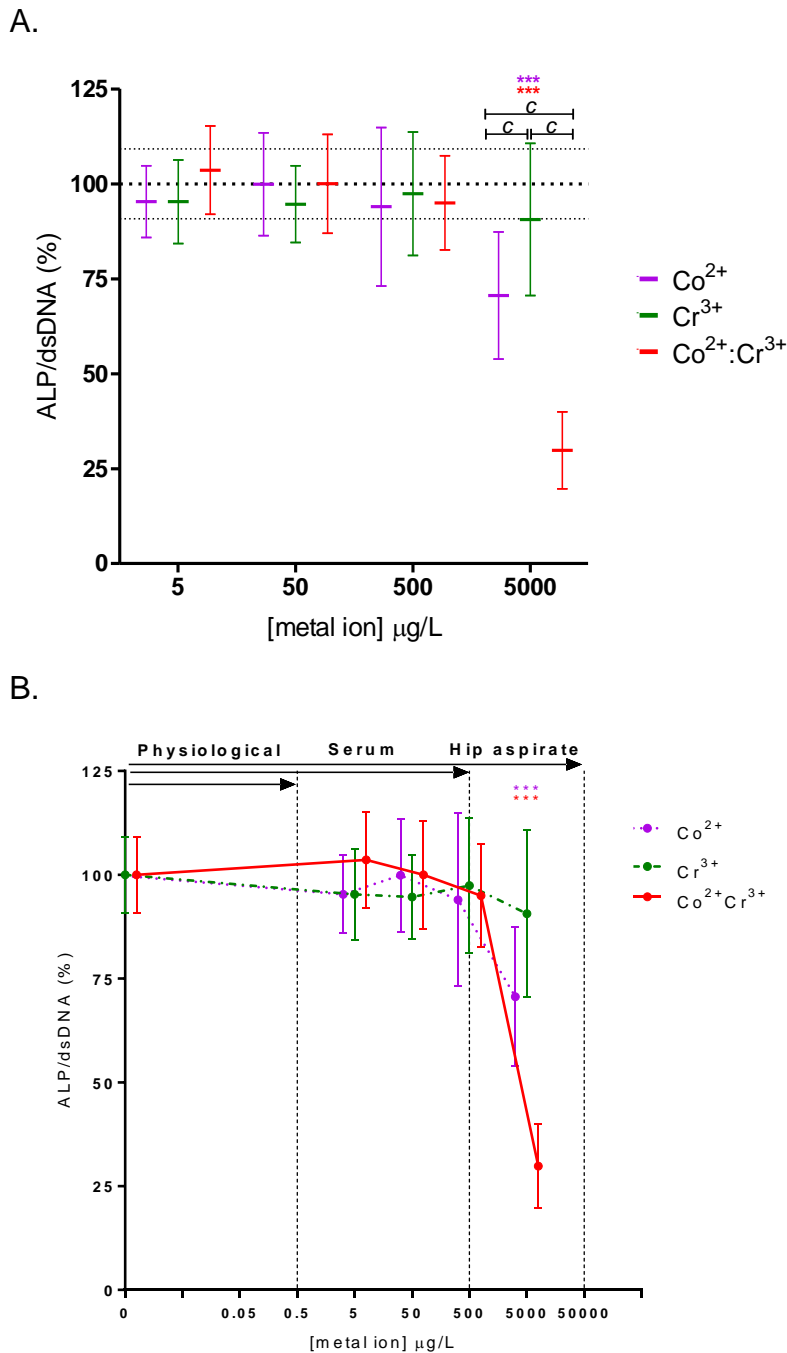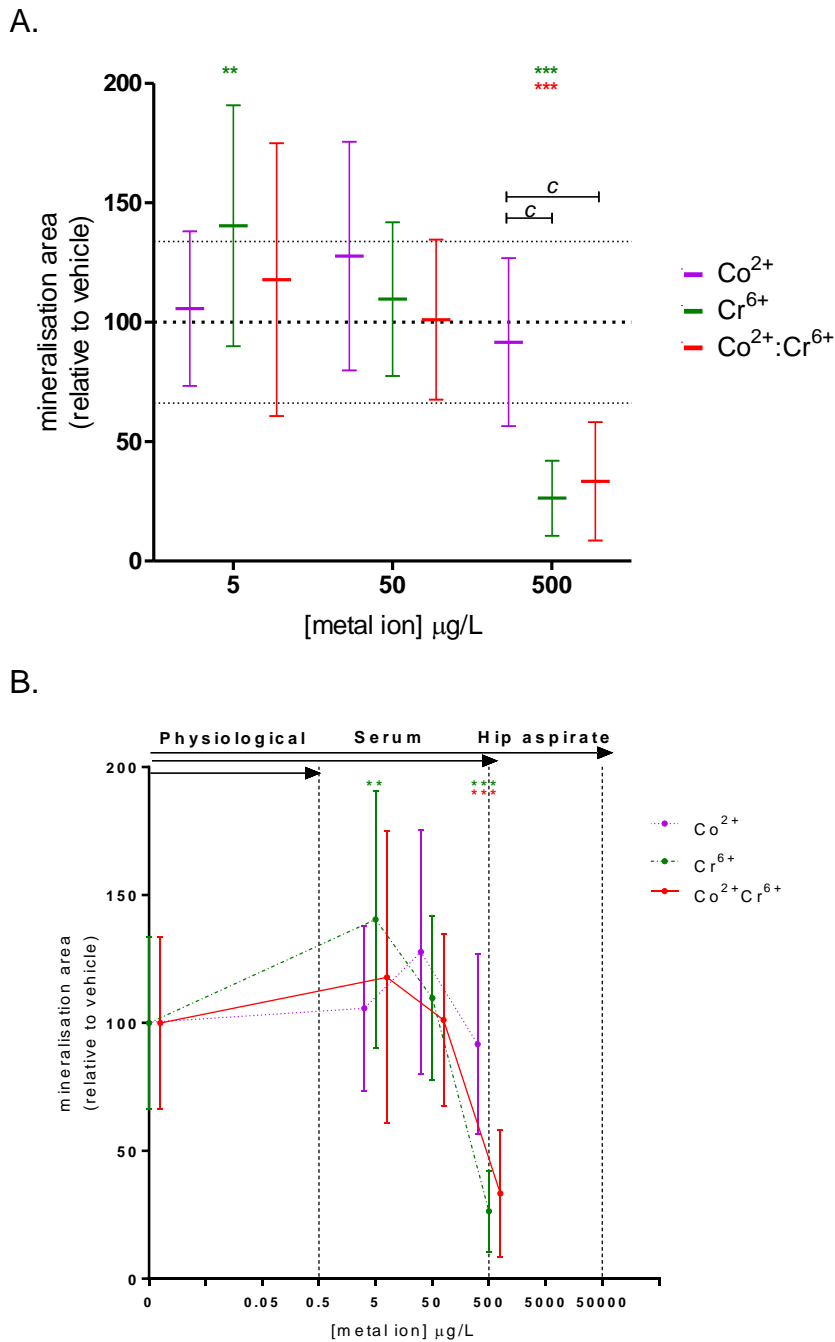
Figure 3.10 Effect of Co²⁺ and Cr⁶⁺ on osteoblast mineralisation over 7 days

Following confluence, SaOS-2 cells were treated with metal ions for 7 days in osteogenic media and mineralisation assessed by Alizarin Red staining. The data is shown relative to mineralisation area of untreated cells. **A)** Comparison between Co²⁺ (purple), Cr⁶⁺ (green) and Co²⁺:Cr⁶⁺ (red) combined treatments. The control and its SD are depicted by dashed lines. **B)** Effect on mineralisation area depicted at clinically relevant concentrations corresponding to normal physiology, patient serum and hip aspirate post-MOMHR. All values are mean ± SD of 3 experiments with 4-6 replicates in each. * indicates significant comparisons between metal concentrations and control, whilst 'c' indicates significance between different metal ion treatments (** $p<0.01$; ***c $p<0.0001$).

3.3 Discussion

Osseointegration of the MOMHR prostheses is vital for its long term survivorship and osteoblast survival and function are integral to this process. Cobalt and chromium ions are known to be released in the periprosthetic environment due to wear and corrosion of the prosthesis and particular debris (Mathew, *et al* 2012). Previous studies have investigated the effects of cobalt and chromium ions on osteoblast survival and function, predominantly in isolation. However, *in situ*, the cells are likely to be exposed to a combination of both cobalt and chromium ions as they release from implant and particle surfaces (Mathew, *et al* 2012, Shahgaldi, *et al* 1995, Witzleb, *et al* 2006). This study examined the effects of Co^{2+}, Cr^{3+} and Cr^{6+} at clinically equivalent combinations on osteoblast-like SaOS-2 cell activity, differentiation and mineralisation ability.

3.3.1 Osteoblast activity

In addition to previously described detrimental effects with individual ions (Andrews, *et al* 2011), we demonstrate an additive detrimental effect on cellular activity with chronic exposure to $Co^{2+}:Cr^{3+}$ at concentrations observed in the hip aspirate (5000µg/L).

The observed additive effect implies the existence of common downstream mechanisms for Co^{2+} and Cr^{3+} mediated effects. The various mechanisms via which the detrimental effects of Co^{2+} are thought to be mediated include generation of reactive oxygen species by Fenton reactions (Leonard, *et al* 1998), mitochondrial stress (Battaglia, *et al* 2009) and genotoxicity (Baldwin, *et al* 2004, Qiao and Ma 2013) with inhibition of DNA repair (Kopera, *et al* 2004). The detrimental effects with Cr^{3+} are more controversial as it is thought to be relatively impermeable to cell membranes (Gray and Sterling 1950) causing little toxicity at clinically observed concentrations (Eastmond, *et al* 2008). Conversely, Cr^{3+} has also been implicated in disruption of cell membrane integrity (Suwalsky, *et al* 2008), and with DNA replication and repair (Dai, *et al* 2009, El-Yamani, *et al* 2011) resulting in genotoxicity and cell apoptosis of mammalian cells (Andersson, *et al* 2007, Rudolf and Cervinka 2009). With the observed additive effect and the reported mechanisms of action, it can be hypothesised that Co^{2+} and Cr^{3+} mediated toxicity at high concentrations occurs via the common pathway of

genotoxicity compounded by impaired ability for DNA repair. In support of this, a study investigating oxidative DNA damage with metal ion combinations described an additive effect with Fe^{2+} and Cr^{3+} (Moriwaki, *et al* 2008). The similarity between the chemistries of Fe^{2+} and Co^{2+} might result in their similar interaction with Cr^{3+}.

These results are however, in contrast to a previous study which reports an increase in SaOS-2 cell activity after 48 hours exposure to $Co^{2+}:Cr^{3+}$ combined treatment (Zijlstra, *et al* 2012). Unlike our study, a ratio of 1:2 for $Co^{2+}:Cr^{3+}$ combined treatment was used in that study. The different metal ion ratio used may result in an altered cellular response, as highlighted by previous studies describing different interactions between metal ions based on their combination ratios (Ince, *et al* 1999).

In contrast to $Co^{2+}:Cr^{3+}$, the combined effect of $Co^{2+}:Cr^{6+}$ at high concentrations is dominated by Cr^{6+} toxicity, with no additive or synergistic effect. Cr^{6+} is a known carcinogen and its high toxicity has been studied extensively for different cell types, including osteoblasts (Andrews, *et al* 2011, Ning and Grant 1999). Exposure to Cr^{6+} has been shown to increase cellular oxidative stress (Fu, *et al* 2008), cause DNA damage (Ovesen, *et al* 2013), lipid peroxidation (Susa, *et al* 1997) and alter protein expression and function (Raghunathan, *et al* 2010). Our previous study with SaOS-2 cells describes a much lower IC_{50} of 114.4µg/L for Cr^{6+} compared to 7955µg/L for Co^{2+} (Andrews, *et al* 2011), and this high toxicity is likely to mask any interactions with Co^{2+}.

However, at lower concentrations (0.5µg/L), acute exposure to $Co^{2+}:Cr^{6+}$ had a synergistic detrimental effect whilst longer exposure did not show any interaction at that concentration. On the contrary, a mild stimulatory effect was observed with longer treatments at concentrations corresponding to patient serum post-MOMHR. The inhibition of DNA repair by Co^{2+} coupled with oxidative stress caused by Cr^{6+} might result in the observed synergistic effect. The difference in cellular response to duration of metal ion exposure suggests an adaptive response with chronic treatments. Indeed, Raghunathan *et al.*, have demonstrated reduced osteoblast toxicity with chronic exposure to Cr^{6+} (2009). They described an increase in reduced glutathione (GSH) expression and

glutathione reductase activity which are cellular defence proteins against oxidative stress (Raghunathan, *et al* 2009).

The mild stimulatory effect observed in cellular activity can be due to metal ion generated ROS, which has been shown to induce *c-fos* expression in chondrocytes, which are cells from the same mesenchymal cell lineage (Lo and Cruz 1995). *C-fos* is an immediate-early gene and a known modulator of cellular activity and proliferation in osteoblasts (Sunters, *et al* 2004).

The data from these studies does not distinguish between the changes in cellular activity as a result of cellular stress or cell death following metal ion treatments. A measure of cell numbers by dsDNA quantification could be used to correct the data for cell death.

3.3.2 Alkaline phosphatase activity

The effect of metal ion treatments on alkaline phosphatase (ALP) activity was more pronounced compared to their effects on cellular activity. Cr^{3+}, which only elicited an effect on cellular activity at hip aspirate concentrations, reduced cellular ALP activity at all concentrations tested after 3 days. A similar reduction in ALP activity was also observed for all concentrations Co^{2+} and $Co^{2+}:Cr^{3+}$ treatments at the same time-point. At the later time-point of 7 days, metal ion treatments did not have the same effect on ALP activity, with significant reduction seen only at the highest concentration. This might be due to the variation in normal expression of ALP by osteoblasts. ALP activity in SaOS-2 cells increases from day 3 of the culture, peaks at day 7 and subsequently falls to baseline levels by day 11 (Appendix 1, Figure A2). With 50% higher ALP activity at day 7 compared to day 3, metal ions fail to elicit an effect except at concentrations corresponding to the hip aspirate. A similar trend is also observed with Cr^{6+} and $Co^{2+}:Cr^{6+}$ treatments, with reduction in ALP activity seen at low concentration after day 3 but not after day 7.

Alkaline phosphatase is a highly conserved metalloenzyme containing two Zn^{2+} and one Mg^{2+} nuclear centres which are vital to its catalytic activity (Kozlenkov, *et al* 2002, Stec, *et al* 2000). Substitution of Zn^{2+} by Co^{2+} has been described for

a variety of proteins (Witkiewicz-Kucharczyk and Bal 2006) including ALP which shows ~500 fold reduction in its enzymatic activity (Wang, *et al* 2005). The difference in ALP activity at two time-points supports the substitution hypothesis as it is likely that with abundance of ALP at day 7, the substitution of Zn^{2+} in a fraction of the enzyme does not result in a significant reduction in overall ALP activity with low metal ion concentrations. In addition, Cr^{6+} has been demonstrated to reduce ALP activity when interacting with the enzyme prior to substrate binding possibly by interacting with residues in the active pocket and/or by oxidative alteration of certain amino acids (Bogé, *et al* 1992). The same study described a restoration of ALP activity by extracellular reduction of Cr^{6+} to Cr^{3+} making reasons for the observed reduction in ALP activity with this species unclear (Bogé, *et al* 1992). It is possible that the effects with Cr^{3+} are more indirect with induced cellular stress described above resulting in a reduction in ALP production.

Previous studies investigating the effects of metal wear on ALP activity in osteoblasts focus on the effects of particulate wear primarily in MG63 cells (Allen, *et al* 1997, Lohmann, *et al* 2000, Ramachandran, *et al* 2006), which a recent study demonstrated to be a poor resemblance to primary osteoblasts compared to SaOS-2 cells when investigating biomaterials (Czekanska, *et al* 2013). The results in this study are in accordance to previous studies which show decrease in ALP activity with Co and Cr ions (Andrews, *et al* 2011, Dai, *et al* 2011, McKay, *et al* 1996), Cr^{6+} being more detrimental than Cr^{3+} (McKay, *et al* 1996).

In addition, this study highlights the interactions of metal ions in combinations, with $Co^{2+}:Cr^{3+}$ exhibiting an additive effect at day 3 but a synergistic effect at day 7. The synergism observed at day 7 is probably due to the different modes action of Co^{2+} and Cr^{3+} described above, with Co^{2+} substituting the Zn^{2+} centre of ALP whilst Cr^{3+} having more indirect effects by causing cellular stress. The effects of Cr^{6+} dominated in the $Co^{2+}:Cr^{6+}$ treatments, similar to the effects observed with cellular activity. The data here suggests that the presence of metal ions have a detrimental effect on cellular differentiation in osteoblasts and subsequently affecting mineralisation and osseointegration.

3.3.3 Mineralisation ability

The metal ion concentrations used in the mineralisation experiments were in the high serum and hip-aspirate range to focus on the effects at the bone/implant surfaces. The results suggest a decrease in mineralisation at hip-aspirate concentrations of all metal ions and no interactions were observed with $Co^{2+}:Cr^{3+}$ and $Co^{2+}:Cr^{6+}$ compared to individual metal ion treatments. These results are in agreement with most studies describing the effect of metal ions on osteoblast mineralisation with individual metal ions (Andrews, *et al* 2011, Anissian, *et al* 2002, Sun, *et al* 1997). These are expected results based on the decreased cellular and ALP activity described in previous sections.

The results show a significant increase in mineralisation with $Co^{2+}:Cr^{3+}$ at systemic concentrations of 500µg/L and Cr^{6+} at 5µg/L. One possible explanation for this, as described previously for chondrocytes (Gibson 1998), could be an increase in nucleation of the matrix around apoptotic bodies formed by slight increase in cell death by the combined treatment (Figure 3.2). A recent study from our Department has reported a 5% increase in total bone mineral density in patients with MOMHR (Prentice, *et al* 2013). The results from this chapter showing small increases in osteoblast activity, ALP activity and mineralisation with combination treatments at serum concentrations are consistent with the clinical observation.

3.4 Conclusion

In conclusion, this study describes the concentration and time dependent detrimental effects of metal ions and their clinically relevant combinations on osteoblasts survival. Metal ions are likely to have severe impact on prosthesis integration and periprosthetic bone health as evidenced by reduced cellular activity, ALP activity and mineralisation observed in our study at concentrations observed in the hip aspirate. In addition, the results suggest that previous studies investigating individual metal ions underestimate the *in situ* clinical effects of wear and corrosion. Co^{2+} and Cr^{3+} combinations predominantly show an additive effect suggesting common downstream mechanisms, whilst Cr^{6+} dominates the effects of $Co^{2+}:Cr^{6+}$ combination.

Chapter 4 - Effect of metal ions on differentiation and function of human osteoclasts

4.1 Introduction

The periprosthetic bone environment is dynamic in nature, involving coordination between several different cell types for successful integration of the implant. In the previous chapter, the effects of prostheses derived metal ions on bone forming osteoblast cells is discussed, while in this chapter their effect on bone resorbing osteoclast cells is explored.

As described in the previous chapter (section 3.1), periprosthetic bone remodelling is essential for proper fixation of cementless components of metal-on-metal hip replacements (MOMHR) and total hip arthroplasty (THA). Osteoclasts play a vital role in this process by remodelling the initial woven bone formed by osteoblasts at the implant surfaces, which is subsequently replaced by lamellar bone that ensures implant fixation (Mavrogenis*, et al* 2009, Reinholt*, et al* 1990). Additionally, osteoclast mediated bone resorption is considered to be the final cellular consequence of implant related adverse reactions, ultimately causing osteolysis and implant failure. Most investigations regarding osteoclasts have focussed on their increased differentiation and activity caused by a monocyte/macrophage mediated inflammatory response to particulate and metal debris in the periprosthetic environment (Lacey*, et al* 2009, Sabokbar*, et al* 1998, Tamaki*, et al* 2008). However, the direct effects of metal ions on osteoclast survival and function remain unclear.

Previous investigations by Nichols and Puleo (1997) (Nichols and Puleo 1997) reported a decrease in rat marrow derived osteoclastic resorption with sub-lethal doses of Co^{2+} and Cr^{6+}. A study with mature rabbit osteoclasts demonstrated a reduction in osteoclast resorption with Co^{2+} but not with Cr^{3+}, while the osteoclast numbers remained unchanged (Rousselle*, et al* 2002). A more recent study by Mabillleau et al. (Mabilleau*, et al* 2012) using primary human osteoclasts reported an increase in osteoclast number accompanied with reduced resorption with Co^{2+}, while a decrease in osteoclast number was observed with Cr^{3+} at concentrations corresponding to hip aspirate (100µM, ~5000µg/L). Although these studies extend our understanding of osteoclast response to metal ions, the

effects of Co and Cr ions on primary human osteoclasts at more clinical concentrations seen systemically and in the local environment are unknown.

This chapter characterises the direct effects of Co and Cr ions at a clinically relevant concentration range on primary human osteoclast survival and function as evaluated *in vitro* by measuring cell number and resorption ability. The concentration range for metal ions (0-10000µg/L) used in this study is derived from previously reported patient levels for different physiological compartments (section 1.5). An increase in the highest concentration from 5000µg/L to 10000 µg/L, was to maintain consistency with previous experiments conducted by Dr Rebecca Andrews, adding biological replicates to the existing data-set (Andrews*, et al* 2011). In addition to characterising the effects of individual metal ions, the effect of combined metal ions on osteoclast survival and function is studied at systemic concentrations post-surgery simulated by culturing osteoclasts derived from MOMHR and THA patients in autologous serum (see section 2.6). This experiment would also highlight any inherent differences in the osteoclastogenic capability of precursors conditioned by post-surgery systemic environment.

4.2 Results

4.2.1 Effect of Co^{2+}, Cr^{3+} and Cr^{6+} on differentiating osteoclasts

Human peripheral blood mononuclear cells were isolated from healthy volunteers and cultured on dentine disks in osteoclastogenic media (see section 2.6). Following a 48h incubation, the media was supplemented with Co^{2+} or Cr^{3+} (0, 0.5, 5, 50, 500 and 10000µg/L), or Cr^{6+} ions (0, 0.5, 5, 50, 500 and 5000µg/L), which was replenished every 2-3 days till end of culture on day 21. A lower range of concentrations was chosen for Cr^{6+} due to its high cellular toxicity observed previously. The dentine disks were fixed in 10% buffered formalin, TRAcP stained and quantified for osteoclast number and percentage resorption by point counting (see section 2.7).

Treatment with Co^{2+} ions had no effect on osteoclast number up to 50µg/L (Figure 4.1A). A decrease was observed with increasing concentrations with significant reduction in number of TRAcP positive osteoclasts observed for 10000µg/L (mean±SD, 24.20±58.31) compared to untreated controls (100.00± 52.88). Total resorption and resorption ability of osteoclasts followed a slightly different pattern, with a transient rise in resorption at lower serum concentrations followed by complete suppression of resorption at 10000µg/L (Figures 4.1B and 4.3A-C).

Treatment with Cr^{3+} resulted in a biphasic response for both osteoclast number and resorption (Figures 4.1A–B and 4.3D–F), with concentrations of up to approximately 5µg/L resulting an increased osteoclast number, total resorption and increased ability to resorb. At higher concentrations, osteoclast number returned to physiological baseline, with resorption (4.46±11.34) and resorption ability (2.71±6.6) significantly reduced at 10000µg/L compared to untreated controls (100.00±96.05 and 100±119.96).

Cr^{6+} ions had the greatest inhibitory effect on the formation of functional osteoclasts. Increasing Cr^{6+} resulted in complete inhibition of osteoclast survival and subsequent resorption at concetrations ≥50µg/L (Figures 4.1A–B and 4.3G–I).
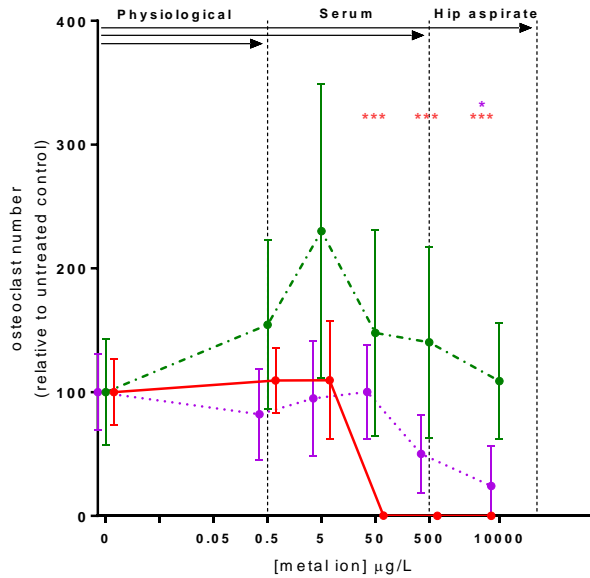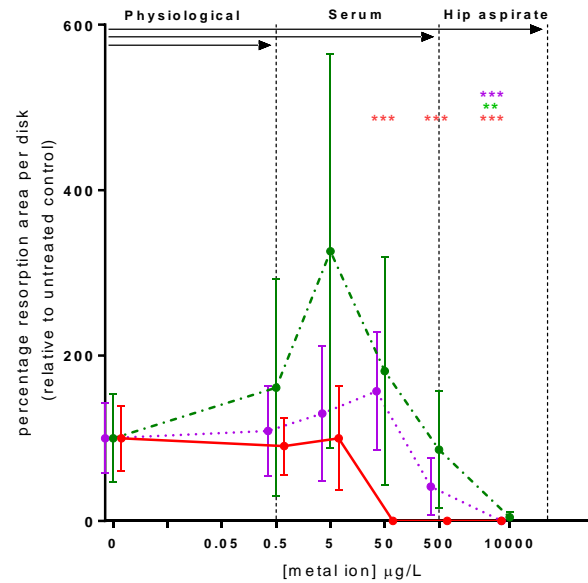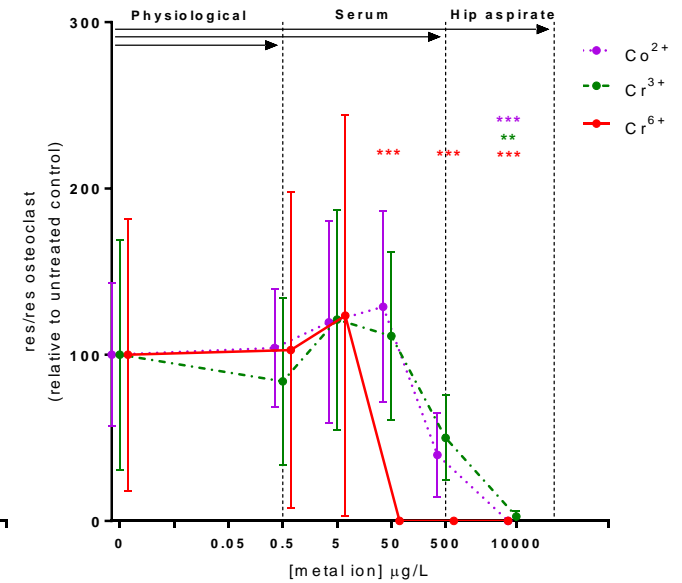
Figure 4.1 Effect of Co²⁺, Cr³⁺ and Cr⁶⁺ on differentiating osteoclasts

Following initial 48h incubation, monocyte isolated from peripheral blood of healthy volunteers were treated with metal ions and the number of osteoclasts and percentage resorption quantified at the end of a 21 day culture. The data shown is relative response to untreated cells from individual experiments for Co²⁺ (purple), Cr³⁺ (green) and Cr⁶⁺ (red) treatments over a clinically relevant concentration range corresponding to normal physiology, patient serum and hip aspirate post-MOMHR. **A)** Effect on osteoclast number, **B)** Effect on percentage resorption by osteoclasts, and **C)** Effect on resorption ability of osteoclasts. All values are mean ± 95%CI of experiments from 3 different volunteers with 4-6 replicates in each (* $p<0.05$; **$p<0.01$; *** $p<0.0001$).

4.2.2 Effect of Co^{2+}, Cr^{3+} and Cr^{6+} on mature osteoclasts

To determine the effects of metal ions on fully functional mature human osteoclasts, human monocytes were isolated, seeded onto dentine disks and cultured in osteoclastogenic media till the onset of resorption (typically day 14). Subsequently, the osteoclast culture medium was replaced to include 0.5µg/L to 1000µg/L Co^{2+} and Cr^{3+}, and 0.5µg/L to 5000µg/L Cr^{6+} ions for the last 7 days of culture.

The response to Co^{2+} and Cr^{3+} treatments was different to that seen for differentiating osteoclasts, with no transient increase in cell number or activity found at lower concentrations. Seven days treatment with Co^{2+} ions ≥500µg/L reduced mature osteoclast number (mean ± SD, 39.76±27.39 and 50.29±88.35) compared to untreated controls (100.00 ± 47.90, Figure 4.2A) whilst, total amount of resorption per disk and percentage resorption per resorbing osteoclasts (resorption ability) was only reduced at the highest concentration (9.56±12.38 and 37.95±77.79) (Figures 4.2B and 4.3 J-L).

Treatment with Cr^{3+} ions significantly reduced mature osteoclast number (55.56±46.43), resorption per disk (29.75±42.55) and resorption ability (35.34±40.14), but only at the 10000µg/L dose (Figures.4.2 A-B and 4.3 M–O). No trend towards increased osteoclast number or resorption was seen for mature osteoclasts at the lower Cr^{3+} concentration range.

Treatment with Cr^{6+} ions had the greatest detrimental effect with no osteoclasts surviving at concentrations of 500µg/L and 5000µg/L, accompanied by a significant reduction in resorption per disk (45.81±62.74 and 12.36±12.02 respectively) (Figures 4.2A-B and 4.3 P–R). Resorption observed at 500µg/L and 10000µg/L (Figure 4.2B) without corresponding viable osteoclasts (Figure 4.2A), reflects the osteoclast activity prior to metal ion treatments after the onset of resorption.
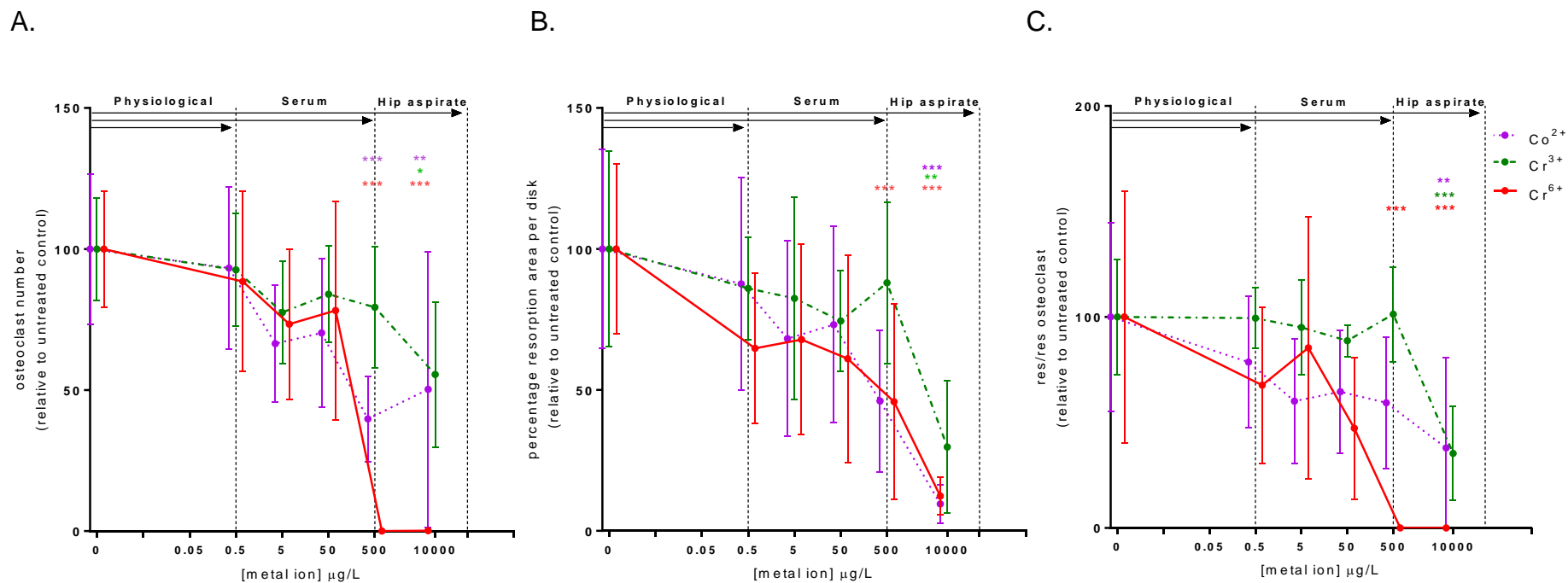
Figure 4.2 Effect of Co^{2+}, Cr^{3+} and Cr^{6+} on mature osteoclasts

Following the onset of resorption, mature osteoclasts differentiated from peripheral blood mononuclear cells of healthy volunteers were treated with metal ions for one week and the number of osteoclasts and percentage resorption quantified at the end of the culture. The data shown is relative response to untreated cells from each individual experiment for Co^{2+} (purple), Cr^{3+} (green) and Cr^{6+} (red) treatments over a clinically relevant concentration range corresponding to normal physiology, patient serum and hip aspirate post-MOMHR. **A)** Effect on osteoclast number, **B)** Effect on percentage resorption by osteoclasts, and **C)** Effect on resorption ability of osteoclasts. All values are mean ± 95%CI of experiments from 3 different volunteers with 4-6 replicates in each (* $p<0.05$; ** $p<0.01$; *** $p<0.0001$).

99
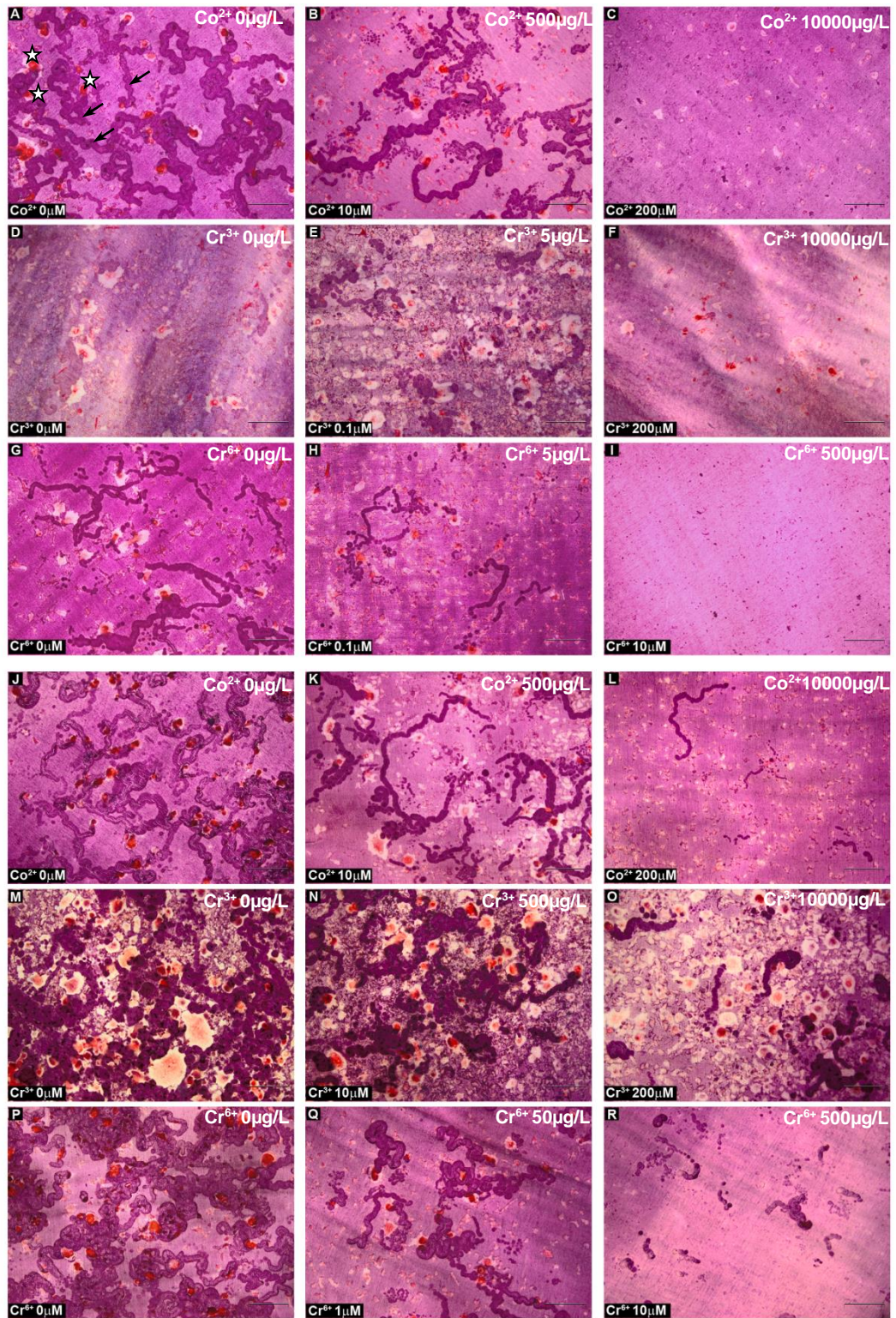
Figure 4.3 Effect of metal ions on osteoclasts – representative images

Representative images of TRAcP stained osteoclasts on dentine discs illustrating the effect of metal ions on differentiating (A–I), and mature osteoclasts (J–R) at the indicated concentrations. Typical fields of view of cells following treatment; A–C and J–L treated with Co^{2+}, D–F and M–O with Cr^{3+}, G-I and P–R with Cr^{6+}. Scale bar 200 µ. Reprinted from Bone, 49 (4); Andrews et al. 'Effects of cobalt and chromium ions at clinically equivalent concentrations after metal-on-metal hip replacement on human osteoblasts and osteoclasts: implications for skeletal health' 717-723, Copyright (2011), with permission from Elsevier.

100

4.2.3 Effect of Co^{2+}, Cr^{3+} and Cr^{6+} on osteoclast TRAcP activity

Total TRAcP activity was assessed for both differentiating and mature osteoclasts by measuring phosphate substrate hydrolysis under acidic conditions, with the data corrected for total protein content as measure by a BCA assay (Figure 4.4) (see section 2.8). To assess the effect of metal ions on efficiency of the enzymatic reaction, the data was corrected for TRAcP content as measured by a sandwich-ELISA (Figure 4.5).

A significant decrease in total TRAcP activity was observed for Cr^{6+} treated differentiating osteoclasts at a concentration of 500µg/L. No changes were observed Co^{2+} and Cr^{3+}, although a trend towards decrease in activity with increasing concentrations was observed. A similar trend in total TRAcP activity was also observed in Co^{2+} and Cr^{6+} treated mature osteoclasts

Differentiating osteoclasts displayed a trend towards increased TRAcP enzyme functioning with all metal ion treatments (Figure 4.5A-C), reaching significance only for Cr^{3+} at a concentration of 500µg/L (mean ± SD, 2.33 ± 0.53) compared to untreated controls (1.0 ± 0.18) (p<0.05, Figure 4.5B). TRAcP enzyme functioning as measured for mature osteoclasts remained unchanged for all concentrations of Co^{2+}, Cr^{3+} and Cr^{6+} (Figure 4.5D-F).
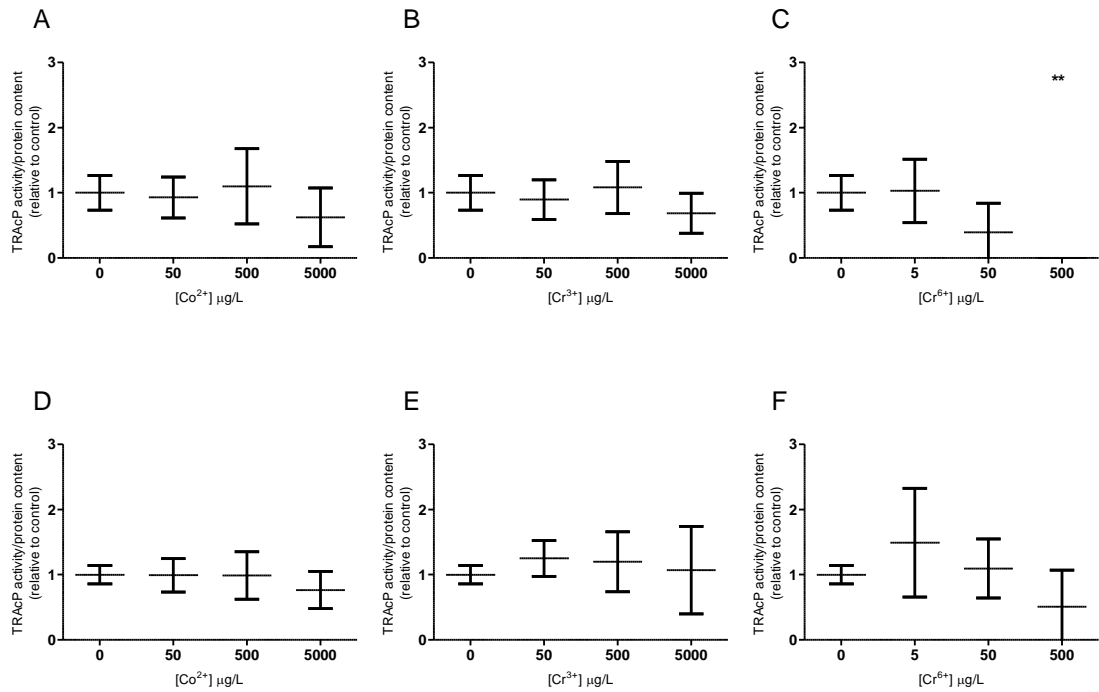
Figure 4.4 Effect of metal ions on osteoclast total TRAcP activity

TRAcP activity was assessed by measuring phosphate substrate hydrolysis for differentiating (A-C) and mature (D-F) osteoclasts exposed to clinically relevant concentrations of Co^{2+} (A,D), Cr^{3+} (B,E) and Cr^{6+} (C,F). Data (mean ± SD) is corrected for total protein content as measured by a BCA assay and represents 3 replicate wells for each treatment from 2 separate experiments (* $p<0.05$).
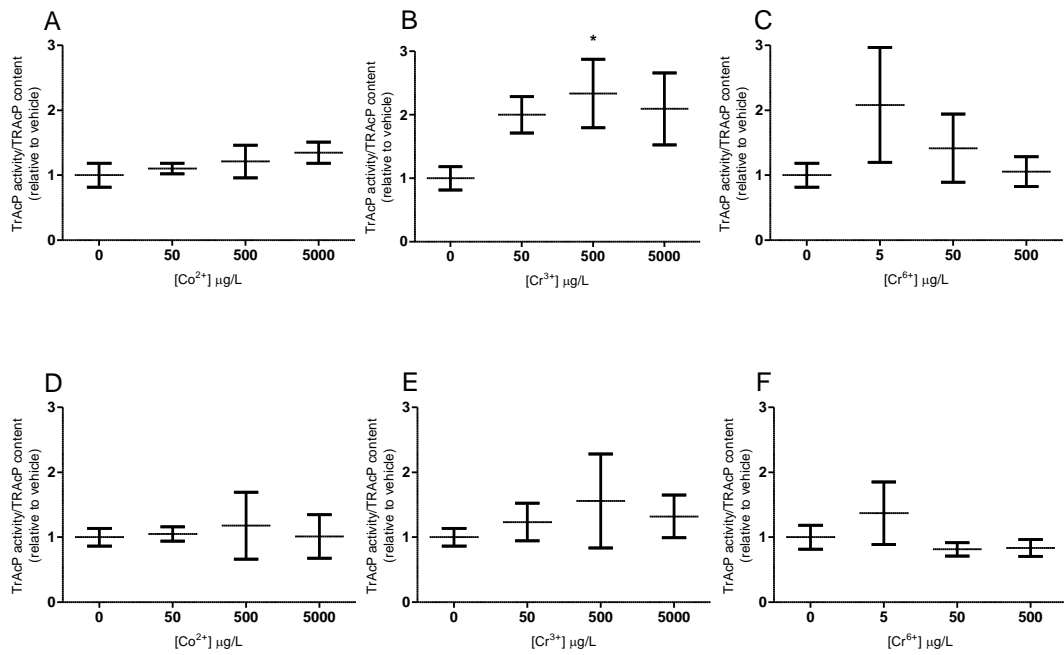
Figure 4.5 Effect of metal ions on osteoclast TRAcP enzymatic activity

TRAcP activity was assessed by measuring phosphate substrate hydrolysis for differentiating (A-C) and mature (D-F) osteoclasts exposed to clinically relevant concentrations of Co^{2+} (A, D), Cr^{3+} (B,E) and Cr^{6+} (C,F). Data (mean ± SD) is corrected for total TRAcP content as measured by ELISA and represents 3 replicate wells for each treatment (* $p<0.05$).

4.2.4 Effect of circulating metal ions on osteoclast survival and function

To investigate the effect of metal ions released into systemic circulation on the survival and function of osteoclasts, monocytes were isolated from donors with well-functioning MOMHR or THA and cultured in media supplemented with RANKL and M-CSF (osteoclastogenic media). In addition, cultures from both sets of donors were monitored for the onset of resorption, at which point the cells were treated with either osteoclastogenic media, autologous serum from the donors or serum from matched case/control donors plus RANKL and M-CSF (Figure 4.6). The rationale behind these set of experiments was to investigate the effect of elevated levels of metal ions in the MOMHR patient circulation on systemic osteoclasts and whether this could be rescued by the serum from THA patients (with low metal ion concentrations).

At the end of the culture, the cells were TRAcP stained and quantified for total osteoclast number, number of resorbing osteoclasts and percentage resorption using CellD Software Package, Olympus (see section 2.7.2). The concentrations of Co and Cr in the donor serum as measured by ICP-MS are detailed below in Table 4.1.

Pairs	MOMHR (Case)			THA (Control)		
	Identifier	[Co]µg/L	[Cr]µg/L	Identifier	[Co]µg/L	[Cr]µg/L
1	MIS14	3.7	3.8	MIS71	0.2	<0.2
2	MIS53	4.6	6.7	MIS63	0.2	<0.2
3	MIS02	13.4	10.1	MIS38	1.8	<0.2
4	MIS26	3.6	6.8	MIS65	0.2	<0.2
5	MIS24	15	21.1	MIS67	0.1	<0.2

Table 4.1 Metal ion levels in MoMHR donors and THA controls

Metal concentration as measured by ICP-MS in serum from donors with well-functioning MOMHR and THA.
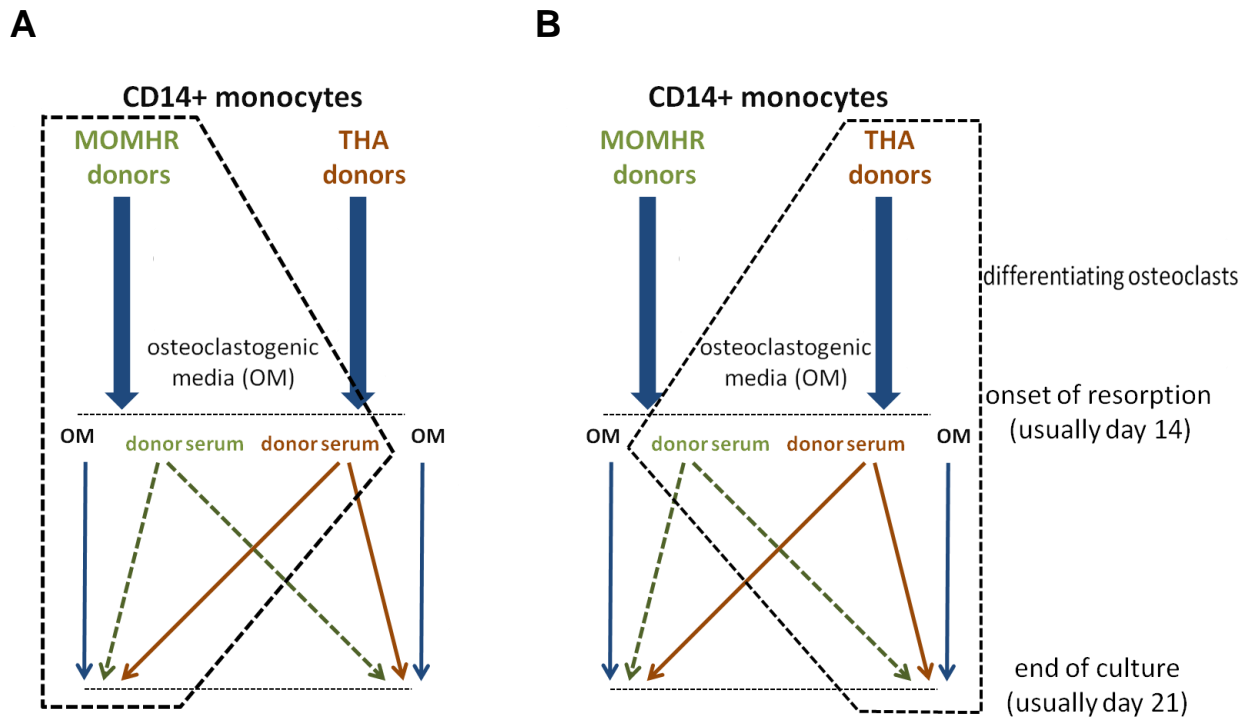
Figure 4.6 Experimental designs to investigate effect of systemic metal ions on osteoclasts survival and function.

CD14+ monocytes from donors with MOMHR **(A)**, and THA **(B)** were cultured on dentine disks in osteoclastogenic media (OM) till maturity. Thereafter, the cells were treated for 7 days with autologous serum, serum from the matched case/control or the normal OM which served as the control. At the end of the experiment, the cells were TRAcP stained and quantified for osteoclast numbers, percentage resorption and resorbing ability of osteoclasts.

4.2.4.1 Effect of MOMHR versus THA on survival and function of osteoclasts

This section highlights any inherent difference between the osteoclastic potential of monocytes from MOMHR and THA donors, when grown in normal osteoclastogenic media.

The results show a significant increase in osteoclast number for cells differentiated from donors with THA (mean ± 95%CI, 280.2 ± 104.2) compared to MOMHR (121.4 ± 32.1) ($p<0.05$, Figure 4.7A). The total resorption by cells isolated from donors with THA (8.62 ± 3.51) was also higher compared to cells from MOMHR (4.56 ± 1.77) ($p<0.05$, Figure 4.7C). There were no differences between the percentage of resorbing osteoclasts and resorption capacity of osteoclasts for cells from the two donor groups.
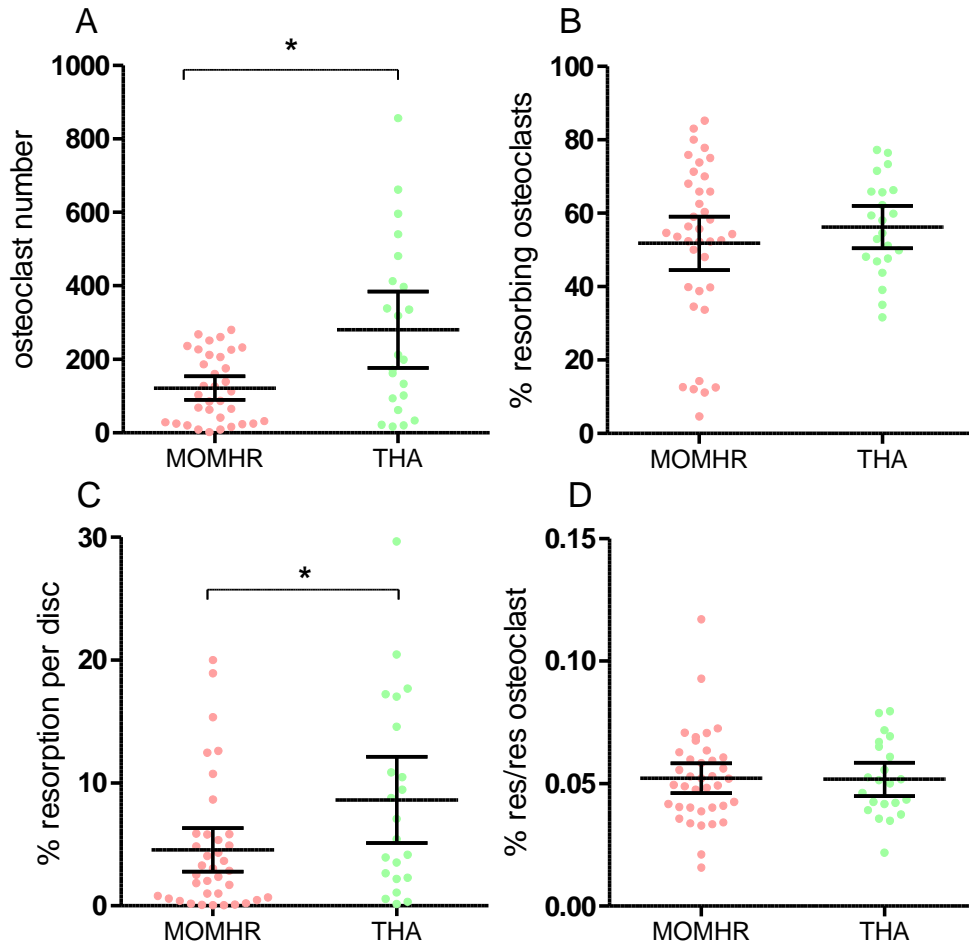
Figure 4.7 Comparison between survival and function of osteoclasts isolated from MOMHR donors and THA controls.

Following the onset of resorption the cells were cultured in normal osteoclastogenic media, serum from donors with MOMHR, or serum from donors with THA for 7 days. Subsequently, the cells were TRAcP stained and quantified. Effect on **A)** osteoclast number, **B)** percentage of resorbing osteoclasts, **C)** percentage resorption, and **D)** resorption per resorbing osteoclast. Graphs represent data (mean ± 95%CI) from 5 case-control pairs, with 4-6 dentine disks per treatment for each donor (* p <0.05).

4.2.4.2 Effect of circulating metal ions on osteoclasts from MOMHR donors

Mature osteoclasts differentiated from donors with MOMHR showed a significant increase in total osteoclast number when cultured in autologous MOMHR serum (mean ± 95%CI, 167.1 ± 41.1) ($p<0.05$) compared to cells grown in osteoclastogenic media (100 ± 21.6) (Figure 4.8A). No significant difference was observed in the fraction of resorbing osteoclasts and percentage resorption per disk between all conditions. However, a significant reduction in the resorption per resorbing osteoclast (resorbing ability) was observed for osteoclasts treated with autologous MOMHR serum (73.9 ± 6.0) compared to the cells in control media (100 ± 9.8) ($p<0.05$) (Figure 4.8D).
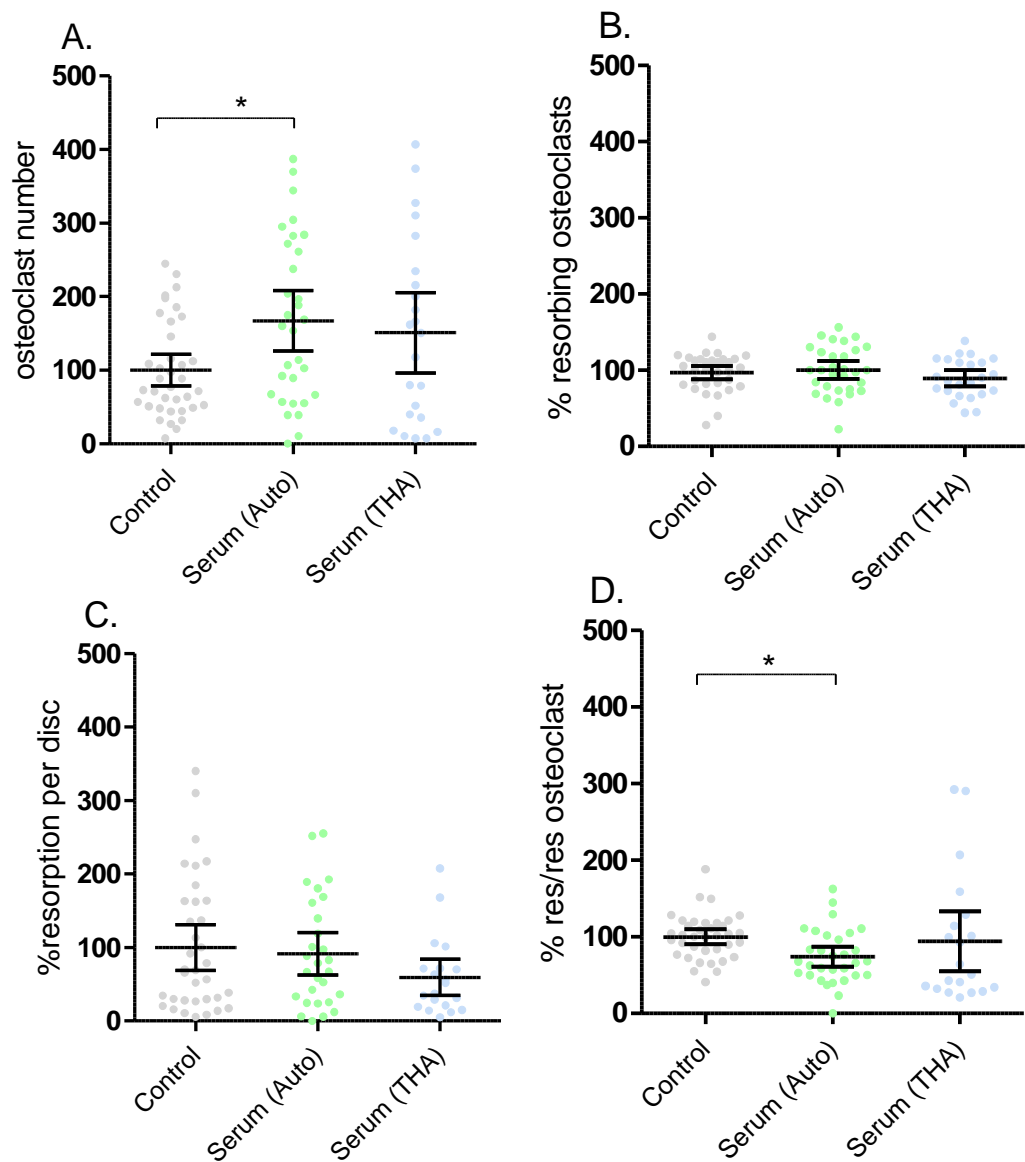
Figure 4.8 Effect of circulating metal ions on survival and function of osteoclasts from donors with MOMHR

Peripheral blood mononuclear cells from MOMHR donors were isolated and differentiated to resorbing osteoclasts on dentine disks. Following the onset of resorption the cells were cultured in normal osteoclastogenic media, autologous serum from the donors, or serum from a control donor with THA for 7days. Subsequently, the cells were TRAcP stained and quantified. Effect on **A)** osteoclast number, **B)** percentage of resorbing osteoclasts, **C)** percentage resorption, and **D)** resorption per resorbing osteoclast. Graphs represent data (mean ± 95%CI) from 5 case-control pairs, with 4-6 dentine disks per treatment for each donor (* $p < 0.05$; ** $p < 0.01$).

4.2.4.3 Effect of circulating metal ions on osteoclasts from THA donors

For osteoclasts cultured from peripheral blood of donors with THA, a significant increase in osteoclast numbers were observed with serum from donors with MOMHR (190.7 ± 37.1) ($p < 0.0001$) compared to cells in control media (100 ± 25.9) (Figure 4.9A). A significant decrease in resorption ability was observed for osteoclasts treated with serum from THA donors (76.4 ± 31.2) ($p < 0.05$) and serum from donors with MOMHR (70.4 ± 21.8) ($p < 0.01$) compared to cells in control media (100 ±11.9) (Figure 4.9D). There were no significant changes observed in resorbing osteoclasts or total resorption between for any treatments.
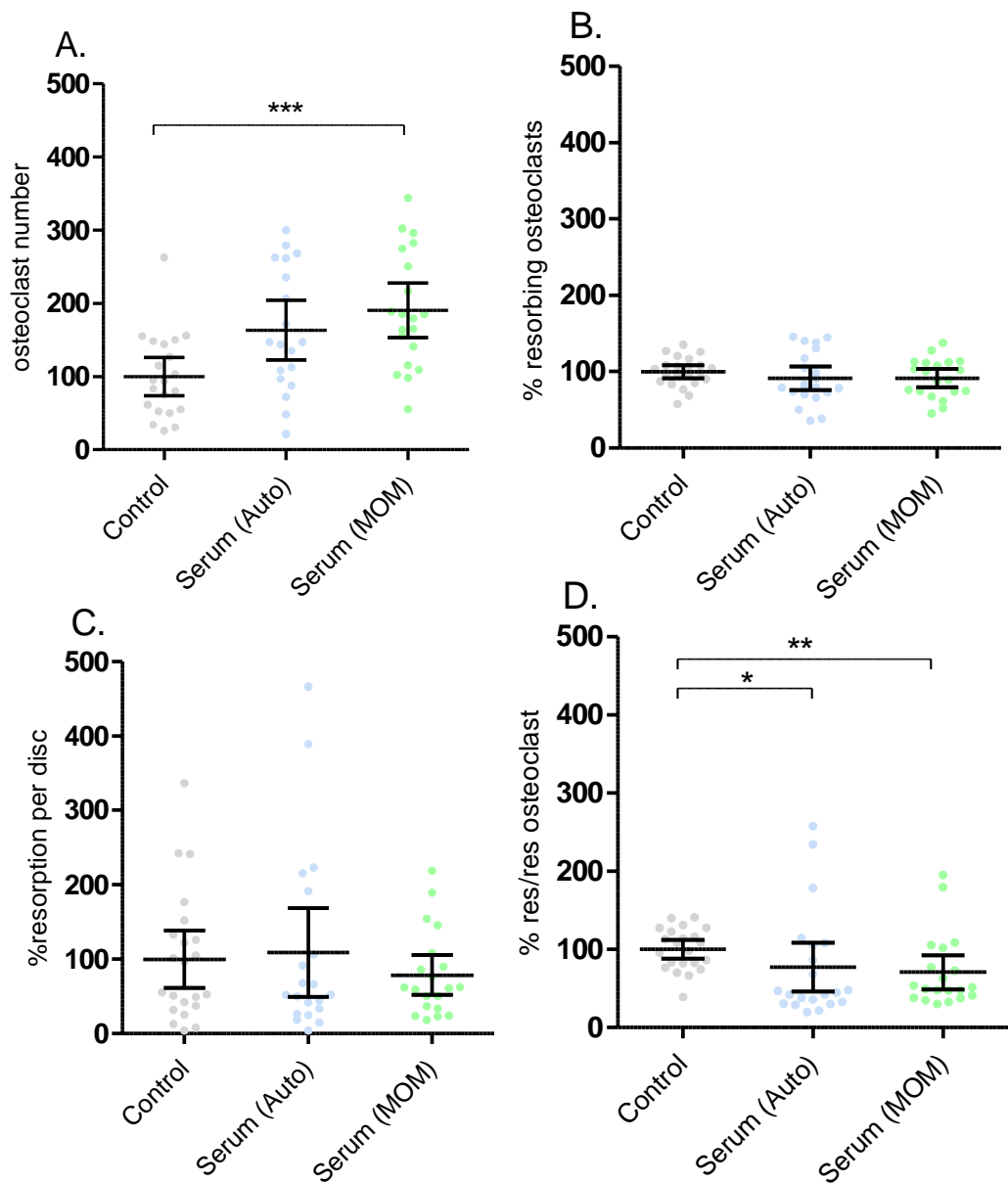
Figure 4.9 Effect of circulating metal ions on survival and function of osteoclasts from donors with THA

Peripheral blood mononuclear cells from THA donor controls were isolated and differentiated to resorbing osteoclasts on dentine disks. Following the onset of resorption the cells were cultured in normal osteoclastogenic media, autologous serum from the donors, or serum from a donor with MOMHR for 7days. Subsequently, the cells were TRAcP stained and quantified. Effect on **A)** osteoclast number, **B)** percentage of resorbing osteoclasts, **C)** percentage resorption, and **D)** resorption per resorbing osteoclast. Graphs represent data (mean ± 95%CI) from 5 case-control pairs, with 4-6 dentine disks per treatment for each donor (* $p < 0.05$; ** $p < 0.01$).

4.3 Discussion

Osteoclast survival and function is integral to balanced periprosthetic bone turnover and thus the survivorship of the implants. The effects of Co and Cr ions on osteoclasts are under-studied with most studies undertaken in animal cells at few concentrations (Mabilleau, *et al* 2012, Nichols and Puleo 1997, Rousselle, *et al* 2002). In this chapter, the direct effect of Co^{2+}, Cr^{3+} and Cr^{6+} at clinically relevant concentrations on the survival and function of differentiating and mature osteoclasts was characterised. In addition, the effect of systemic metal exposure on osteoclast survival and function was investigated using cells and serum from donors with well-functioning MOMHR and THA.

4.3.1 Effect of individual metal ions on osteoclast differentiation and function

A reduction in survival and activity was observed with increasing concentrations corresponding to hip aspirates, with Cr^{6+} being most detrimental, followed by Co^{2+} and Cr^{3+} being the least toxic.

The detrimental effects observed with high concentrations of Co and Cr ions are likely to be via similar mechanisms to that in osteoblasts (described in Chapter 3). Mature resorbing osteoclasts showed a monophasic decrease in cell number and activity with Cr^{6+} being the most toxic and Cr^{3+} being the least detrimental, consistent with the results of osteoblasts. A previous study by Rousselle *et al* (2002) on mature osteoclasts isolated from long bones of rabbits demonstrated no decrease in osteoclast number with Co and Cr ions. This inconsistency in the results may be attributed to the difference in the treatment regime between the two studies. While Rousselle *et al* treated bone cells with metal ions for 24 hours; the cells in this study were treated for considerably longer (7 days), with the observed effect likely to represent a response to chronic exposure. The results of this study suggest an inhibition of osteoclast activity at the implant surface and a reduction systemically. These changes would likely affect the balance of bone remodelling in both these compartments with implication for implant survivorship and skeletal bone health. Indeed, a recent study from our Department has reported a decrease bone turnover markers in patients with MOMHR compared to conventional THA (Prentice, *et al* 2013).

A trend towards increase in osteoclast number and resorption was observed for differentiating osteoclasts when treated with Cr^{3+}, and only for resorption with Co^{2+} at concentrations corresponding to patient serum. The trend towards a stimulatory effect at systemic concentrations was consistent for all experimental cultures hinting at an actual effect rather than a spurious result masked by the variation in the data. More experimental repeats with more replicates in each repeat are needed to validate the trend.

4.3.2 Effect of individual metal ions on TRAcP activity

TRAcP is thought to play a role in osteoclast bone resorption, as knock-out mice having a mild osteopetrotic phenotype with reduced osteoclast activity (Hayman, *et al* 1996). Total TRAcP activity was measured to assess its association with reduced osteoclast activity observed with metal ions. The results suggest a decrease in total TRAcP activity in differentiating osteoclasts with increasing concentrations of Cr^{6+}. To correct the data for reduced cell number at higher concentrations of metal ions, the TRAcP activity was corrected by the total protein content in the sample. The reduction in TRAcP activity could be due to the reduction in the production of TRAcP or in the functionality of the metalloenzyme.

The functionality of TRAcP was assessed by correcting the activity results with total TRAcP present as measured by a sandwich-ELISA. The results show increased TRAcP functionality in differentiating osteoclasts grown in presence of low concentrations of Cr^{3+} and Cr^{6+}, reaching significance for 500µg/L Cr^{3+}. The mechanism for the observed increase in phosphatase activity is yet unknown, with only one study linking Cr to 50% increment in acid phosphatase activity *in vivo* (Sivalingam 1989). A separate study demonstrating a similar increase in acid phosphatase enzymatic activity, albeit in a fungal system, suggests a role of conserved amino acids in mediating these effects (Raman*, et al* 2002). Multiple sequence alignment of fungal and human acid phosphatase sequences show several conserved residues (Appendix 3) some of which may play a role in the observed effects. Further investigations are required to elucidate these interactions and the effect of Cr on TRAcP.

The above results suggest a reduced production of TRAcP in differentiating osteoclasts exposed to metal ions, possibly due to increased cellular stress. The observation of unchanged activity for mature osteoclasts, which would have abundant TRAcP already, further supports this hypothesis.

4.3.3 Effect of MOMHR versus THA on osteoclast survival and function

On comparing osteoclasts grown in normal osteoclastogenic media from precursors isolated from MOMHR or THA donors, a higher osteoclastogenic response was observed for cells from THA compared to MOMHR. An increase in osteoclast number and total resorption was observed for THA cells, but there were no changes in percentage of resorbing osteoclasts and resorbing ability of osteoclasts between the two groups. Although the mechanism for this is unclear, increased osteoclast response for cells from THA donors suggests a relative difference in potential for osteoclastogenesis for osteoclast precursors derived from THA versus MOMHR patients. This may be due to the relative difference in circulating metal to which each cell population is exposed prior to extraction, or may be due to factors derived from the conventional THA exposure that are important in osteoclast differentiation, and this observation requires further study.

4.3.4 Effect of circulating metal ions on osteoclast survival and function

An autologous serum culture of osteoclasts was developed to mimic the systemic environment with clinically relevant combinations of metal ions (section 2.6). Autologous serum was used at 100% concentration, as diluting the serum would result in reducing the metal exposure to the cells and hence underestimating their effects (Appendix 4).

An increase in osteoclast number was observed for cells isolated from MOMHR donors when cultured in autologous serum (containing higher metal ion concentrations than the THA subject-derived serum). This increase in osteoclast number suggests improved survival of mature osteoclasts at systemic concentrations of metal ions. The increase in survival could be attributed to the generation of intracellular ROS in response to metal ions in the patient serum. Previous studies have described the role of ROS in mediating downstream RANK signalling, promoting osteoclast survival (Ha, *et al* 2004).

However, a decrease in resorption ability was observed for mature osteoclasts from MOMHR donors treated with autologous serum. This is in accordance to our *in vitro* data for mature osteoclasts and a previous clinical study that reports a reduction in bone resorption markers observed in MOMHR patient group compared to THA (Prentice*, et al* 2013). The reduction in resorption ability is recovered in the presence of THA serum, suggesting the factors responsible are most likely to be the increased metal exposure. A reduction in resorption ability was also observed for osteoclasts obtained from precursors from THA donors cultured in serum from MOMHR patients.

This study, however, does not take into consideration the differences in the levels of several other circulating factors including several cytokines and hormones that are known to modulate osteoclast responses (Aeschlimann and Evans 2004). An in-depth analysis of patient serum samples used to treat the cells is required to further understand the role of MOMHR on systemic osteoclast survival and function.

4.4 Conclusion

In conclusion, this study characterises the concentration and stage of differentiation dependent detrimental effects of individual metal ions on osteoclast survival and function, and the effects of genuine patient-derived circulating metal on primary osteoclasts derived from arthroplasty patients. A reduced cellular activity was observed at hip aspirate concentrations which is likely to have a severe impact on periprosthetic bone remodelling and thus osseointegration of the implant. In addition, the effects of metal ions on osteoclasts using autologous patient serum that represent the systemic effects post-surgery suggests that MOMHR insertion has implications for systemic bone health that warrant further study. The dominant effect here appears to be a reduction in osteoclast resorptive activity.

Chapter 5 - Effect of metal ions on survival and function of immature and mature osteocytes

5.1 Introduction

Osseointegration of the prostheses relies on the process of new bone modelling in the periprosthetic environment, and is akin to the callus formation process and subsequent remodelling observed in fracture healing. Osteocytes regulate bone remodelling in response to loading and mechanical strain by orchestrating the activities of both osteoblasts and osteoclasts. It is therefore necessary to investigate the effects of clinically relevant concentrations of metal ions on osteocyte survival and function

The transition of osteoblasts to a mature osteocyte involves several intermediate cell types (Figure 5.1) based on the changes in the cellular morphology and expression of specific genes. The most frequently used cell models for investigating osteocyte are the MLO-A5 and the MLO-Y4 cells which represent different stages of osteoblast to osteocyte differentiation. MLO-A5 cells are derived from osteocalcin promoter-driven T-antigen transgenic mice and have higher expression of ALP and osteocalcin compared to primary osteoblasts and MLO-Y4 osteocytes (Kato*, et al* 2001). They mineralise spontaneously in culture, even in absence of phosphate supplementation and are thought to represent pre-osteocytes that mineralise the osteoid matrix they are embedded in (Kato*, et al* 2001).

MLO-Y4 cells are a mature osteocyte cell model, also derived from the same transgenic mice used for the generation of MLO-A5 cells. These cells have a stellate morphology, with dendritic processes typical of mature osteocytes. They have relatively high expression of osteocalcin and connexin 43 with low collagen type 1, periostin and alkaline phosphatase activity compared to osteoblast primary and clonal cells (Kato*, et al* 2001, Kato*, et al* 1997). MLO-Y4 cells also possess the ability to respond to mechanical strain by releasing PGE_2 (Kamel*, et al* 2010), ATP (Genetos*, et al* 2007) and NO (Vatsa*, et al* 2006), integral to osteocytes' orchestration of adaptive bone remodelling.

While there is extensive evidence for the importance of osteocytes in regulation of bone health, their role in metal mediated adverse events following MOMHR is

largely unexplored. A recent study demonstrated an increase in pro-inflammatory cytokine (TNF-alpha) production by MLO-Y4 cells in presence of Co-Cr-Mo microparticles (Kanaji*, et al* 2009). This increase in TNF-alpha production was subsequently attributed to transcriptional activation downstream of the calcineurin-NFAT signalling pathway (Orhue*, et al* 2011). TNF-alpha is known to promote osteoclastogenesis (Kobayashi*, et al* 2000) and inhibit osteoblast differentiation (Gilbert*, et al* 2000), with severe consequences to local bone health. This is further evidenced by its positive association with severity of aseptic loosening (He*, et al* 2013).

Although these studies describe the effects of metal particles on osteocytes, the role of clinically relevant concentrations of Co and Cr ions remains unclear. In this chapter, the effect of Co and Cr ions on the *in-vitro* function of cells undergoing transition from osteoblast to osteocyte (MLO-A5 cells), and on viability and dendritic morphology of osteocytes (MLO-A4 cells) is investigated.
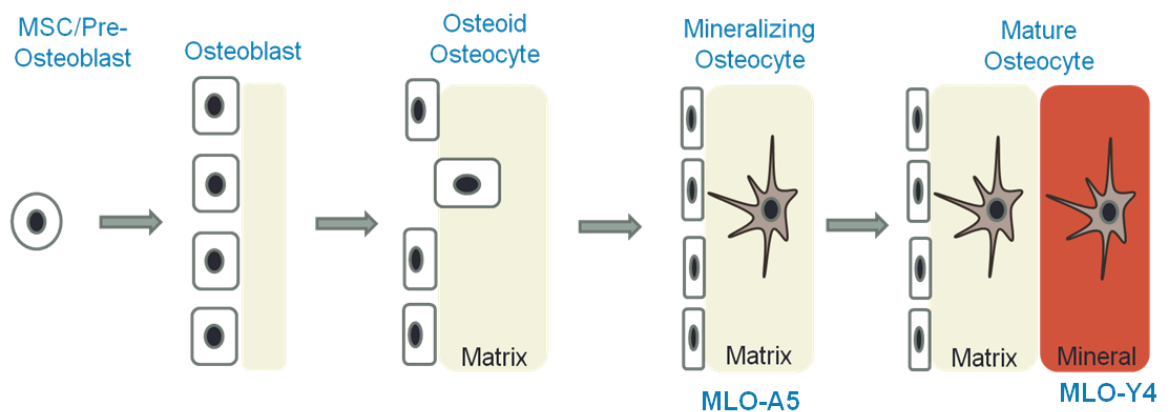
Figure 5.1 Stages of osteoblast differentiation.
Mesenchymal stem cells (MSCs) differentiate in matrix mineralising osteoblasts. Some osteoblasts get embedded into the osteoid matrix and differentiate into mineralising osteocytes (MLO-A5). Subsequent to mineralisation of the surrounding matrix, the cells develop a dendritic morphology forming connections to the surrounding cells and cells on the bone surface, characteristic of mature osteocytes (MLO-Y4). *Adapted from 'The amazing osteocyte', LF Bonewald (2011), with permission from American Society for Bone and Mineral Research copyright © 2011.*

5.2 Results

Murine early osteocyte cells (MLO-A5) were treated with Co^{2+} and Cr^{3+} ions for 7 days and mineralisation assessed by measuring the area of alizarin red stained calcium deposits (section 2.5.1). The mature osteocyte cells (MLO-Y4) were treated with the metal ions for 24h following which they were stained with crystal-violet and cell numbers, average number of dendrites per cell (>5µm) and their length assessed by manual counting. Both cell types were treated with a range of clinically relevant concentrations (0, 5, 50, 500 and 5000µg/L) of Co^{2+}, Cr^{3+} or a combination of Co^{2+} and Cr^{3+} ($Co^{2+}:Cr^{3+}$) at equal concentrations. Cr^{6+} ions were not included in this study due to its high cellular toxicity established in these cells previously in the group. Mr Peter Orton and Ms Katie Deaton, SSC students under my supervision, characterised the individual effects of Co^{2+}, Cr^{3+} and Cr^{6+} on MLO-A5 mineralisation. The results suggested a decrease in MLO-A5 mineralisation with Cr^{6+} being the most detrimental ($IC_{50}=75µg/L$). Similarly, Mr Nick Mani, an Arthritis Research UK summer intern characterised the effects of individual metal ions on MLO-Y4 cells and observed reduced viability for Cr^{6+} at hip aspirate concentrations ($IC_{50} = 2200µg/L$).

5.2.1 Effect of Co^{2+} and Cr^{3+} on mineralisation by – MLO-A5

A significant increase in mineralisation was observed for 5µg/L Co^{2+} (mean±95%CI; 120.6±9.4), with no change observed at higher concentrations, compared to the untreated control (100±5.2) (Figure 5.2A). A reduction in mineralisation was observed for Cr^{3+} treatments, reaching significance for concentrations of 50µg/L (70.9±16.4) and higher (Figure 5.2A). The combination treatments with $Co^{2+}:Cr^{3+}$ resulted in a biphasic response, having a significant increase with 5µg/L (121.9±5.6) and decreases with 500µg/L (32.7±8.1) and 5000µg/L (0.02±0.04) (Figure 5.2A). The results corresponding to metal ion concentrations for clinically relevant compartments are illustrated in Figure 5.2B

For $Co^{2+}:Cr^{3+}$ treatments up to 50µg/L, the effect of Co^{2+} was dominant whilst the response at higher concentrations seemed to be due to the effect of Cr^{3+} (Figure 5.2A). Both Cr^{3+} and $Co^{2+}:Cr^{3+}$ were significantly lower compared to Co^{2+} at 500µg/L and 5000µg/L, with no significant difference between them (Figure 5.2A).

A.
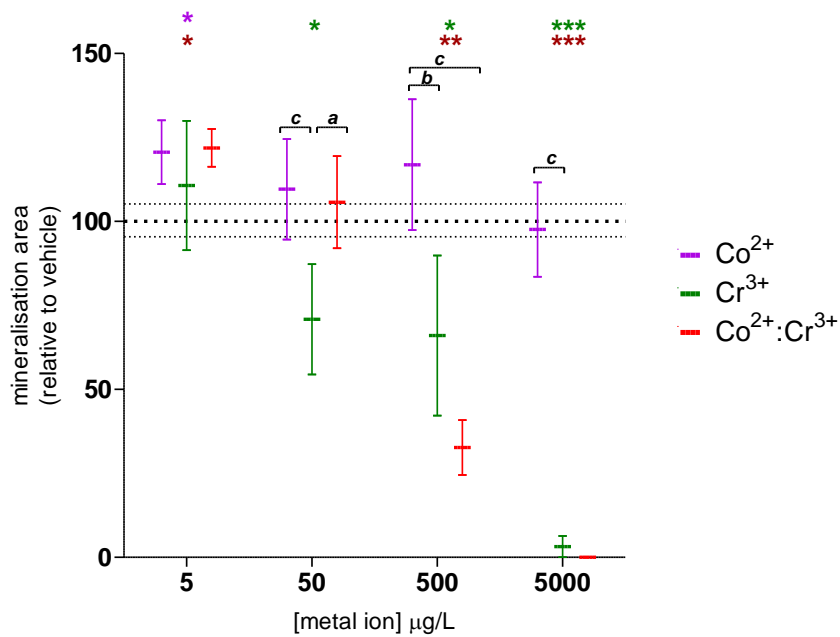
B.
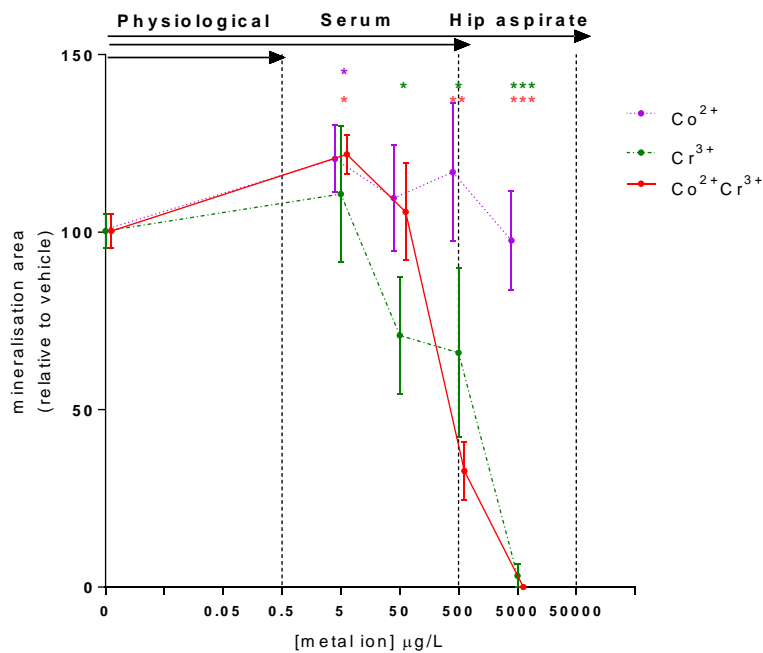
Figure 5.2 Effect of Co²⁺ and Cr³⁺ on MLO-A5 mineralisation

Following confluence, MLO-A5 cells were treated with metal ions for 7 days in osteogenic media and mineralisation assessed by Alizarin Red staining. The data is shown relative to mineralisation by untreated cells. **A)** Comparisons between Co^{2+} (purple), Cr^{3+} (green) and $Co^{2+}:Cr^{3+}$ (red) combined treatments. The mean± 95%CI for control is depicted by dashed lines. **B)** Effect on mineralisation area depicted at clinically relevant concentrations corresponding to normal physiology, patient serum and hip aspirate post-MOMHR. All values are mean ± 95%CI of 4 experiments with 4-6 replicates in each. ([a] * $p<0.01$; [b] ** $p<0.01$; [c] *** $p<0.0001$).

5.2.2 Effect of Co^{2+} and Cr^{3+} on MLO-Y4 osteocyte cell number

Whilst no change in osteocyte cell number was observed with Cr^{3+} treatments, a significant decrease was seen with 5000µg/L Co^{2+} (mean±95%CI; 62.4±7.7) compared to the untreated controls (100.0±7.3) (Figure 5.3A). A decrease was observed with Co^{2+}:Cr^{3+} treatment which was significant at 500µg/L (62.8±10.2) and 5000µg/L (48.4±7.9) (Figure 5.3A). The results corresponding to metal ion concentrations for clinically relevant compartments are illustrated in Figure 5.3B.

Combination treatment at 500µg/L (62.8±10.2) had a synergistic effect, being significantly lower to Co^{2+} (89.9±10.5) and Cr^{3+} (103.3±24.5) (Figure 5.3A). At the highest concentration of 5000µg/L, Co^{2+} (62.4±7.7) and Co^{2+}:Cr^{3+} (48.4±7.9) treatments had no difference between them but were significantly lower compared to Cr^{3+} (88.6±16.2) (Figure 5.3A).
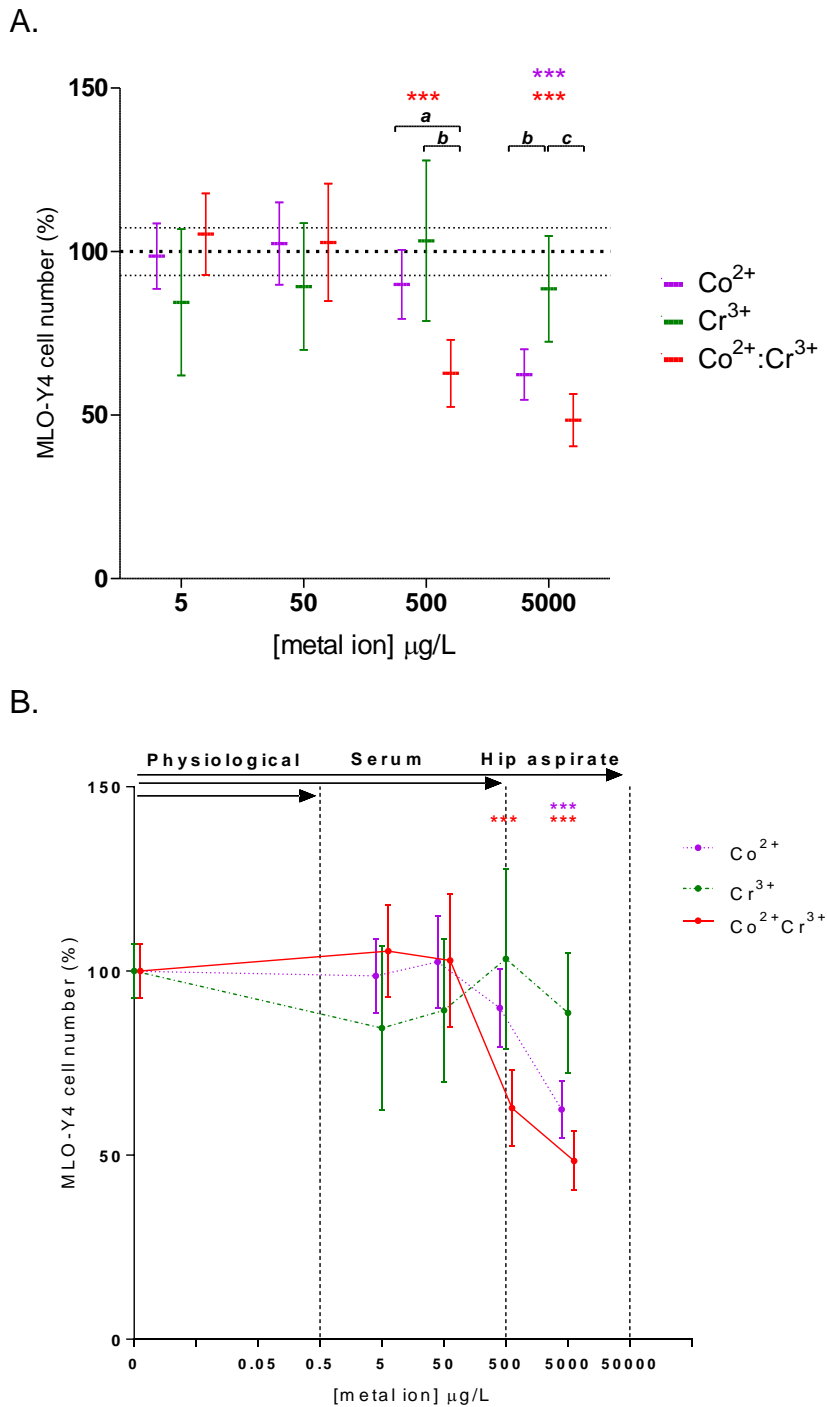
Figure 5.3 Effect of Co^{2+} and Cr^{3+} on MLO-Y4 cell number

Following 24h treatment with metal ions, crystal-violet stained MLO-Y4 cells were counted from 4 random fields per well using cellID. The data shown is relative to cell numbers of untreated controls. **A)** Comparison between Co^{2+} (purple), Cr^{3+} (green) and Co^{2+}:Cr^{3+} (red) combined treatments. The mean± 95%CI for control is depicted by dashed lines. **B)** Effect on cell number depicted at clinically relevant concentrations corresponding to normal physiology, patient serum and hip aspirate post-MOMHR. All values are mean ± 95%CI of 3 experiments with 3 replicate wells each ([a] * $p<0.01$; [b] ** $p<0.01$; [c] *** $p<0.0001$).

5.2.3 Effect of Co^{2+} and Cr^{3+} on MLO-Y4 dendricity

5.2.3.1 Dendrite number

A biphasic response in dendrites per cell was observed for Co^{2+} treatment, with a significant decrease seen at 500µg/L (87.1±5.7) and a significant increase at 5000µg/L (126.4±10.1) compared to untreated control (100.0±4.3) (Figure 5.4A). Cr^{3+} treatments lowered the average number of dendrites per cell with a significant reduction observed at 5µg/L (85.4±8.0), 500µg/L (86.6±9.2) and 5000µg/L (81.8±9.5) (Figure 5.4A). The number of dendrites remained unchanged with Co^{2+}:Cr^{3+} treatment, except for a significant reduction at the highest concentration of 5000µg/L (86.1±8.4) (Figure 5.4A). The results corresponding to metal ion concentrations for clinically relevant compartments are illustrated in Figure 5.4B.

Comparisons amongst the different treatment groups showed a significant reduction for Cr^{3+} (81.8±9.5) and Co^{2+}:Cr^{3+} (86.1±8.4) compared to Co^{2+} (126.4±10.1) ($p < 0.0001$) at 5000µg/L (Figure 5.4A).

5.2.3.2 Dendrite length

An increase in dendritic length was observed for Co^{2+} and Co^{2+}:Cr^{3+} treatments, with increase being significant at 500µg/L for Co^{2+} (110.3±4.7) and 5000µg/L for Co^{2+} (144.7±10.6) and Co^{2+}:Cr^{3+} (151.3±12.3) compared to the untreated controls (100.0±3.1) (Figure 5.5A). Cr^{3+} had no effect on the dendritic length of MLO-Y4 cells at any concentrations. The results corresponding to metal ion concentrations for clinically relevant compartments are illustrated in Figure 5.5B. Comparisons amongst the different treatment groups showed a significant increase for Co^{2+} (144.7±10.6) and Co^{2+}:Cr^{3+} (151.3±12.3) compared to Cr^{3+} (100.3±8.6) ($p < 0.0001$) at 5000µg/L (Figure 5.5A).
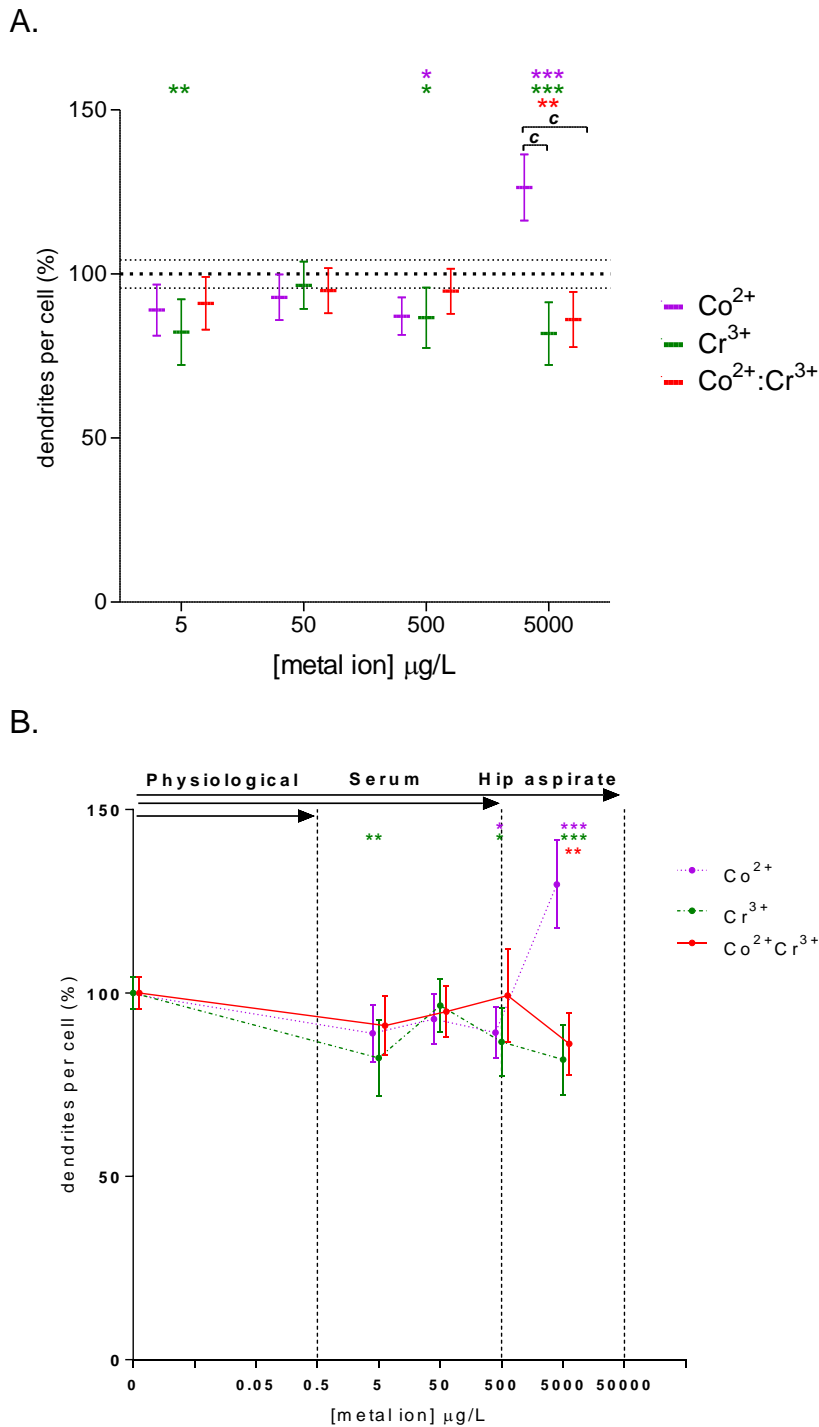
Figure 5.4 Effect of Co^{2+} and Cr^{3+} on MLO-Y4 dendrite number

Following 24h treatment with metal ions, average number of dendrites per crystal-violet stained MLO-Y4 cells was counted using cellD. The data shown is relative to cell numbers of untreated controls. **A)** Comparison between Co^{2+} (purple), Cr^{3+} (green) and Co^{2+}:Cr^{3+} (red) combined treatments. The mean± 95%CI for control is depicted by dashed lines. **B)** Effect on dendrite number depicted at clinically relevant concentrations corresponding to normal physiology, patient serum and hip aspirate post-MOMHR. All values are mean ± 95%CI of 3 experiments with 3 replicate wells each (* $p<0.01$; ** $p<0.01$; ^{c} *** $p<0.0001$)

A.

B.
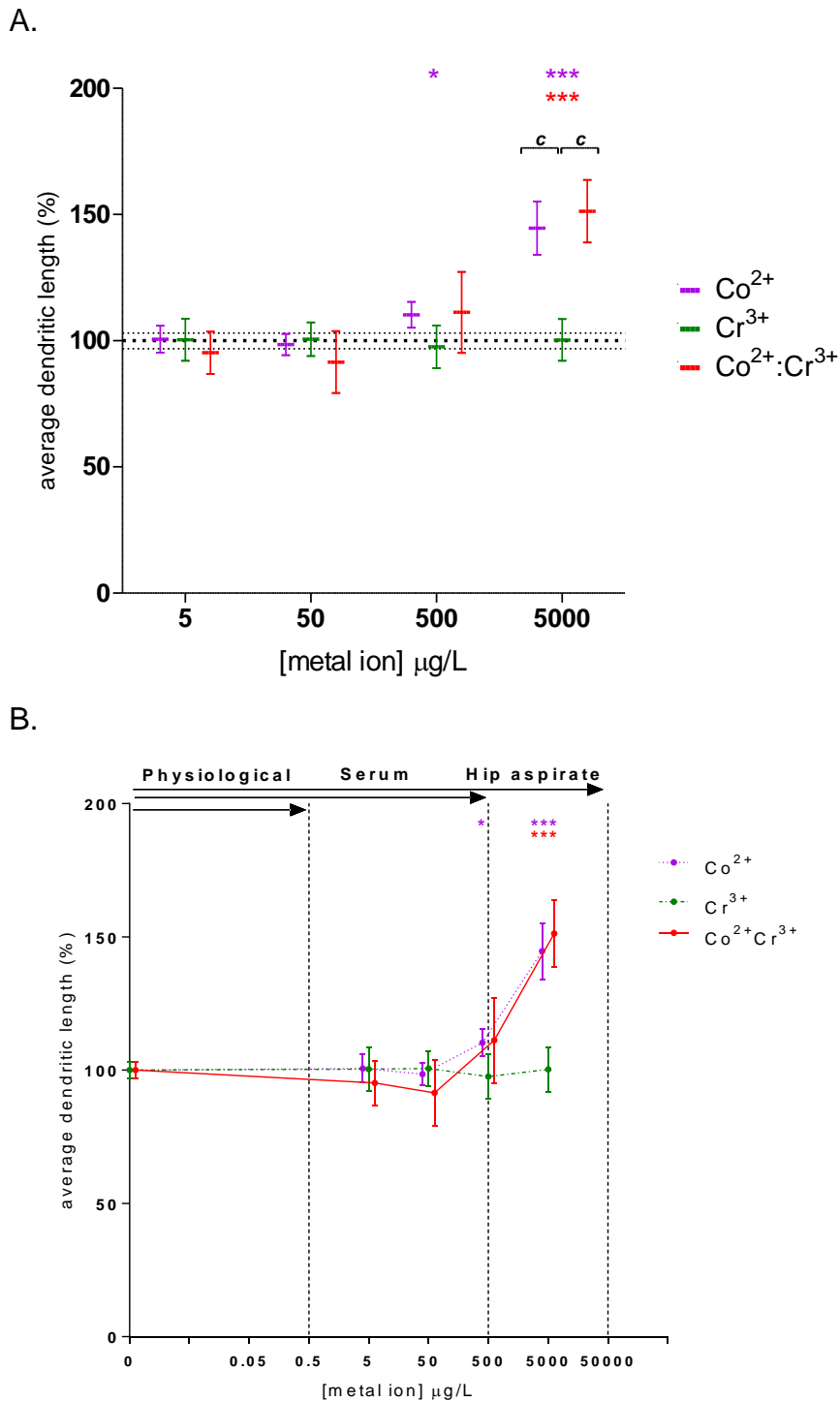
Figure 5.5 Effect of Co^{2+} and Cr^{3+} on MLO-Y4 dendritic length

Following 24h treatment with metal ions, average dendritic length of MLO-Y4 cells was measured using cellD. The data shown is relative to cell numbers of untreated controls. A) Comparison between Co^{2+} (purple), Cr^{3+} (green) and Co^{2+}:Cr^{3+} (red) combined treatments. The mean± 95%CI for control is depicted by dashed lines. B) Effect on dendritic length depicted at clinically relevant concentrations corresponding to normal physiology, patient serum and hip aspirate post-MOMHR. All values are mean ± 95%CI of 3 experiments with 3 replicate wells each (* $p < 0.01$; ** $p < 0.01$; ^{c} *** $p < 0.0001$).
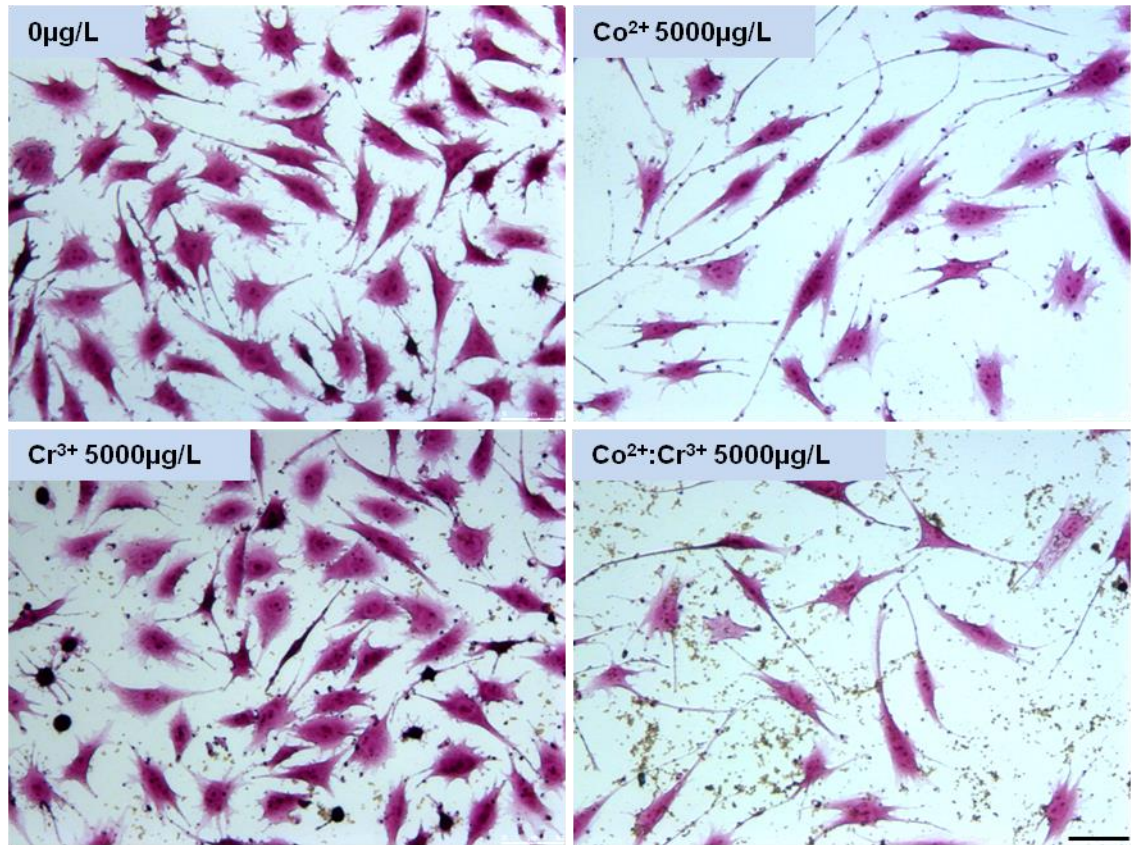
Figure 5.6 MLO-Y4 cells with metal ion treatments – representative images

Representative images of crystal-violet stained MLO-Y4 cells, treated with vehicle (0µg/L), Co^{2+} (5000 µg/L), Cr^{3+} (5000 µg/L) and $Co^{2+}:Cr^{3+}$ (5000 µg/L) for 24hrs. Scale bar = 50µm.

5.3 Discussion

Osteocytes are integral to the regulation of bone remodelling and its response to mechanical strain. In view of this, the effects of clinically relevant concentrations and combinations of metal ions are explored for osteocyte-like cells – the late osteoblasts/early osteocytes (MLO-A5) and mature osteocytes (MLO-Y4). The study investigated the mineralisation ability for MLO-A5 cells, and the cell number and dendricity for MLO-Y4 cells, to understand if there is a mechanistic explanation for the observed clinical effects.

5.3.1 MLO-A5 mineralisation

The increase in mineralisation observed with low concentrations of Co^{2+} and $Co^{2+}:Cr^{3+}$, but not Cr^{3+}, suggests a Co^{2+} mediated effect. At low concentrations, Co^{2+} can cause an increase in intracellular reactive oxygen species (ROS) via Fenton-like reactions – a catalytic reaction of metal ions and hydrogen peroxide that produces free radicals (Leonard, *et al* 1998). There is growing evidence for a role of ROS in the regulation of osteogenic response with several studies, suggesting in increase in osteoblast differentiation and mineralisation (Arakaki, *et al* 2013, Choe, *et al* 2012, Lee, *et al* 2006, Mandal, *et al* 2011, Nicolaije, *et al* 2012). The lack of a stimulatory effect by Cr^{3+} further supports the hypothesis of ROS-mediated increase in mineralisation as the metal ion species is relatively redox stable, and fails to generate ROS in osteoblast cells (Fu, *et al* 2008).

In addition, unlike SaOS-2 cells (section 3.2.5), Co^{2+} treatment at hip aspirate concentrations did not result in a reduction of mineralisation by MLO-A5 cells. This discrepancy could be attributed to the high ALP activity in MLO-A5 cells compared to primary osteoblasts and osteoblast cell lines (Kato, *et al* 2001). As mentioned in the previous chapter, Co^{2+} can substitute the Zn^{2+} centres in ALP, rendering it less active (Wang, *et al* 2005). The importance of Zn^{2+} in osteoblast function is further evidenced by a study which describes increased ALP activity and subsequent mineralisation in cultures supplemented with the metal ion (Cerovic, *et al* 2007). With an abundance of ALP in MLO-A5 relative to osteoblast-like SaOS-2 cells, its inhibition by Co^{2+}, even at high concentrations, may be insubstantial to cause a subsequent reduction in mineralisation. Moreover, difference in species and stage of differentiation of the two cell types are likely to

affect the expression and affinity of certain transporters and receptors implicated in cellular entry of Co^{2+}, such as divalent metal transporter-1 and P2X7R (Donnelly-Roberts, *et al* 2009, Mabilleau, *et al* 2008), contributing to the differential effect.

The decrease in mineralisation with Cr^{3+} treatments observed in MLO-A5 cells is similar to its effect in SaOS-2 cells, although the effect appears more pronounced in MLO-A5 cells with reduction reaching significance at 50µg/L compared to 500µg/L. Mineralisation by primary osteoblasts and osteoblast-like cell lines, including SaOS-2 cells, is believed to be mediated via the release of matrix vesicles (MVs) (Mahamid, *et al* 2011, Thouverey, *et al* 2011). MVs contain hydroxyapatite 'seeds' which are formed within its lumen by coordinated activities of several enzymes (ALP, NPP-1 and PHOSPHO-1) (Golub 2009). The nucleation of matrix, at least in part, is due the association of vesicular membrane proteins to the collagenous matrix (Wu, *et al* 1991). In contrast, mineralisation by MLO-A5 cells occurs via the release of mineralised spheres that nucleate collagen fibrils and propagate calcification (Barragan-Adjemian, *et al* 2006). There is evidence suggesting that increasing concentrations of Cr^{3+} complexes with amino acids in collagen distorting its helical backbone (Wu, *et al* 2009). This Cr^{3+}-related distortion of the collagen structure might hamper the vesicle-free mode of matrix nucleation and eventual mineralisation by MLO-A5 cells seen in this study.

In support of this, microscopic examination of the mineralisation cultures suggested that the decrease in SaOS-2 mineralisation at high concentrations is due to the reduced cell number and absence of extracellular matrix, whereas MLO-A5 remain viable and produce a matrix which is left unmineralised (Figure 5.7). The difference in cellular toxicity of Cr^{3+} between the two cell types could be attributed to their stage of differentiation. MLO-A5, being late osteoblast/early osteocyte cells, are more differentiated than the osteoblast-like SaOS-2 cells and are therefore likely to be less proliferative. The toxicity of Cr^{3+} is primarily due to its ability to interfere with DNA replication and repair (Dai, *et al* 2009, El-Yamani, *et al* 2011) and thus may manifest less in MLO-A5 cells compared to the more proliferative SaOS-2 cells. Additionally, the cellular uptake of relatively

impermeable Cr^{3+} might differ based on the endocytic ability of the two cell types, contributing to the difference in their toxicity.

The combination treatment of Co^{2+}:Cr^{3+} exhibited interactions between the effects of individual Co^{2+} and Cr^{3+} treatments, with Co^{2+} having a protective role at 50µg/L while the effect of Cr^{3+} was more dominant at higher concentrations of 500µg/L and 5000µg/L. This protective effect with Co^{2+} at lower concentrations could be due to the increase in ROS-mediated mineralisation described earlier, sufficient to overcome the negative effects of Cr^{3+} resulting in no net change in overall mineralisation compared to the untreated control.

A recent gene expression study has demonstrated that extracellular matrix mineralisation is integral to osteocytic differentiation of MLO-A5 cells (Prideaux*, et al* 2012). The reduction in mineralisation observed with metal ion treatments is therefore likely to be detrimental to osteoblast-osteocyte transitions in the periprosthetic environment, potentially compromising the response of bone to mechanically loading and thus implant fixation.
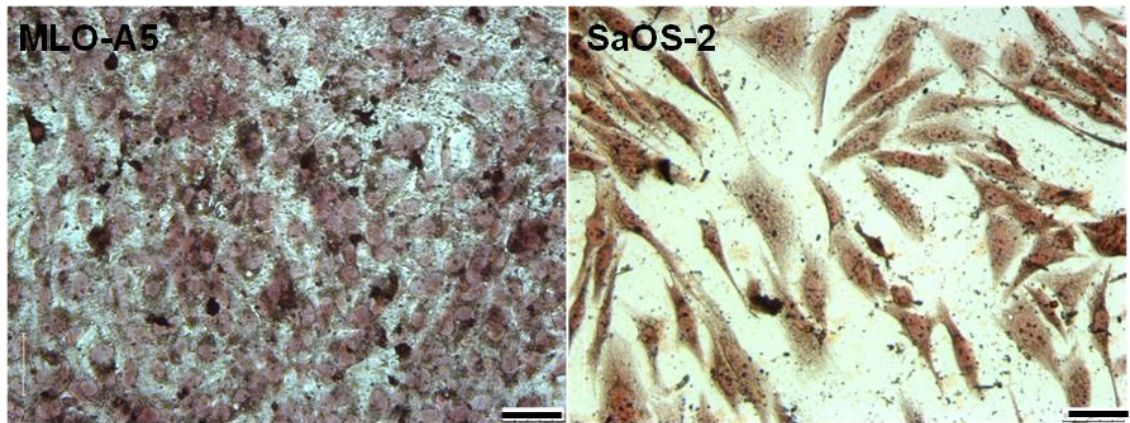
Figure 5.7. Cr³⁺ treated MLO-A5 vs SaOS-2 cells.

MLO-A5 cells treated with 5000µg/L Cr^{3+} remain confluent and generate ECM compared to SaOS-2 cells which appear sub-confluent. Scale bar 50µm

5.3.2 MLO-Y4 osteocyte number

The treatments with increasing concentration of Cr^{3+} did not have any effect on MLO-Y4 cell number. This could be, at least in part, due to its relative inability to cross cell-membranes (Gray and Sterling 1950). Additionally, the 24h exposure time in this study might be insufficient to elicit an effect and may explain the inconsistency compared to the response of SaOS-2 osteoblast-like cells at concentrations corresponding to the hip aspirate, observed in the previous chapter (section 3.2.1).

In contrast, the decrease in cell number at high concentrations of Co^{2+} is consistent with its detrimental cellular effects observed with osteoblasts in the previous chapter. The similar detrimental effect observed with Co^{2+} in this study, even with a shorter exposure to the metal ion, maybe explained via increased cellular entry of Co^{2+}. Osteocytes, including MLO-Y4 cells, respond to mechanical loading by releasing osteogenic factors including PGE_2 (Jiang and Cheng 2001). This release of PGE_2 has been shown to be mediated via the activation of ATP-gated P2X7 receptor (P2X7R) (Li, *et al* 2005a). Functional P2X7R has been implicated to play a role in metal ion mediated toxicity and its expression on MLO-Y4 cells may contribute to the uptake of extracellular Co^{2+}, causing intracellular mitochondrial and oxidative stress and subsequent cell apoptosis (Battaglia, *et al* 2009, Bhabra, *et al* 2009, Leonard, *et al* 1998). Whilst the role of P2X7R in uptake of Co^{2+} in bone cells has been investigated in chapter 7, the difference in the species specific activation of P2X7R (Hibell, *et al* 2000) in presence of Co^{2+}, and its potential role as an allosteric modulator (Coddou, *et al* 2011) needs to be investigated for the two species to validate this hypothesis.

The Co^{2+}:Cr^{3+} combined treatment exhibited a synergistic effect at 500µg/L, with significantly lower cell number compared to individual Co^{2+} and Cr^{3+} treatments. The reason for this is unclear, especially as both Co^{2+} and Cr^{3+} do not elicit an effect significantly different to the untreated control. At higher concentrations, corresponding to hip aspirate, the effects of Co^{2+} dominates with no additive or synergistic effect observed in the presence of Cr^{3+}.

An inflammatory, pro-osteoclastic environment prevails locally at the hip as a response to prosthetic derived metal ions and particles (Nawabi, *et al* 2013). The decrease in osteocyte cell number is known to promote osteoclastic resorption, adding to the already osteolytic environment (Cardoso, *et al* 2009, Verborgt, *et al* 2000), with possible negative implications to implant survivorship.

5.3.3 MLO-Y4 dendricity

The dendrites connect osteocytes to osteoblasts and osteoclasts via gap junctions (GJs) and regulate their functions by signalling via calcium and ATP (Huo*, et al* 2010). The reduced dendrites per cell with Cr^{3+} and $Co^{2+}:Cr^{3+}$ treatments are likely to affect the osteocyte connectivity to other cells and thus its efficacy at orchestrating bone remodelling. In contrast, Co^{2+} treatments resulted in a significant increase in dendrite number at 5000µg/L. The number of dendrite processes in osteocytes is thought to be regulated to some extent by the expression of membrane type-1 metalloproteinase (MT1-MMP), a collagenase enzyme (Bonewald 2005). A study with MT1-MMP deficient mice demonstrated a reduction in osteocyte processes, with no change in osteocyte number (Holmbeck*, et al* 2005). There is evidence that suggests the up regulation of MMP gene and protein expression in presence of Co^{2+}, but not Cr^{3+} (Luo*, et al* 2005), which might explain the increased dendrite numbers in Co^{2+} treated MLO-Y4 cells. The contradictory effect with $Co^{2+}:Cr^{3+}$ treatments could be due to an inability of MT1-MMP to catalyse the lysis of Cr^{3+}-distorted collagen fibrils described previously.

The average dendritic length increased with Co^{2+} and $Co^{2+}:Cr^{3+}$ treatments at concentrations corresponding to patient serum and hip aspirates, whilst Cr^{3+} did not elicit any effect. The regulation of osteocytic dendritic length is still unclear but it is shown to be influenced by mechanical loading in the form of fluid shear stress (Zhang*, et al* 2006). Application of shear stress increases the expression of E11/gp38, a gene associated with formation and elongation of dendrites in osteocytes (Zhang*, et al* 2006). However, there is no evidence yet suggesting an association between the expression of E11/gp38 and presence of metal ions. A reduced cell number observed with Co^{2+} and $Co^{2+}:Cr^{3+}$ may induce elongation of dendrites to maintain the connectivity between cells. The absence of change in dendritic length with Cr^{3+} treatments, which had no effect on cell number, further supports this hypothesis. This could be tested by seeding MLO-Y4 cells at different cell densities and assessing the corresponding change in their dendritic length. An absence of change would suggest the role of cell death or metal mediated regulation of dendritic length as the cause for the observed effect. Alternatively, genes associated with osteocyte differentiation and dendricity such

as Dmp-1 and Cx43 are upregulated under hypoxic conditions (Hirao, *et al* 2007), and Co^{2+} being a hypoxia mimic may promote osteocyte differentiation with increased dendritic number and length.

The importance of altered osteocyte dendricity is highlighted by its association with several diseased states. Decreased interconnectivity has been observed in osteoporotic and osteoarthritic bone, whilst osteomalacic bone exhibits an increased interconnectivity which is chaotic (Jaiprakash, *et al* 2012, Knothe Tate, *et al* 2004). The metal ion induced changes in the osteocyte dendricity could compromise the adaptive remodelling ability of bone under mechanical loading, increasing the risk of fractures and ultimate failure of the implant.

Whilst MLO-A5 and MLO-Y4 cells possess a phenotype similar to pre-osteocytic and osteocytic cells respectively (Kato, *et al* 2001, Kato, *et al* 1997), they do not express certain proteins including sclerostin which are characteristic of primary osteocytes (Yang, *et al* 2009). Moreover, they are murine cell lines and thus the results should be treated with caution when extrapolating their responses to patient osteocytes. Nevertheless, the technical difficulties associated with obtaining primary osteocytes, and their inability to proliferate *ex vivo* make these cell lines convenient and useful tools to study osteocytic responses (Stern, *et al* 2012).

5.4 Conclusion

The data from this chapter suggests that the direct effects of metal ions on osteocytic cells may alter its orchestration of bone remodelling and contribute to the already descirbed effects on osteoblast and osteoclasts, especially in the periprosthetic environment. In addition, detection of stress transfer from the implant onto the bone might also be affected resulting in loss of adaptive remodelling periprosthetically, potentially increasing the risk of fractures. Further studies evaluating key bone remodelling associated events and gene expression such as osteocyte apoptosis (integral to osteoclast recruitment), RANKL and OPG in response to metal exposure would strengthen the present set of data.

Chapter 6 - Intracellular distribution and speciation of cobalt and chromium in osteoblasts and osteoclasts

6.1 Introduction

In the previous chapters, the detrimental effects of Co^{2+}, Cr^{3+} and Cr^{6+} at clinically-equivalent concentrations on human osteoblast and osteoclast survival and function *in-vitro* have been described. While the effects of metal ions on bone cells are being established, it remains unclear what the intracellular distribution of these metal ion species is, and how they interact with cells to mediate their effects. The presence of Cr(III) phosphate (Huber*, et al* 2009) and Cr(III) hydroxide (Catelas*, et al* 2006) was observed in periprosthetic tissue of patients with failed MOMHR using energy dispersive X-ray analysis (EDXA). Cr(III) phosphate and metallic cobalt was also found in hip capsule tissue from patients with failed MOMHR using synchrotron based microfocus X-ray fluorescence (μ-XRF) and X-ray absorption spectroscopy (XAS) (Hart*, et al* 2010a). A more recent study described the wear debris phagocytosed within macrophages in the periprosthetic tissue to be chromium in the +3 oxidation state and cobalt in the +2 oxidation state using XAS in combination with electron energy-loss spectroscopy (Goode*, et al* 2012). However, metal distribution and speciation at the sub-cellular level in bone cells, the key downstream cell types in bone-related adverse effects, are unstudied.

The aims of this study were to investigate the intracellular distribution and speciation of cobalt and chromium in human osteoblasts and primary human osteoclasts when treated with specific ionic forms of cobalt and chromium using high-sensitivity μ-XRF and XAS. Knowledge of the intracellular distribution and oxidation state of cobalt and chromium in bone cells would provide us with a valuable understanding of the potential mechanisms of toxicity associated with these metal ions.

6.2 Results

To observe the intracellular state of metal ions, osteoblasts (SaOS-2) were treated with 5000µg/L Co^{2+}, 5000µg/L Cr^{3+} or 50µg/L Cr^{6+} for 3 days whilst differentiating osteoclasts were treated with 500µg/L Co^{2+}, 500µg/L Cr^{3+} or 50µg/L Cr^{6+} from day 3 till the onset of resorption (typically day 14). Osteoclasts that had differentiated into multinuclear resorbing osteoclasts were treated with 500µg/L Co^{2+}, 5000µg/L Cr^{3+} or 500µg/L Cr^{6+} for a week from the onset of resorption. Sub-toxic concentrations of metal ions were chosen for all cell types based on previous studies (Chapters 3 and 4).

6.2.1 Localisation and speciation of cobalt in Co^{2+} treated osteoblasts and osteoclasts

Intracellular cobalt was found in all cell sample XRF elemental maps (Figure 6.1). Cobalt was present throughout the osteoblast cell body, but found at a relatively higher concentration in the area corresponding to the cell nucleus (Figure 6.1a). Localisation of cobalt signals were to discrete areas within both developing and mature osteoclasts, and corresponded to areas on basolateral membrane in phase contrast images (Figure 6.1b-c). K-edge µ-XANES spectra from intracellular sites with high cobalt concentrations were compared to standards of cobalt at different oxidation states (Co-metal, CoO, Co_2O_3 and Co(II)acetate) (Figure 6.4A). Osteoblasts and mature osteoclasts showed the presence of cobalt in the +2 oxidation state based on the Co(II)Acetate standard spectra, indicating that no intracellular redox change occurs in osteoblasts or mature osteoclasts. No µ-XANES spectra could be obtained for osteoclasts exposed to cobalt during days 0-14, due to the very low concentrations present, potentially indicating no cellular entry during this time period.

6.2.2 Localisation and speciation of chromium in Cr^{3+} treated osteoblasts and osteoclasts

The XRF maps for all Cr^{3+} treated cells showed the presence of intracellular chromium (Figure 6.2). Chromium was seen throughout the osteoblast cell body, but with relatively greater localisation at perinuclear sites (Figure 6.2a). Both developing and mature osteoclasts showed chromium localisation to the basolateral membrane (Figure 6.2b-c). Chromium K-edge µ-XANES spectra from

all cell samples were compared to chromium standards (Cr-metal, Cr(III)OH, $Cr(III)PO_4$, Cr_2O_3 and CrO_3) (Figure 6.4B). Spectra from osteoblasts and both osteoclasts samples were similar to Cr(III)OH and $Cr(III)PO_4$ indicating chromium in the +3 oxidation state.
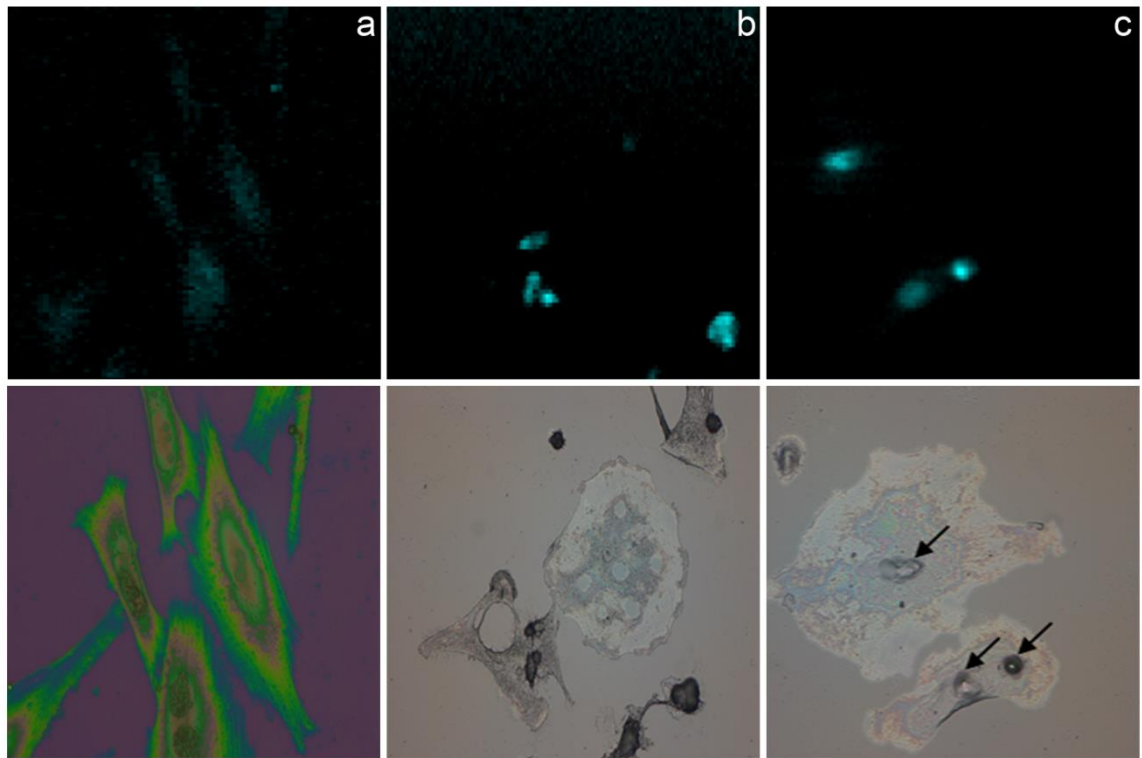
Figure 6.1 µ-XRF maps of osteoblasts and osteoclasts treated with Co^{2+}

Top-panel represents Co^{2+} treated osteoblasts (a), developing osteoclasts (b), and mature osteoclasts (c), with corresponding microscope images (bottom panel). Distribution of metal ions in osteoblast samples is throughout the cell body, whereas osteoclast cells show discrete localization to basolateral membrane within the cell (arrows).
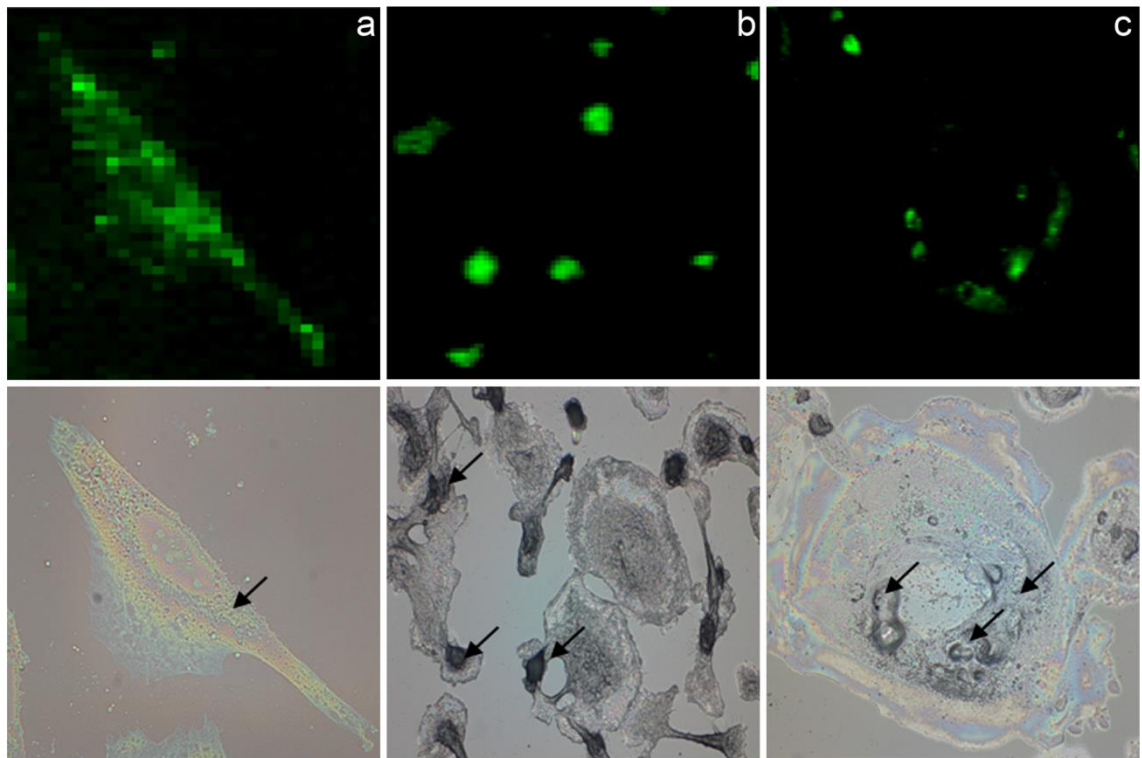
Figure 6.2 μ-XRF maps of osteoblasts and osteoclasts treated with Cr³⁺

Top panel represents Cr^{3+} treated osteoblasts (a), developing osteoclasts (b), and mature osteoclasts (c), with corresponding microscope images (bottom panel). Distribution of metal ions in osteoblast samples localised to perinuclear regions (arrows). Osteoclast cells show discrete localization to basolateral membrane within the cell (arrows).

6.2.3 Localisation and speciation of chromium in Cr^{6+} treated osteoblasts and osteoclasts

All Cr^{6+} treated osteoblasts and osteoclasts samples showed the presence of intracellular elemental chromium (Figure 6.3). Both in osteoblast and osteoclast cells, chromium was diffusely distributed, in contrast to the focal distributions seen with Co^{2+} and Cr^{3+} treated cells, suggesting a different mechanism of cellular entry or intra-cellular processing. The characteristic pre-edge feature for Cr^{6+} (seen in CrO_3) was absent in μ-XANES spectra from all cell samples showing an intracellular redox change (Figure 6.4C). The spectral features were similar to $Cr(III)OH$ and $Cr(III)PO_4$ indicating intracellular reduction of $Cr6+$ to Cr^{3+}.
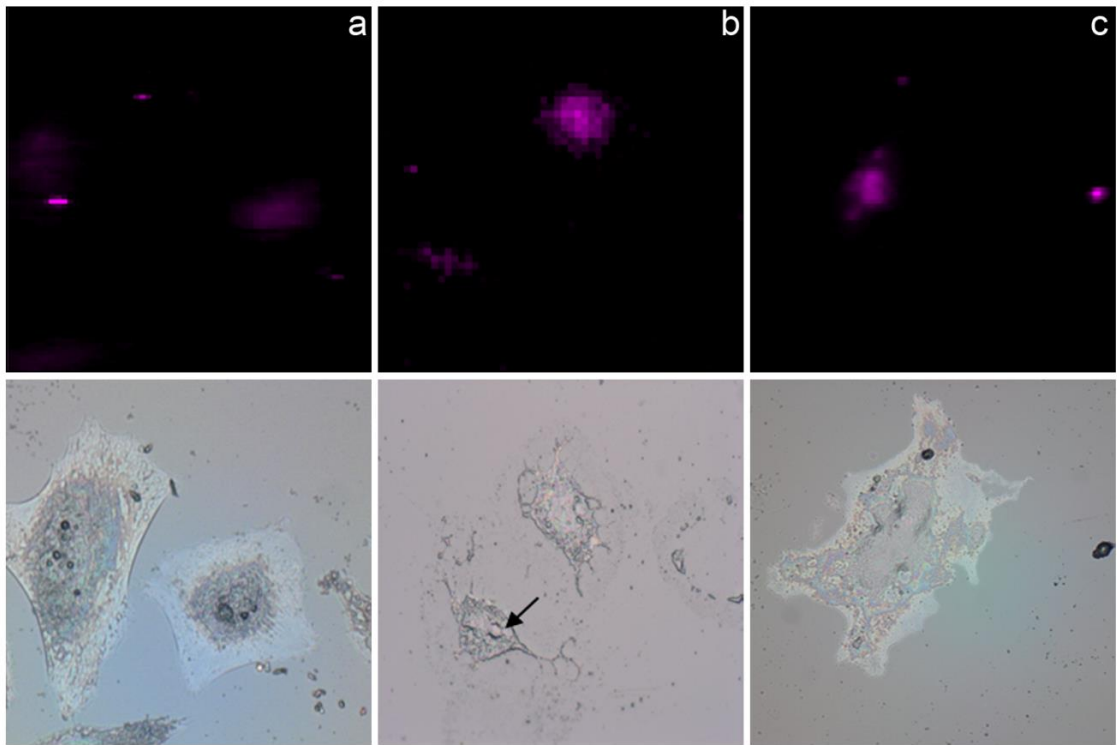
Figure 6.3 μ-XRF maps of osteoblasts and osteoclasts treated with Cr^{6+}

Top panel represents Cr^{6+} treated osteoblasts (a), developing osteoclasts (b), and mature osteoclasts (c), with corresponding microscope images (bottom panel). Chromium diffused throughout the cell body (arrow) with no localisation to specific areas within osteoblasts and osteoclasts.
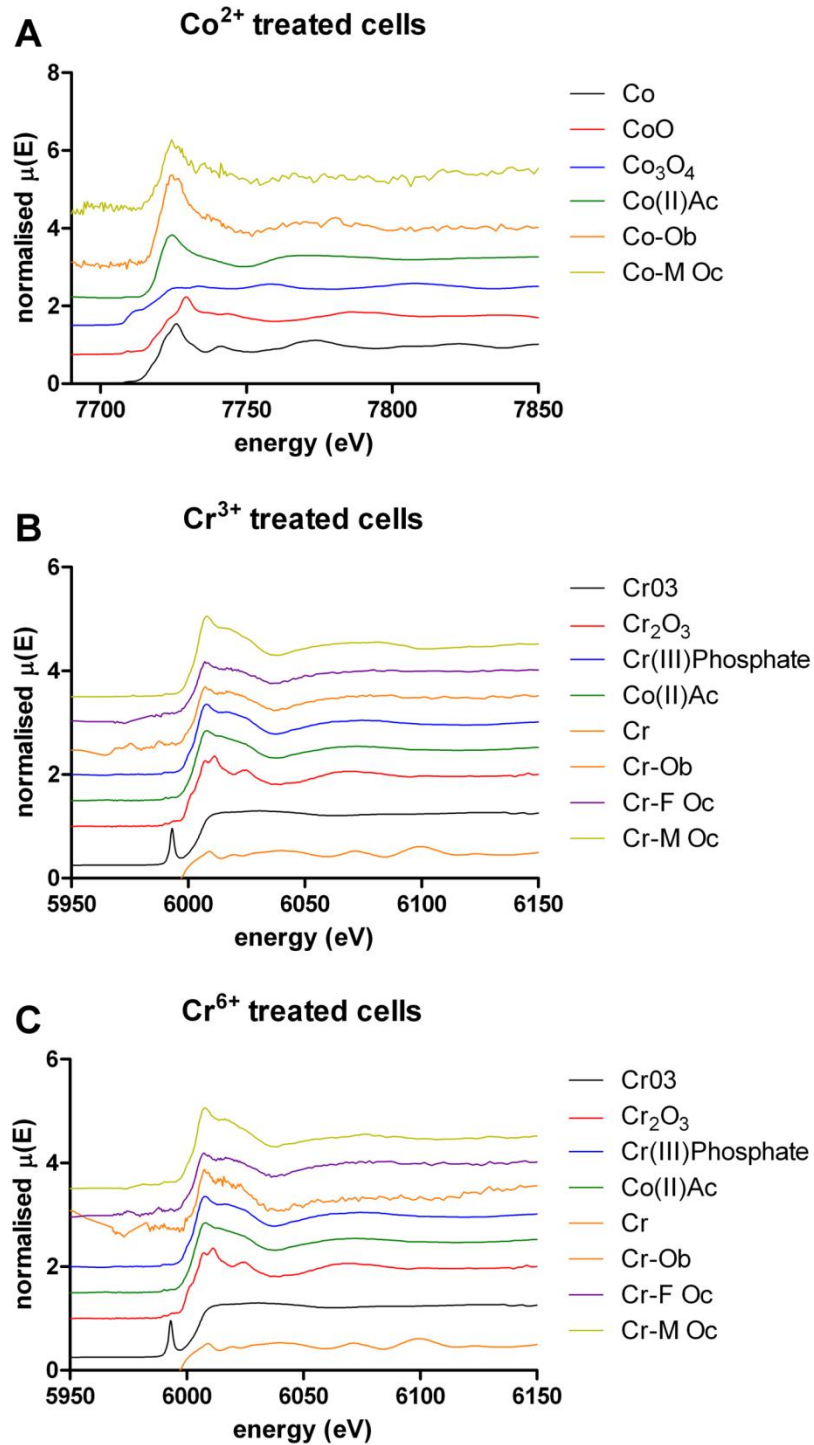
Figure 6.4 μ-XANES spectra for cells treated with metal ions

Co²⁺ (A), Cr³⁺ (B) and Cr⁶⁺(C) treated cells compared to standards of different oxidation states. 'Ob' – osteoblasts, 'F-Oc' – forming osteoclasts and 'M-Oc' – mature osteoclasts. Spectra for cells treated with Co²⁺ correlates closely with that of Co(II) acetate standard suggesting a +2 oxidation state. Cr in +3 oxidation states observed for all cells treated with Cr³⁺ and Cr⁶⁺ (Cr(III)PO₄ and Cr(III)OH standards) with the absence of distinctive pre-edge feature of Cr⁶⁺ (CrO₃ standard).

6.3 Discussion

Cobalt and chromium ions have detrimental effects on osteoblast and osteoclast survival and function; however, the mechanisms that mediate these effects are unclear. We examined the intracellular distribution and speciation of cobalt and chromium ions in treated human osteoblasts and primary human osteoclasts in order to better understand their sites and mechanisms of action within these cells. Co^{2+} and Cr^{3+} are distributed differently within osteoblasts versus osteoclasts; however Cr^{6+} is similarly distributed. The different elemental metals also had different intracellular distributions within the different cell types, with osteoblasts showing predominantly nuclear localisation of cobalt when treated with Co^{2+}, Cr^{3+} treated cells showing perinuclear chromium distribution, and Cr^{6+} treated cells showing chromium throughout the cell body. In both forming and mature osteoclasts, Co^{2+} and Cr^{3+} treated cells showed the metals localised to the basolateral membrane, whilst Cr^{6+} treated cells showed a diffuse pattern of chromium distribution. We found no evidence of intracellular change in oxidation state for Co^{2+} and Cr^{3+}, but observed intracellular reduction of Cr^{6+} to Cr^{3+}.

In a previous study we demonstrated that Cr^{6+} had the most detrimental effect on bone cells (Andrews*, et al* 2011). In this study, the µ-XANES spectra determined the localisation of Cr^{3+} in Cr^{6+} treated cells. The presence of Cr^{3+} is consistent with the intracellular reduction of Cr^{6+} and its observed toxicity through generation of reactive oxygen species and subsequent DNA damage (Patlolla*, et al* 2009). In addition, these observations support the notion that Cr^{6+} is not detected in explant tissues from patients, as it is present only in the reduced Cr^{3+} state (Hart*, et al* 2010a). The diffuse localisation of chromium in both Cr^{6+} treated osteoblasts and osteoclasts suggest a similar mechanism of metal uptake in these cell types. Cr^{6+} exists as divalent chromate ion (CrO_4^{2-}) at physiological pH that is analogous to phosphates and sulphates, which readily enter cells via their anion transporters (Arslan*, et al* 1987, Chiu*, et al* 2004).

The observed increased nuclear localisation of cobalt in osteoblasts may represent a possible target of action. Intracellular Co^{2+} interacts with genomic DNA and nuclear proteins associated with DNA repair (Bresson*, et al* 2006,

Kasten, *et al* 1997), and may explain its preferential localisation to nuclear and perinuclear sites. Co^{2+} is known to substitute zinc in zinc-fingers (Kopera, *et al* 2004); a structural motif present in many transcription factors and integral to protein-DNA interactions and subsequent gene transcription.

In osteoblasts, cobalt was also found at a relatively lower level throughout the cell body, in keeping with other divalent cations that have established membrane channels and transporters, such as Ca^{2+} and Zn^{2+} (Sheridan, *et al* 2013). Therefore, this distribution may be indicative of the cellular entry of cobalt via plasma membrane bound channels and transporters. Indeed, cellular entry of Co^{2+} is mediated, at least in part, via the proton-coupled divalent transporter DMT-1, a Fe^{2+} transporter (Forbes and Gros 2003, Garrick, *et al* 2006, Sacher, *et al* 2001, Yeung, *et al* 2005). More recently, inhibition of Ca^{2+} influx in presence of Co^{2+} has suggested a role of Ca^{2+}-channel transporters in cellular entry of Co^{2+} (Simonsen, *et al* 2011).

In osteoclasts the localisation of cobalt to the basolateral membrane may be indicative of sequestered cobalt in vesicles undergoing exocytosis through a functional secretory domain (FSD). In support of this, previous studies have shown that metal ions including cobalt and chromium are taken up by osteoclasts cultured on metal surfaces (such as titanium, aluminium and stainless steel) most likely by endocytosis and are released into the culture supernatant via the transcytotic pathway (Cadosch, *et al* 2010, Cadosch, *et al* 2009).

The observation that cobalt exists in its +2 oxidised state within both osteoblasts and mature osteoclasts is consistent with previous *ex-vivo* studies (Goode, *et al* 2012, Hart, *et al* 2012) and suggests the absence of any intracellular redox changes. Nevertheless, Co^{2+} is known to catalyse Fenton-like reactions that generate ROS and free radicals, before returning to its +2 oxidation state (Leonard, *et al* 1998, Valko, *et al* 2006). Alternative mechanisms of cytotoxicity such as disruption of vital enzymatic activities by displacement of divalent cation centres (Maxwell and Salnikow 2004) and interaction with zinc-finger structures of transcription factors may be more likely. The absence of μ-XANES spectra for cobalt in the developing osteoclast is due to its presence at relatively low

concentrations. The relatively under-developed endocytic and transcytotic machinery in developing osteoclasts compared to mature osteoclasts (Nesbitt and Horton 1997) might explain this difference. A lower concentration of cobalt observed in developing osteoclasts also supports our hypothesis of endocytosis being the predominant mechanism of cobalt uptake in osteoclasts.

Cr^{3+} is thought to be impermeable to cell membranes with no specific system for membrane transport (Ramirez-Diaz, *et al* 2008). In contrast with the current dogma, we found intracellular chromium following Cr^{3+} treatment. One explanation for the peri-nuclear localisation of Cr^{3+} in osteoblasts is its ability to bind to proteins within the extracellular milieu such as albumin (Tkaczyk, *et al* 2010) which enters cells via endocytosis. Once internalised the albumin-Cr^{3+} will be trafficked in lysosomes and returned to the golgi apparatus for recycling (Yokota and Fahimi 1987). A similar mechanism may exist in osteoclasts whereby the recycled proteins undergo exocytosis from the basolateral FSD. Whilst Cr^{3+} has a high affinity for DNA in a cell-free system (Dai, *et al* 2009, Macfie, *et al* 2010), our observation that Cr^{3+} was not localised to the nuclear region may suggest that Cr^{3+} bound to proteins once internalised is preferentially targeted to the golgi for recycling.

The µ-XANES spectra demonstrated that chromium exists in the +3 oxidation states in all Cr^{3+} treated cells and is consistent with previous findings in periprosthetic tissues (Goode, *et al* 2012, Hart, *et al* 2012, Hart, *et al* 2010a, Huber, *et al* 2009) confirming the importance of this ion species in MOMHR complications. Given the lack of nuclear localisation and chromium existing in its lowest redox state in cells treated with sub-toxic levels of Cr^{3+}, the observed toxic effect at higher concentrations may occur via disruption of the cell membrane integrity (Rudolf and Cervinka 2005, Suwalsky, *et al* 2008) and induction of necrosis (Huk, *et al* 2004).

6.4 Conclusion

In summary, the study describes the sub-cellular localisation and speciation of soluble metal ion species in human osteoblasts and osteoclasts using synchrotron-based μ-XRF and μ-XANES. The intracellular distribution of metal ions highlights a cell- and metal-specific mode of cellular entry, whilst speciation confirms no redox change in Co^{2+} or Cr^{3+}, but an intracellular reduction of Cr^{6+} to Cr^{3+}. Our study is the first to show that Cr^{3+} can cross bone cell membranes to enter the cell. The difference in cellular distribution between Cr^{3+} and Cr^{6+} derived chromium may represent a possible way to identify the parent species in pathological tissue samples. The data suggests possible mechanisms of cellular entry of metal ions which may provide therapeutic targets to ameliorate the adverse effects of MOMHR.

Chapter 7 - The role of P2X7R and DMT-1 in cellular uptake of Co^{2+} in osteoblasts and osteoclasts

7.1 Introduction

In the previous chapters, the detrimental effects of cobalt (Co) and chromium (Cr) ions (Co^{2+}, Cr^{3+} and Cr^{6+}) have been described, together with their intracellular distribution and speciation in osteoblasts and osteoclasts. The results suggest a cell-specific mechanism for cellular uptake of these metal ions with several putative receptors and transporters implicated. This chapter explores the role of both a plasma membrane ion channel (P2X7R) and a transporter (divalent metal ion transporter-1; DMT-1) in the cellular entry of Co^{2+}, as its prevention is likely to be of therapeutic value.

7.1.1 P2X7R

The P2X7 receptor (P2X7R) is a member of P2 family of receptors that are activated by extracellular nucleotides. Brief activation by its physiological agonist adenosine triphosphate (ATP) causes the P2X7R to function as a cation channel, increasing the levels of intracellular Ca^{2+}. However, sustained or repeated activation results in formation of a non-selective aqueous pore permeable to solutes up to 900Da (Di Virgilio 1995). Functional P2X7R are expressed on all bone cells and its role in regulation of bone is well established (Gartland, *et al* 2001, Rumney, *et al* 2012).

A study investigating the effects of Co and Cr nanoparticles demonstrated DNA damage in fibroblasts separated by an intact cellular barrier, without the metal debris crossing of the barrier (Bhabra, *et al* 2009). They further described a possible role of ATP release and P2X7R activation in mediating these indirect effects across the barrier (Bhabra, *et al* 2009). In addition to indirect effects of metal ions via ATP release, Co^{2+} has been shown to be a negative allosteric modulator of rat P2X7R (Virginio C, *et al* 1997), whilst other members of the P2X family - P2X2R and P2X4R - are potentiated by Co^{2+} in the range of 500-5000µg/L (Coddou, *et al* 2003, Lorca, *et al* 2005). These contrasting effects are thought to be due to different positions of the metal ion binding histidine residues in the different receptors (Coddou, *et al* 2011). Sequence alignment of rat and human P2X7R shows inconsistencies in histidine residue positions (Figure 7.1) that might result in a different action of Co^{2+} for these receptors. A highly specific

competitive antagonist for P2X7R (A740003) has been used in this study to assess its role in Co^{2+} uptake (Honore*, et al* 2006).

```
CLUSTAL O(1.2.0) multiple sequence alignment


ratP2X7R      MPACCSWNDVFQYETNKVTRIQSVNYGTIKWILHMTVFSYVSFALMSDKLYQRKEPLISS
humanP2X7R    MPACCSCSDVFQYETNKVTRIQSMNYGTIKWFFHVIIFSYVCFALVSDKLYQRKEPVISS
              ****** .***************:*******::*: :****.***:**********:***


ratP2X7R      VHTKVKGVAEVTENVTEGGVTKLVHGIFDTADYTLPLQGNSFFVMTNYLKSEGQEQKLCP
humanP2X7R    VHTKVKGIAEVKEEIVENGVKKLVHSVFDTADYTFPLQGNSFFVMTNFLKTEGQEQRLCP
              *******:***.*::.* **.****.:*******:***********:**:*****:***


ratP2X7R      EYPSRGKQCHSDQGCIKGWMDPQSKGIQTGRCIPYDQKRKTCEIFAWCPAEEGKEAPRPA
humanP2X7R    EYPTRRTLCSSDRGCKKGWMDPQSKGIQTGRCVVYEGNQKTCEVSAWCPIEAVEEAPRPA
              ***:*  . * **:** ****************: *: ::****: **** *  :******


ratP2X7R      LLRSAENFTVLIKNNIDFPGHNYTTRNILPGMNISCTFHKTWNPQCPIFRLGDIFQEIGE
humanP2X7R    LLNSAENFTVLIKNNIDFPGHNYTTRNILPGLNITCTFHKTQNPQCPIFRLGDIFRETGD
              **.************************:**:***** ************:* *:


ratP2X7R      NFTEVAVQGGIMGIEIYWDCNLDSWSHRCQPKYSFRRLDDKYTNESLFPGYNFRYAKYYK
humanP2X7R    NFSDVAIQGGIMGIEIYWDCNLDRWFHHCRPKYSFRRLDDKTTNVSLYPGYNFRYAKYYK
              **::**:****************** * *:*:************ ** **:*********


ratP2X7R      ENGMEKRTLIKAFGVRFDILVFGTGGKFDIIQLVVYIGSTLSYFGLATVCIDLIINTYAS
humanP2X7R    ENNVEKRTLIKVFGIRFDILVFGTGGKFDIIQLVVYIGSTLSYFGLAAVFIDFLIDTYSS
              ** :*******.**:***********************************: **:*:*:**:*


ratP2X7R      TCCRSRVYPSCKCCEPCAVNEYYYRKKCEPIVEPKPTLKYVSFVDEPHIWMVDQQLLGKS
humanP2X7R    NCCRSHIYPWCKCCQPCVVNEYYYRKKCESIVEPKPTLKYVSFVDESHIRMVNQQLLGRS
              .****::** ****:**.***********: ****************** ** **:*****:*


ratP2X7R      LQDVKGQEVPRPQTDFLELSRLSLSLHHSPPIPGQPEEMQLLQIEAVPRSRDSPDWCQCG
humanP2X7R    LQDVKGQEVPRPAMDFTDLSRLPLALHDTPPIPGQPEEIQLLRKEATPRSRDSPVWCQCG
              ************  ** :**** *:**.:*********::**: ***. **.****** *****


ratP2X7R      NCLPSQLPENRRALEELCCRRKPGQCITTSELFSKIVLSREALQLLLLYQEPLLALEGEA
humanP2X7R    SCLPSQLPESHRCLEELCCRKKPGACITTSELFRKLVLSRHVLQFLLLYQEPLLALDVDS
              .********:.:*.******:***.********:*:****:.**:**:************: ::


ratP2X7R      INSKLRHCAYRSYATWRFVSQDMADFAILPSCCRWKIRKEFPKTQGQYSGFKYPY
humanP2X7R    TNSRLRHCAYRCYATWRFGSQDMADFAILPSCCRWRIRKEFPKSEGQYSGFKSPY
              **:*******.****** ****************:******:.*****: ******* **
```

Figure 7.1 Sequence alignment of rat P2X7R and human P2X7R

Rat and human protein sequences were aligned using Clustal Omega (www.ebi.ac.uk). The differences in the histidine residues (H) between the two sequences are highlighted with black stars. These amino acids are sites for metal ion binding and the differences in their positions could result in a different effect upon metal binding with the first two stars corresponding to the H residues in the extracellular loop.

7.1.2 DMT-1

DMT-1, also known as natural resistance-associated macrophage protein 2 (NRAMP2), is a proton-coupled iron (Fe^{2+}) transporter protein that is responsible for the transferrin-independent cellular uptake of Fe^{2+} in intestines and its release from transferrin containing endosomal compartments (Gruenheid, *et al* 1999). In addition to its role in cellular uptake of Fe^{2+}, DMT-1 is known to have a broad specificity, and has been described to allow entry Co^{2+}, Ni^{2+}, Mn^{2+}, Cd^{2+}, Zn^{2+} and Cu^{2+} in oocytes overexpressing the protein (Gunshin, *et al* 1997, Illing, *et al* 2012, Picard, *et al* 2000).

DMT-1 is thought to be present ubiquitously, with expression confirmed in various tissues such as kidneys, skeletal muscle, liver, brain and bone marrow (Gunshin, *et al* 1997). Its expression is well established in macrophage cells which are responsible for recycling of iron-rich erythrocytes by phagocytosis (Jabado, *et al* 2002). Osteoclasts, which belong to the same lineage, are likely to express DMT-1, especially with their known high transferrin internalisation (Stenbeck and Horton 2004). Investigation of sub-cellular distribution of DMT-1 using immunofluorescence against HA-tag epitopes demonstrated that approximately 40% of the total DMT-1 expression is on the cell surface (Touret, *et al* 2003). Taken together, this suggests that DMT-1 is likely to be expressed on osteoclast cell surface and has been proposed to be responsible for cellular entry of Co^{2+} in the periprosthetic environment (Keegan, *et al* 2007, Mabilleau, *et al* 2008). In this study, we make use of a DMT-1 specific inhibitor (NSC306711) identified from National Cancer Institute's Diversity Set (Buckett and Wessling-Resnick 2009).

This chapter presents the results for cellular uptake of Co^{2+} as assessed by measuring the intracellular quenching of fluorescent Calcein-AM over time (Breuer, *et al* 1995, Forbes and Gros 2003), the technique detailed in section 2.13.

7.2 Results

7.2.1 Calcein-AM quenching by Co^{2+}

Osteoblasts (SaOS-2) and primary human osteoclasts were incubated 0.25µM Calcein AM, which was quenched in presence of extracellular Co^{2+} over time (Figures 7.2 and 7.3). The concentrations of Co^{2+} are in the clinically relevant range of patient serum and hip aspirate (5-5000µg/L). A supraphysiological concentration of 50000µg/L was used to engender an acute response within 1 hour. The fluorescence intensities relative to the cellular baseline of osteoblasts for increasing concentrations of Co^{2+} are plotted in Figure 7.4A. To represent these results as an increasing change in cellular fluorescence with increasing cellular entry of Co^{2+}, the quenching data was inversed and plotted as in Figure 7.4B.

The area-under-curve (AUC), plotted to represent the data as increased entry of Co^{2+} into the cells, was significantly higher for 5000µg/L (mean ± 95%CI; 1.49 ± 0.151) and 50000µg/L (1.66 ± 0.148) compared to untreated control (1.0 ± 0.168) (Figure 7.4C). Subsequent data in this chapter has been represented in this format.
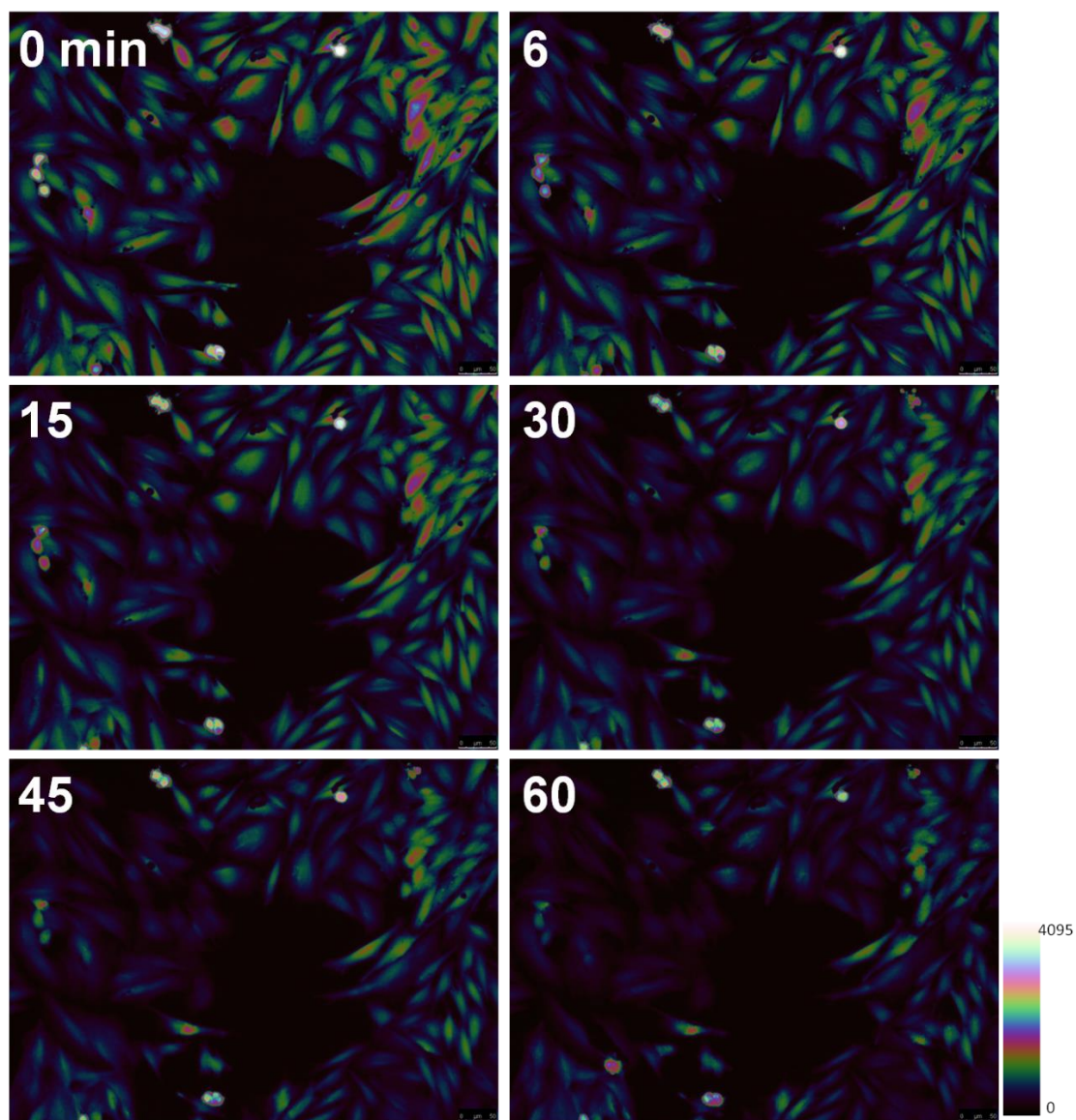
Figure 7.2 Fluorescence quenching in osteoblasts

Time lapse images of fluorescence in SaOS-2 cells loaded with 0.25µM Calcein-AM being quenched with 5000µg/L Co^{2+} over 60 min. The heat-map alongside corresponds to the intensity of cellular fluorescence.
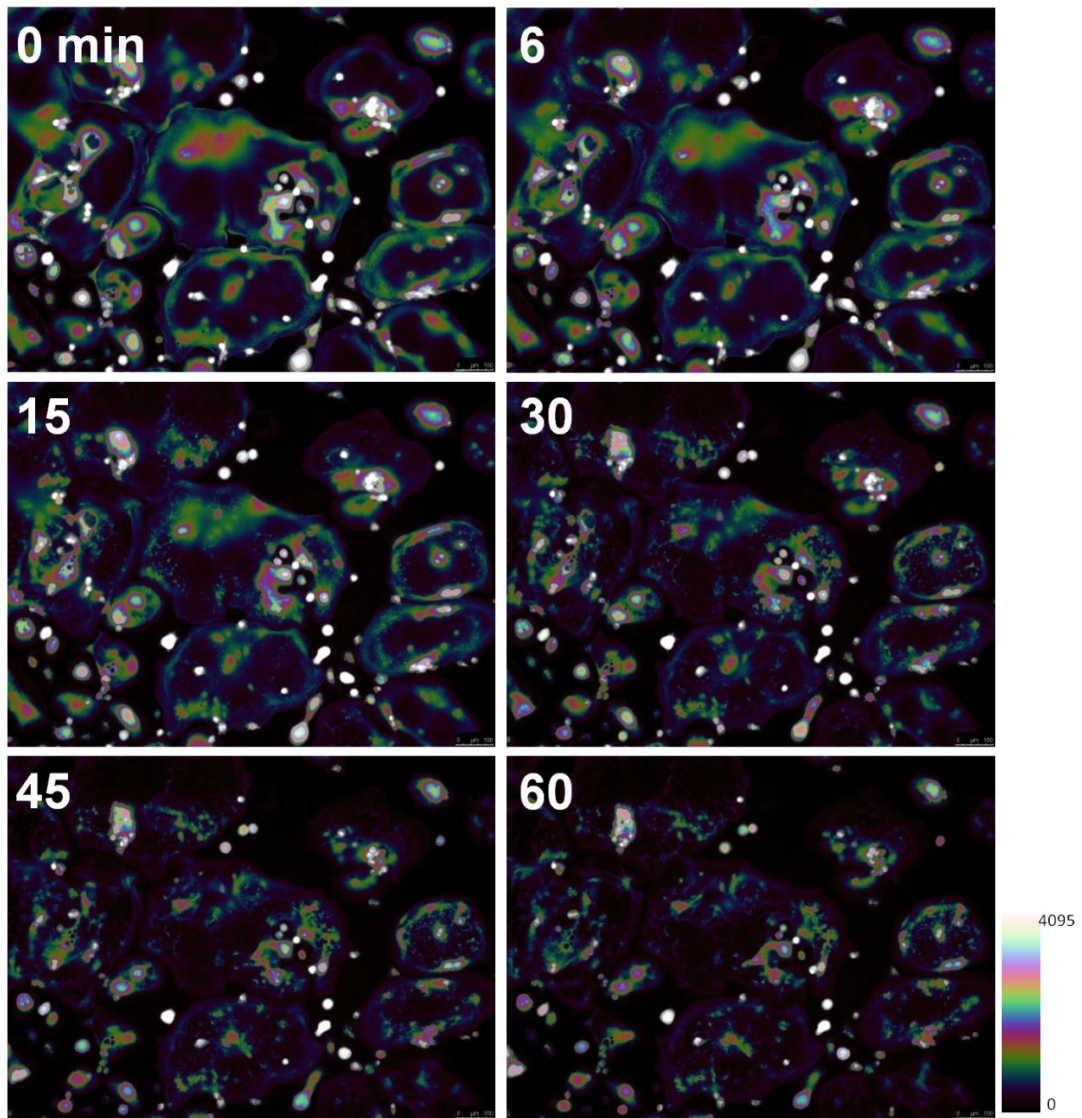
Figure 7.3 Fluorescence quenching in osteoclasts

Time lapse images of fluorescence in primary human osteoclasts cells loaded with 0.25µM Calcein-AM being quenched with 50000µg/L Co^{2+} over 60 min. The heat-map alongside corresponds to the intensity of cellular fluorescence.
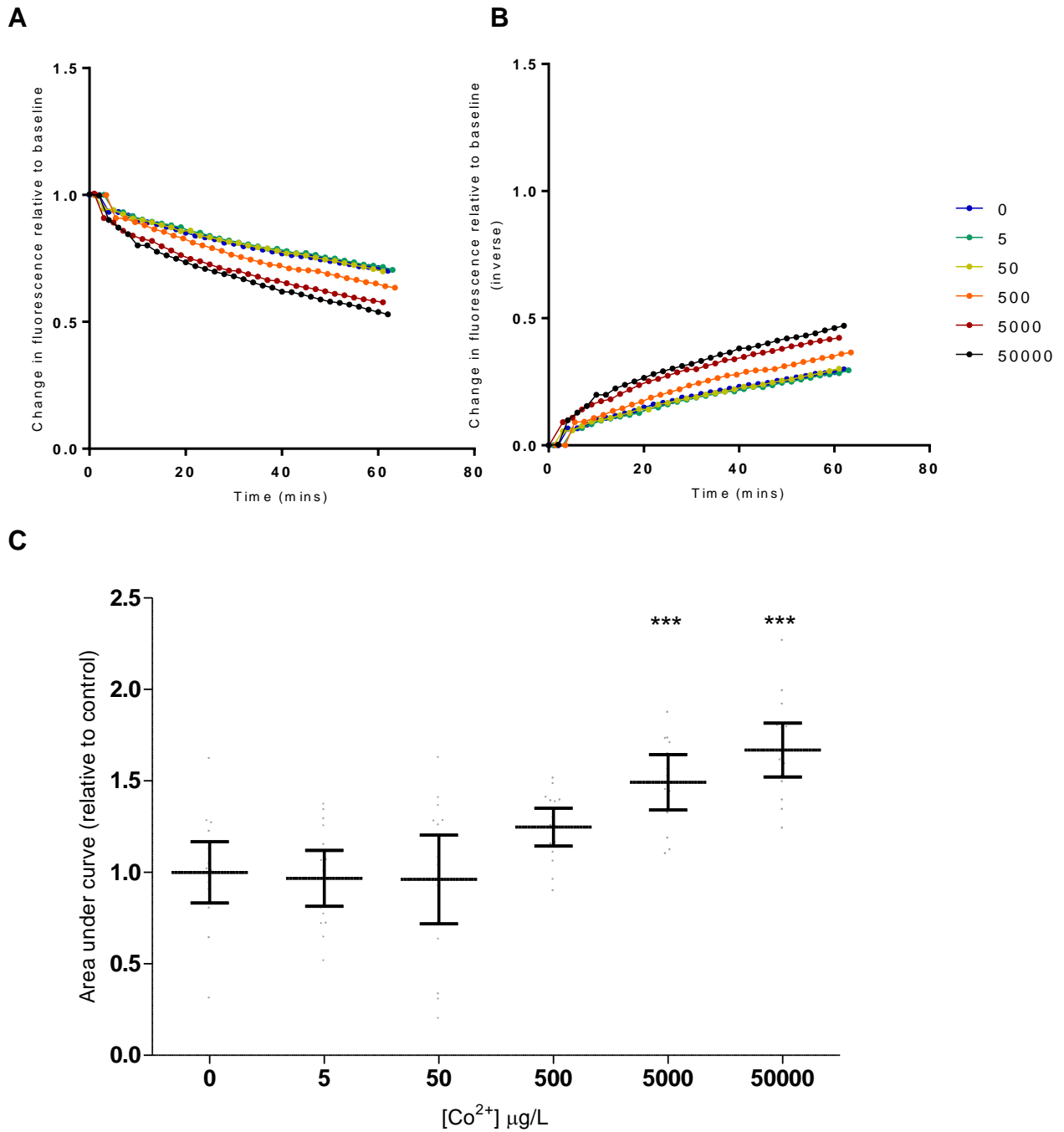
Figure 7.4 Quenching of cellular fluorescence by Co^{2+} in osteoblasts.

A) Quenching of intracellular Calcein-AM with increasing concentrations of Co^{2+}. B) Inverse of the quenching curves to represent increased cellular entry of Co2+ with increase in concentrations. C) The data represented as area-under-curve relative to untreated control. Data from 15 individual cells per concentration (mean ± 95%CI) analysed by One-way ANOVA with Dunnett's multiple comparison test (***p<0.0001).

7.2.2 DMT-1 expression in osteoblasts and osteoclasts

Expression of DMT-1 was assessed for non-permeabilsed osteoblasts and osteoclasts cultured on glass coverslips, using an anti-DMT-1 rabbit polyclonal antibody (section 2.13). No primary and isotype IgG controls were used to assess the primary antibody specificity.

Both cell types expressed DMT-1 as illustrated in Figure 7.5. The control staining suggest no cross reactivity as illustrated in Figure 7.6.
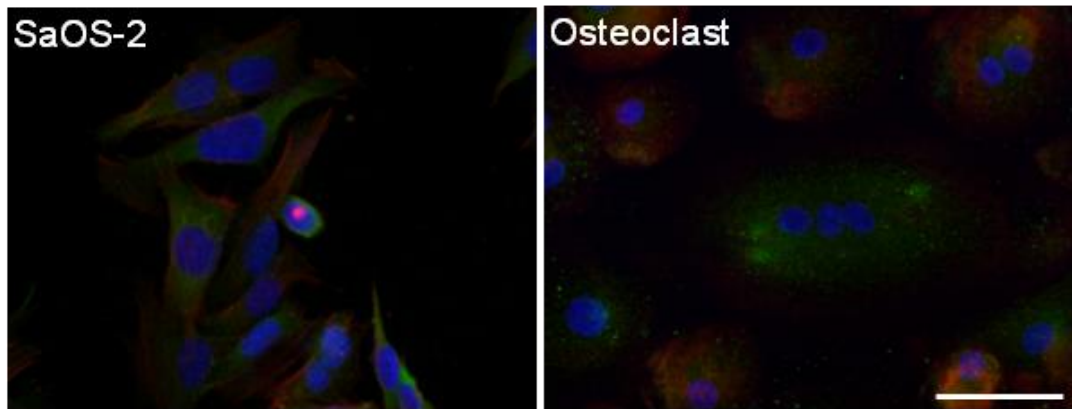
Figure 7.5 DMT-1 expression in osteoblasts and osteoclasts - immunofluorescence

SaOS-2 osteoblasts and primary human osteoclasts stained with rabbit polyclonal antibody against DMT-1. Both cells express DMT-1 (green); with nucleus (blue) and F-actin staining (red). Scale bar = 50μm
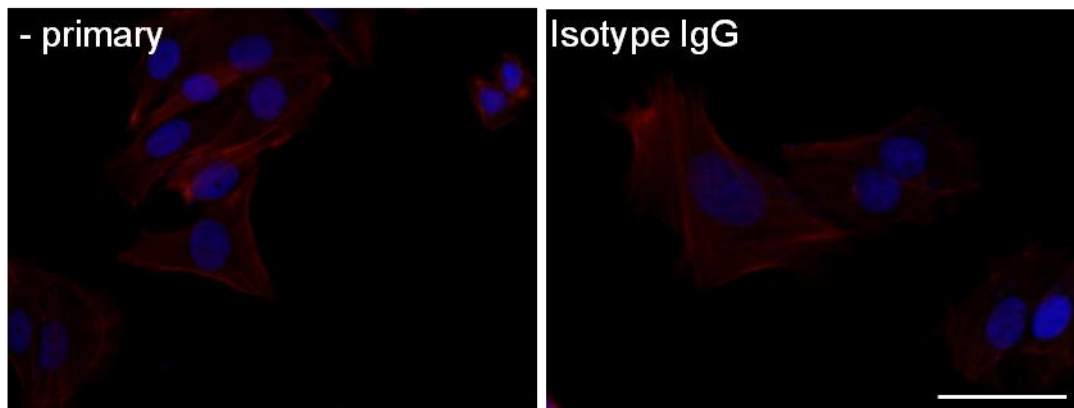
Figure 7.6 Immunofluorescence controls

No primary control and isotype IgG control for the antibody specificity on SaOS-2 cells with nucleus (blue) and F-actin (red).Scale bar = 50μm

7.2.3 Role of P2X7R in uptake of Co^{2+}

Cellular entry of Co^{2+} was measured as the area-under-curve of fluorescent intensities measured over time for individual osteoblasts and osteoclasts. The concentrations of Co^{2+} ranged from 0-50000µg/L with P2X7R antagonist A740003 used at a fixed concentration of 40nM.

The results show a significant increase in Co^{2+} mediated change in fluorescence for osteoblasts at treatments of 5000µg/L (mean ± 95%CI; 1.22 ± 0.10) and 50000µg/L (1.55 ± 0.08) compared to untreated controls (1.0 ± 0.08). The P2X7R antagonist abrogated this effect, and hence reduced the cellular entry of Co^{2+} at 500µg/L ($p<0.01$), 5000µg/L ($p<0.05$) and 50000µg/L ($p<0.0001$) compared to cells with no antagonist treatment (Figure 7.5A-B).

In case of osteoclasts, a significant increase in Co^{2+} mediated change in fluorescence was observed for the highest concentration of 50000µg/L (1.46 ± 0.11) compared to untreated controls. However, unlike osteoblasts, no reduction was observed in presence P2X7R antagonist at that concentration.
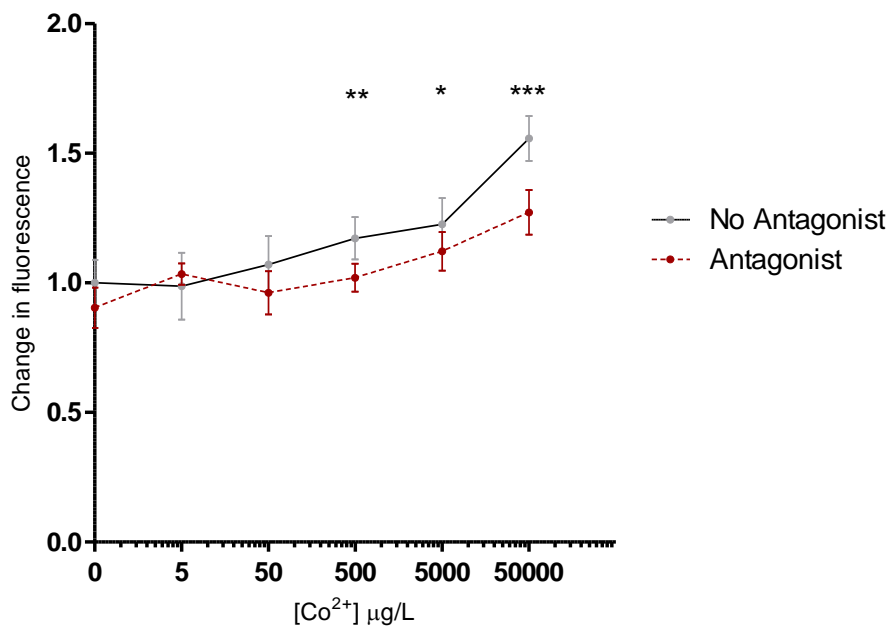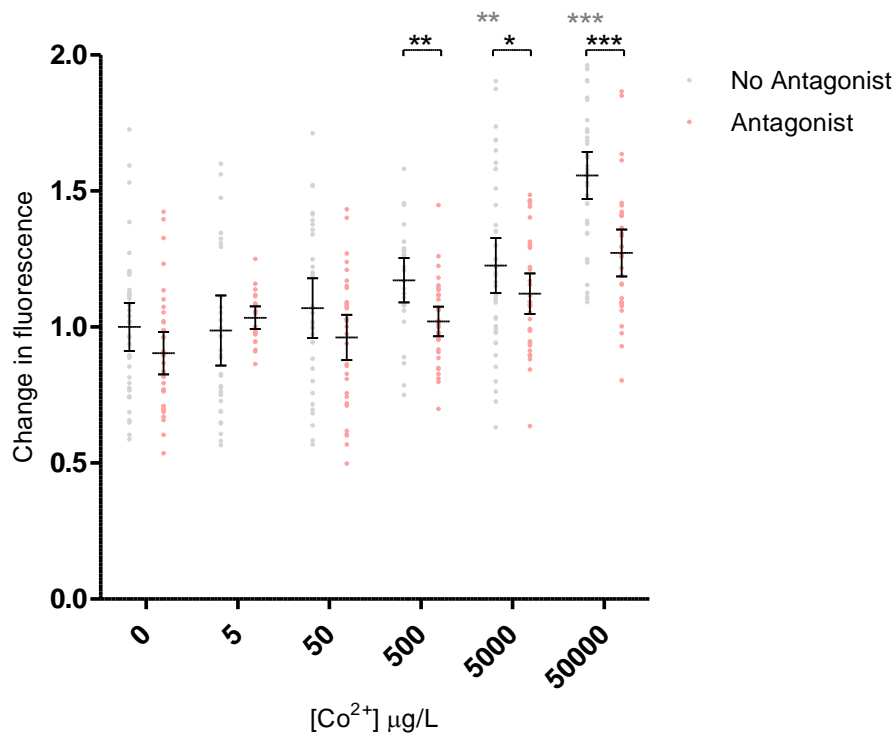
Figure 7.7 Effect of P2X7R antagonist on Co²⁺ entry in SaOS-2

Co²⁺ entry was assessed by measuring quenching of Calcein-AM over one hour, in presence of 40nM P2X7R specific antagonist (A740003). Area-under-curves for different concentrations of Co²⁺ plotted relative to untreated control in absence (gray) and presence of P2X7R antagonist (red). All values are mean ± 95%CI from 3 separate experiments with 10-15 cells assessed from each experiment. Students t-test is used to compare differences between no agonist and agonist treated cells at each concentration (*$p<0.05$; **$p<0.01$; ***$p<0.0001$).
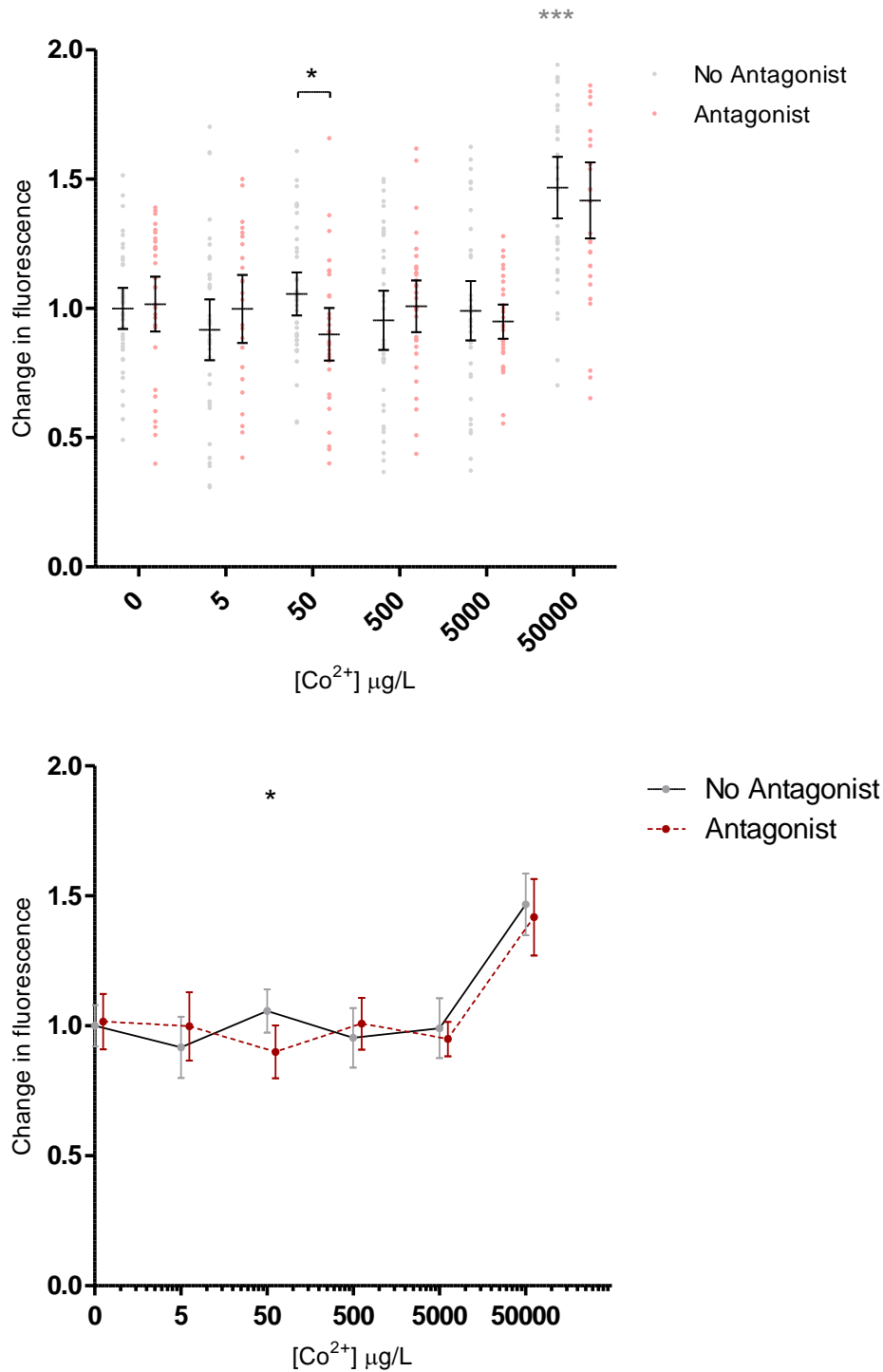
Figure 7.8 Effect of P2X7R antagonist on Co²⁺ entry in primary human osteoclasts

Co²⁺ entry was assessed by measuring quenching of Calcein-AM over one hour, in presence of 40nM P2X7R specific antagonist (A740003). Area-under-curves for different concentrations of Co²⁺ plotted relative to untreated control in absence (gray) and presence of P2X7R antagonist (red). All values are mean ± 95%CI from 3 separate experiments with 10-15 cells assessed from each experiment. Students t-test is used to compare differences between no agonist and agonist treated cells at each concentration (*$p<0.05$; ***$p<0.0001$).

7.2.4 Role of DMT-1 in uptake of Co^{2+}

Cellular entry of Co^{2+} was measured as the area-under-curve of fluorescent intensities measured over time for individual osteoblasts and osteoclasts. The concentrations of Co^{2+} ranged from 0-50000µg/L with DMT-1 antagonist NSC306711 used at a fixed concentration of 50µM.

A significant increase in Co^{2+} mediated change in fluorescence for osteoblasts at treatments of 5000µg/L (mean ± 95%CI; 1.40 ± 0.12) and 50000µg/L (1.60 ± 0.17) compared to untreated controls (1.0 ± 0.18). DMT-1 antagonist treatment had no effect on cellular entry of Co^{2+} at any concentrations (Figure7.7A-B).

In osteoclasts, Co^{2+} mediated change in fluorescence was significantly higher for 50000µg/L (1.29 ± 0.13) compared to untreated control (1.0 ± 0.09), with DMT-1 antagonist having no effect at any concentrations of Co^{2+} (Figure 7.8A-B).
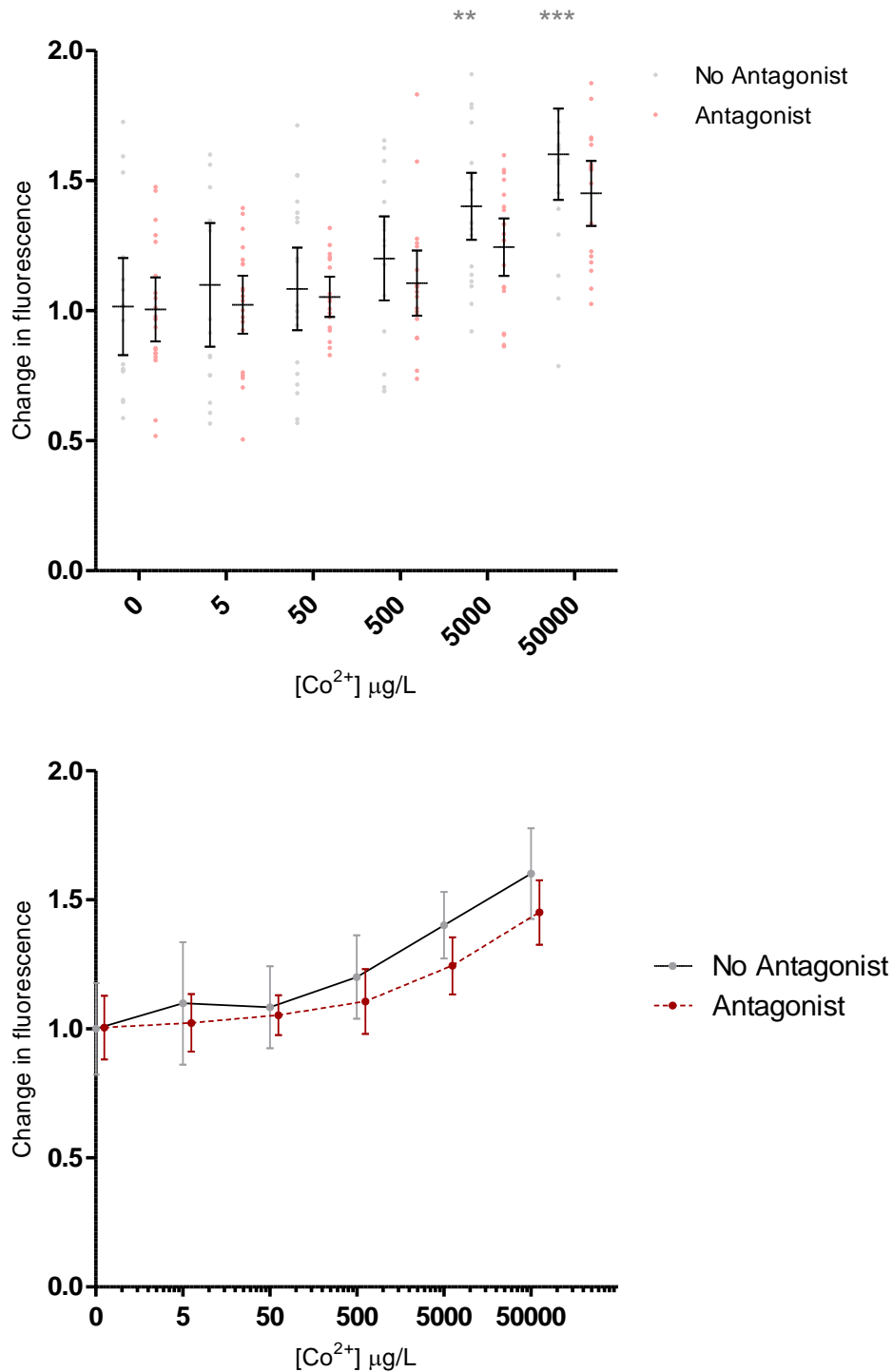
Figure 7.9 Effect of DMT-1 antagonist on Co^{2+} entry in SaOS-2

Co^{2+} entry was assessed by measuring quenching of Calcein-AM over one hour, in presence of 50µM DMT-1 specific antagonist (NSC306711). Area-under-curves for different concentrations of Co^{2+} plotted relative to untreated control in absence (gray) and presence of DMT-1 antagonist (red). All values are mean ± 95%CI from 3 separate experiments with 10-15 cells assessed from each experiment. Students t-test is used to compare differences between no agonist and agonist treated cells at each concentration (**$p<0.01$; ***$p<0.0001$).
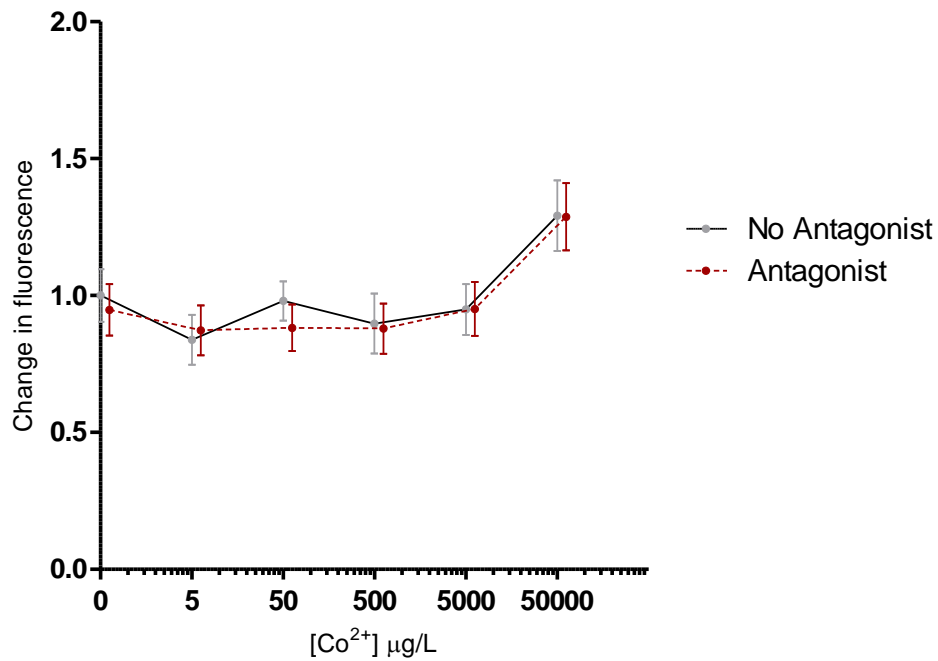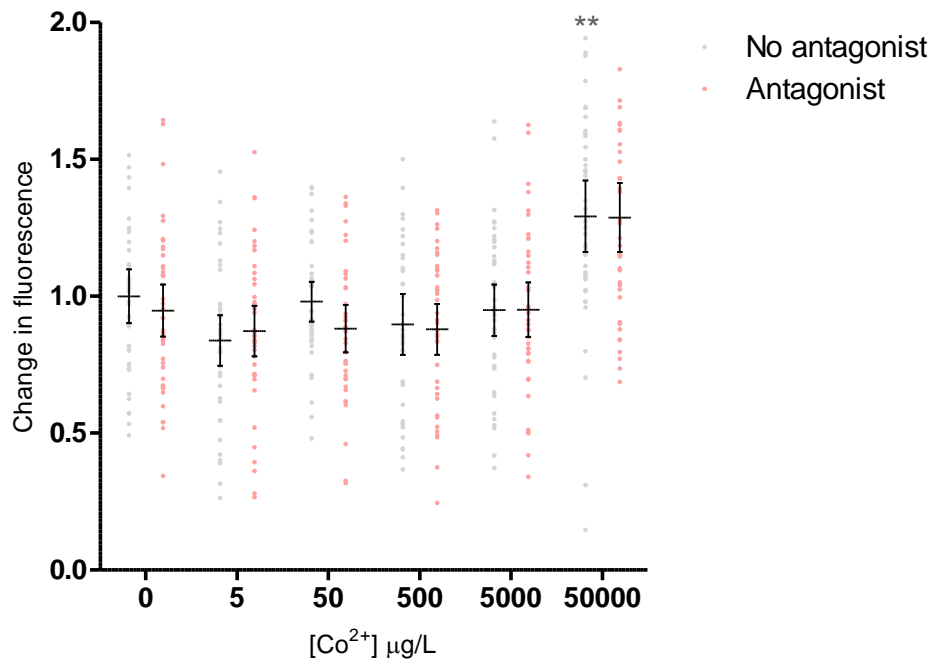
Figure 7.10 Effect of DMT-1 antagonist on Co^{2+} entry in primary human osteoclasts

Co^{2+} entry was assessed by measuring quenching of Calcein-AM over one hour, in presence of 50µM DMT-1 specific antagonist (NSC306711). Area-under-curves for different concentrations of Co^{2+} plotted relative to untreated control in absence (gray) and presence of DMT-1 antagonist (red). All values are mean ± 95%CI from 3 separate experiments with 10-15 cells assessed from each experiment. Students t-test is used to compare differences between no agonist and agonist treated cells at each concentration (**$p<0.01$).

7.3 Discussion

The prevention of metal ion entry into cells of the periprosthetic environment may serve as a therapeutic intervention to reduce for metal-related adverse events after MOMHR and MOMTHR. In this study, we explored the role of P2X7R ATP-gated ion channel and divalent metal transporter-1 (DMT-1) in the cellular uptake of Co^{2+} in human osteoblast-like SaOS-2 cells and primary human osteoclasts. The results suggest a role of P2X7R in the uptake of Co^{2+} in osteoblasts, but not in osteoclasts, at concentrations equivalent to serum and hip aspirates in patients after MoMHR. DMT-1 did not seem to play a role in uptake of Co^{2+} in either cell types.

A possible role of P2X7R in CoCr mediated toxicity was hypothesised by Bhabra et al. (2009). In their study, a trophoblast cell barrier when treated with CoCr particles and ions resulted in DNA damage in fibroblasts seeded below the barrier. A decrease in DNA damage was observed when the fibroblasts were treated with a P2X7R antagonist. DNA damage was also reduced in presence of apyrase, an enzyme that hydrolyses ATP, suggesting that these effects are mediated via ATP (Bhabra, *et al* 2009).

The results from our study suggest that Co^{2+} results in the activation of P2X7R in osteoblasts that permits its entry into the cell. Whilst the ATP for P2X7R activation may have been released by the trophoblast cell barrier in the study by Bhabra et al. (2009), the activation of P2X7R in our study could occur via autocrine/paracrine mechanisms. A study in primary rat osteoblasts has demonstrated a significant increase in ATP release (~1µM) with transient exposure to hypoxia (0.5-1.5 min) (Orriss, *et al* 2009). The effect of Co^{2+} as a mimic of hypoxia is well-established and is thought to occur via stabilisation of hypoxia-inducible factor 1-alpha (HIF1α) which translocates to the nucleus and regulates the transcription of hypoxic genes (Salnikow, *et al* 2004, Vengellur and LaPres 2004). Taken together, Co^{2+} might cause the release of ATP by mimicking hypoxic conditions, with relatively higher concentrations of ATP at the cell surface likely to activate the P2X7R in an autocrine/paracrine manner allowing the cellular entry of Co^{2+}. Furthermore, the reduced entry of Co^{2+} with P2X7R antagonist is

observed at concentrations equivalent to those observed in patient serum and hip aspirate. At these concentrations of Co^{2+}, osteoblast cell death might contribute to ATP release in the local environment. A schematic of mechanisms described above is illustrated in Figure 7.9.

The P2X7R antagonist used in this study (A740003), being a competitive inhibitor of the receptor (Honore, *et al* 2006), would prevent ATP-binding and activation of P2X7R and subsequent cellular entry of Co^{2+} via the ion channel or non-selective pore. Additionally, the antagonist is also likely to reduce P2X7R mediated release of ATP (Suadicani, *et al* 2006), potentially decreasing its autocrine and paracrine actions. Antagonist binding may also prevent possible allosteric modulation of P2X7R by Co^{2+} described previously (section 7.1.1).

The additional role of P2X7R in regulating inflammation increases its potential value as a therapeutic target. During injury or cellular stress, extracellular ATP levels increase causing receptor activation and subsequent release of pro-inflammatory cytokines from immune cells. Previous studies have demonstrated the release of IL-1β (Ferrari, *et al* 1997), IL-1α, IL-4, IL-6, IL-13, IL-18 and TNFα (Alves, *et al* 2013) with P2X7R activation. Metal ions and particles released from the implant create an inflammatory environment in the surrounding tissue that drives periprosthetic osteolysis. Targeting P2X7R can have an anti-inflammatory effect in the periprosthetic environment, in addition to preventing detrimental effects of Co^{2+} on osteoblasts. Indeed, several phase I and II clinical trials have investigated P2X7R inhibition in inflammatory diseases such as rheumatoid arthritis, osteoarthritis and Crohn's disease (Arulkumaran, *et al* 2011).

Nevertheless, further investigations are required to support this study in establishing the role of P2X7R in cellular entry of Co^{2+} in osteoblasts. Firstly, the activation of P2X7R ion channel or the formation of a non-selective pore could be assessed in presence of extracellular Co^{2+}. The former would be evaluated by changes in intracellular Ca^{2+} as measured by Fura-2AM (Chao, *et al* 2012, Paredes-Gamero, *et al* 2004), and the latter by the cellular uptake of ethidium bromide (Gartland, *et al* 2001). In addition, the observed effects should be rescued in presence of specific P2X7R antagonists. Secondly, Co^{2+} mediated

ATP release could be confirmed by measuring its concentration in the media supernatant. Lastly, the detrimental effects of Co^{2+} on osteoblast survival and function described in previous chapters should be rescued in presence of P2X7R antagonists for it to be a target of therapeutic value.

In contrast to P2X7R antagonist, DMT-1 specific antagonist had no effect on cellular entry of Co^{2+} in osteoblasts and osteoclasts, although both cell types expressed the transporter. The absence of an effect in both cell types may be due the lack of sensitivity of the technique at lower concentrations of Co^{2+}. A Co^{2+} mediated change in fluorescence is observed for concentrations above 500µg/L for osteoblasts and only at the highest concentration of 50000µg/L for osteoclasts. The inability to detect changes at lower concentrations might mask any small effects the implicated receptors have at those concentrations. Additionally, the results with osteoclasts suggests that DMT-1 may not be the predominant mechanism for cellular entry of Co^{2+}, which is in support of our previous hypothesis based on the localisation of metal ions in the vesicular compartment of these cells (section 6.2.1).

7.4 Conclusion

In conclusion, the results from this chapter suggest a role of P2X7R in cellular entry of Co^{2+} in osteoblasts, but not osteoclasts. Our data suggest P2X7R are a potential therapeutic target to increase osseointegration of the prosthesis.
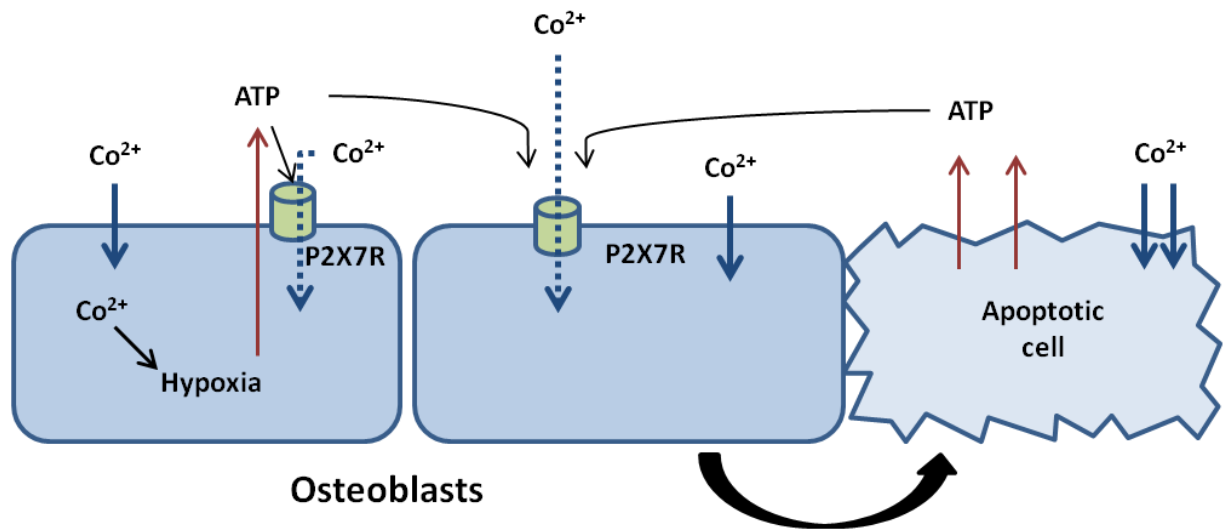
Figure 7.11 Schematic for the role of P2X7R in Co²⁺ uptake in osteoblasts

Cellular entry of Co^{2+} mimics hypoxic conditions that cause extracellular release of ATP. The released ATP can activate P2X7R in an autocrine or paracrine manner causing increased cellular entry of Co^{2+}. Increased Co^{2+} uptake causes cell apoptosis, releasing more ATP in extracellular milieu.

Chapter 8 - Effect of metal ions and particles on osteoblast mineralisation on grit-blasted, titanium-coated and hydroxyapatite-coated prosthesis surfaces

8.1 Introduction

The majority of hip prostheses (resurfacing and stemmed) currently in use are cementless (NJR 2013), and rely on osseointegration by osteoblasts for their long term survival. The detrimental effects of clinically relevant concentrations of cobalt and chromium ions (Co^{2+}, Cr^{3+} and Cr^{6+}) on osteoblast-like cell survival and function, and on early clinical loosening of prostheses in the presence of poor osseointegration have been described previously in Chapter 3.

Modulation of uncemented prosthesis surfaces is commonly used to enhance bone growth and osseointegration. Surfaces are modified topographically or chemically to alter their surface energy and wettability, facilitating protein adsorption, cell adhesion and subsequent bio-integration (Hallab*, et al* 2001, Webb*, et al* 1998). Some of the most commonly used alterations to implant surfaces include grit-blasting, plasma spray, and hydroxyapatitie coating. Grit blasting creates a roughened implant surface by impinging abrasive particles onto the surfaces, whilst in plasma spraying and hydroxyapatite-coating a thin layer of molten metal or hydroxyapatite is applied onto the implant surface creating a textured osteoconductive interface for bone ongrowth.

Previous studies with grit-blasted implant surfaces in animal models describe a significantly greater bone growth observed histologically compared to polished surfaces, which consequently results in its better mechanical fixation (Abe*, et al* 2008, Feighan*, et al* 1995, Jinno*, et al* 1998). A multicentre study by Delaunay *et al.* (2001) reported a 10 year survival rate of 92.4% for grit-blasted femoral stems. Implant surfaces coated with plasma sprayed titanium demonstrate higher long term survival, with studies describing up to 98.4% survival at 10 years post surgery (Lombardi*, et al* 2009, Park*, et al* 2003). Whilst studies have demonstrated significantly better bone growth and fixation of hydroxyapatite coated implant surfaces compared to grit-blasted (Eckardt*, et al* 2003, Park*, et al* 2005b), they seem to offer no significant benefit in survivorship compared to plasma sprayed titanium coated surfaces. A study using Swedish Hip Registry data found no difference between the 10 year survival of hydroxyapatite coated (98%) and plasma sprayed titanium stem (Lazarinis*, et al* 2011). This evidence

is further supported by a prospective long term follow-up study which also observed similar survivorship for hydroxyapatite coated and porous-coated titanium stems (Kim, *et al* 2012).

Although, the effects of surface modulation on osseointegration and survivorship are extensively studied, the change in osteogenic response in presence of metal ions and particles remains unclear. In spite of the recent decline in the use of MOMHR (NJR 2013), the release of metal ions and particles from wear and corrosion of Co-Cr from the modular junctions of conventional total hip arthroplasties remains a persistent problem for their survivorship (Cook, *et al* 2013, Cook, *et al* 1994). To take our previous *in vitro* study forward and understand the effect of implant surfaces on the osteogenic response of osteoblasts to metal exposure, a collaboration with JRI Orthopaedics Ltd (Sheffield, UK) who provided with titanium grit-blasted (GB) (areal surface roughness Sz = 57µm), plasma sprayed titanium (Ti) (Sz = 79µm) and hydroxyapatite coated (HA) (Sz = 66µm) Ti6Al4V alloy surfaces. In this chapter, the effects of metal ions and nanoparticles (mean size–30-40nm) on mineralisation by osteoblast-like cell on these implant surfaces were investigated.

8.2 Results

In this study, a combination of Co^{2+} and Cr^{3+} at 1000µg/L each was used to represent the concentration of metal ions in the synovial fluid (Davda, *et al* 2011, Kwon, *et al* 2011), with bone-implant interfaces likely to have similar concentrations. Cr^{6+} was disregarded for this study due to its high cellular toxicity established in previous chapters. Further, the effect of particulate wear debris was mimicked by treating the cells with 100 nanoparticles per cell of Co and Cr oxide (~30nm) in accordance to previous studies (Brown, *et al* 2007, Polyzois, *et al* 2012) (section 2.5.2, Materials and methods). The mineralisation by osteoblast-like cells on implant surfaces (Figure 8.1A) was visualised by supplementing the feeding media with xylenol orange, a fluorochrome that is incorporated into newly deposited mineral (Figure 8.1B) and does not bind to hydroxyapatite coatings (Kuhn, *et al* 2010, Shu, *et al* 2003, Wang, *et al* 2006), unlike traditional techniques of Alizarin red and von Kossa staining.

8.2.1 Effect of implant surfaces on SaOS-2 mineralisation

Mineralisation by SaOS-2 cells on grit-blasted (GB), titanium coated (Ti) and hydroxyapatite coated (HA) surfaces was assessed by measuring the percentage area of xylenol orange incorporated mineral deposits.

HA coated implant surfaces showed significantly higher mineralisation by SaOS-2 cells (mean ± 95%CI; 91.73 ± 4.59), compared to cells grown on GB (0.82 ± 0.38; $p<0.0001$) and Ti (0.15 ± 0.14; $p<0.0001$) surfaces (Figure 8.2A). The percentage area of mineralisation on GB surfaces was also significantly higher than on Ti surfaces ($p<0.05$) (Figure 8.2A).

A

B

C
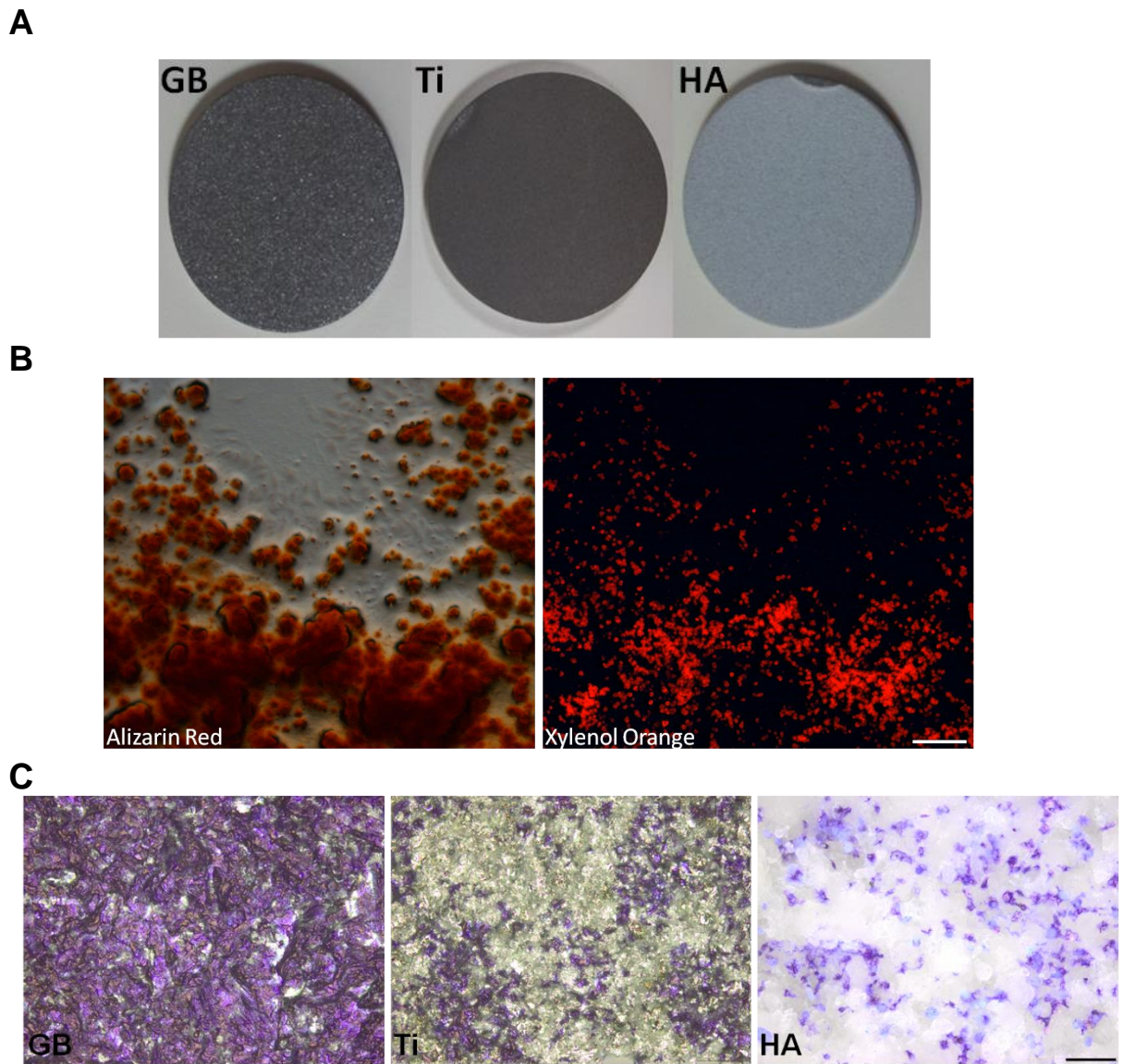
Figure 8.1 Osteoblast culture on implant surfaces

A) Implant surfaces that are grit-blasted (GB), titanium-coated (Ti) and hydroxyapatite-coated (HA). **B)** Images of mineralising osteoblasts stained with Alizarin red and xylenol orange.**C)** Toluidine blue stained cells after 24 hours on GB, Ti and HA surfaces. Scale bar = 200μm

A
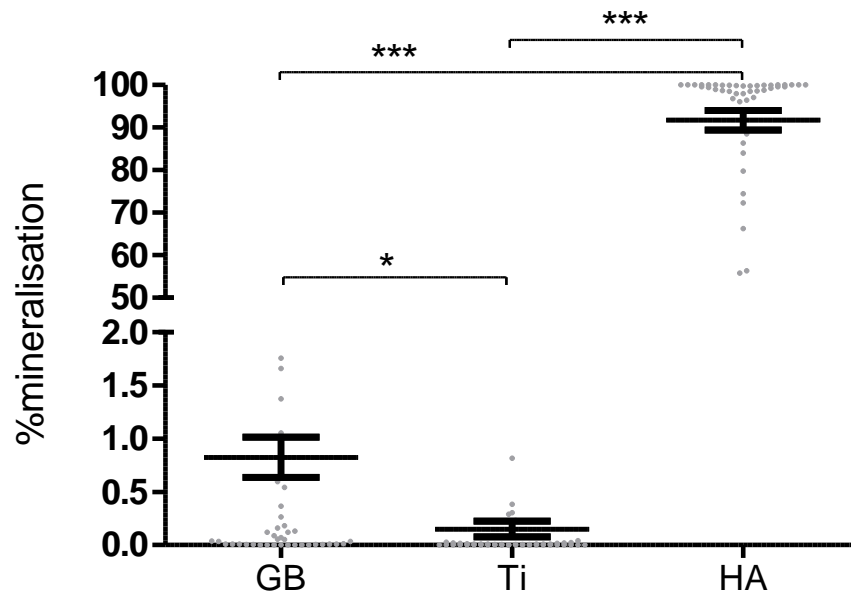
B
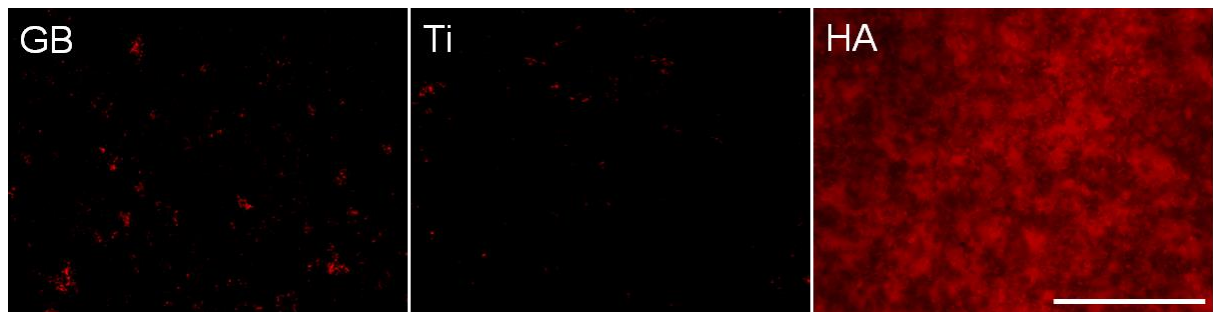
Figure 8.2 Mineralisation by SaOS-2 cells on implant surfaces

A) SaOS-2 cells were seeded onto different implant surfaces (GB: grit-blasted; Ti: titanium coated; HA: hydroxyapatite coated) and cultured in osteogenic media for 3 weeks. Percentage mineralisation was assessed by quantifying the red fluorescence corresponding to xylenol orange incorporated mineral deposits. **B)** Representative images of mineralisation GB, Ti and HA surfaces. Data from 3 repeat experiments with 3 replicates in each experiment (mean ± 95%CI). Data analysed with One-way ANOVA with Dunns multiple comparison test (*p<0.05; ***p<0.0001). Scale bar = 200μ

8.2.2 Effect of metal ions and nanoparticles on SaOS-2 mineralisation on implant surfaces

Mineralisation by SaOS-2 cells on implant surfaces was assessed by measuring the percentage area of xylenol orange incorporated mineral deposits in the presence of 1000µg/L Co^{2+} and Cr^{3+} each ($Co^{2+}:Cr^{3+}$), or 100 nanoparticles of Co and Cr oxide per cell (Co-Cr NP). The rationale for using metal debris in equal ratios is based on the correlation observed for their concentrations measured in serum from patients with well-functioning MOMHR (Appendix 2).

Grit-blasted

A reduction in mineralisation was observed for Co-Cr NPs (mean ± 95%CI; 0.06 ± 0.005) compared to the untreated control (0.82 ± 0.38; p<0.0001). No reduction was seen for $Co^{2+}:Cr^{3+}$ metal ion treatments (0.44 ± 0.15) compared to the untreated control. Mineralisation by SaOS-2 cells in presence of Co-Cr NP was significantly lower compared to $Co^{2+}:Cr^{3+}$ treatments (p<0.0001) (Figure 8.3). Representative images of the cultures are also illustrated in Figure 8.3.

Titanium coated

Mineralisation by SaOS-2 cells was poor on Ti surfaces under all conditions, with area fraction for untreated controls being (mean ± 95%CI; 0.03 ± 0.02), $Co^{2+}:Cr^{3+}$ (0.006 ± 0.004) and Co-Cr NPs (0.005 ± 0.002) (Figure 8.4). There were no significant differences observed between the treatment groups. Representative images of the cultures are also illustrated in Figure 8.4.
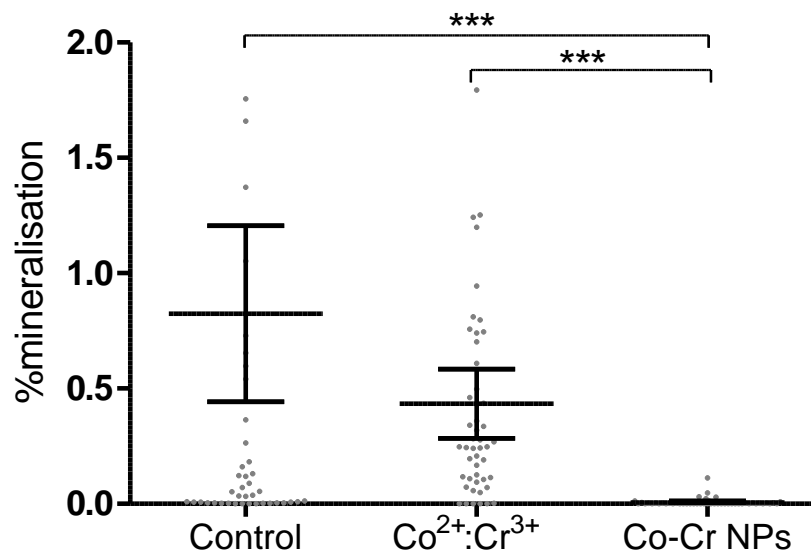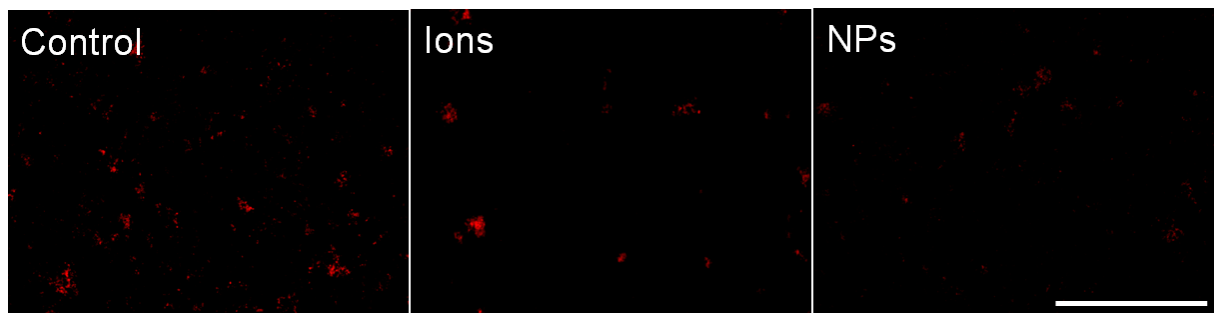
Figure 8.3 Effect of metal ions and nanoparticles on mineralisation by SaOS-2 cells on grit-blasted surface

A) SaOS-2 cells were seeded onto grit-blasted surfaces and cultured in osteogenic media for 3 weeks supplemented with 1000µg/LCo^{2+}:Cr^{3+} or 100 nanoparticles of Co and Cr oxide per cell (based on the initial seeding density). Percentage mineralisation was assessed by quantifying the red fluorescence corresponding to xylenol orange incorporated mineral deposits. **B)** Representative images from the cultures are illustrated below the graph. Data from 3 repeat experiments with 3 replicates in each experiment (mean ± 95%CI). Data analysed with One-way ANOVA with Dunns multiple comparison test (***p<0.0001). Scale bar = 200µ

A

B

Figure 8.4 Effect of metal ions and nanoparticles on mineralisation by SaOS-2 cells on titanium coated surface

A) SaOS-2 cells were seeded onto titanium coated surfaces and cultured in osteogenic media for 3 weeks supplemented with $1000\mu g/L Co^{2+}:Cr^{3+}$ or 100 nanoparticles of Co and Cr oxide per cell (based on the initial seeding density). Percentage mineralisation was assessed by quantifying the red fluorescence corresponding to xylenol orange incorporated mineral deposits. **B)** Representative images from the cultures are illustrated below the graph. Data from 3 repeat experiments with 3 replicates in each experiment (mean ± 95%CI). Data analysed with One-way ANOVA with Dunns multiple comparison test. Scale bar = 200μ

Hydroxyapatite coated

For the HA coated surface, mineralisation by osteoblasts was reduced with $Co^{2+}:Cr^{3+}$ (mean ± 95%CI; 72.3 ± 6.46; $p<0.0001$) and Co-Cr NP (58.72 ± 8.89; $p<0.0001$) treatments compared to untreated controls (91.73 ± 4.59) (Figure 8.5). There was no difference observed between $Co^{2+}:Cr^{3+}$ metal ions and Co-Cr NP treated cells. Representative images of the cultures are also illustrated in Figure 8.5.

8.2.3 Percentage response for mineralisation on implant surfaces with metal ion and nanoparticles exposure

Data from previous section (section 8.2.2) were also expressed as a percentage response to the untreated controls for each surface to explore the relative effect of different surfaces in modulating SaOS-2 cell response to metal ions and nanoparticles challenge, (Figure 8.6). The decrease in mineralisation in presence of $Co^{2+}:Cr^{3+}$ and Co-Cr NP respectively was ameliorated on HA surfaces (mean ± 95%CI; 78.82 ±.7.05; 64.02 ± 9.69) compared to GB (52.65 ± 18.09; 0.78 ± 0.63) and Ti (21.48 ± 12.26; 15.60 ± 8.49) surfaces (Figure 8.6).

Surprisingly, whilst GB surfaces had significantly higher mineralisation compared to Ti surfaces in presence of $Co^{2+}:Cr^{3+}$ (52.65 ± 18.09 versus 21.48 ± 12.26), lower mineralisation was observed with Co-Cr NP (0.78 ± 0.63 versus 15.60 ± 8.41) (Figure 8.6).

A
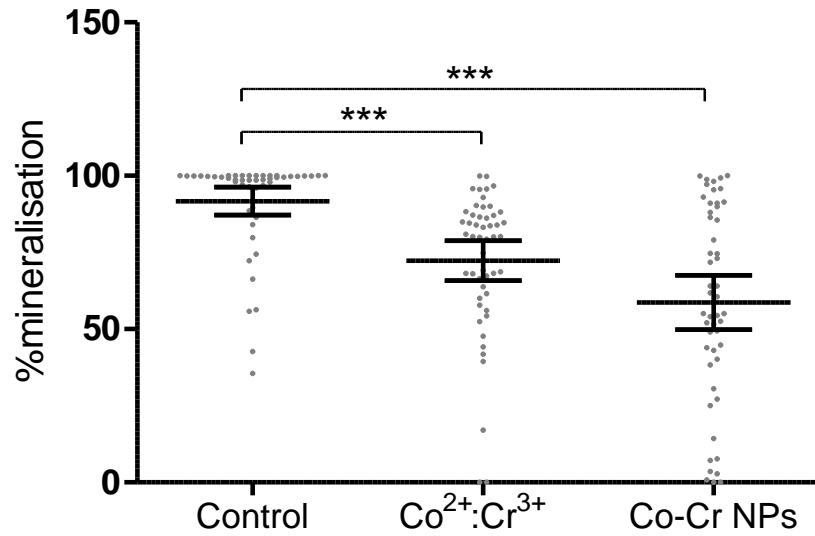
B
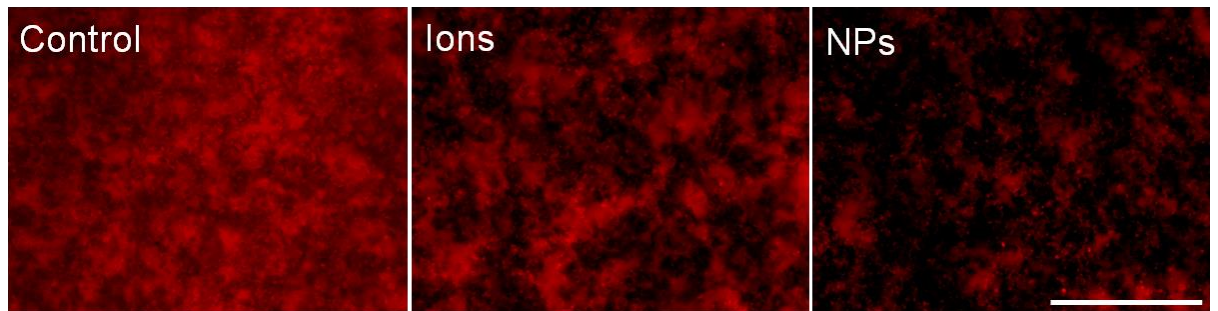
Figure 8.5 Effect of metal ions and nanoparticles on mineralisation by SaOS-2 cells on hydroxyapatite coated surface

A) SaOS-2 cells were seeded onto hydroxyapatite coated surfaces and cultured in osteogenic media for 3 weeks supplemented with 1000µg/LCo^{2+}:Cr^{3+} or 100 nanoparticles of Co and Cr oxide per cell (based on the initial seeding density). Percentage mineralisation was assessed by quantifying the red fluorescence corresponding to xylenol orange incorporated mineral deposits. **B)** Representative images from the cultures are illustrated below the graph. Data from 3 repeat experiments with 3 replicates in each experiment (mean ± 95%CI). Data analysed with One-way ANOVA with Dunns multiple comparison test (***p<0.0001). Scale bar = 200µ

Figure 8.6 Effect of metal ions and nanoparticles on mineralisation by SaOS-2 cells on implant surfaces – percentage response

Mineralisation by osteoblasts on implant surfaces with metal ions and nanoparticles treatments is represented as percentage response to the untreated control. Data from 3 repeat experiments with 3 replicates in each experiment (mean ± 95%CI). Data analysed with One-way ANOVA with Dunns multiple comparison test (***p<0.0001).

8.2.4 Effect of metal ions and nanoparticles on ALP activity in SaOS-2 cells on implant surfaces

ALP activity of SaOS-2 cells on implant surfaces was assessed by pNPP hydrolysis after 7 day exposure to metal ions (1000µg/L Co^{2+} and Cr^{3+}) or nanoparticles (100 particles of Co and Cr oxide each, per cell).

For untreated controls, the ALP activity was lower on HA surfaces (mean ± 95%CI; 2.65 ± 1.08) compared to GB (8.24 ± 0.91) and Ti (8.98 ± 0.90). SaOS-2 cell ALP activity on HA coated surface was also lower with $Co^{2+}:Cr^{3+}$ (2.98 ± 1.28) and Co-Cr NP (2.94 ± 1.15) treatments compared to GB (5.79 ± 1.62; 6.59 ± 1.61) and Ti (5.70 ± 0.85; 5.42 ± 1.74). There was no difference in ALP activity for cells grown on GB and Ti surfaces for all conditions
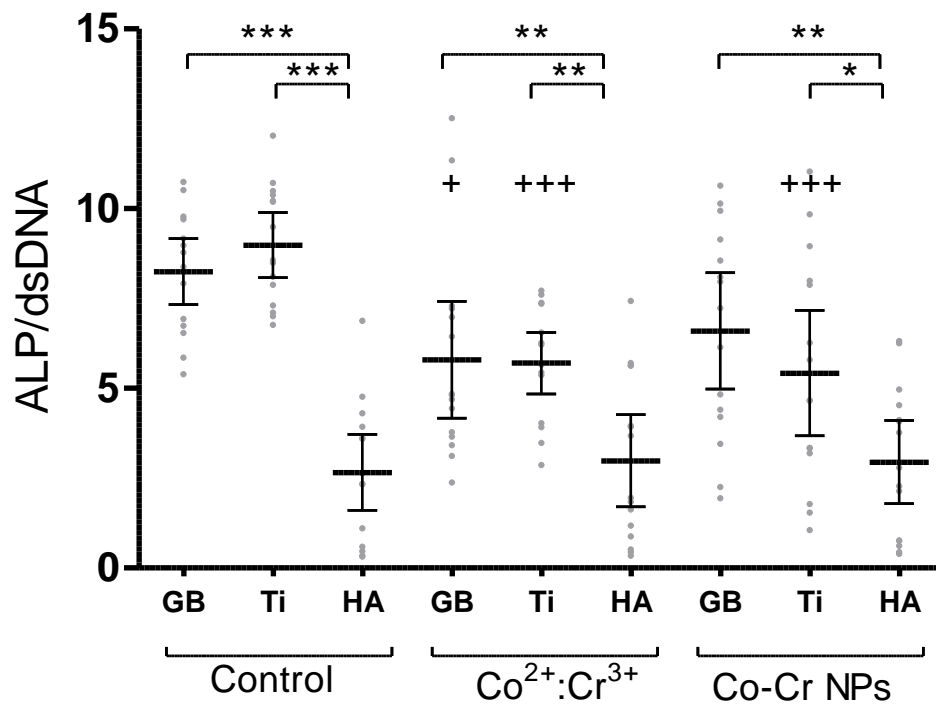
Figure 8.7 ALP activity of SaOS-2 cells on implant surfaces

ALP activity of SaOS-2 cells on implant surfaces with metal ions and nanoparticles treatments was measured after 7 days. Data from 3 repeat experiments with 5 replicates in each experiment (mean ± 95%CI). Data analysed with One-way ANOVA with Tukey's multiple comparison test (*$p<0.05$; **$p<0.01$; ***$p<0.0001$) (+ signifies comparison with control)

8.3 Discussion

The modulation of implant surfaces is a common modality to enhance prostheses osseointegration by improving surface osteo-conduction and bone on-growth. Previous studies by us and others have demonstrated the detrimental effects of metal ions and particles on osteoblast survival and function *in vitro* (Andrews*, et al* 2011, Anissian*, et al* 2002, Fleury*, et al* 2006)*.* However, the effect of implant surface topography and chemistry on their response to such metal exposure remains unclear. This study describes the effects of Co^{2+} and Cr^{3+} and nanoparticles on mineralisation by SaOS-2 cells on titanium grit-blasted (GB), plasma sprayed titanium (Ti) and plasma sprayed hydroxyapaptite (HA) implant surfaces.

The finding of increased mineralisation on HA coated surfaces compared to GB and Ti is consistent with its greater osteoconductive properties described in previous studies. The osteoconductivity of HA surfaces is manifested as an increase in osteoblast attachment and spreading compared to other surfaces (Malik*, et al* 1992, Okumura*, et al* 2001). The basis for increased cell attachment is thought to occur via the adsorption of adhesive proteins such as fibronectin and vitronectin which contain Asp-Gly-Asp (RGD) motifs that bind to integrins on cell membranes (Hennessy*, et al* 2008, Kilpadi*, et al* 2001). Molecular studies have further confirmed the higher affinity of these adhesive proteins for HA compared to titanium (Saju*, et al* 2011). The binding of cell surface integrins to RGD-motif containing adhesive proteins results in intracellular rearrangement of the cytoskeleton, forming focal adhesions, with subsequent downstream signalling directed towards cell survival and differentiation (Giancotti and Ruoslahti 1999). Indeed, the gene expression of osteoblasts on HA surfaces shifts towards differentiation within the first 24 hours (Lehmann*, et al* 2012, Xie*, et al* 2004), which might explain the difference in mineralisation observed in our study.

Mineralisation by SaOS-2 cells on titanium grit-blasted and plasma sprayed titanium surfaces was surprisingly low compared to the HA surface. Previous *in vitro* and *in vivo* studies have observed substantial bone growth and

osseointegration with these surfaces. The low mineralisation observed in our study could be attributed to the relatively low adsorption of proteins on their surfaces compared to HA (Kilpadi, *et al* 2001). In our study, prior to cell seeding, all three surfaces (GB, Ti and HA) were pre-wetted in serum-free culture media. The absence of serum in the wetting media would have led to low protein being adsorbed on the surfaces before the cells were seeded. The slower adsorption of adhesive proteins for GB and Ti surfaces (Kilpadi, *et al* 2001, Saju, *et al* 2011) from serum containing cell suspension media could have affected the initial cell attachment and subsequent differentiation.

Additionally, investigations using RGD blocking peptides have demonstrated that cell attachment on titanium surfaces is not via RGD-motifs containing adsorbed proteins (Okamoto, *et al* 1998). With the absence of RGD mediated downstream signalling, osteoblast differentiation is likely to be affected on titanium surfaces compared to HA. Furthermore, in support of this reasoning, immobilisation of RGD peptides on titanium surfaces significantly improves osteoblast adhesion, mineralisation and osseointegration (Chollet, *et al* 2009, Germanier, *et al* 2006, Oya, *et al* 2009).

A decrease in mineralisation was observed in presence of $Co^{2+}:Cr^{3+}$ and Co-Cr NP treatments for HA surfaces, with NPs being more detrimental than metal ions. The concentrations of metal ions used in the present study are similar to those observed in the hip aspirates of patients with MoMHR, and the observed decrease in mineralisation is in accordance to previous *in vitro* studies by us and others (Chapter 3, section 3.2.5) (Andrews, *et al* 2011, Anissian, *et al* 2002, Fleury, *et al* 2006). A decrease in the osteogenic response with Co and Cr wear particles reported previously is also in keeping with the results of this study (Allen, *et al* 1997, Lohmann, *et al* 2000). A novel finding of this study is the lower percentage of detrimental response to metal ions and nanoparticles by osteogenic cells on HA surface compared to GB and Ti surfaces. The mechanism for this protective effect of HA surfaces is not clearly understood, but the integrin based upregulation of cell survival genes might play a role. Further studies investigating the gene expression of osteogenic cells on implant surfaces in

presence of metal ions and nanoparticles are required to discern the involved mechanisms.

To support our observations of increased cell differentiation on HA surfaces, ALP activity of SaOS-2 cells on different implant surfaces was measured at day 7 in presence of metal ions and nanoparticles. Cells on HA surfaces had lower ALP activity compared to both GB and Ti surfaces, and remained lower in the presence of metal ions and nanoparticles. The ALP activity of SaOS-2 cells usually peaks at day 7, before decreasing to near-basal levels by day 11, prior to mineralisation (Appendix 1). An early peaking of ALP activity for cells on HA surfaces due to their accelerated differentiation described above, might explain the observed results. The protective role of HA surfaces in presence of metal ions and nanoparticles is further evidenced by unchanging ALP activity of SaOS-2 cells in presence of metal debris, whereas a decrease was observed for both GB and Ti surfaces.

A fluorochrome was used to quantitate mineralisation on the substrate because of its opacity to transmitted light microscopy. Moreover, conventional Alizarin red and von Kossa staining could not be employed as they also bind existing mineral, such as HA, and therefore does not exclusively stain newly mineralised matrix laid down by osteoblasts. Xylenol orange, a fluorochrome that has been previously used to investigate osteogenesis on biomaterials, was used in this study (Kuhn, *et al* 2010, Shu, *et al* 2003, Wang, *et al* 2006). Like tetracycline derivatives, xylenol orange is widely used in labelling bones *in vivo* where it incorporates at sites of calcification (Rahn 2003, Rahn and Perren 1971). This is evident from the comparison between Alizarin red and xylenol orange stained images of *in vitro* mineralisation by SaOS-2 cells (Figure 8.1A). Whilst alizarin red stains all the calcium deposited throughout the culture, xylenol orange is localised to the mineral that is deposited after the feeding media has been supplemented with the fluorochrome (day 17 in this study). The lack of HA surface staining was observed in the absence of cells, which further supports a cell mediated mechanism of fluorochrome incorporation into the newly deposited mineral.

8.4 Conclusion

In summary, the findings of this study suggest that HA coating of implant surfaces offer better mineralisation by osteoblasts in presence of metal ions and debris released from MOMHR and other modular prostheses, compared to GB and Ti coated surfaces. Thus, HA coatings may improve the survivorship of implants by promoting osseointegration.

Chapter 9 - General Discussion

9.1 Thesis summary

Over the last decade, there has been a 4-fold increase in patients undergoing primary hip replacements in England and Wales (NJR 2013) (http://www.njrcentre.org.uk/), with increasing number of younger more active patients undergoing hip arthroplasty. In recent years, MOMHR has been a popular alternative to conventional THA due to its better wear and lubrication characteristics that permitted higher rates of activity (Chan, *et al* 1999, Clarke, *et al* 2000), and conserved femoral bone aiding revision at later stages. However, MOMHR have a poor clinical outcome with 5-year revision rates of 5.8% (5.5-6.1) compared to 1.5% (1.4-1.6) for cemented and 2.5% (2.3-2.6) uncemented conventional total hip arthroplasty (NJR 2013). In fact, the clinical outcomes are poor for all MOM bearing hip implants with 5-year revision rates of 6.3% (95%CI, 4.9-8.0) for cemented and 7.6% (7.3-8.0) for uncemented MOM total hip replacements (NJR 2013).

The reduced survivorship of these implants is attributed to adverse reactions in the surrounding tissue to metal ions and particles released from the prostheses. These reactions most commonly manifest as osteolysis and aseptic loosening, femoral neck fractures, periprosthetic inflammatory masses and pain (NJR 2013). Moreover, the problems associated with metal release are not restricted to hip implants with MOM bearings, with recent studies reporting increase in serum metal ion concentrations and consequent adverse reactions for other modular prostheses (Cooper, *et al* 2012, Cooper, *et al* 2013). Modular junctions are present in all modern hip replacements. Even with the sharp decline in the use of MOM hip replacement (NJR 2013) observed over the last few years, modular implants provide an urgent clinical need to address the issue of adverse reactions to metal debris.

For better revision outcomes, the Medicines and Healthcare Regulatory Agency (MHRA) has recommended monitoring blood cobalt and chromium levels for patients with MOMHR with serum concentrations of 7µg/L as a threshold for further investigations. While the effects of prosthesis derived metal ions and particles on survivorship of prostheses is being established, and the various

adverse events characterised, the mechanisms mediating these observed effects are yet unclear and requires further research.

The overall aim of this thesis was to investigate the effects of prosthesis related metal ions (Co^{2+}, Cr^{3+} and Cr^{6+}) at clinically relevant concentrations on bone cell physiology. In the first study, I characterised the response of bone cells - osteoblasts, osteoclasts and osteocytes – to clinically relevant concentrations and combinations of metal ions (Co^{2+}, Cr^{3+} and Cr^{6+}). With most previous studies investigating the effect of individual metal ions, the combination treatment used in this study was more representative of the clinical setting (Appendix 2). The results from these investigations provide insights into dynamics of periprosthetic bone remodelling which is integral to osseointegration and implant survivorship. Furthermore, the effect of metal ions at systemic concentrations was assessed to understand the implications for global skeletal health.

A reduction in viability and osteogenic potential was observed for human osteoblast-like SaOS-2 cells at periprosthetic concentrations as assessed by ALP activity and mineralisation ability (Chapter 3). A more mature phenotype of osteoblast cells represented by murine MLO-A5 cells also showed a similar decrease in mineralisation with metal ions combinations at periprosthetic concentrations. The above findings with osteoblasts coupled with reduced osteoclast number and activity described in Chapter 4 suggests inhibition of bone remodelling in the periprosthetic environment as a consequence of direct effects of metal ions on these cells. Taken together, these results imply a risk of failure of primary implant osseo-integration due to metal ion exposure, rather than secondary osteolysis and aseptic loosening of a previously fixed implant (Figure 9.1B). Moreover, these effects are likely to be compounded by the decreased number of viable osteocytes with altered dendricity affecting its orchestration of adaptive bone remodelling under mechanical loading (Chapter 5).

Manipulation of implant surfaces to alter its osseoconductivity has been a common modality to promote osseointegration of the prosthesis. In view of the detrimental effects of metal ions on osteoblasts described in chapter 3, the osteogenic response of osteoblasts was assessed in presence of metal ions and

nanoparticles on implant surfaces. These surfaces were either grit-blasted, plasma-sprayed titanium coated or hydroxyapatite coated, obtained in collaboration with JRI Orthopaedics Ltd. (Sheffield, UK). Mineralisation by osteoblasts reduced in the presence of metal exposure, supporting the initial inference of failure of primary fixation. Nevertheless, hydroxyapatite-coated surfaces offered some resistance against the detrimental effects of metal ions and particles on osteoblast function, and thus may prove beneficial for implant osseointegration.

At concentrations corresponding to the patient serum, the *in vitro* results showed an increase in osteoblast synthetic function accompanied by a reduction in the number and activity of mature osteoclasts (Figure 9.1C). The results suggest a net osteogenic response systemically which is in keeping with a recent cross-sectional study that described increased total BMD for patients with MOMHR compared those with THA (Prentice*, et al* 2013). They attributed the increase in total BMD to reduced bone turnover as inferred from reduction in biomarkers of bone turnover (TRAP5b and osteocalcin) (Prentice*, et al* 2013). Whilst the clinical observation of reduced TRAP5b could be attributed to a reduction in mature osteoclast numbers activity as observed in the *in vitro* results from Chapter 4, the reduction in osteocalcin levels is contrary to the increase in osteoblast activity described above. This inconsistency may be attributed to a reduced release of osteocalcin from the bone matrix following decrease in osteoclastic resorption (Cloos and Christgau 2004).

The use of *in vitro* cell lines as cellular models to characterise the effects of metal ions on human cells is one of the limitations of this study. In mitigation of this, a recent study by Czenkanska et al. compared the phenotypic profile of different immortalised osteoblast-like cell-lines to primary human osteoblasts (Czekanska*, et al* 2013). Their results demonstrate good resemblance between SaOS-2 and primary human osteoblasts in their gene expression profile, ALP activity and mineralising ability. Nevertheless, the results could be validated in primary human cells to better understand the quantitative effects of metal ions on systemic and periprosthetic osteoblasts. Additionally, the effects described in the results are likely to vary between patients as the concentration combinations of 1:1 for Co

and Cr is an approximation of the physiological setting based on clinical observation described earlier (section 3.1 and Appendix 2). The ratio of Co and Cr may differ between patients based on their activity levels and time since surgery as evidenced previously in section 1.5 and Table 1.1. Nevertheless, the combinations used in this study are a conservative approximation of the *in-situ* environment and significantly improves our understanding of the effects of metal ions on bone cells.

Sub-cellular distribution and speciation of prostheses related metal ions were explored in bone cells for the first time, using synchrotron based X-ray absorption spectroscopy (Diamond Light Source Ltd, Didcot, UK) (Chapter 6). The study aimed to provide an insight into the mechanisms for metal ion entry and their intracellular sites of action. The data from these studies suggest cell-specific mechanisms of cellular entry for metal ions which could be specifically targeted to alter the balance of bone remodelling in the periprosthetic environment. The results confirmed the intracellular entry of Cr^{3+} in both osteoblasts and osteoclasts, a metal species previously thought to be relatively impermeable to cell membranes. Moreover, the intracellular reduction of Cr^{6+} supported the notion of its ROS-mediated cellular toxicity reported in previous studies, while the distribution and unchanged speciation of Co^{2+} implied interactions with metalloenzymes or DNA as its mechanism for detrimental effects.

Although the synchrotron based investigations provided us with unparalleled accuracy in determining the intracellular chemical form of a metal, only a few cells from each treatment group were examined because of the long scan times. Moreover, intracellular distribution of Co and Cr did offer us insights into putative mechanisms of cellular entry, but the localisation of metal at organelle level was undetermined. This could be achieved in the future using specific labels for different organelles and scanning for co-localisation of different metal species as described previously (McRae*, et al* 2006).

A.

B.

C.
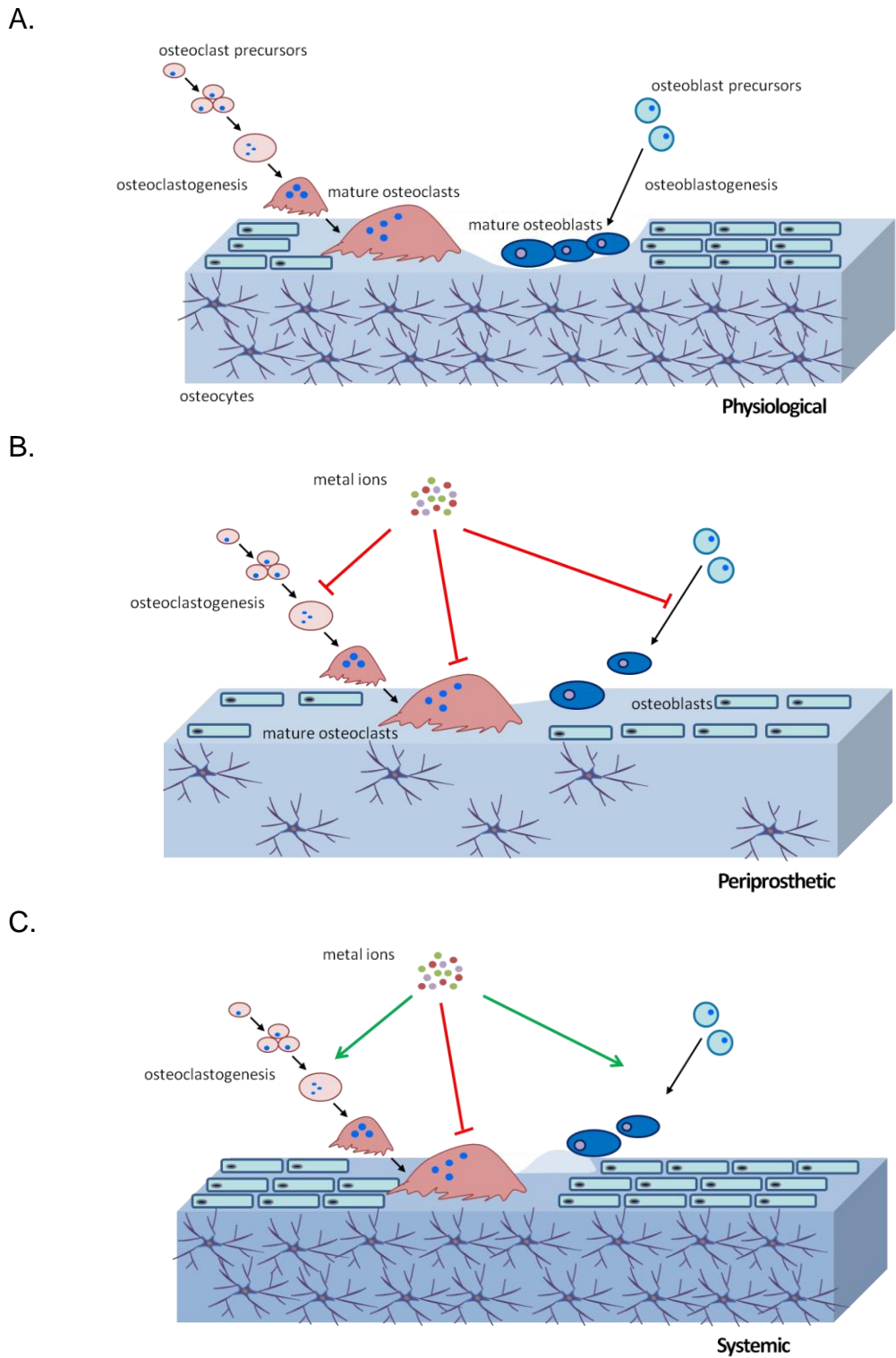
Figure 9.1 Effect of metal ions on bone cells at periprosthetic and systemic concentrations. **A)** Represents the bone remodelling cycle under physiological conditions with osteoclastogenesis, bone resorption followed by bone formation by mature osteoblasts. **B)** In the periprosthetic environment, there is complete inhibition (red arrows) of the bone remodelling cycle, and **C)** in the systemic environment, there is an increase in osteoblast survival and function, with reduction in viability and activity of mature osteoclasts suggesting a net increase in bone formation.

In chapter 7, a novel approach of targeting cellular entry of metal ions as a possible therapeutic intervention against detrimental cellular effects was explored. P2X7R, an implicated ATP-gated ion channel, was found to play a role in cellular entry Co^{2+} at periprosthetic concentrations in osteoblasts but not in osteoclasts. With several P2X7R antagonists in clinical trials (Arulkumaran, *et al* 2011), this provides an immediate opportunity to specifically target osteoblasts for protection against metal ions in the local environment, but further investigations are warranted to validate it as a suitable target.

This study extends our understanding of Co^{2+} entry into bone cells, however the mechanisms by which Cr^{3+} and Cr^{6+} enter cells is un-explored. The mechanisms underlying the entry of Cr^{6+} are of particular importance because of its higher toxicity demonstrated in previous chapters. Due to its paramagnetic nature and absence of selective chelators, fluorescent probes for observing intracellular Cr^{3+} remains poorly developed. In recent years, a few ratiometric detectors for aqueous Cr^{3+} have been reported (Lohar, *et al* 2013, Zhou, *et al* 2008) and we have recently obtained a cell-permeant napthalamide-rhodamine based fluorescent probe that works on the principle of fluorescence resonance energy transfer (Mahato, *et al* 2012). To take this study forward, the role of nonspecific phosphate/sulphate ion channels and endocytosis in cellular uptake of Cr^{3+} and Cr^{6+} could be assessed in osteoblasts and osteoclasts using the new probe.

9.2 Future directions

This project provides an insight into the effects metal ions released due to tribo-corrosion have on the local and systemic bone and introduces several new questions that can take this study forward with clinical implications.

The results generated in this study have not been validated against the conditions observe clinically. Histological examination of the periprosthetic tissue from patients with failed MOM hip replacement may prove useful to verify the suggested inferences of the data. However, obtaining uncompromised tissue is a challenge and alternatively imaging techniques such as computed tomography could be employed to observe changes in the periprosthetic bone over time.

Furthermore, the mechanisms involved for the observed cellular responses to metal ions are left unexplored. Although there are studies which describe changes in expression of a few key genes important in bone biology in response to metal exposure, none have explored changes corresponding to different clinical concentrations and cell differentiation stages. In view of this, investigations for changes in gene expression using custom TaqMan microarrays (consisting of genes governing cell survival, differentiation and function, responses to stress, and factors responsible for cell-to-cell communication) for osteoblasts and osteoclasts exposed to a clinically relevant range of metal ions, at different stages of differentiation could be performed. Transcriptional level changes corroborated with corresponding protein expression changes could help identify cellular pathways that could be targeted to ameliorate the detrimental effects of metal ions.

Bone is a dynamic tissue with interactions between osteoblasts, osteoclasts and osteocytes crucial for its maintenance, and responses to stress and strain. This study explores the effects of metal ions on different bone cells in isolation, ignoring the regulatory effects they have on each other. This could be overcome to a certain extent by assessing the changes in gene expression of several regulatory molecules in these cells response to metal ions. However, the effects of metal ions investigated in a co-culture system involving different cell types (Vazquez, *et al* 2012) would provide a greater insight into the dynamics of periprosthetic and systemic bone after surgery.

Additionally, it would be useful to incorporate effects of metal ions on immune cells as several studies have described the release of pro-inflammatory cytokines from them in presence of metal debris. One possible way to take into consideration the contribution of an immune response is to develop a multicellular transwell *in vitro* system which incorporates an immune component on the transwell membrane, while the survival and functional outcomes for bone cells can be assessed in the bottom well separated by the transwell insert. To further mimic the physiological setting and model responses on prostheses surfaces,

bone cells could be cultured on various implant surfaces and outcomes of cell viability and mineralisation assessed.

Lastly, survival and functional studies with osteoblasts should be conducted in presence of P2X7R antagonists to validate if the reduced metal ion entry, described in chapter 7, translates into a potential therapeutic option. The study should be supplemented by assessing ATP release from cells and the activation of P2X7R with metal ion exposure.

9.3 Conclusion

In conclusion, the results from this group of related studies suggest that Co and Cr ions inhibit bone cell activity at concentrations found in the periprosthetic environment, and also the potential to alter bone physiology at concentrations found systemically. These findings have implications both for implant fixation and survivorship and for general skeletal health. Furthermore, it identifies the intracellular distribution and speciation of metal ions in bone cells extending our understanding of cellular effects, and explores mechanisms of cellular entry that can be exploited to ameliorate the detrimental effects.

Although, the worldwide use of hip replacements with metal-on-metal bearings is sharply decreasing, modular prostheses that release similar metal debris through fretting and corrosion are unlikely to be phased out. Thus, the findings from this study form a strong platform for further investigations with potential clinical applications which are likely to be important in the long term, as well as for the large number of patients who have indwelling prosthesis that include a MoM bearing or taper junctions that include a Co/Cr component.

Appendices

Appendix 1:

Optimisation of seeding density for SaOS-2 cells

SaOS-2 cells were cultured in 96 well-plates upto 15 days with varying cell densities and concentrations of FCS. Cellular activity was measured using MTS based assay described in section 2.3 at different time points. Based on the linear range for the cell activity assays (described as optical densities between 0.25 and 1.2, according to the manufacturer's guide), the cell density of 5000 cells per well cultured in 0.5% FCS containing media with time-points of day 3 and 7 was selected for further experimentation (Figure A1). This allowed sufficient margins above and below the expected optical density values for control treatments, to observe changes in the cellular activity.
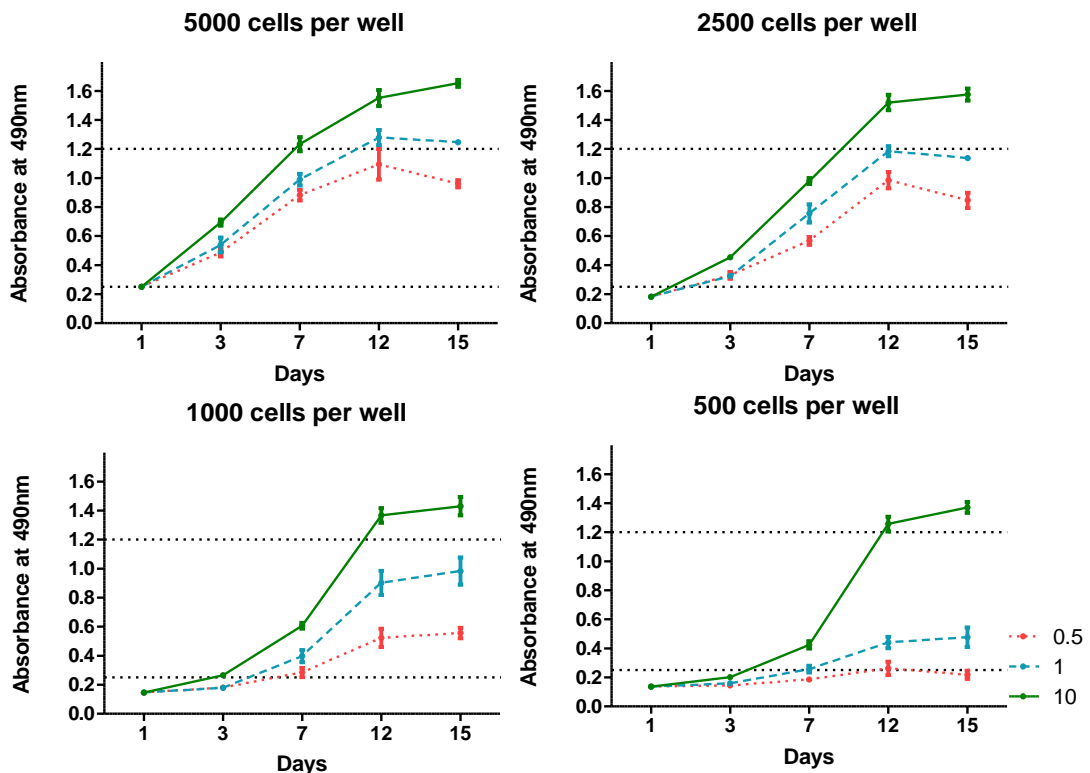
Figure A1. Optimal seeding density and FCS supplementation for osteoblast experiments Graphs represent cellular activity of osteoblasts cultured in media containing 0.5% (red), 1% (blue) and 10% (green) FCS, measured using and MTS based assay. The horizontal lines highlight the linear range of the assay.

Change in ALP activity for SaOS-2 cells

The change in alkaline phosphatase activity of SaOS-2 cells cultured in control media (containing 0.5% FCS) over time as measured using the ALP assay described in section 2.4 suggests a peak at day 7, before returning to basal levels day 15 onwards (Figure A2).
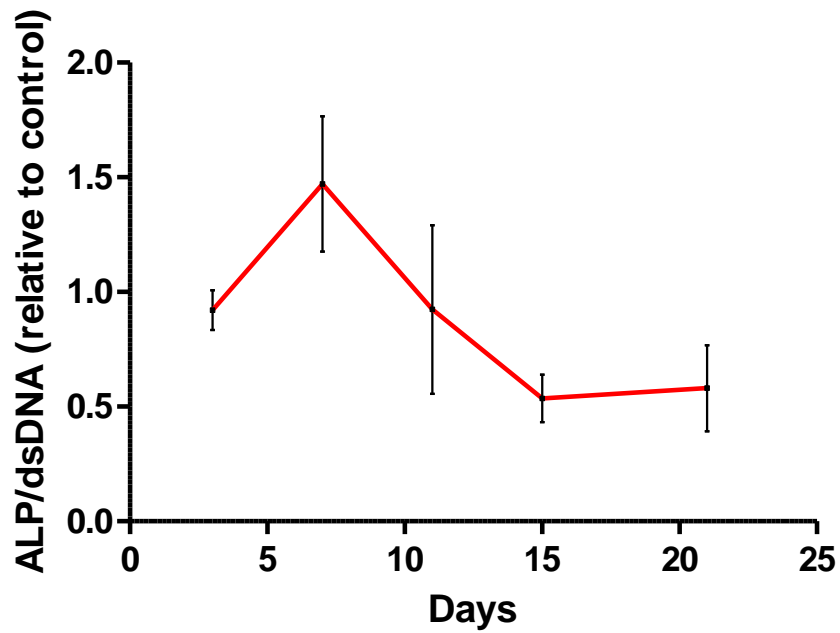
Figure A2 Change in ALP activity over time for SaOS-2 cells

Appendix 2

Correlation between Co and Cr in serum from patients well-functioning MOMHR

A plot showing $R^2 = 0.9635$ with y-axis labeled [chromium] µg/L (0 to 8) and x-axis labeled [cobalt] µg/L (0 to 8).
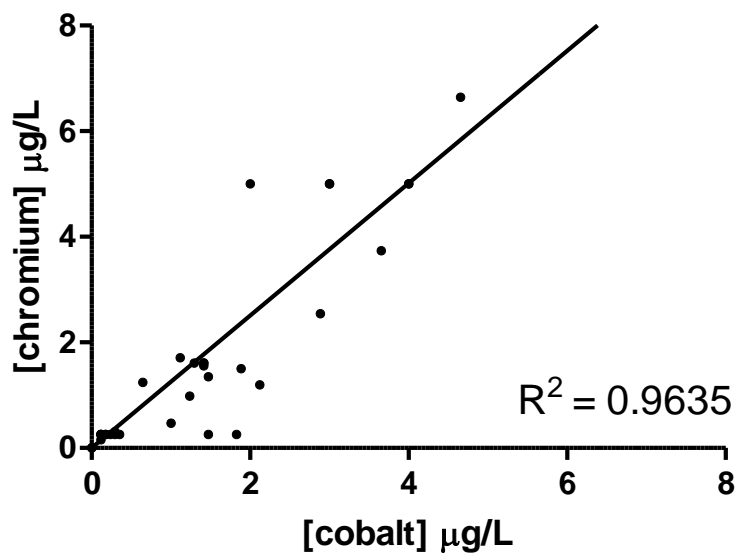
Figure A3. Correlation between Co and Cr serum concentrations from 24 patients with well-functioning MOMHR.

A positive correlation (R^2=0.9635) was observed suggesting that the cells are exposed to broadly similar concentrations of Co and Cr.

Appendix 3

Multiple sequence alignment for fungal and humanTRAcP
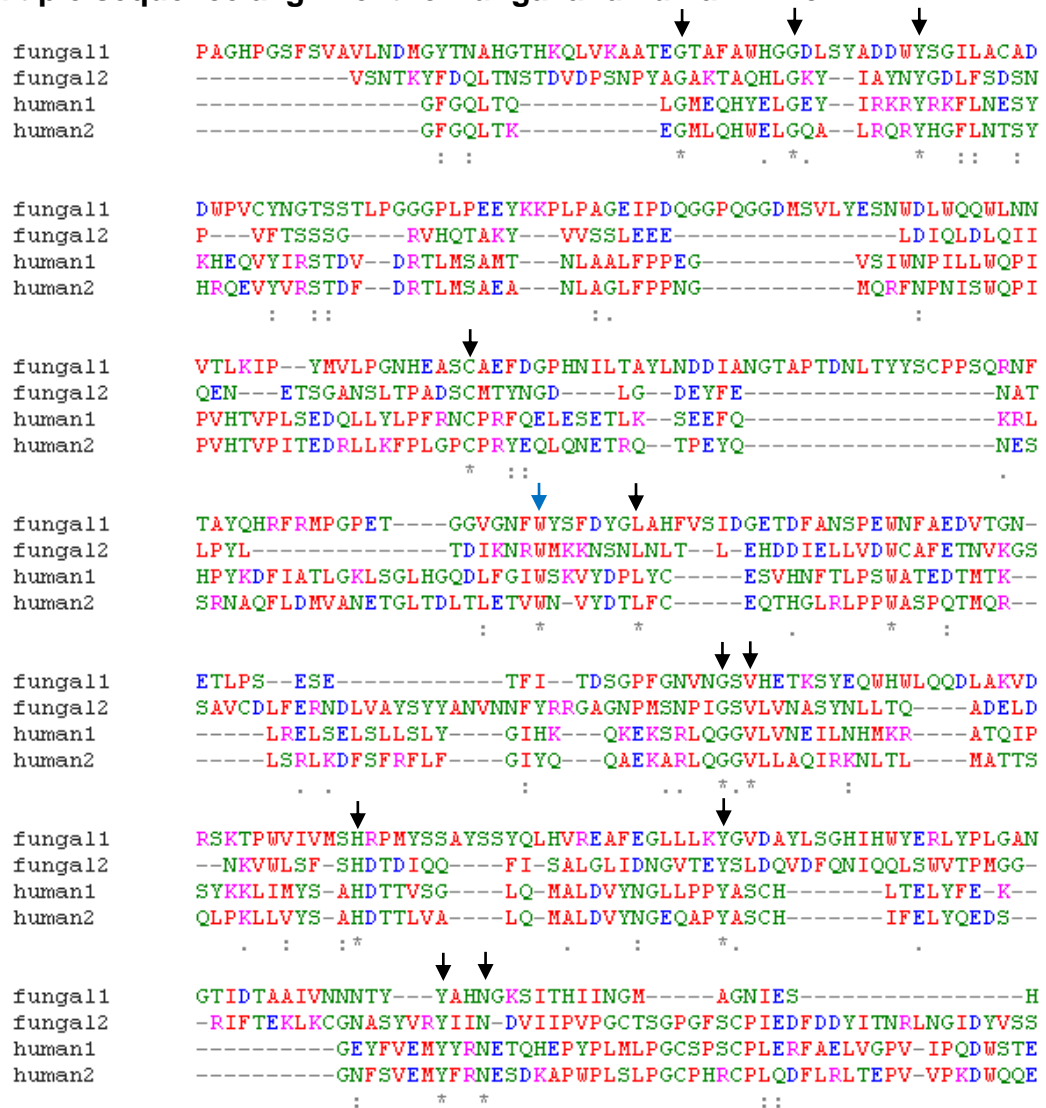
Figure A4 Multiple sequence alignment of acid phosphatases. Conserved residues between the different sequences are marked with black arrows.

Appendix 4

Autologous serum dilutions on osteoclast survival and function

Mature osteoclasts were cultured in different dilutions of autolous serum in normal osteoclastogenic media to investigate its effect on the survival and function of osteoclasts (section 2.6). All treatments were supplemented with equivalent amounts of RANKL and M-CSF. The results show no change in osteoclast number, percentage resorption and the resorbing ability of osteoclasts for any concentration of serum compared to normal osteoclastogenic media (10%).
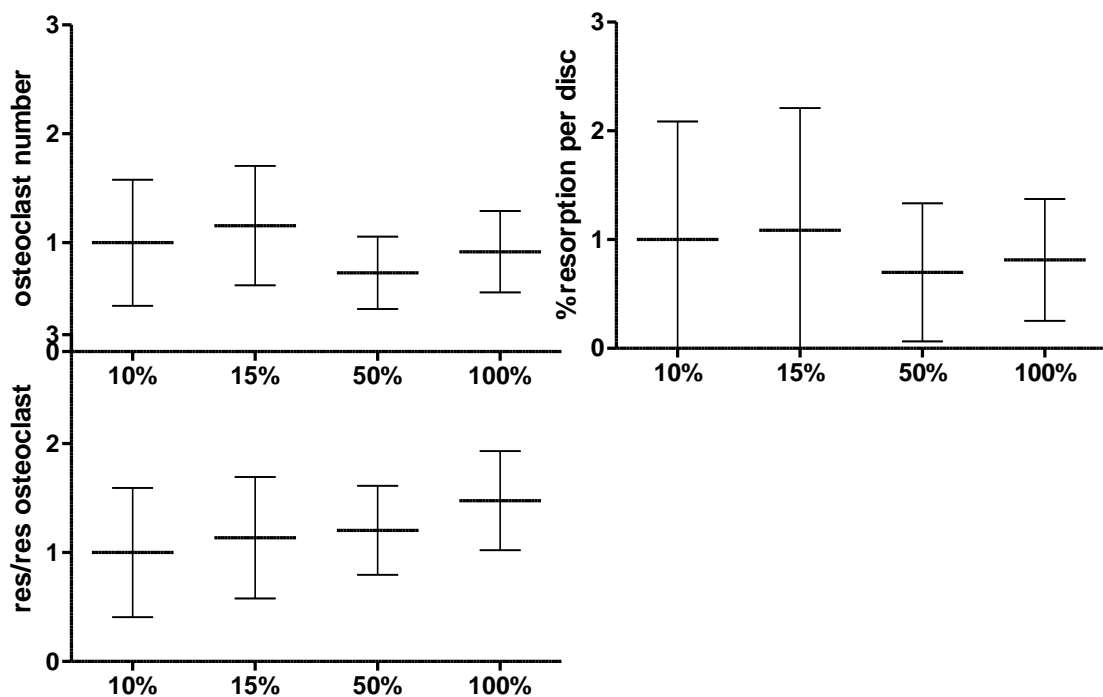
Figure A5 Effects of autologous serum on osteoclast survival and function. Mature osteoclasts were treated with varying concentrations of autologous serum. The graphs represent effects on A) osteoclast number, B) total resorptionand C) resorbing ability. Data represent as mean ± 95%CI for 2 experiments.

Appendix 5

Bibliography

(2013) The Canadian Arthroplasty Society's experience with hip resurfacing arthroplasty. An analysis of 2773 hips. *Bone Joint J,* **95-B,** 1045-1051.

Abe, L., Nishimura, I. & Izumisawa, Y. (2008) Mechanical and histological evaluation of improved grit-blast implant in dogs: pilot study. *J Vet Med Sci,* **70,** 1191-1198.

Adams, F., Janssens, K. & Snigirev, A. (1998) Microscopic X-ray fluorescence analysis and related methods with laboratory and synchrotron radiation sources. *Journal of Analytical Atomic Spectrometry,* **13**.

Addison, W.N., Azari, F., Sorensen, E.S., Kaartinen, M.T. & McKee, M.D. (2007) Pyrophosphate inhibits mineralization of osteoblast cultures by binding to mineral, up-regulating osteopontin, and inhibiting alkaline phosphatase activity. *J Biol Chem,* **282,** 15872-15883.

Aeschlimann, D. & Evans, B.A. (2004) The vital osteoclast: how is it regulated? *Cell Death Differ,* **11 Suppl 1,** S5-7.

Aguirre, J.I., Plotkin, L.I., Stewart, S.A., Weinstein, R.S., Parfitt, A.M., Manolagas, S.C. & Bellido, T. (2006) Osteocyte apoptosis is induced by weightlessness in mice and precedes osteoclast recruitment and bone loss. *J Bone Miner Res,* **21,** 605-615.

Ajubi, N.E., Klein-Nulend, J., Alblas, M.J., Burger, E.H. & Nijweide, P.J. (1999) Signal transduction pathways involved in fluid flow-induced PGE2 production by cultured osteocytes. *Am J Physiol,* **276,** E171-178.

Al-Dujaili, S.A., Lau, E., Al-Dujaili, H., Tsang, K., Guenther, A. & You, L. (2011) Apoptotic osteocytes regulate osteoclast precursor recruitment and differentiation in vitro. *J Cell Biochem,* **112,** 2412-2423.

Albarracin, C.A., Fuqua, B.C., Evans, J.L. & Goldfine, I.D. (2008) Chromium picolinate and biotin combination improves glucose metabolism in treated, uncontrolled overweight to obese patients with type 2 diabetes. *Diabetes Metab Res Rev,* **24,** 41-51.

Allen, M.J., Myer, B.J., Millett, P.J. & Rushton, N. (1997) The effects of particulate cobalt, chromium and cobalt-chromium alloy on human osteoblast-like cells in vitro. *J Bone Joint Surg Br,* **79,** 475-482.

Alves, L., Bezerra, R., Faria, R., Ferreira, L. & da Silva Frutuoso, V. (2013) Physiological Roles and Potential Therapeutic Applications of the P2X7 Receptor in Inflammation and Pain. *Molecules,* **18,** 10953-10972.

Amstutz, H.C., Campbell, P.A. & Le Duff, M.J. (2004) Fracture of the neck of the femur after surface arthroplasty of the hip. *J Bone Joint Surg Am,* **86-A,** 1874-1877.

Amstutz, H.C. & Grigoris, P. (1996) Metal on metal bearings in hip arthroplasty. *Clin Orthop Relat Res,* S11-34.

Amstutz, H.C., Grigoris, P. & Dorey, F.J. (1998) Evolution and future of surface replacement of the hip. *J Orthop Sci,* **3,** 169-186.

Anderson, R.A., Cheng, N., Bryden, N.A., Polansky, M.M., Chi, J. & Feng, J. (1997) Elevated intakes of supplemental chromium improve glucose and insulin variables in individuals with type 2 diabetes. *Diabetes,* **46,** 1786-1791.

Andersson, M.A., Petersson Grawe, K.V., Karlsson, O.M., Abramsson-Zetterberg, L.A. & Hellman, B.E. (2007) Evaluation of the potential

genotoxicity of chromium picolinate in mammalian cells in vivo and in vitro. *Food Chem Toxicol,* **45,** 1097-1106.

Andrew, T.A., Berridge, D., Thomas, A. & Duke, R.N. (1985) Long-term review of ring total hip arthroplasty. *Clin Orthop Relat Res,* 111-122.

Andrews, R.E., Shah, K.M., Wilkinson, J.M. & Gartland, A. (2011) Effects of cobalt and chromium ions at clinically equivalent concentrations after metal-on-metal hip replacement on human osteoblasts and osteoclasts: implications for skeletal health. *Bone,* **49,** 717-723.

Anissian, L., Stark, A., Dahlstrand, H., Granberg, B., Good, V. & Bucht, E. (2002) Cobalt ions influence proliferation and function of human osteoblast-like cells. *Acta Orthop Scand,* **73,** 369-374.

Arakaki, N., Yamashita, A., Niimi, S. & Yamazaki, T. (2013) Involvement of reactive oxygen species in osteoblastic differentiation of MC3T3-E1 cells accompanied by mitochondrial morphological dynamics. *Biomed Res,* **34,** 161-166.

Arslan, P., Beltrame, M. & Tomasi, A. (1987) Intracellular chromium reduction. *Biochim Biophys Acta,* **931,** 10-15.

Arulkumaran, N., Unwin, R.J. & Tam, F.W. (2011) A potential therapeutic role for P2X7 receptor (P2X7R) antagonists in the treatment of inflammatory diseases. *Expert Opin Investig Drugs,* **20,** 897-915.

Askew, M.J., Steege, J.W., Lewis, J.L., Ranieri, J.R. & Wixson, R.L. (1984) Effect of cement pressure and bone strength on polymethylmethacrylate fixation. *J Orthop Res,* **1,** 412-420.

August, A.C., Aldam, C.H. & Pynsent, P.B. (1986) The McKee-Farrar hip arthroplasty. A long-term study. *J Bone Joint Surg Br,* **68,** 520-527.

Baldwin, E.L., Byl, J.A. & Osheroff, N. (2004) Cobalt enhances DNA cleavage mediated by human topoisomerase II alpha in vitro and in cultured cells. *Biochemistry,* **43,** 728-735.

Baron, R., Neff, L., Tran Van, P., Nefussi, J.R. & Vignery, A. (1986) Kinetic and cytochemical identification of osteoclast precursors and their differentiation into multinucleated osteoclasts. *Am J Pathol,* **122,** 363-378.

Barragan-Adjemian, C., Nicolella, D., Dusevich, V., Dallas, M.R., Eick, J.D. & Bonewald, L.F. (2006) Mechanism by which MLO-A5 late osteoblasts/early osteocytes mineralize in culture: Similarities with mineralization of lamellar bone. *Calcified Tissue International,* **79,** 340-353.

Battaglia, V., Compagnone, A., Bandino, A., Bragadin, M., Rossi, C.A., Zanetti, F., Colombatto, S., Grillo, M.A. & Toninello, A. (2009) Cobalt induces oxidative stress in isolated liver mitochondria responsible for permeability transition and intrinsic apoptosis in hepatocyte primary cultures. *Int J Biochem Cell Biol,* **41,** 586-594.

Beaule, P.E., Kim, P.R., Hamdi, A. & Fazekas, A. (2011) A prospective metal ion study of large-head metal-on-metal bearing: a matched-pair analysis of hip resurfacing versus total hip replacement. *Orthop Clin North Am,* **42,** 251-257, ix.

Beaumont, J.J., Sedman, R.M., Reynolds, S.D., Sherman, C.D., Li, L.H., Howd, R.A., Sandy, M.S., Zeise, L. & Alexeeff, G.V. (2008) Cancer mortality in a Chinese population exposed to hexavalent chromium in drinking water. *Epidemiology,* **19,** 12-23.

Bellows, C.G., Heersche, J.N. & Aubin, J.E. (1992) Inorganic phosphate added exogenously or released from beta-glycerophosphate initiates mineralization of osteoid nodules in vitro. *Bone Miner,* **17,** 15-29.

Berridge, M.V., Herst, P.M. & Tan, A.S. (2005) Tetrazolium dyes as tools in cell biology: new insights into their cellular reduction. *Biotechnol Annu Rev,* **11,** 127-152.

Berry, D.J., Harmsen, W.S., Cabanela, M.E. & Morrey, B.F. (2002) Twenty-five-year survivorship of two thousand consecutive primary Charnley total hip replacements: factors affecting survivorship of acetabular and femoral components. *J Bone Joint Surg Am,* **84-A,** 171-177.

Beveridge, R., Pintos, J., Parent, M.E., Asselin, J. & Siemiatycki, J. (2010) Lung cancer risk associated with occupational exposure to nickel, chromium VI, and cadmium in two population-based case-control studies in Montreal. *Am J Ind Med,* **53,** 476-485.

Bhabra, G., Sood, A., Fisher, B., Cartwright, L., Saunders, M., Evans, W.H., Surprenant, A., Lopez-Castejon, G., Mann, S., Davis, S.A., Hails, L.A., Ingham, E., Verkade, P., Lane, J., Heesom, K., Newson, R. & Case, C.P. (2009) Nanoparticles can cause DNA damage across a cellular barrier. *Nat Nanotechnol,* **4,** 876-883.

Bisschop, R., Boomsma, M.F., Van Raay, J.J., Tiebosch, A.T., Maas, M. & Gerritsma, C.L. (2013) High prevalence of pseudotumors in patients with a Birmingham Hip Resurfacing prosthesis: a prospective cohort study of one hundred and twenty-nine patients. *J Bone Joint Surg Am,* **95,** 1554-1560.

Blair, H.C., Teitelbaum, S.L., Ghiselli, R. & Gluck, S. (1989) Osteoclastic bone resorption by a polarized vacuolar proton pump. *Science,* **245,** 855-857.

Blasiak, J. & Kowalik, J. (2000) A comparison of the in vitro genotoxicity of tri- and hexavalent chromium. *Mutat Res,* **469,** 135-145.

Bogé, G., Leydet, M. & Houvet, D. (1992) The effects of hexavalent chromium on the activity of alkaline phosphatase in the intestine of rainbow trout (Oncorhynchus mykiss). *Aquatic Toxicology,* **23,** 247-260.

Bonewald, L.F. (2005) Generation and function of osteocyte dendritic processes. *J Musculoskelet Neuronal Interact,* **5,** 321-324.

Bosker, B.H., Ettema, H.B., Boomsma, M.F., Kollen, B.J., Maas, M. & Verheyen, C.C. (2012) High incidence of pseudotumour formation after large-diameter metal-on-metal total hip replacement: a prospective cohort study. *J Bone Joint Surg Br,* **94,** 755-761.

Boyle, W.J., Simonet, W.S. & Lacey, D.L. (2003) Osteoclast differentiation and activation. *Nature,* **423,** 337-342.

Brennan, S.A., Khan, F., McQuillan, J., O'Neill, C.J., Kenny, P., O'Rourke, S.K. & O'Byrne, J.M. (2013) Neck narrowing in resurfacing hip arthroplasty: a vascular insult? *Ir J Med Sci,* **182,** 201-205.

Bresson, C., Lamouroux, C., Sandre, C., Tabarant, M., Gault, N., Poncy, J.L., Lefaix, J.L., Den Auwer, C., Spezia, R., Gaigeot, M.P., Ansoborlo, E., Mounicou, S., Fraysse, A., Deves, G., Bacquart, T., Seznec, H., Pouthier, T., Moretto, P., Ortega, R., Lobinski, R. & Moulin, C. (2006) An interdisciplinary approach to investigate the impact of cobalt in a human keratinocyte cell line. *Biochimie,* **88,** 1619-1629.

Breuer, W., Epsztejn, S., Millgram, P. & Cabantchik, I.Z. (1995) Transport of iron and other transition metals into cells as revealed by a fluorescent probe. *Am J Physiol,* **268,** C1354-1361.

Breusch, S.J., Norman, T.L., Schneider, U., Reitzel, T., Blaha, J.D. & Lukoschek, M. (2000) Lavage technique in total hip arthroplasty: jet lavage produces better cement penetration than syringe lavage in the proximal femur. *J Arthroplasty,* **15,** 921-927.

Brown, C., Williams, S., Tipper, J.L., Fisher, J. & Ingham, E. (2007) Characterisation of wear particles produced by metal on metal and ceramic on metal hip prostheses under standard and microseparation simulation. *J Mater Sci Mater Med,* **18,** 819-827.

Buckett, P.D. & Wessling-Resnick, M. (2009) Small molecule inhibitors of divalent metal transporter-1. *Am J Physiol Gastrointest Liver Physiol,* **296,** G798-804.

Cadosch, D., Al-Mushaiqri, M.S., Gautschi, O.P., Meagher, J., Simmen, H.P. & Filgueira, L. (2010) Biocorrosion and uptake of titanium by human osteoclasts. *J Biomed Mater Res A,* **95,** 1004-1010.

Cadosch, D., Chan, E., Gautschi, O.P., Simmen, H.P. & Filgueira, L. (2009) Bio-corrosion of stainless steel by osteoclasts--in vitro evidence. *J Orthop Res,* **27,** 841-846.

Callaghan, J.J., Albright, J.C., Goetz, D.D., Olejniczak, J.P. & Johnston, R.C. (2000) Charnley total hip arthroplasty with cement. Minimum twenty-five-year follow-up. *J Bone Joint Surg Am,* **82,** 487-497.

Canalis, E. (2009) Growth factor control of bone mass. *J Cell Biochem,* **108,** 769-777.

Cardoso, L., Herman, B.C., Verborgt, O., Laudier, D., Majeska, R.J. & Schaffler, M.B. (2009) Osteocyte apoptosis controls activation of intracortical resorption in response to bone fatigue. *J Bone Miner Res,* **24,** 597-605.

Carrothers, A.D., Gilbert, R.E., Jaiswal, A. & Richardson, J.B. (2010) Birmingham hip resurfacing: the prevalence of failure. *J Bone Joint Surg Br,* **92,** 1344-1350.

Cartwright, G.E. (1955) The relationship of copper, cobalt, and other trace elements to hemopoiesis. *Am J Clin Nutr,* **3,** 11-19.

Catelas, I., Campbell, P.A., Bobyn, J.D., Medley, J.B. & Huk, O.L. (2006) Wear particles from metal-on-metal total hip replacements: effects of implant design and implantation time. *Proc Inst Mech Eng H,* **220,** 195-208.

Catelas, I. & Wimmer, M.A. (2011) New insights into wear and biological effects of metal-on-metal bearings. *J Bone Joint Surg Am,* **93 Suppl 2,** 76-83.

Cerovic, A., Miletic, I., Sobajic, S., Blagojevic, D., Radusinovic, M. & El-Sohemy, A. (2007) Effects of zinc on the mineralization of bone nodules from human osteoblast-like cells. *Biol Trace Elem Res,* **116,** 61-71.

Chan, F.W., Bobyn, J.D., Medley, J.B., Krygier, J.J. & Tanzer, M. (1999) The Otto Aufranc Award. Wear and lubrication of metal-on-metal hip implants. *Clin Orthop Relat Res*, 10-24.

Chang, Y.L., Stanford, C.M. & Keller, J.C. (2000) Calcium and phosphate supplementation promotes bone cell mineralization: implications for hydroxyapatite (HA)-enhanced bone formation. *J Biomed Mater Res,* **52,** 270-278.

Chao, C.C., Huang, C.C., Lu, D.Y., Wong, K.L., Chen, Y.R., Cheng, T.H. & Leung, Y.M. (2012) Ca2+ store depletion and endoplasmic reticulum

stress are involved in P2X7 receptor-mediated neurotoxicity in differentiated NG108-15 cells. *J Cell Biochem,* **113,** 1377-1385.

Chiu, A., Katz, A.J., Beaubier, J., Chiu, N. & Shi, X. (2004) Genetic and cellular mechanisms in chromium and nickel carcinogenesis considering epidemiologic findings. *Mol Cell Biochem,* **255,** 181-194.

Choe, Y., Yu, J.Y., Son, Y.O., Park, S.M., Kim, J.G., Shi, X. & Lee, J.C. (2012) Continuously generated H2O2 stimulates the proliferation and osteoblastic differentiation of human periodontal ligament fibroblasts. *J Cell Biochem,* **113,** 1426-1436.

Chollet, C., Chanseau, C., Remy, M., Guignandon, A., Bareille, R., Labrugere, C., Bordenave, L. & Durrieu, M.C. (2009) The effect of RGD density on osteoblast and endothelial cell behavior on RGD-grafted polyethylene terephthalate surfaces. *Biomaterials,* **30,** 711-720.

Chou, T.-C. (2006) Theoretical Basis, Experimental Design, and Computerized Simulation of Synergism and Antagonism in Drug Combination Studies. *Pharmacological Reviews,* **58,** 621-681.

Clarke, I.C., Good, V., Williams, P., Schroeder, D., Anissian, L., Stark, A., Oonishi, H., Schuldies, J. & Gustafson, G. (2000) Ultra-low wear rates for rigid-on-rigid bearings in total hip replacements. *Proc Inst Mech Eng H,* **214,** 331-347.

Clarke, M.T., Lee, P.T., Arora, A. & Villar, R.N. (2003a) Levels of metal ions after small- and large-diameter metal-on-metal hip arthroplasty. *J Bone Joint Surg Br,* **85,** 913-917.

Clarke, M.T., Lee, P.T. & Villar, R.N. (2003b) Dislocation after total hip replacement in relation to metal-on-metal bearing surfaces. *J Bone Joint Surg Br,* **85,** 650-654.

Cloos, P.A. & Christgau, S. (2004) Characterization of aged osteocalcin fragments derived from bone resorption. *Clin Lab,* **50,** 585-598.

Coddou, C., Morales, B., Gonzalez, J., Grauso, M., Gordillo, F., Bull, P., Rassendren, F. & Huidobro-Toro, J.P. (2003) Histidine 140 plays a key role in the inhibitory modulation of the P2X4 nucleotide receptor by copper but not zinc. *J Biol Chem,* **278,** 36777-36785.

Coddou, C., Yan, Z., Obsil, T., Huidobro-Toro, J.P. & Stojilkovic, S.S. (2011) Activation and regulation of purinergic P2X receptor channels. *Pharmacol Rev,* **63,** 641-683.

Coelho, D., Suormala, T., Stucki, M., Lerner-Ellis, J.P., Rosenblatt, D.S., Newbold, R.F., Baumgartner, M.R. & Fowler, B. (2008) Gene identification for the cblD defect of vitamin B12 metabolism. *N Engl J Med,* **358,** 1454-1464.

Coelho, M.J. & Fernandes, M.H. (2000) Human bone cell cultures in biocompatibility testing. Part II: effect of ascorbic acid, beta-glycerophosphate and dexamethasone on osteoblastic differentiation. *Biomaterials,* **21,** 1095-1102.

Cole, A.A. & Walters, L.M. (1987) Tartrate-resistant acid phosphatase in bone and cartilage following decalcification and cold-embedding in plastic. *J Histochem Cytochem,* **35,** 203-206.

Cook, R.B., Bolland, B.J., Wharton, J.A., Tilley, S., Latham, J.M. & Wood, R.J. (2013) Pseudotumour formation due to tribocorrosion at the taper interface of large diameter metal on polymer modular total hip replacements. *J Arthroplasty,* **28,** 1430-1436.

Cook, S.D., Barrack, R.L. & Clemow, A.J. (1994) Corrosion and wear at the modular interface of uncemented femoral stems. *J Bone Joint Surg Br,* **76,** 68-72.

Cooper, H.J., Della Valle, C.J., Berger, R.A., Tetreault, M., Paprosky, W.G., Sporer, S.M. & Jacobs, J.J. (2012) Corrosion at the head-neck taper as a cause for adverse local tissue reactions after total hip arthroplasty. *J Bone Joint Surg Am,* **94,** 1655-1661.

Cooper, H.J., Urban, R.M., Wixson, R.L., Meneghini, R.M. & Jacobs, J.J. (2013) Adverse local tissue reaction arising from corrosion at the femoral neck-body junction in a dual-taper stem with a cobalt-chromium modular neck. *J Bone Joint Surg Am,* **95,** 865-872.

Cory, A.H., Owen, T.C., Barltrop, J.A. & Cory, J.G. (1991) Use of an aqueous soluble tetrazolium/formazan assay for cell growth assays in culture. *Cancer Commun,* **3,** 207-212.

Crockett, J.C., Rogers, M.J., Coxon, F.P., Hocking, L.J. & Helfrich, M.H. (2011) Bone remodelling at a glance. *J Cell Sci,* **124,** 991-998.

Czekanska, E.M., Stoddart, M.J., Ralphs, J.R., Richards, R.G. & Hayes, J.S. (2013) A phenotypic comparison of osteoblast cell lines versus human primary osteoblasts for biomaterials testing. *J Biomed Mater Res A.*

Dai, H., Liu, J., Malkas, L.H., Catalano, J., Alagharu, S. & Hickey, R.J. (2009) Chromium reduces the in vitro activity and fidelity of DNA replication mediated by the human cell DNA synthesome. *Toxicol Appl Pharmacol,* **236,** 154-165.

Dai, M., Zhou, T., Xiong, H., Zou, W., Zhan, P. & Fu, W. (2011) [Effect of metal ions Co2+ and Cr3+ on osteoblast apoptosis, cell cycle distribution, and secretion of alkaline phosphatase]. *Zhongguo Xiu Fu Chong Jian Wai Ke Za Zhi,* **25,** 56-60.

Dalal, A., Pawar, V., McAllister, K., Weaver, C. & Hallab, N.J. (2012) Orthopedic implant cobalt-alloy particles produce greater toxicity and inflammatory cytokines than titanium alloy and zirconium alloy-based particles in vitro, in human osteoblasts, fibroblasts, and macrophages. *J Biomed Mater Res A,* **100,** 2147-2158.

Davda, K., Lali, F.V., Sampson, B., Skinner, J.A. & Hart, A.J. (2011) An analysis of metal ion levels in the joint fluid of symptomatic patients with metal-on-metal hip replacements. *J Bone Joint Surg Br,* **93,** 738-745.

Davies, A.P., Willert, H.G., Campbell, P.A., Learmonth, I.D. & Case, C.P. (2005) An unusual lymphocytic perivascular infiltration in tissues around contemporary metal-on-metal joint replacements. *J Bone Joint Surg Am,* **87,** 18-27.

De Boeck, M., Kirsch-Volders, M. & Lison, D. (2003) Cobalt and antimony: genotoxicity and carcinogenicity. *Mutat Res,* **533,** 135-152.

Di Virgilio, F. (1995) The P2Z purinoceptor: an intriguing role in immunity, inflammation and cell death. *Immunol Today,* **16,** 524-528.

Diaz, G.J., Julian, R.J. & Squires, E.J. (1994) Cobalt-induced polycythaemia causing right ventricular hypertrophy and ascites in meat-type chickens. *Avian Pathol,* **23,** 91-104.

Donkena, K.V., Young, C.Y. & Tindall, D.J. (2010) Oxidative stress and DNA methylation in prostate cancer. *Obstet Gynecol Int,* **2010,** 302051.

Donnelly-Roberts, D.L., Namovic, M.T., Han, P. & Jarvis, M.F. (2009) Mammalian P2X7 receptor pharmacology: comparison of recombinant mouse, rat and human P2X7 receptors. *Br J Pharmacol,* **157,** 1203-1214.

Dorr, L.D., Kane, T.J., 3rd & Conaty, J.P. (1994) Long-term results of cemented total hip arthroplasty in patients 45 years old or younger. A 16-year follow-up study. *J Arthroplasty,* **9,** 453-456.

Dror, D.K. & Allen, L.H. (2008) Effect of vitamin B12 deficiency on neurodevelopment in infants: current knowledge and possible mechanisms. *Nutr Rev,* **66,** 250-255.

Eastmond, D.A., Macgregor, J.T. & Slesinski, R.S. (2008) Trivalent chromium: assessing the genotoxic risk of an essential trace element and widely used human and animal nutritional supplement. *Crit Rev Toxicol,* **38,** 173-190.

Eckardt, A., Aberman, H.M., Cantwell, H.D. & Heine, J. (2003) Biological fixation of hydroxyapatite-coated versus grit-blasted titanium hip stems: a canine study. *Arch Orthop Trauma Surg,* **123,** 28-35.

El-Yamani, N., Zuniga, L., Stoyanova, E., Creus, A. & Marcos, R. (2011) Chromium-induced genotoxicity and interference in human lymphoblastoid cell (TK6) repair processes. *J Toxicol Environ Health A,* **74,** 1030-1039.

Eskelinen, A., Remes, V., Helenius, I., Pulkkinen, P., Nevalainen, J. & Paavolainen, P. (2006) Uncemented total hip arthroplasty for primary osteoarthritis in young patients: a mid-to long-term follow-up study from the Finnish Arthroplasty Register. *Acta Orthop,* **77,** 57-70.

Feighan, J.E., Goldberg, V.M., Davy, D., Parr, J.A. & Stevenson, S. (1995) The influence of surface-blasting on the incorporation of titanium-alloy implants in a rabbit intramedullary model. *J Bone Joint Surg Am,* **77,** 1380-1395.

Ferrari, D., Chiozzi, P., Falzoni, S., Hanau, S. & Di Virgilio, F. (1997) Purinergic modulation of interleukin-1 beta release from microglial cells stimulated with bacterial endotoxin. *J Exp Med,* **185,** 579-582.

Fleury, C., Petit, A., Mwale, F., Antoniou, J., Zukor, D.J., Tabrizian, M. & Huk, O.L. (2006) Effect of cobalt and chromium ions on human MG-63 osteoblasts in vitro: morphology, cytotoxicity, and oxidative stress. *Biomaterials,* **27,** 3351-3360.

Forbes, J.R. & Gros, P. (2003) Iron, manganese, and cobalt transport by Nramp1 (Slc11a1) and Nramp2 (Slc11a2) expressed at the plasma membrane. *Blood,* **102,** 1884-1892.

Forwood, M.R. (1996) Inducible cyclo-oxygenase (COX-2) mediates the induction of bone formation by mechanical loading in vivo. *J Bone Miner Res,* **11,** 1688-1693.

Franceschi, R.T., Iyer, B.S. & Cui, Y. (1994) Effects of ascorbic acid on collagen matrix formation and osteoblast differentiation in murine MC3T3-E1 cells. *J Bone Miner Res,* **9,** 843-854.

Frost, J.W. & Goldwein, M.I. (1958) Observations on vitamin B12 absorption in primary pernicious anemia during administration of adrenocortical steroids. *N Engl J Med,* **258,** 1096-1098.

Fu, J., Liang, X., Chen, Y., Tang, L., Zhang, Q.H. & Dong, Q. (2008) Oxidative stress as a component of chromium-induced cytotoxicity in rat calvarial osteoblasts. *Cell Biol Toxicol,* **24,** 201-212.

Garbuz, D.S., Tanzer, M., Greidanus, N.V., Masri, B.A. & Duncan, C.P. (2010) The John Charnley Award: Metal-on-metal hip resurfacing versus large-diameter head metal-on-metal total hip arthroplasty: a randomized clinical trial. *Clin Orthop Relat Res,* **468,** 318-325.

Garrick, M.D., Singleton, S.T., Vargas, F., Kuo, H.C., Zhao, L., Knopfel, M., Davidson, T., Costa, M., Paradkar, P., Roth, J.A. & Garrick, L.M. (2006) DMT1: which metals does it transport? *Biol Res,* **39,** 79-85.

Gartland, A., Hipskind, R.A., Gallagher, J.A. & Bowler, W.B. (2001) Expression of a P2X7 receptor by a subpopulation of human osteoblasts. *J Bone Miner Res,* **16,** 846-856.

Gatto, N.M., Kelsh, M.A., Mai, D.H., Suh, M. & Proctor, D.M. (2010) Occupational exposure to hexavalent chromium and cancers of the gastrointestinal tract: a meta-analysis. *Cancer Epidemiol,* **34,** 388-399.

Genetos, D.C., Kephart, C.J., Zhang, Y., Yellowley, C.E. & Donahue, H.J. (2007) Oscillating fluid flow activation of gap junction hemichannels induces ATP release from MLO-Y4 osteocytes. *J Cell Physiol,* **212,** 207-214.

Germanier, Y., Tosatti, S., Broggini, N., Textor, M. & Buser, D. (2006) Enhanced bone apposition around biofunctionalized sandblasted and acid-etched titanium implant surfaces. A histomorphometric study in miniature pigs. *Clin Oral Implants Res,* **17,** 251-257.

Giancotti, F.G. & Ruoslahti, E. (1999) Integrin signaling. *Science,* **285,** 1028-1032.

Gibson, G. (1998) Active role of chondrocyte apoptosis in endochondral ossification. *Microsc Res Tech,* **43,** 191-204.

Gilbert, L., He, X., Farmer, P., Boden, S., Kozlowski, M., Rubin, J. & Nanes, M.S. (2000) Inhibition of osteoblast differentiation by tumor necrosis factor-alpha. *Endocrinology,* **141,** 3956-3964.

Glant, T.T., Jacobs, J.J., Molnar, G., Shanbhag, A.S., Valyon, M. & Galante, J.O. (1993) Bone resorption activity of particulate-stimulated macrophages. *J Bone Miner Res,* **8,** 1071-1079.

Golub, E.E. (2009) Role of matrix vesicles in biomineralization. *Biochim Biophys Acta,* **1790,** 1592-1598.

Gomez, P.F. & Morcuende, J.A. (2005) Early attempts at hip arthroplasty--1700s to 1950s. *Iowa Orthop J,* **25,** 25-29.

Goode, A.E., Perkins, J.M., Sandison, A., Karunakaran, C., Cheng, H., Wall, D., Skinner, J.A., Hart, A.J., Porter, A.E., McComb, D.W. & Ryan, M.P. (2012) Chemical speciation of nanoparticles surrounding metal-on-metal hips. *Chem Commun (Camb),* **48,** 8335-8337.

Grammatopoulos, G., Pandit, H., Kamali, A., Maggiani, F., Glyn-Jones, S., Gill, H.S., Murray, D.W. & Athanasou, N. (2013) The correlation of wear with histological features after failed hip resurfacing arthroplasty. *J Bone Joint Surg Am,* **95,** e81.

Gray, S.J. & Sterling, K. (1950) The tagging of red cells and plasma proteins with radioactive chromium. *J Clin Invest,* **29,** 1604-1613.

Gruenheid, S., Canonne-Hergaux, F., Gauthier, S., Hackam, D.J., Grinstein, S. & Gros, P. (1999) The iron transport protein NRAMP2 is an integral membrane glycoprotein that colocalizes with transferrin in recycling endosomes. *J Exp Med,* **189,** 831-841.

Gunshin, H., Mackenzie, B., Berger, U.V., Gunshin, Y., Romero, M.F., Boron, W.F., Nussberger, S., Gollan, J.L. & Hediger, M.A. (1997) Cloning and characterization of a mammalian proton-coupled metal-ion transporter. *Nature,* **388,** 482-488.

Ha, H., Kwak, H.B., Lee, S.W., Jin, H.M., Kim, H.M., Kim, H.H. & Lee, Z.H. (2004) Reactive oxygen species mediate RANK signaling in osteoclasts. *Exp Cell Res,* **301,** 119-127.

Halasova, E., Matakova, T., Kavcova, E., Musak, L., Letkova, L., Adamkov, M., Ondrusova, M., Bukovska, E. & Singliar, A. (2009) Human lung cancer and hexavalent chromium exposure. *Neuro Endocrinol Lett,* **30 Suppl 1,** 182-185.

Hallab, N.J., Bundy, K.J., O'Connor, K., Moses, R.L. & Jacobs, J.J. (2001) Evaluation of metallic and polymeric biomaterial surface energy and surface roughness characteristics for directed cell adhesion. *Tissue Eng,* **7,** 55-71.

Hallab, N.J., Vermes, C., Messina, C., Roebuck, K.A., Glant, T.T. & Jacobs, J.J. (2002) Concentration- and composition-dependent effects of metal ions on human MG-63 osteoblasts. *J Biomed Mater Res,* **60,** 420-433.

Hallam, P., Haddad, F. & Cobb, J. (2004) Pain in the well-fixed, aseptic titanium hip replacement. The role of corrosion. *J Bone Joint Surg Br,* **86,** 27-30.

Han, Y., Cowin, S.C., Schaffler, M.B. & Weinbaum, S. (2004) Mechanotransduction and strain amplification in osteocyte cell processes. *Proceedings of the National Academy of Sciences of the United States of America,* **101,** 16689-16694.

Harp, M.J. & Scoular, F.I. (1952) Cobalt metabolism of young college women on self-selected diets. *J Nutr,* **47,** 67-72.

Harris, W.H., Schiller, A.L., Scholler, J.M., Freiberg, R.A. & Scott, R. (1976) Extensive localized bone resorption in the femur following total hip replacement. *J Bone Joint Surg Am,* **58,** 612-618.

Harrison, G., Shapiro, I.M. & Golub, E.E. (1995) The phosphatidylinositol-glycolipid anchor on alkaline phosphatase facilitates mineralization initiation in vitro. *J Bone Miner Res,* **10,** 568-573.

Hart, A.J., Quinn, P.D., Lali, F., Sampson, B., Skinner, J.A., Powell, J.J., Nolan, J., Tucker, K., Donell, S., Flanagan, A. & Mosselmans, J.F. (2012) Cobalt from metal-on-metal hip replacements may be the clinically relevant active agent responsible for periprosthetic tissue reactions. *Acta Biomater,* **8,** 3865-3873.

Hart, A.J., Quinn, P.D., Sampson, B., Sandison, A., Atkinson, K.D., Skinner, J.A., Powell, J.J. & Mosselmans, J.F. (2010a) The chemical form of metallic debris in tissues surrounding metal-on-metal hips with unexplained failure. *Acta Biomater,* **6,** 4439-4446.

Hart, A.J., Quinn, P.D., Sampson, B., Sandison, A., Atkinson, K.D., Skinner, J.A., Powell, J.J. & Mosselmans, J.F.W. (2010b) The chemical form of metallic debris in tissues surrounding metal-on-metal hips with unexplained failure. *Acta Biomaterialia,* **6,** 4439-4446.

Hartke, J.R. & Lundy, M.W. (2001) Bone anabolic therapy with selective prostaglandin analogs. *J Musculoskelet Neuronal Interact,* **2,** 25-31.

Hartwig, A. & Schwerdtle, T. (2002) Interactions by carcinogenic metal compounds with DNA repair processes: toxicological implications. *Toxicol Lett,* **127,** 47-54.

Hausser, H.J. & Brenner, R.E. (2005) Phenotypic instability of Saos-2 cells in long-term culture. *Biochem Biophys Res Commun,* **333,** 216-222.

Hayman, A.R., Bune, A.J., Bradley, J.R., Rashbass, J. & Cox, T.M. (2000) Osteoclastic tartrate-resistant acid phosphatase (Acp 5): its localization to dendritic cells and diverse murine tissues. *J Histochem Cytochem,* **48,** 219-228.

Hayman, A.R., Jones, S.J., Boyde, A., Foster, D., Colledge, W.H., Carlton, M.B., Evans, M.J. & Cox, T.M. (1996) Mice lacking tartrate-resistant acid phosphatase (Acp 5) have disrupted endochondral ossification and mild osteopetrosis. *Development,* **122,** 3151-3162.

Haynes, D.R., Rogers, S.D., Hay, S., Pearcy, M.J. & Howie, D.W. (1993) The differences in toxicity and release of bone-resorbing mediators induced by titanium and cobalt-chromium-alloy wear particles. *J Bone Joint Surg Am,* **75,** 825-834.

He, T., Wu, W., Huang, Y., Zhang, X., Tang, T. & Dai, K. (2013) Multiple biomarkers analysis for the early detection of prosthetic aseptic loosening of hip arthroplasty. *Int Orthop,* **37,** 1025-1031.

Heisel, C., Streich, N., Krachler, M., Jakubowitz, E. & Kretzer, J.P. (2008) Characterization of the running-in period in total hip resurfacing arthroplasty: an in vivo and in vitro metal ion analysis. *J Bone Joint Surg Am,* **90 Suppl 3,** 125-133.

Hennessy, K.M., Clem, W.C., Phipps, M.C., Sawyer, A.A., Shaikh, F.M. & Bellis, S.L. (2008) The effect of RGD peptides on osseointegration of hydroxyapatite biomaterials. *Biomaterials,* **29,** 3075-3083.

Herberts, P. & Malchau, H. (2000) Long-term registration has improved the quality of hip replacement: a review of the Swedish THR Register comparing 160,000 cases. *Acta Orthop Scand,* **71,** 111-121.

Hessle, L., Johnson, K.A., Anderson, H.C., Narisawa, S., Sali, A., Goding, J.W., Terkeltaub, R. & Millan, J.L. (2002) Tissue-nonspecific alkaline phosphatase and plasma cell membrane glycoprotein-1 are central antagonistic regulators of bone mineralization. *Proc Natl Acad Sci U S A,* **99,** 9445-9449.

Hibell, A.D., Kidd, E.J., Chessell, I.P., Humphrey, P.P. & Michel, A.D. (2000) Apparent species differences in the kinetic properties of P2X(7) receptors. *Br J Pharmacol,* **130,** 167-173.

Hillam, R.A. & Skerry, T.M. (1995) Inhibition of bone resorption and stimulation of formation by mechanical loading of the modeling rat ulna in vivo. *J Bone Miner Res,* **10,** 683-689.

Hirao, M., Hashimoto, J., Yamasaki, N., Ando, W., Tsuboi, H., Myoui, A. & Yoshikawa, H. (2007) Oxygen tension is an important mediator of the transformation of osteoblasts to osteocytes. *J Bone Miner Metab,* **25,** 266-276.

Holland, J.P., Langton, D.J. & Hashmi, M. (2012) Ten-year clinical, radiological and metal ion analysis of the Birmingham Hip Resurfacing: from a single, non-designer surgeon. *J Bone Joint Surg Br,* **94,** 471-476.

Holmbeck, K., Bianco, P., Pidoux, I., Inoue, S., Billinghurst, R.C., Wu, W., Chrysovergis, K., Yamada, S., Birkedal-Hansen, H. & Poole, A.R. (2005) The metalloproteinase MT1-MMP is required for normal development and maintenance of osteocyte processes in bone. *J Cell Sci,* **118,** 147-156.

Honore, P., Donnelly-Roberts, D., Namovic, M.T., Hsieh, G., Zhu, C.Z., Mikusa, J.P., Hernandez, G., Zhong, C., Gauvin, D.M., Chandran, P., Harris, R., Medrano, A.P., Carroll, W., Marsh, K., Sullivan, J.P., Faltynek, C.R. & Jarvis, M.F. (2006) A-740003 [N-(1-{[(cyanoimino)(5-quinolinylamino) methyl]amino}-2,2-dimethylpropyl)-2-(3,4-dimethoxyphenyl)acetamide], a novel and selective P2X7 receptor antagonist, dose-dependently reduces neuropathic pain in the rat. *J Pharmacol Exp Ther,* **319,** 1376-1385.

Howie, D.W., Cornish, B.L. & Vernon-Roberts, B. (1993) The viability of the femoral head after resurfacing hip arthroplasty in humans. *Clin Orthop Relat Res,* 171-184.

Huber, M., Reinisch, G., Trettenhahn, G., Zweymuller, K. & Lintner, F. (2009) Presence of corrosion products and hypersensitivity-associated reactions in periprosthetic tissue after aseptic loosening of total hip replacements with metal bearing surfaces. *Acta Biomater,* **5,** 172-180.

Huk, O.L., Catelas, I., Mwale, F., Antoniou, J., Zukor, D.J. & Petit, A. (2004) Induction of apoptosis and necrosis by metal ions in vitro. *The Journal of Arthroplasty,* **19,** 84-87.

Huo, B., Lu, X.L., Costa, K.D., Xu, Q. & Guo, X.E. (2010) An ATP-dependent mechanism mediates intercellular calcium signaling in bone cell network under single cell nanoindentation. *Cell Calcium,* **47,** 234-241.

Hussein, S.M., Duff, E.K. & Sirard, C. (2003) Smad4 and beta-catenin co-activators functionally interact with lymphoid-enhancing factor to regulate graded expression of Msx2. *J Biol Chem,* **278,** 48805-48814.

Illing, A.C., Shawki, A., Cunningham, C.L. & Mackenzie, B. (2012) Substrate profile and metal-ion selectivity of human divalent metal-ion transporter-1. *J Biol Chem,* **287,** 30485-30496.

Ince, N.H., Dirilgen, N., Apikyan, I.G., Tezcanli, G. & Ustun, B. (1999) Assessment of toxic interactions of heavy metals in binary mixtures: A statistical approach. *Arch Environ Contam Toxicol,* **36,** 365-372.

Jabado, N., Canonne-Hergaux, F., Gruenheid, S., Picard, V. & Gros, P. (2002) Iron transporter Nramp2/DMT-1 is associated with the membrane of phagosomes in macrophages and Sertoli cells. *Blood,* **100,** 2617-2622.

Jaiprakash, A., Prasadam, I., Feng, J.Q., Liu, Y., Crawford, R. & Xiao, Y. (2012) Phenotypic characterization of osteoarthritic osteocytes from the sclerotic zones: a possible pathological role in subchondral bone sclerosis. *Int J Biol Sci,* **8,** 406-417.

Jasty, M., Goetz, D.D., Bragdon, C.R., Lee, K.R., Hanson, A.E., Elder, J.R. & Harris, W.H. (1997) Wear of polyethylene acetabular components in total hip arthroplasty. An analysis of one hundred and twenty-eight components retrieved at autopsy or revision operations. *J Bone Joint Surg Am,* **79,** 349-358.

Jefferson, J.A., Escudero, E., Hurtado, M.E., Pando, J., Tapia, R., Swenson, E.R., Prchal, J., Schreiner, G.F., Schoene, R.B., Hurtado, A. & Johnson, R.J. (2002) Excessive erythrocytosis, chronic mountain sickness, and serum cobalt levels. *Lancet,* **359,** 407-408.

Jensen, E.D., Gopalakrishnan, R. & Westendorf, J.J. (2010) Regulation of gene expression in osteoblasts. *Biofactors,* **36,** 25-32.

Jiang, J.X. & Cheng, B. (2001) Mechanical stimulation of gap junctions in bone osteocytes is mediated by prostaglandin E2. *Cell Commun Adhes,* **8,** 283-288.

Jiang, L., Cui, Y., Luan, J., Zhou, X., Zhou, X. & Han1, J. (2013) A comparative proteomics study on matrix vesicles of osteoblast-like SaOS-2 and U2-OS cells. *Intractable and Rare Diseases Research,* **2,** 59-62.

Jin, Z.M., Dowson, D. & Fisher, J. (1997) Analysis of fluid film lubrication in artificial hip joint replacements with surfaces of high elastic modulus. *Proc Inst Mech Eng H,* **211,** 247-256.

Jinno, T., Goldberg, V.M., Davy, D. & Stevenson, S. (1998) Osseointegration of surface-blasted implants made of titanium alloy and cobalt-chromium alloy in a rabbit intramedullary model. *J Biomed Mater Res,* **42,** 20-29.

Kamel, M.A., Picconi, J.L., Lara-Castillo, N. & Johnson, M.L. (2010) Activation of beta-catenin signaling in MLO-Y4 osteocytic cells versus 2T3 osteoblastic cells by fluid flow shear stress and PGE2: Implications for the study of mechanosensation in bone. *Bone,* **47,** 872-881.

Kanaji, A., Caicedo, M.S., Virdi, A.S., Sumner, D.R., Hallab, N.J. & Sena, K. (2009) Co-Cr-Mo alloy particles induce tumor necrosis factor alpha production in MLO-Y4 osteocytes: a role for osteocytes in particle-induced inflammation. *Bone,* **45,** 528-533.

Kasten, U., Mullenders, L.H. & Hartwig, A. (1997) Cobalt(II) inhibits the incision and the polymerization step of nucleotide excision repair in human fibroblasts. *Mutat Res,* **383,** 81-89.

Kato, Y., Boskey, A., Spevak, L., Dallas, M., Hori, M. & Bonewald, L.F. (2001) Establishment of an osteoid preosteocyte-like cell MLO-A5 that spontaneously mineralizes in culture. *J Bone Miner Res,* **16,** 1622-1633.

Kato, Y., Windle, J.J., Koop, B.A., Mundy, G.R. & Bonewald, L.F. (1997) Establishment of an osteocyte-like cell line, MLO-Y4. *J Bone Miner Res,* **12,** 2014-2023.

Keegan, G.M., Learmonth, I.D. & Case, C.P. (2007) Orthopaedic metals and their potential toxicity in the arthroplasty patient: A review of current knowledge and future strategies. *J Bone Joint Surg Br,* **89,** 567-573.

Kemner, K.M., Kelly, S.D., Lai, B., Maser, J., O'Loughlin E, J., Sholto-Douglas, D., Cai, Z., Schneegurt, M.A., Kulpa, C.F., Jr. & Nealson, K.H. (2004) Elemental and redox analysis of single bacterial cells by x-ray microbeam analysis. *Science,* **306,** 686-687.

Kilgus, D.J., Dorey, F.J., Finerman, G.A. & Amstutz, H.C. (1991) Patient activity, sports participation, and impact loading on the durability of cemented total hip replacements. *Clin Orthop Relat Res,* 25-31.

Kilpadi, K.L., Chang, P.L. & Bellis, S.L. (2001) Hydroxylapatite binds more serum proteins, purified integrins, and osteoblast precursor cells than titanium or steel. *J Biomed Mater Res,* **57,** 258-267.

Kim, R.H., Dennis, D.A. & Carothers, J.T. (2008) Metal-on-metal total hip arthroplasty. *J Arthroplasty,* **23,** 44-46.

Kim, Y.H., Kim, J.S., Joo, J.H. & Park, J.W. (2012) Is hydroxyapatite coating necessary to improve survivorship of porous-coated titanium femoral stem? *J Arthroplasty,* **27,** 559-563.

Klaunig, J.E. & Kamendulis, L.M. (2004) The role of oxidative stress in carcinogenesis. *Annu Rev Pharmacol Toxicol,* **44,** 239-267.

Knothe Tate, M.L., Adamson, J.R., Tami, A.E. & Bauer, T.W. (2004) The osteocyte. *Int J Biochem Cell Biol,* **36,** 1-8.

Kobayashi, K., Takahashi, N., Jimi, E., Udagawa, N., Takami, M., Kotake, S., Nakagawa, N., Kinosaki, M., Yamaguchi, K., Shima, N., Yasuda, H.,

Morinaga, T., Higashio, K., Martin, T.J. & Suda, T. (2000) Tumor necrosis factor alpha stimulates osteoclast differentiation by a mechanism independent of the ODF/RANKL-RANK interaction. *J Exp Med,* **191,** 275-286.

Koerten, H.K., Onderwater, J.J., Koerten, E.W., Bernoski, F.P. & Nelissen, R.G. (2001) Observations at the articular surface of hip prostheses: an analytical electron microscopy study on wear and corrosion. *J Biomed Mater Res,* **54,** 591-596.

Kogianni, G., Mann, V. & Noble, B.S. (2008) Apoptotic Bodies Convey Activity Capable of Initiating Osteoclastogenesis and Localized Bone Destruction. *Journal of Bone and Mineral Research,* **23,** 915-927.

Koh, J.M., Lee, Y.S., Kim, Y.S., Kim, D.J., Kim, H.H., Park, J.Y., Lee, K.U. & Kim, G.S. (2006) Homocysteine enhances bone resorption by stimulation of osteoclast formation and activity through increased intracellular ROS generation. *J Bone Miner Res,* **21,** 1003-1011.

Komori, T., Yagi, H., Nomura, S., Yamaguchi, A., Sasaki, K., Deguchi, K., Shimizu, Y., Bronson, R.T., Gao, Y.H., Inada, M., Sato, M., Okamoto, R., Kitamura, Y., Yoshiki, S. & Kishimoto, T. (1997) Targeted disruption of Cbfa1 results in a complete lack of bone formation owing to maturational arrest of osteoblasts. *Cell,* **89,** 755-764.

Kong, Y.Y., Yoshida, H., Sarosi, I., Tan, H.L., Timms, E., Capparelli, C., Morony, S., Oliveira-dos-Santos, A.J., Van, G., Itie, A., Khoo, W., Wakeham, A., Dunstan, C.R., Lacey, D.L., Mak, T.W., Boyle, W.J. & Penninger, J.M. (1999) OPGL is a key regulator of osteoclastogenesis, lymphocyte development and lymph-node organogenesis. *Nature,* **397,** 315-323.

Kopera, E., Schwerdtle, T., Hartwig, A. & Bal, W. (2004) Co(II) and Cd(II) substitute for Zn(II) in the zinc finger derived from the DNA repair protein XPA, demonstrating a variety of potential mechanisms of toxicity. *Chem Res Toxicol,* **17,** 1452-1458.

Korovessis, P., Petsinis, G., Repanti, M. & Repantis, T. (2006) Metallosis after contemporary metal-on-metal total hip arthroplasty. Five to nine-year follow-up. *J Bone Joint Surg Am,* **88,** 1183-1191.

Kozlenkov, A., Manes, T., Hoylaerts, M.F. & Millan, J.L. (2002) Function assignment to conserved residues in mammalian alkaline phosphatases. *J Biol Chem,* **277,** 22992-22999.

Krakowiak, A., Dudek, W., Tarkowski, M., Swiderska-Kielbik, S., Niescierenko, E. & Palczynski, C. (2005) Occupational asthma caused by cobalt chloride in a diamond polisher after cessation of occupational exposure: a case report. *Int J Occup Med Environ Health,* **18,** 151-158.

Krantz, N., Miletic, B., Migaud, H. & Girard, J. (2012) Hip resurfacing in patients under thirty years old: an attractive option for young and active patients. *Int Orthop,* **36,** 1789-1794.

Kuhn, L.T., Liu, Y., Advincula, M., Wang, Y.H., Maye, P. & Goldberg, A.J. (2010) A nondestructive method for evaluating in vitro osteoblast differentiation on biomaterials using osteoblast-specific fluorescence. *Tissue Eng Part C Methods,* **16,** 1357-1366.

Kurtz, S.M., Kocagoz, S.B., Hanzlik, J.A., Underwood, R.J., Gilbert, J.L., MacDonald, D.W., Lee, G.C., Mont, M.A., Kraay, M.J., Klein, G.R., Parvizi, J. & Rimnac, C.M. (2013) Do ceramic femoral heads reduce

taper fretting corrosion in hip arthroplasty? A retrieval study. *Clin Orthop Relat Res, 471,* 3270-3282.

Kwon, Y.M., Ostlere, S.J., McLardy-Smith, P., Athanasou, N.A., Gill, H.S. & Murray, D.W. (2011) "Asymptomatic" pseudotumors after metal-on-metal hip resurfacing arthroplasty: prevalence and metal ion study. *J Arthroplasty, 26,* 511-518.

Lacey, D.C., De Kok, B., Clanchy, F.I., Bailey, M.J., Speed, K., Haynes, D., Graves, S.E. & Hamilton, J.A. (2009) Low dose metal particles can induce monocyte/macrophage survival. *J Orthop Res, 27,* 1481-1486.

Langard, S. & Norseth, T. (1975) A cohort study of bronchial carcinomas in workers producing chromate pigments. *Br J Ind Med, 32,* 62-65.

Langton, D.J., Jameson, S.S., Joyce, T.J., Hallab, N.J., Natu, S. & Nargol, A.V. (2010) Early failure of metal-on-metal bearings in hip resurfacing and large-diameter total hip replacement: A consequence of excess wear. *J Bone Joint Surg Br, 92,* 38-46.

Langton, D.J., Sidaginamale, R.P., Joyce, T.J., Natu, S., Blain, P., Jefferson, R.D., Rushton, S. & Nargol, A.V. (2013) The clinical implications of elevated blood metal ion concentrations in asymptomatic patients with MoM hip resurfacings: a cohort study. *BMJ Open, 3.*

Langton, D.J., Sprowson, A.P., Joyce, T.J., Reed, M., Carluke, I., Partington, P. & Nargol, A.V. (2009) Blood metal ion concentrations after hip resurfacing arthroplasty: a comparative study of articular surface replacement and Birmingham Hip Resurfacing arthroplasties. *J Bone Joint Surg Br, 91,* 1287-1295.

Lazarinis, S., Karrholm, J. & Hailer, N.P. (2011) Effects of hydroxyapatite coating on survival of an uncemented femoral stem. A Swedish Hip Arthroplasty Register study on 4,772 hips. *Acta Orthop, 82,* 399-404.

Learmonth, I.D., Young, C. & Rorabeck, C. (2007) The operation of the century: total hip replacement. *Lancet, 370,* 1508-1519.

Lee, D.H., Lim, B.S., Lee, Y.K. & Yang, H.C. (2006) Effects of hydrogen peroxide (H2O2) on alkaline phosphatase activity and matrix mineralization of odontoblast and osteoblast cell lines. *Cell Biol Toxicol, 22,* 39-46.

Leggett, R.W. (2008) The biokinetics of inorganic cobalt in the human body. *Sci Total Environ, 389,* 259-269.

Lehmann, G., Cacciotti, I., Palmero, P., Montanaro, L., Bianco, A., Campagnolo, L. & Camaioni, A. (2012) Differentiation of osteoblast and osteoclast precursors on pure and silicon-substituted synthesized hydroxyapatites. *Biomed Mater, 7,* 055001.

Leonard, S., Gannett, P.M., Rojanasakul, Y., Schwegler-Berry, D., Castranova, V., Vallyathan, V. & Shi, X. (1998) Cobalt-mediated generation of reactive oxygen species and its possible mechanism. *J Inorg Biochem, 70,* 239-244.

Lewin, M.R., Wills, M.R. & Baron, D.N. (1969) Ultramicrofluorimetric determination of calcium in plasma. *J Clin Pathol, 22,* 222-225.

Li, J., Liu, D., Ke, H.Z., Duncan, R.L. & Turner, C.H. (2005a) The P2X7 nucleotide receptor mediates skeletal mechanotransduction. *J Biol Chem, 280,* 42952-42959.

Li, J., Sarosi, I., Yan, X.Q., Morony, S., Capparelli, C., Tan, H.L., McCabe, S., Elliott, R., Scully, S., Van, G., Kaufman, S., Juan, S.C., Sun, Y., Tarpley,

J., Martin, L., Christensen, K., McCabe, J., Kostenuik, P., Hsu, H., Fletcher, F., Dunstan, C.R., Lacey, D.L. & Boyle, W.J. (2000) RANK is the intrinsic hematopoietic cell surface receptor that controls osteoclastogenesis and regulation of bone mass and calcium metabolism. *Proc Natl Acad Sci U S A,* **97,** 1566-1571.

Li, X., Qin, L., Bergenstock, M., Bevelock, L.M., Novack, D.V. & Partridge, N.C. (2007) Parathyroid hormone stimulates osteoblastic expression of MCP-1 to recruit and increase the fusion of pre/osteoclasts. *J Biol Chem,* **282,** 33098-33106.

Li, X., Zhang, Y., Kang, H., Liu, W., Liu, P., Zhang, J., Harris, S.E. & Wu, D. (2005b) Sclerostin binds to LRP5/6 and antagonizes canonical Wnt signaling. *J Biol Chem,* **280,** 19883-19887.

Liao, Y., Hoffman, E., Wimmer, M., Fischer, A., Jacobs, J. & Marks, L. (2013) CoCrMo metal-on-metal hip replacements. *Phys Chem Chem Phys,* **15,** 746-756.

Lieske, S., John, M., Rimasch, C. & Mahlfeld, K. (2008) [Dislocation as a rare complication of resurfacing of the hip joint. Case report and meta-analysis]. *Unfallchirurg,* **111,** 637-640.

Lin, G.L. & Hankenson, K.D. (2011) Integration of BMP, Wnt, and notch signaling pathways in osteoblast differentiation. *J Cell Biochem,* **112,** 3491-3501.

Liu, F., Udofia, I., Jin, Z., Hirt, F., Rieker, C., Roberts, P. & Grigoris, P. (2005) Comparison of contact mechanics between a total hip replacement and a hip resurfacing with a metal-on-metal articulation. *Proceedings of the Institution of Mechanical Engineers, Part C: Journal of Mechanical Engineering Science,* **219,** 727-732.

Lo, Y.Y. & Cruz, T.F. (1995) Involvement of reactive oxygen species in cytokine and growth factor induction of c-fos expression in chondrocytes. *J Biol Chem,* **270,** 11727-11730.

Lochner, K., Fritsche, A., Jonitz, A., Hansmann, D., Mueller, P., Mueller-Hilke, B. & Bader, R. (2011) The potential role of human osteoblasts for periprosthetic osteolysis following exposure to wear particles. *Int J Mol Med,* **28,** 1055-1063.

Lohar, S., Banerjee, A., Sahana, A., Banik, A., Mukhopadhyay, S.K. & Das, D. (2013) A rhodamine-naphthalene conjugate as a FRET based sensor for Cr3+ and Fe3+ with cell staining application. *Analytical Methods,* **5,** 442-445.

Lohmann, C.H., Schwartz, Z., Koster, G., Jahn, U., Buchhorn, G.H., MacDougall, M.J., Casasola, D., Liu, Y., Sylvia, V.L., Dean, D.D. & Boyan, B.D. (2000) Phagocytosis of wear debris by osteoblasts affects differentiation and local factor production in a manner dependent on particle composition. *Biomaterials,* **21,** 551-561.

Lombardi, A.V., Jr., Berend, K.R., Mallory, T.H., Skeels, M.D. & Adams, J.B. (2009) Survivorship of 2000 tapered titanium porous plasma-sprayed femoral components. *Clin Orthop Relat Res,* **467,** 146-154.

Long, W.T. (2005) The clinical performance of metal-on-metal as an articulation surface in total hip replacement. *Iowa Orthop J,* **25,** 10-16.

Lorca, R.A., Coddou, C., Gazitua, M.C., Bull, P., Arredondo, C. & Huidobro-Toro, J.P. (2005) Extracellular histidine residues identify common

structural determinants in the copper/zinc P2X2 receptor modulation. *J Neurochem,* **95,** 499-512.

Luo, L., Petit, A., Antoniou, J., Zukor, D.J., Huk, O.L., Liu, R.C., Winnik, F.M. & Mwale, F. (2005) Effect of cobalt and chromium ions on MMP-1, TIMP-1, and TNF-alpha gene expression in human U937 macrophages: a role for tyrosine kinases. *Biomaterials,* **26,** 5587-5593.

Ma, Y.L., Cain, R.L., Halladay, D.L., Yang, X., Zeng, Q., Miles, R.R., Chandrasekhar, S., Martin, T.J. & Onyia, J.E. (2001) Catabolic effects of continuous human PTH (1--38) in vivo is associated with sustained stimulation of RANKL and inhibition of osteoprotegerin and gene-associated bone formation. *Endocrinology,* **142,** 4047-4054.

Mabilleau, G., Gill, R. & Sabokbar, A. (2012) Cobalt and Chromium Ions Affect Human Osteoclast and Human Osteoblast Physiology In vitro.

Mabilleau, G., Kwon, Y.M., Pandit, H., Murray, D.W. & Sabokbar, A. (2008) Metal-on-metal hip resurfacing arthroplasty: a review of periprosthetic biological reactions. *Acta Orthop,* **79,** 734-747.

Macfie, A., Hagan, E. & Zhitkovich, A. (2010) Mechanism of DNA-protein cross-linking by chromium. *Chem Res Toxicol,* **23,** 341-347.

Mahamid, J., Sharir, A., Gur, D., Zelzer, E., Addadi, L. & Weiner, S. (2011) Bone mineralization proceeds through intracellular calcium phosphate loaded vesicles: a cryo-electron microscopy study. *J Struct Biol,* **174,** 527-535.

Mahato, P., Saha, S., Suresh, E., Di Liddo, R., Parnigotto, P.P., Conconi, M.T., Kesharwani, M.K., Ganguly, B. & Das, A. (2012) Ratiometric detection of Cr3+ and Hg2+ by a naphthalimide-rhodamine based fluorescent probe. *Inorg Chem,* **51,** 1769-1777.

Makela, K.T., Matilainen, M., Pulkkinen, P., Fenstad, A.M., Havelin, L., Engesaeter, L., Furnes, O., Pedersen, A.B., Overgaard, S., Karrholm, J., Malchau, H., Garellick, G., Ranstam, J. & Eskelinen, A. (2014) Failure rate of cemented and uncemented total hip replacements: register study of combined Nordic database of four nations. *BMJ,* **348,** f7592.

Malchau, H., Herberts, P., Eisler, T., Garellick, G. & Soderman, P. (2002) The Swedish Total Hip Replacement Register. *J Bone Joint Surg Am,* **84-A Suppl 2,** 2-20.

Malik, M.A., Puleo, D.A., Bizios, R. & Doremus, R.H. (1992) Osteoblasts on hydroxyapatite, alumina and bone surfaces in vitro: morphology during the first 2 h of attachment. *Biomaterials,* **13,** 123-128.

Mandal, C.C., Ganapathy, S., Gorin, Y., Mahadev, K., Block, K., Abboud, H.E., Harris, S.E., Ghosh-Choudhury, G. & Ghosh-Choudhury, N. (2011) Reactive oxygen species derived from Nox4 mediate BMP2 gene transcription and osteoblast differentiation. *Biochem J,* **433,** 393-402.

Manley, M.T. & Sutton, K. (2008) Bearings of the future for total hip arthroplasty. *J Arthroplasty,* **23,** 47-50.

Marks, S. & Odgren, P. (2002) *Principles of Bone Biology.* Academic Press.

Mason, D.J., Hillam, R.A. & Skerry, T.M. (1996) Constitutive in vivo mRNA expression by osteocytes of beta-actin, osteocalcin, connexin-43, IGF-I, c-fos and c-jun, but not TNF-alpha nor tartrate-resistant acid phosphatase. *J Bone Miner Res,* **11,** 350-357.

Masui, T., Sakano, S., Hasegawa, Y., Warashina, H. & Ishiguro, N. (2005) Expression of inflammatory cytokines, RANKL and OPG induced by

titanium, cobalt-chromium and polyethylene particles. *Biomaterials,* **26,** 1695-1702.

Mathew, M.T., Jacobs, J.J. & Wimmer, M.A. (2012) Wear-corrosion synergism in a CoCrMo hip bearing alloy is influenced by proteins. *Clin Orthop Relat Res,* **470,** 3109-3117.

Matthies, A.K., Racasan, R., Bills, P., Blunt, L., Cro, S., Panagiotidou, A., Blunn, G., Skinner, J. & Hart, A.J. (2013) Material loss at the taper junction of retrieved large head metal-on-metal total hip replacements. *J Orthop Res,* **31,** 1677-1685.

Mavrogenis, A.F., Dimitriou, R., Parvizi, J. & Babis, G.C. (2009) Biology of implant osseointegration. *J Musculoskelet Neuronal Interact,* **9,** 61-71.

Maxwell, P. & Salnikow, K. (2004) HIF-1: an oxygen and metal responsive transcription factor. *Cancer Biol Ther,* **3,** 29-35.

McKay, G.C., Macnair, R., MacDonald, C. & Grant, M.H. (1996) Interactions of orthopaedic metals with an immortalized rat osteoblast cell line. *Biomaterials,* **17,** 1339-1344.

McQuillan, D.J., Richardson, M.D. & Bateman, J.F. (1995) Matrix deposition by a calcifying human osteogenic sarcoma cell line (SAOS-2). *Bone,* **16,** 415-426.

McRae, R., Lai, B., Vogt, S. & Fahrni, C.J. (2006) Correlative microXRF and optical immunofluorescence microscopy of adherent cells labeled with ultrasmall gold particles. *J Struct Biol,* **155,** 22-29.

Mertz, W. (1969) Chromium occurrence and function in biological systems. *Physiol Rev,* **49,** 163-239.

Minkin, C. (1982) Bone acid phosphatase: tartrate-resistant acid phosphatase as a marker of osteoclast function. *Calcif Tissue Int,* **34,** 285-290.

Mont, M.A., McGrath, M.S., Ulrich, S.D., Seyler, T.M., Marker, D.R. & Delanois, R.E. (2008) Metal-on-metal total hip resurfacing arthroplasty in the presence of extra-articular deformities or implants. *J Bone Joint Surg Am,* **90 Suppl 3,** 45-51.

Moore, A.T. & Bohlman, H.R. (2006) Metal hip joint: a case report. 1942. *Clin Orthop Relat Res,* **453,** 22-24.

Moretti, R., Torre, P., Antonello, R.M., Cattaruzza, T., Cazzato, G. & Bava, A. (2004) Vitamin B12 and folate depletion in cognition: a review. *Neurol India,* **52,** 310-318.

Morin, Y. & Daniel, P. (1967) Quebec beer-drinkers' cardiomyopathy: etiological considerations. *Can Med Assoc J,* **97,** 926-928.

Moriwaki, H., Osborne, M.R. & Phillips, D.H. (2008) Effects of mixing metal ions on oxidative DNA damage mediated by a Fenton-type reduction. *Toxicol In Vitro,* **22,** 36-44.

Moroni, A., Savarino, L., Cadossi, M., Baldini, N. & Giannini, S. (2008) Does ion release differ between hip resurfacing and metal-on-metal THA? *Clin Orthop Relat Res,* **466,** 700-707.

Moukarzel, A. (2009) Chromium in parenteral nutrition: too little or too much? *Gastroenterology,* **137,** S18-28.

Murad, S., Grove, D., Lindberg, K.A., Reynolds, G., Sivarajah, A. & Pinnell, S.R. (1981) Regulation of collagen synthesis by ascorbic acid. *Proceedings of the National Academy of Sciences,* **78,** 2879-2882.

Nabavi, A., Yeoh, K.M., Shidiac, L., Appleyard, R., Gillies, R.M. & Turnbull, A. (2009) Effects of positioning and notching of resurfaced femurs on

femoral neck strength: a biomechanical test. *J Orthop Surg (Hong Kong),* **17,** 47-50.

Nakashima, Y., Sun, D.H., Trindade, M.C., Chun, L.E., Song, Y., Goodman, S.B., Schurman, D.J., Maloney, W.J. & Smith, R.L. (1999) Induction of macrophage C-C chemokine expression by titanium alloy and bone cement particles. *J Bone Joint Surg Br,* **81,** 155-162.

Nasab, M. & Hassan, M. (2010) Metallic Biomaterials of Knee and Hip - A Review. *Trends Biomater. Artif. Organs,* **24,** 69-82.

Nassif, N.A., Nawabi, D.H., Stoner, K., Elpers, M., Wright, T. & Padgett, D.E. (2014) Taper Design Affects Failure of Large-head Metal-on-metal Total Hip Replacements. *Clin Orthop Relat Res,* **472,** 564-571.

Navarro, M., Michiardi, A., Castano, O. & Planell, J.A. (2008) Biomaterials in orthopaedics. *J R Soc Interface,* **5,** 1137-1158.

Nawabi, D.H., Hayter, C.L., Su, E.P., Koff, M.F., Perino, G., Gold, S.L., Koch, K.M. & Potter, H.G. (2013) Magnetic resonance imaging findings in symptomatic versus asymptomatic subjects following metal-on-metal hip resurfacing arthroplasty. *J Bone Joint Surg Am,* **95,** 895-902.

Neale, S.D., Haynes, D.R., Howie, D.W., Murray, D.W. & Athanasou, N.A. (2000) The effect of particle phagocytosis and metallic wear particles on osteoclast formation and bone resorption in vitro. *J Arthroplasty,* **15,** 654-662.

Nemery, B., Verbeken, E.K. & Demedts, M. (2001) Giant cell interstitial pneumonia (hard metal lung disease, cobalt lung). *Semin Respir Crit Care Med,* **22,** 435-448.

Nesbitt, S.A. & Horton, M.A. (1997) Trafficking of matrix collagens through bone-resorbing osteoclasts. *Science,* **276,** 266-269.

Nichols, K.G. & Puleo, D.A. (1997) Effect of metal ions on the formation and function of osteoclastic cells in vitro. *J Biomed Mater Res,* **35,** 265-271.

Nickens, K.P., Patierno, S.R. & Ceryak, S. (2010) Chromium genotoxicity: A double-edged sword. *Chem Biol Interact.*

Nicolaije, C., Koedam, M. & van Leeuwen, J.P. (2012) Decreased oxygen tension lowers reactive oxygen species and apoptosis and inhibits osteoblast matrix mineralization through changes in early osteoblast differentiation. *J Cell Physiol,* **227,** 1309-1318.

Ning, J. & Grant, M.H. (1999) Chromium (VI)-induced cytotoxicity to osteoblast-derived cells. *Toxicol In Vitro,* **13,** 879-887.

NJR (2013) National Joint Registry 9th Annual Report. National Joint registry of England and Wales.

O'Brien, T., Xu, J. & Patierno, S.R. (2001) Effects of glutathione on chromium-induced DNA crosslinking and DNA polymerase arrest. *Mol Cell Biochem,* **222,** 173-182.

Okamoto, K., Matsuura, T., Hosokawa, R. & Akagawa, Y. (1998) RGD peptides regulate the specific adhesion scheme of osteoblasts to hydroxyapatite but not to titanium. *J Dent Res,* **77,** 481-487.

Okumura, A., Goto, M., Goto, T., Yoshinari, M., Masuko, S., Katsuki, T. & Tanaka, T. (2001) Substrate affects the initial attachment and subsequent behavior of human osteoblastic cells (Saos-2). *Biomaterials,* **22,** 2263-2271.

Olsson, S.S., Jernberger, A. & Tryggo, D. (1981) Clinical and radiological long-term results after Charnley-Muller total hip replacement. A 5 to 10 year

follow-up study with special reference to aseptic loosening. *Acta Orthop Scand,* **52,** 531-542.

Orhue, V., Kanaji, A., Caicedo, M.S., Virdi, A.S., Sumner, D.R., Hallab, N.J., Jahr, H. & Sena, K. (2011) Calcineurin/nuclear factor of activated T cells (NFAT) signaling in cobalt-chromium-molybdenum (CoCrMo) particles-induced tumor necrosis factor-alpha (TNFalpha) secretion in MLO-Y4 osteocytes. *J Orthop Res,* **29,** 1867-1873.

Orriss, I.R., Knight, G.E., Utting, J.C., Taylor, S.E., Burnstock, G. & Arnett, T.R. (2009) Hypoxia stimulates vesicular ATP release from rat osteoblasts. *J Cell Physiol,* **220,** 155-162.

Ortega, R., Bresson, C., Fraysse, A., Sandre, C., Deves, G., Gombert, C., Tabarant, M., Bleuet, P., Seznec, H., Simionovici, A., Moretto, P. & Moulin, C. (2009) Cobalt distribution in keratinocyte cells indicates nuclear and perinuclear accumulation and interaction with magnesium and zinc homeostasis. *Toxicol Lett,* **188,** 26-32.

Ovesen, J.L., Fan, Y., Chen, J., Medvedovic, M., Xia, Y. & Puga, A. (2013) Long-term exposure to low-concentrations of Cr(VI) induce DNA damage and disrupt the transcriptional response to benzo[a]pyrene. *Toxicology,* **316C,** 14-24.

Oya, K., Tanaka, Y., Saito, H., Kurashima, K., Nogi, K., Tsutsumi, H., Tsutsumi, Y., Doi, H., Nomura, N. & Hanawa, T. (2009) Calcification by MC3T3-E1 cells on RGD peptide immobilized on titanium through electrodeposited PEG. *Biomaterials,* **30,** 1281-1286.

Pandey, R., Quinn, J., Joyner, C., Murray, D.W., Triffitt, J.T. & Athanasou, N.A. (1996) Arthroplasty implant biomaterial particle associated macrophages differentiate into lacunar bone resorbing cells. *Ann Rheum Dis,* **55,** 388-395.

Pandit, H., Glyn-Jones, S., McLardy-Smith, P., Gundle, R., Whitwell, D., Gibbons, C.L., Ostlere, S., Athanasou, N., Gill, H.S. & Murray, D.W. (2008) Pseudotumours associated with metal-on-metal hip resurfacings. *J Bone Joint Surg Br,* **90,** 847-851.

Paredes-Gamero, E.J., Franca, J.P., Moraes, A.A., Aguilar, M.O., Oshiro, M.E. & Ferreira, A.T. (2004) Problems caused by high concentration of ATP on activation of the P2X7 receptor in bone marrow cells loaded with the Ca2+ fluorophore fura-2. *J Fluoresc,* **14,** 711-722.

Park, M.S., Choi, B.W., Kim, S.J. & Park, J.H. (2003) Plasma spray-coated Ti femoral component for cementless total hip arthroplasty. *J Arthroplasty,* **18,** 626-630.

Park, Y.S., Moon, Y.W., Lim, S.J., Yang, J.M., Ahn, G. & Choi, Y.L. (2005a) Early osteolysis following second-generation metal-on-metal hip replacement. *J Bone Joint Surg Am,* **87,** 1515-1521.

Park, Y.S., Yi, K.Y., Lee, I.S., Han, C.H. & Jung, Y.C. (2005b) The effects of ion beam-assisted deposition of hydroxyapatite on the grit-blasted surface of endosseous implants in rabbit tibiae. *Int J Oral Maxillofac Implants,* **20,** 31-38.

Patlolla, A.K., Barnes, C., Hackett, D. & Tchounwou, P.B. (2009) Potassium dichromate induced cytotoxicity, genotoxicity and oxidative stress in human liver carcinoma (HepG2) cells. *Int J Environ Res Public Health,* **6,** 643-653.

Patntirapong, S., Habibovic, P. & Hauschka, P.V. (2009) Effects of soluble cobalt and cobalt incorporated into calcium phosphate layers on osteoclast differentiation and activation. *Biomaterials,* **30,** 548-555.

Paustenbach, D.J., Tvermoes, B.E., Unice, K.M., Finley, B.L. & Kerger, B.D. (2013) A review of the health hazards posed by cobalt. *Crit Rev Toxicol,* **43,** 316-362.

Pederson, L., Ruan, M., Westendorf, J.J., Khosla, S. & Oursler, M.J. (2008) Regulation of bone formation by osteoclasts involves Wnt/BMP signaling and the chemokine sphingosine-1-phosphate. *Proc Natl Acad Sci U S A,* **105,** 20764-20769.

Peters, C.L., McPherson, E., Jackson, J.D. & Erickson, J.A. (2007) Reduction in early dislocation rate with large-diameter femoral heads in primary total hip arthroplasty. *J Arthroplasty,* **22,** 140-144.

Picard, V., Govoni, G., Jabado, N. & Gros, P. (2000) Nramp 2 (DCT1/DMT1) expressed at the plasma membrane transports iron and other divalent cations into a calcein-accessible cytoplasmic pool. *J Biol Chem,* **275,** 35738-35745.

Plate, J.F., Seyler, T.M., Stroh, D.A., Issa, K., Akbar, M. & Mont, M.A. (2012) Risk of dislocation using large- vs. small-diameter femoral heads in total hip arthroplasty. *BMC Res Notes,* **5,** 553.

Polyzois, I., Nikolopoulos, D., Michos, I., Patsouris, E. & Theocharis, S. (2012) Local and systemic toxicity of nanoscale debris particles in total hip arthroplasty. *J Appl Toxicol,* **32,** 255-269.

Poole, K.E.S., van Bezooijen, R.L., Loveridge, N., Hamersma, H., Papapoulos, S.E., Löwik, C.W. & Reeve, J. (2005) Sclerostin is a delayed secreted product of osteocytes that inhibits bone formation. *The FASEB Journal.*

Prentice, J.R., Clark, M.J., Hoggard, N., Morton, A.C., Tooth, C., Paley, M.N., Stockley, I., Hadjivassiliou, M. & Wilkinson, J.M. (2013) Metal-on-metal hip prostheses and systemic health: a cross-sectional association study 8 years after implantation. *PLoS One,* **8,** e66186.

Preuss, H.G. & Anderson, R.A. (1998) Chromium update: examining recent literature 1997-1998. *Curr Opin Clin Nutr Metab Care,* **1,** 509-512.

Prideaux, M., Loveridge, N., Pitsillides, A.A. & Farquharson, C. (2012) Extracellular matrix mineralization promotes E11/gp38 glycoprotein expression and drives osteocytic differentiation. *PLoS One,* **7,** e36786.

Purdue, P.E., Koulouvaris, P., Nestor, B.J. & Sculco, T.P. (2006) The central role of wear debris in periprosthetic osteolysis. *HSS J,* **2,** 102-113.

Qiao, Y. & Ma, L. (2013) Quantification of metal ion induced DNA damage with single cell array based assay. *Analyst.*

Queally, J.M., Devitt, B.M., Butler, J.S., Malizia, A.P., Murray, D., Doran, P.P. & O'Byrne, J.M. (2009) Cobalt ions induce chemokine secretion in primary human osteoblasts. *J Orthop Res,* **27,** 855-864.

Quinn, J., Joyner, C., Triffitt, J.T. & Athanasou, N.A. (1992) Polymethylmethacrylate-induced inflammatory macrophages resorb bone. *J Bone Joint Surg Br,* **74,** 652-658.

Raggatt, L.J. & Partridge, N.C. (2010) Cellular and molecular mechanisms of bone remodeling. *J Biol Chem,* **285,** 25103-25108.

Raghunathan, V.K., Grant, M.H. & Ellis, E.M. (2010) Changes in protein expression associated with chronic in vitro exposure of hexavalent

chromium to osteoblasts and monocytes: a proteomic approach. *J Biomed Mater Res A,* **92,** 615-625.

Raghunathan, V.K., Tettey, J.N., Ellis, E.M. & Grant, M.H. (2009) Comparative chronic in vitro toxicity of hexavalent chromium to osteoblasts and monocytes. *J Biomed Mater Res A,* **88,** 543-550.

Rahn, B. (2003) Fluorochrome labelling of bone dynamics. *Eur Cells and Mater,* **5,** 41.

Rahn, B.A. & Perren, S.M. (1971) Xylenol orange, a fluorochrome useful in polychrome sequential labeling of calcifying tissues. *Stain Technol,* **46,** 125-129.

Ramachandran, R., Goodman, S.B. & Smith, R.L. (2006) The effects of titanium and polymethylmethacrylate particles on osteoblast phenotypic stability. *J Biomed Mater Res A,* **77,** 512-517.

Raman, N., Srinivasan, V. & Ravi, M. (2002) Effect of chromium on the axenic growth and phosphatase activity of ectomycorrhizal fungi, Laccaria laccata and Suillus bovinus. *Bull Environ Contam Toxicol,* **68,** 569-575.

Ramazanoglu, M. & Oshida, Y. (2011) Osseointegration and Bioscience of Implant Surfaces-Current Concepts at Bone-Implant Interface. *Implant Dentistry-A Rapidly Evolving Practice, InTech Publisher, Croatia.*

Ramirez-Diaz, M.I., Diaz-Perez, C., Vargas, E., Riveros-Rosas, H., Campos-Garcia, J. & Cervantes, C. (2008) Mechanisms of bacterial resistance to chromium compounds. *Biometals,* **21,** 321-332.

Rastogi, S.K., Pandey, A. & Tripathi, S. (2008) Occupational health risks among the workers employed in leather tanneries at Kanpur. *Indian J Occup Environ Med,* **12,** 132-135.

Ravel, B. & Newville, M. (2005) ATHENA, ARTEMIS, HEPHAESTUS: data analysis for X-ray absorption spectroscopy using IFEFFIT. *J Synchrotron Radiat,* **12,** 537-541.

Reinholt, F.P., Hultenby, K., Oldberg, A. & Heinegard, D. (1990) Osteopontin--a possible anchor of osteoclasts to bone. *Proc Natl Acad Sci U S A,* **87,** 4473-4475.

Reito, A., Eskelinen, A., Puolakka, T. & Pajamaki, J. (2013) Results of metal-on-metal hip resurfacing in patients 40 years old and younger. *Arch Orthop Trauma Surg,* **133,** 267-273.

Richards, C.J., Giannitsios, D., Huk, O.L., Zukor, D.J., Steffen, T. & Antoniou, J. (2008) Risk of periprosthetic femoral neck fracture after hip resurfacing arthroplasty: valgus compared with anatomic alignment. A biomechanical and clinical analysis. *J Bone Joint Surg Am,* **90 Suppl 3,** 96-101.

Rickard, D.J., Sullivan, T.A., Shenker, B.J., Leboy, P.S. & Kazhdan, I. (1994) Induction of rapid osteoblast differentiation in rat bone marrow stromal cell cultures by dexamethasone and BMP-2. *Dev Biol,* **161,** 218-228.

Robling, A.G., Niziolek, P.J., Baldridge, L.A., Condon, K.W., Allen, M.R., Alam, I., Mantila, S.M., Gluhak-Heinrich, J., Bellido, T.M., Harris, S.E. & Turner, C.H. (2008) Mechanical stimulation of bone in vivo reduces osteocyte expression of Sost/sclerostin. *J Biol Chem,* **283,** 5866-5875.

Rodan, S.B., Imai, Y., Thiede, M.A., Wesolowski, G., Thompson, D., Bar-Shavit, Z., Shull, S., Mann, K. & Rodan, G.A. (1987) Characterization of a human osteosarcoma cell line (Saos-2) with osteoblastic properties. *Cancer Res,* **47,** 4961-4966.

Rodda, S.J. & McMahon, A.P. (2006) Distinct roles for Hedgehog and canonical Wnt signaling in specification, differentiation and maintenance of osteoblast progenitors. *Development,* **133,** 3231-3244.

Rosser, J. & Bonewald, L.F. (2012) Studying osteocyte function using the cell lines MLO-Y4 and MLO-A5. *Methods Mol Biol,* **816,** 67-81.

Rousselle, A.V., Heymann, D., Demais, V., Charrier, C., Passuti, N. & Basle, M.F. (2002) Influence of metal ion solutions on rabbit osteoclast activities in vitro. *Histol Histopathol,* **17,** 1025-1032.

Rudolf, E. & Cervinka, M. (2005) The role of biomembranes in chromium (III)-induced toxicity in vitro. *Altern Lab Anim,* **33,** 249-259.

Rudolf, E. & Cervinka, M. (2009) Trivalent chromium activates Rac-1 and Src and induces switch in the cell death mode in human dermal fibroblasts. *Toxicol Lett,* **188,** 236-242.

Rumney, R.M., Wang, N., Agrawal, A. & Gartland, A. (2012) Purinergic signalling in bone. *Front Endocrinol (Lausanne),* **3,** 116.

Sabokbar, A., Pandey, R., Quinn, J.M. & Athanasou, N.A. (1998) Osteoclastic differentiation by mononuclear phagocytes containing biomaterial particles. *Arch Orthop Trauma Surg,* **117,** 136-140.

Sacher, A., Cohen, A. & Nelson, N. (2001) Properties of the mammalian and yeast metal-ion transporters DCT1 and Smf1p expressed in Xenopus laevis oocytes. *J Exp Biol,* **204,** 1053-1061.

Saju, K.K., Jayadas, N.H., Vidyanand, S. & James, J. (2011) Investigations into the molecular-level adhesion characteristics of hydroxyapatite-coated and anodized titanium surfaces using the molecular orbital approach. *Proc Inst Mech Eng H,* **225,** 246-254.

Salnikow, K., Donald, S.P., Bruick, R.K., Zhitkovich, A., Phang, J.M. & Kasprzak, K.S. (2004) Depletion of intracellular ascorbate by the carcinogenic metals nickel and cobalt results in the induction of hypoxic stress. *J Biol Chem,* **279,** 40337-40344.

Savarino, L., Padovani, G., Ferretti, M., Greco, M., Cenni, E., Perrone, G., Greco, F., Baldini, N. & Giunti, A. (2008) Serum ion levels after ceramic-on-ceramic and metal-on-metal total hip arthroplasty: 8-year minimum follow-up. *J Orthop Res,* **26,** 1569-1576.

Schmalzried, T.P., Jasty, M. & Harris, W.H. (1992) Periprosthetic bone loss in total hip arthroplasty. Polyethylene wear debris and the concept of the effective joint space. *J Bone Joint Surg Am,* **74,** 849-863.

Schneider, C.A., Rasband, W.S. & Eliceiri, K.W. (2012) NIH Image to ImageJ: 25 years of image analysis. *Nat Methods,* **9,** 671-675.

Scholes, S.C., Green, S.M. & Unsworth, A. (2001) The wear of metal-on-metal total hip prostheses measured in a hip simulator. *Proc Inst Mech Eng H,* **215,** 523-530.

Seetharam, B. & Alpers, D.H. (1982) Absorption and transport of cobalamin (vitamin B12). *Annu Rev Nutr,* **2,** 343-369.

Shahgaldi, B.F., Heatley, F.W., Dewar, A. & Corrin, B. (1995) In vivo corrosion of cobalt-chromium and titanium wear particles. *J Bone Joint Surg Br,* **77,** 962-966.

Shelnutt, S.R., Goad, P. & Belsito, D.V. (2007) Dermatological toxicity of hexavalent chromium. *Crit Rev Toxicol,* **37,** 375-387.

Sheridan, E.J., Austin, C.J., Aitken, J.B., Vogt, S., Jolliffe, K.A., Harris, H.H. & Rendina, L.M. (2013) Synchrotron X-ray fluorescence studies of a

bromine-labelled cyclic RGD peptide interacting with individual tumor cells. *J Synchrotron Radiat,* **20,** 226-233.

Shu, R., McMullen, R., Baumann, M.J. & McCabe, L.R. (2003) Hydroxyapatite accelerates differentiation and suppresses growth of MC3T3-E1 osteoblasts. *J Biomed Mater Res A,* **67,** 1196-1204.

Simonsen, L.O., Harbak, H. & Bennekou, P. (2011) Passive transport pathways for Ca(2+) and Co(2+) in human red blood cells. (57)Co(2+) as a tracer for Ca(2+) influx. *Blood Cells Mol Dis,* **47,** 214-225.

Singer, V.L., Jones, L.J., Yue, S.T. & Haugland, R.P. (1997) Characterization of PicoGreen reagent and development of a fluorescence-based solution assay for double-stranded DNA quantitation. *Anal Biochem,* **249,** 228-238.

Singh, G., Meyer, H., Ruetschi, M., Chamaon, K., Feuerstein, B. & Lohmann, C.H. (2013) Large-diameter metal-on-metal total hip arthroplasties: a page in orthopedic history? *J Biomed Mater Res A,* **101,** 3320-3326.

Siopack, J.S. & Jergesen, H.E. (1995) Total hip arthroplasty. *West J Med,* **162,** 243-249.

Sivalingam, P.M. (1989) Enzymatic and cellular level effects of chromium∗. *Toxicological & Environmental Chemistry,* **19,** 119-123.

Smith-Petersen, M.N. (2006) Evolution of mould arthroplasty of the hip joint. 1948. *Clin Orthop Relat Res,* **453,** 17-21.

Smith, A.J., Dieppe, P., Howard, P.W. & Blom, A.W. (2012a) Failure rates of metal-on-metal hip resurfacings: analysis of data from the National Joint Registry for England and Wales. *Lancet,* **380,** 1759-1766.

Smith, A.J., Dieppe, P., Vernon, K., Porter, M. & Blom, A.W. (2012b) Failure rates of stemmed metal-on-metal hip replacements: analysis of data from the National Joint Registry of England and Wales. *Lancet,* **379,** 1199-1204.

Smith, T.M., Berend, K.R., Lombardi, A.V., Jr., Emerson, R.H., Jr. & Mallory, T.H. (2005) Metal-on-metal total hip arthroplasty with large heads may prevent early dislocation. *Clin Orthop Relat Res,* **441,** 137-142.

Solé, V.A., Papillon, E., Cotte, M., Walter, P. & Susini, J. (2007) A multiplatform code for the analysis of energy-dispersive X-ray fluorescence spectra. *Spectrochimica Acta Part B: Atomic Spectroscopy,* **62,** 63-68.

Speetjens, J.K., Collins, R.A., Vincent, J.B. & Woski, S.A. (1999) The nutritional supplement chromium(III) tris(picolinate) cleaves DNA. *Chem Res Toxicol,* **12,** 483-487.

Spencer, S., Carter, R., Murray, H. & Meek, R.M. (2008) Femoral neck narrowing after metal-on-metal hip resurfacing. *J Arthroplasty,* **23,** 1105-1109.

Stec, B., Holtz, K.M. & Kantrowitz, E.R. (2000) A revised mechanism for the alkaline phosphatase reaction involving three metal ions. *J Mol Biol,* **299,** 1303-1311.

Steffen, R.T., Smith, S.R., Urban, J.P., McLardy-Smith, P., Beard, D.J., Gill, H.S. & Murray, D.W. (2005) The effect of hip resurfacing on oxygen concentration in the femoral head. *J Bone Joint Surg Br,* **87,** 1468-1474.

Stenbeck, G. & Horton, M.A. (2004) Endocytic trafficking in actively resorbing osteoclasts. *J Cell Sci,* **117,** 827-836.

Stern, A.R., Stern, M.M., Van Dyke, M.E., Jahn, K., Prideaux, M. & Bonewald, L.F. (2012) Isolation and culture of primary osteocytes from the long bones of skeletally mature and aged mice. *Biotechniques,* **52,** 361-373.

Stevens, A. & Lowe, J. (1997) *Human Histology.* Mosby.

Stroh, D.A., Issa, K., Johnson, A.J., Delanois, R.E. & Mont, M.A. (2013) Reduced dislocation rates and excellent functional outcomes with large-diameter femoral heads. *J Arthroplasty,* **28,** 1415-1420.

Suadicani, S.O., Brosnan, C.F. & Scemes, E. (2006) P2X7 receptors mediate ATP release and amplification of astrocytic intercellular Ca2+ signaling. *J Neurosci,* **26,** 1378-1385.

Sun, Z.L., Wataha, J.C. & Hanks, C.T. (1997) Effects of metal ions on osteoblast-like cell metabolism and differentiation. *J Biomed Mater Res,* **34,** 29-37.

Sundaram, P., Agrawal, K., Mandke, J.V. & Joshi, J.M. (2001) Giant cell pneumonitis induced by cobalt. *Indian J Chest Dis Allied Sci,* **43,** 47-49.

Sunters, A., Thomas, D.P., Yeudall, W.A. & Grigoriadis, A.E. (2004) Accelerated cell cycle progression in osteoblasts overexpressing the c-fos proto-oncogene: induction of cyclin A and enhanced CDK2 activity. *J Biol Chem,* **279,** 9882-9891.

Susa, N., Ueno, S., Furukawa, Y., Ueda, J. & Sugiyama, M. (1997) Potent protective effect of melatonin on chromium(VI)-induced DNA single-strand breaks, cytotoxicity, and lipid peroxidation in primary cultures of rat hepatocytes. *Toxicol Appl Pharmacol,* **144,** 377-384.

Suwalsky, M., Castro, R., Villena, F. & Sotomayor, C.P. (2008) Cr(III) exerts stronger structural effects than Cr(VI) on the human erythrocyte membrane and molecular models. *J Inorg Biochem,* **102,** 842-849.

Tamaki, Y., Sasaki, K., Sasaki, A., Takakubo, Y., Hasegawa, H., Ogino, T., Konttinen, Y.T., Salo, J. & Takagi, M. (2008) Enhanced osteolytic potential of monocytes/macrophages derived from bone marrow after particle stimulation. *J Biomed Mater Res B Appl Biomater,* **84,** 191-204.

Tan, S.D., Bakker, A.D., Semeins, C.M., Kuijpers-Jagtman, A.M. & Klein-Nulend, J. (2008) Inhibition of osteocyte apoptosis by fluid flow is mediated by nitric oxide. *Biochem Biophys Res Commun,* **369,** 1150-1154.

Tan, S.D., de Vries, T.J., Kuijpers-Jagtman, A.M., Semeins, C.M., Everts, V. & Klein-Nulend, J. (2007) Osteocytes subjected to fluid flow inhibit osteoclast formation and bone resorption. *Bone,* **41,** 745-751.

Tenderholt, A., Hedman, B. & Hodgson, K.O. (2007) PySpline: A modern, cross-platform program for the processing of raw averaged XAS edge and EXAFS data. In: *X-Ray Absorption Fine Structure-XAFS13* (ed. by Hedman, B. & Painetta, P.), Vol. 882, pp. 105-107.

Thomas, F., Serratrice, G., Beguin, C., Aman, E.S., Pierre, J.L., Fontecave, M. & Laulhere, J.P. (1999) Calcein as a fluorescent probe for ferric iron. Application to iron nutrition in plant cells. *J Biol Chem,* **274,** 13375-13383.

Thouverey, C., Malinowska, A., Balcerzak, M., Strzelecka-Kiliszek, A., Buchet, R., Dadlez, M. & Pikula, S. (2011) Proteomic characterization of biogenesis and functions of matrix vesicles released from mineralizing human osteoblast-like cells. *J Proteomics,* **74,** 1123-1134.

Tkaczyk, C., Huk, O.L., Mwale, F., Antoniou, J., Zukor, D.J., Petit, A. & Tabrizian, M. (2010) Investigation of the binding of Cr(III) complexes to bovine and human serum proteins: a proteomic approach. *J Biomed Mater Res A,* **94,** 214-222.

Touret, N., Furuya, W., Forbes, J., Gros, P. & Grinstein, S. (2003) Dynamic traffic through the recycling compartment couples the metal transporter Nramp2 (DMT1) with the transferrin receptor. *J Biol Chem,* **278,** 25548-25557.

Ubara, Y., Fushimi, T., Tagami, T., Sawa, N., Hoshino, J., Yokota, M., Katori, H., Takemoto, F. & Hara, S. (2003) Histomorphometric features of bone in patients with primary and secondary hypoparathyroidism. *Kidney Int,* **63,** 1809-1816.

Ubara, Y., Tagami, T., Nakanishi, S., Sawa, N., Hoshino, J., Suwabe, T., Katori, H., Takemoto, F., Hara, S. & Takaichi, K. (2005) Significance of minimodeling in dialysis patients with adynamic bone disease. *Kidney Int,* **68,** 833-839.

Ullmark, G., Sundgren, K., Milbrink, J., Nilsson, O. & Sorensen, J. (2009) Osteonecrosis following resurfacing arthroplasty. *Acta Orthop,* **80,** 670-674.

Ulrich, S.D., Seyler, T.M., Bennett, D., Delanois, R.E., Saleh, K.J., Thongtrangan, I., Kuskowski, M., Cheng, E.Y., Sharkey, P.F., Parvizi, J., Stiehl, J.B. & Mont, M.A. (2008) Total hip arthroplasties: what are the reasons for revision? *Int Orthop,* **32,** 597-604.

Unceta, N., Seby, F., Malherbe, J. & Donard, O.F. (2010) Chromium speciation in solid matrices and regulation: a review. *Anal Bioanal Chem,* **397,** 1097-1111.

Upreti, R.K., Shrivastava, R., Kannan, A. & Chaturvedi, U.C. (2005) A comparative study on rat intestinal epithelial cells and resident gut bacteria: (I) effect of hexavalent chromium. *Toxicol Mech Methods,* **15,** 331-338.

Vail, T.P., Mina, C.A., Yergler, J.D. & Pietrobon, R. (2006) Metal-on-metal hip resurfacing compares favorably with THA at 2 years followup. *Clin Orthop Relat Res,* **453,** 123-131.

Valko, M., Rhodes, C.J., Moncol, J., Izakovic, M. & Mazur, M. (2006) Free radicals, metals and antioxidants in oxidative stress-induced cancer. *Chem Biol Interact,* **160,** 1-40.

Vatsa, A., Mizuno, D., Smit, T.H., Schmidt, C.F., MacKintosh, F.C. & Klein-Nulend, J. (2006) Bio imaging of intracellular NO production in single bone cells after mechanical stimulation. *J Bone Miner Res,* **21,** 1722-1728.

Vazquez, M., Evans, B.A.J., Ralphs, J.R., Riccardi, D. & D.J., M. (2012) In vitro 3D osteoblast-osteocyte co-culture model. *European Cells and Materials,* **24,** 7.

Vengellur, A. & LaPres, J.J. (2004) The role of hypoxia inducible factor 1alpha in cobalt chloride induced cell death in mouse embryonic fibroblasts. *Toxicol Sci,* **82,** 638-646.

Verborgt, O., Gibson, G.J. & Schaffler, M.B. (2000) Loss of osteocyte integrity in association with microdamage and bone remodeling after fatigue in vivo. *J Bone Miner Res,* **15,** 60-67.

Vincent, J.B. (2010) Chromium: celebrating 50 years as an essential element? *Dalton Trans,* **39,** 3787-3794.

Virginio C, Church D, North RA & A., S. (1997) Effects of divalent cations, protons and calmidazolium at the rat P2X7 receptor. *Neuropharmacology,* **36,** 1285-1294.

von Schenck, U., Bender-Gotze, C. & Koletzko, B. (1997) Persistence of neurological damage induced by dietary vitamin B-12 deficiency in infancy. *Arch Dis Child,* **77,** 137-139.

Vos, T. & Flaxman, A.D. & Naghavi, M. & Lozano, R. & Michaud, C. & Ezzati, M. & Shibuya, K. & Salomon, J.A. & Abdalla, S. & Aboyans, V. & Abraham, J. & Ackerman, I. & Aggarwal, R. & Ahn, S.Y. & Ali, M.K. & Alvarado, M. & Anderson, H.R. & Anderson, L.M. & Andrews, K.G. & Atkinson, C. & Baddour, L.M. & Bahalim, A.N. & Barker-Collo, S. & Barrero, L.H. & Bartels, D.H. & Basanez, M.G. & Baxter, A. & Bell, M.L. & Benjamin, E.J. & Bennett, D. & Bernabe, E. & Bhalla, K. & Bhandari, B. & Bikbov, B. & Bin Abdulhak, A. & Birbeck, G. & Black, J.A. & Blencowe, H. & Blore, J.D. & Blyth, F. & Bolliger, I. & Bonaventure, A. & Boufous, S. & Bourne, R. & Boussinesq, M. & Braithwaite, T. & Brayne, C. & Bridgett, L. & Brooker, S. & Brooks, P. & Brugha, T.S. & Bryan-Hancock, C. & Bucello, C. & Buchbinder, R. & Buckle, G. & Budke, C.M. & Burch, M. & Burney, P. & Burstein, R. & Calabria, B. & Campbell, B. & Canter, C.E. & Carabin, H. & Carapetis, J. & Carmona, L. & Cella, C. & Charlson, F. & Chen, H. & Cheng, A.T. & Chou, D. & Chugh, S.S. & Coffeng, L.E. & Colan, S.D. & Colquhoun, S. & Colson, K.E. & Condon, J. & Connor, M.D. & Cooper, L.T. & Corriere, M. & Cortinovis, M. & de Vaccaro, K.C. & Couser, W. & Cowie, B.C. & Criqui, M.H. & Cross, M. & Dabhadkar, K.C. & Dahiya, M. & Dahodwala, N. & Damsere-Derry, J. & Danaei, G. & Davis, A. & De Leo, D. & Degenhardt, L. & Dellavalle, R. & Delossantos, A. & Denenberg, J. & Derrett, S. & Des Jarlais, D.C. & Dharmaratne, S.D. & Dherani, M. & Diaz-Torne, C. & Dolk, H. & Dorsey, E.R. & Driscoll, T. & Duber, H. & Ebel, B. & Edmond, K. & Elbaz, A. & Ali, S.E. & Erskine, H. & Erwin, P.J. & Espindola, P. & Ewoigbokhan, S.E. & Farzadfar, F. & Feigin, V. & Felson, D.T. & Ferrari, A. & Ferri, C.P. & Fevre, E.M. & Finucane, M.M. & Flaxman, S. & Flood, L. & Foreman, K. & Forouzanfar, M.H. & Fowkes, F.G. & Franklin, R. & Fransen, M. & Freeman, M.K. & Gabbe, B.J. & Gabriel, S.E. & Gakidou, E. & Ganatra, H.A. & Garcia, B. & Gaspari, F. & Gillum, R.F. & Gmel, G. & Gosselin, R. & Grainger, R. & Groeger, J. & Guillemin, F. & Gunnell, D. & Gupta, R. & Haagsma, J. & Hagan, H. & Halasa, Y.A. & Hall, W. & Haring, D. & Haro, J.M. & Harrison, J.E. & Havmoeller, R. & Hay, R.J. & Higashi, H. & Hill, C. & Hoen, B. & Hoffman, H. & Hotez, P.J. & Hoy, D. & Huang, J.J. & Ibeanusi, S.E. & Jacobsen, K.H. & James, S.L. & Jarvis, D. & Jasrasaria, R. & Jayaraman, S. & Johns, N. & Jonas, J.B. & Karthikeyan, G. & Kassebaum, N. & Kawakami, N. & Keren, A. & Khoo, J.P. & King, C.H. & Knowlton, L.M. & Kobusingye, O. & Koranteng, A. & Krishnamurthi, R. & Lalloo, R. & Laslett, L.L. & Lathlean, T. & Leasher, J.L. & Lee, Y.Y. & Leigh, J. & Lim, S.S. & Limb, E. & Lin, J.K. & Lipnick, M. & Lipshultz, S.E. & Liu, W. & Loane, M. & Ohno, S.L. & Lyons, R. & Ma, J. & Mabweijano, J. & MacIntyre, M.F. & Malekzadeh, R. & Mallinger, L. & Manivannan, S. & Marcenes, W. & March, L. & Margolis, D.J. & Marks, G.B. & Marks, R.

& Matsumori, A. & Matzopoulos, R. & Mayosi, B.M. & McAnulty, J.H. & McDermott, M.M. & McGill, N. & McGrath, J. & Medina-Mora, M.E. & Meltzer, M. & Mensah, G.A. & Merriman, T.R. & Meyer, A.C. & Miglioli, V. & Miller, M. & Miller, T.R. & Mitchell, P.B. & Mocumbi, A.O. & Moffitt, T.E. & Mokdad, A.A. & Monasta, L. & Montico, M. & Moradi-Lakeh, M. & Moran, A. & Morawska, L. & Mori, R. & Murdoch, M.E. & Mwaniki, M.K. & Naidoo, K. & Nair, M.N. & Naldi, L. & Narayan, K.M. & Nelson, P.K. & Nelson, R.G. & Nevitt, M.C. & Newton, C.R. & Nolte, S. & Norman, P. & Norman, R. & O'Donnell, M. & O'Hanlon, S. & Olives, C. & Omer, S.B. & Ortblad, K. & Osborne, R. & Ozgediz, D. & Page, A. & Pahari, B. & Pandian, J.D. & Rivero, A.P. & Patten, S.B. & Pearce, N. & Padilla, R.P. & Perez-Ruiz, F. & Perico, N. & Pesudovs, K. & Phillips, D. & Phillips, M.R. & Pierce, K. & Pion, S. & Polanczyk, G.V. & Polinder, S. & Pope, C.A., 3rd & Popova, S. & Porrini, E. & Pourmalek, F. & Prince, M. & Pullan, R.L. & Ramaiah, K.D. & Ranganathan, D. & Razavi, H. & Regan, M. & Rehm, J.T. & Rein, D.B. & Remuzzi, G. & Richardson, K. & Rivara, F.P. & Roberts, T. & Robinson, C. & De Leon, F.R. & Ronfani, L. & Room, R. & Rosenfeld, L.C. & Rushton, L. & Sacco, R.L. & Saha, S. & Sampson, U. & Sanchez-Riera, L. & Sanman, E. & Schwebel, D.C. & Scott, J.G. & Segui-Gomez, M. & Shahraz, S. & Shepard, D.S. & Shin, H. & Shivakoti, R. & Singh, D. & Singh, G.M. & Singh, J.A. & Singleton, J. & Sleet, D.A. & Sliwa, K. & Smith, E. & Smith, J.L. & Stapelberg, N.J. & Steer, A. & Steiner, T. & Stolk, W.A. & Stovner, L.J. & Sudfeld, C. & Syed, S. & Tamburlini, G. & Tavakkoli, M. & Taylor, H.R. & Taylor, J.A. & Taylor, W.J. & Thomas, B. & Thomson, W.M. & Thurston, G.D. & Tleyjeh, I.M. & Tonelli, M. & Towbin, J.A. & Truelsen, T. & Tsilimbaris, M.K. & Ubeda, C. & Undurraga, E.A. & van der Werf, M.J. & van Os, J. & Vavilala, M.S. & Venketasubramanian, N. & Wang, M. & Wang, W. & Watt, K. & Weatherall, D.J. & Weinstock, M.A. & Weintraub, R. & Weisskopf, M.G. & Weissman, M.M. & White, R.A. & Whiteford, H. & Wiersma, S.T. & Wilkinson, J.D. & Williams, H.C. & Williams, S.R. & Witt, E. & Wolfe, F. & Woolf, A.D. & Wulf, S. & Yeh, P.H. & Zaidi, A.K. & Zheng, Z.J. & Zonies, D. & Lopez, A.D. & Murray, C.J. & AlMazroa, M.A. & Memish, Z.A. (2012) Years lived with disability (YLDs) for 1160 sequelae of 289 diseases and injuries 1990-2010: a systematic analysis for the Global Burden of Disease Study 2010. *Lancet,* **380,** 2163-2196.

Walker, P.S. & Gold, B.L. (1971) The tribology (friction, lubrication and wear) of all-metal artificial hip joints. *Wear,* **17,** 285-299.

Walsh, C.A., Beresford, J.N., Birch, M.A., Boothroyd, B. & Gallagher, J.A. (1991) Application of reflected light microscopy to identify and quantitate resorption by isolated osteoclasts. *J Bone Miner Res,* **6,** 661-671.

Wang, J., Stieglitz, K.A. & Kantrowitz, E.R. (2005) Metal specificity is correlated with two crucial active site residues in Escherichia coli alkaline phosphatase. *Biochemistry,* **44,** 8378-8386.

Wang, W., Geller, J.A., Hasija, R., Choi, J.K., Patrick, D.A., Jr. & Macaulay, W. (2013) Longitudinal evaluation of time related femoral neck narrowing after metal-on-metal hip resurfacing. *World J Orthop,* **4,** 75-79.

Wang, Y., McNamara, L.M., Schaffler, M.B. & Weinbaum, S. (2007) A model for the role of integrins in flow induced mechanotransduction in osteocytes. *Proceedings of the National Academy of Sciences,* **104,** 15941-15946.

Wang, Y.H., Liu, Y., Maye, P. & Rowe, D.W. (2006) Examination of mineralized nodule formation in living osteoblastic cultures using fluorescent dyes. *Biotechnol Prog,* **22,** 1697-1701.

Webb, K., Hlady, V. & Tresco, P.A. (1998) Relative importance of surface wettability and charged functional groups on NIH 3T3 fibroblast attachment, spreading, and cytoskeletal organization. *J Biomed Mater Res,* **41,** 422-430.

Weiss, M.J., Cole, D.E., Ray, K., Whyte, M.P., Lafferty, M.A., Mulivor, R.A. & Harris, H. (1988) A missense mutation in the human liver/bone/kidney alkaline phosphatase gene causing a lethal form of hypophosphatasia. *Proc Natl Acad Sci U S A,* **85,** 7666-7669.

Weissbach, H. & Dickerman, H. (1965) BIOCHEMICAL ROLE OF VITAMIN B12. *Physiol Rev,* **45,** 80-97.

Willert, H.G., Buchhorn, G.H., Fayyazi, A., Flury, R., Windler, M., Koster, G. & Lohmann, C.H. (2005) Metal-on-metal bearings and hypersensitivity in patients with artificial hip joints. A clinical and histomorphological study. *J Bone Joint Surg Am,* **87,** 28-36.

Williams, D.H., Greidanus, N.V., Masri, B.A., Duncan, C.P. & Garbuz, D.S. (2011) Prevalence of pseudotumor in asymptomatic patients after metal-on-metal hip arthroplasty. *J Bone Joint Surg Am,* **93,** 2164-2171.

Witkiewicz-Kucharczyk, A. & Bal, W. (2006) Damage of zinc fingers in DNA repair proteins, a novel molecular mechanism in carcinogenesis. *Toxicol Lett,* **162,** 29-42.

Witzleb, W.C., Ziegler, J., Krummenauer, F., Neumeister, V. & Guenther, K.P. (2006) Exposure to chromium, cobalt and molybdenum from metal-on-metal total hip replacement and hip resurfacing arthroplasty. *Acta Orthop,* **77,** 697-705.

Wu, B., Mu, C., Zhang, G. & Lin, W. (2009) Effects of Cr3+ on the structure of collagen fiber. *Langmuir,* **25,** 11905-11910.

Wu, L.N., Genge, B.R., Lloyd, G.C. & Wuthier, R.E. (1991) Collagen-binding proteins in collagenase-released matrix vesicles from cartilage. Interaction between matrix vesicle proteins and different types of collagen. *J Biol Chem,* **266,** 1195-1203.

Xie, J., Baumann, M.J. & McCabe, L.R. (2004) Osteoblasts respond to hydroxyapatite surfaces with immediate changes in gene expression. *J Biomed Mater Res A,* **71,** 108-117.

Yamada, H., Yoshihara, Y., Henmi, O., Morita, M., Shiromoto, Y., Kawano, T., Kanaji, A., Ando, K., Nakagawa, M., Kosaki, N. & Fukaya, E. (2009) Cementless total hip replacement: past, present, and future. *J Orthop Sci,* **14,** 228-241.

Yang, L., McRae, R., Henary, M.M., Patel, R., Lai, B., Vogt, S. & Fahrni, C.J. (2005) Imaging of the intracellular topography of copper with a fluorescent sensor and by synchrotron x-ray fluorescence microscopy. *Proc Natl Acad Sci U S A,* **102,** 11179-11184.

Yang, W., Harris, M.A., Heinrich, J.G., Guo, D., Bonewald, L.F. & Harris, S.E. (2009) Gene expression signatures of a fibroblastoid preosteoblast and cuboidal osteoblast cell model compared to the MLO-Y4 osteocyte cell model. *Bone,* **44,** 32-45.

Yeung, C.K., Glahn, R.P. & Miller, D.D. (2005) Inhibition of iron uptake from iron salts and chelates by divalent metal cations in intestinal epithelial cells. *J Agric Food Chem,* **53,** 132-136.

Yokota, S. & Fahimi, D.H. (1987) Intracellular transport of albumin through the secretory apparatus of rat liver parenchymal cells. An immunocytochemical study. *Cell Struct Funct,* **12,** 251-264.

Yoshida, H., Hayashi, S., Kunisada, T., Ogawa, M., Nishikawa, S., Okamura, H., Sudo, T. & Shultz, L.D. (1990) The murine mutation osteopetrosis is in the coding region of the macrophage colony stimulating factor gene. *Nature,* **345,** 442-444.

You, L.-D., Weinbaum, S., Cowin, S.C. & Schaffler, M.B. (2004) Ultrastructure of the osteocyte process and its pericellular matrix. *The Anatomical Record Part A: Discoveries in Molecular, Cellular, and Evolutionary Biology,* **278A,** 505-513.

Zhang, K., Barragan-Adjemian, C., Ye, L., Kotha, S., Dallas, M., Lu, Y., Zhao, S., Harris, M., Harris, S.E., Feng, J.Q. & Bonewald, L.F. (2006) E11/gp38 selective expression in osteocytes: regulation by mechanical strain and role in dendrite elongation. *Mol Cell Biol,* **26,** 4539-4552.

Zhang, R., Oyajobi, B.O., Harris, S.E., Chen, D., Tsao, C., Deng, H.W. & Zhao, M. (2013) Wnt/beta-catenin signaling activates bone morphogenetic protein 2 expression in osteoblasts. *Bone,* **52,** 145-156.

Zhao, C., Irie, N., Takada, Y., Shimoda, K., Miyamoto, T., Nishiwaki, T., Suda, T. & Matsuo, K. (2006) Bidirectional ephrinB2-EphB4 signaling controls bone homeostasis. *Cell Metab,* **4,** 111-121.

Zhou, Z., Yu, M., Yang, H., Huang, K., Li, F., Yi, T. & Huang, C. (2008) FRET-based sensor for imaging chromium(III) in living cells. *Chem Commun (Camb)***,** 3387-3389.

Zijlstra, W.P., Bulstra, S.K., van Raay, J.J., van Leeuwen, B.M. & Kuijer, R. (2012) Cobalt and chromium ions reduce human osteoblast-like cell activity in vitro, reduce the OPG to RANKL ratio, and induce oxidative stress. *J Orthop Res,* **30,** 740-747.

Zustin, J., Hahn, M., Morlock, M.M., Ruther, W., Amling, M. & Sauter, G. (2010) Femoral component loosening after hip resurfacing arthroplasty. *Skeletal Radiol,* **39,** 747-756.